Mechanistic insights into the regulation of inflammatory pathology by A20

Arne Martens

Thesis submitted in partial fulfilment of the requirements for the degree of
DOCTOR OF SCIENCE: BIOTECHNOLOGY

Promoter: Prof. Dr. Geert van Loo

Academic year: 2019-2020
Faculty of Sciences, Ghent University
Department of Biomedical Molecular Biology

GHENT UNIVERSITY

FACULTY OF SCIENCES

VIB-UGENT CENTER FOR INFLAMMATION RESEARCH

Arne Martens was supported by a grant from the “Concerted Research Actions” (GOA) of the Ghent University. Research in the G. van Loo lab is supported by research grants from the FWO, the “Geneeskundige Stichting Koningin Elisabeth” (GSKE), the CBC Banque Prize, the Charcot Foundation, the “Belgian Foundation against Cancer”, “Kom op tegen Kanker”, and the GOA of the Ghent University.

Mechanistic insights into the regulation of inflammatory pathology by A20

By Arne Martens
Unit of Cellular and Molecular (Patho)physiology
Department of Biomedical Molecular Biology, Ghent University
Center for Inflammation Research, Flanders Institute for Biotechnology (VIB)
Technologiepark 71
9052 Zwijnaarde, Belgium

Academic year 2019-2020

Promoter
Prof. Dr. Geert van Loo

Examination committee

Chair:	Prof. Dr. Peter Brouckaert[1,2]
Secretary:	Prof. Dr. Mathieu Bertrand[1,2]
Other voting members:	Prof. Dr. Nelson O Gekara[3]
	Prof. Dr. Emmanuel Dejardin[4]
	Prof. Dr. Tom Vanden Berghe[1,2,5]
	Prof. Dr. Wim Declercq[1,2]
	Prof. Dr. Mohamed Lamkanfi[6,7]
Other members:	Prof. Dr. Geert van Loo[1,2]

[1]Department of Biomedical Molecular Biology, Ghent University, Belgium
[2]Center for Inflammation Research, VIB, Belgium
[3]Department of Molecular Biosciences, The Wenner-Gren Institute, Stockholm University, Sweden
[4]Laboratory of Molecular Immunology and Signal Transduction, GIGA-Research, University of Liège, Belgium
[5]Laboratory of Pathophysiology, Faculty of Biomedical Sciences, University of Antwerp, Wilrijk, Belgium
[6]Department of Internal Medicine and Pediatrics, Ghent University, Belgium
[7]Janssen Immunosciences, World Without Disease Accelerator, Pharmaceutical Companies of Johnson & Johnson, Belgium

General summary

Inflammation is a protective response of the body which is activated upon the detection of foreign molecules, pathogens or damaged cells, and is important to eliminate the danger and initiate tissue repair. Inflammation is a tightly controlled process and uncontrolled activation can lead to the development of several autoinflammatory and autoimmune diseases and eventually to the development of cancer. The NF-κB family of transcription factors are crucial regulators of inflammatory pathways and immune responses, but are also involved in cell survival, development, cell proliferation, differentiation and metabolism. Several (auto)regulatory mechanisms control NF-κB signaling in order to maintain tissue homeostasis and prevent sustained inflammation. In this PhD thesis, I will focus on the protein A20 (also known as Tumor Necrosis Factor alpha induced protein 3, TNFAIP3), a critical regulator of NF-κB signaling. Genome wide association studies have linked the *A20/TNFAIP3* locus to a variety of human inflammatory and autoimmune diseases, including rheumatoid arthritis (RA), systemic lupus erythematosus (SLE) and inflammatory bowel disease (IBD). Moreover, whole exome sequencing has identified heterozygous loss-of-function mutations in the *A20/TNFAIP3* gene (A20 haploinsufficiency, HA20) in patients with a rare, early-onset autoinflammatory syndrome, and bi-allelic somatic mutations are frequently observed in several B-cell lymphomas. Experimental studies in mice have confirmed the importance of A20 for the prevention of inflammatory pathology. However, how A20 controls inflammatory signaling still remains elusive. The main aim of this PhD thesis was to understand the molecular mechanisms by which A20 regulates inflammatory signaling *in vivo*.

In the first part of this thesis we investigated *in vivo* the importance of different A20 functionalities, by generating and characterizing new A20 mutant mouse lines which were engineered through CRISPR-Cas9 genome-editing technology to carry disruptive mutations in their ZnF7 domain ($A20^{ZnF7}$) or in both the ZnF4 and ZnF7 domains ($A20^{ZnF4ZnF7}$). Initially, A20 was described as a ubiquitin-editing enzyme that regulates NF-κB signaling by interfering with the ubiquitination status of target proteins, via its OTU and ZnF4 domains which have deubiquitinating and E3-ligase activities, respectively. However, mice with disruptive mutations in these domains do not develop spontaneous disease, questioning the *in vivo* role of these domains. $A20^{ZnF7}$ mice, which are defective in their ability to bind linear ubiquitin, do develop a spontaneous disease, characterized by a reduced bodyweight, the presence of splenomegaly and lymphadenopathy, increased levels of inflammatory cytokines in serum, and the detection of tissue inflammation. Furthermore, these mice are hypersensitive to a sublethal dose of TNF leading to severe hypothermia and death. Mechanistically, we demonstrated that the ZnF7 mutation abolishes the recruitment of A20 to the TNFR1 complex, reducing the amount

of linear ubiquitin chains detected at the complex, leading to the destabilization of complex I and the induction of cell death. By the additional mutation of A20's ZnF4 domain, known to have K63-ubiquitin binding activity, we have generated mice that die perinatally due to severe multi-organ inflammation, phenocopying A20 deficient mice. In conclusion, with these studies we have demonstrated that A20 primarily functions as a ubiquitin-binding protein to prevent cell death and inflammation.

In the second part of this thesis we further unraveled the role of A20 in preventing polyarthritis development in mice. Previous research from the group demonstrated that mice lacking A20 in their myeloid cells ($A20^{myel\text{-}KO}$) spontaneously develop polyarthritis with many features of human rheumatoid arthritis. This was shown to be caused by enhanced Nlrp3 inflammasome-mediated caspase-1 activation, pyroptosis and IL-1β secretion in macrophages of these mice. However, how A20 regulates Nlrp3 inflammasome activation was still not clear. In collaboration with the group of Manolis Pasparakis (University of Cologne), we could show that A20 prevents NLRP3 inflammasome-mediated arthritis development by preventing macrophage necroptosis, since $A20^{myel\text{-}KO}$ mice crossed into a RIPK3 or MLKL knockout background, or in a background of mice that express a kinase-dead RIPK1 mutant, no longer develop arthritis. We could further show that A20 prevents macrophage necroptosis, at least partly, by its ZnF7 function mediating linear ubiquitin binding, since mice mutated in their ZnF7 domain ($A20^{ZnF7}$) spontaneously develop polyarthritis, comparable to $A20^{myel\text{-}KO}$ mice. LPS stimulation of BMDMs isolated from $A20^{ZnF7}$ mice induced the release of bioactive IL-1β as well as IL-1α. IL-1α and IL-1β likely together with IL-18 and other DAMPs released by necroptotic macrophages activate MyD88-dependent proinflammatory signalling in synovial fibroblasts causing the development of arthritis.

Finally, in the last part of this thesis, we have identified a role for A20 in the process of osteoclastogenesis by regulating signaling downstream the receptor activator of nuclear factor kappa-B (RANK). Previous research from the group showed that $A20^{myel\text{-}KO}$ mice have increased numbers of $CD115^{+}CD117^{+}$ osteoclast precursors *in vivo,* and also produce more osteoclasts *in vitro* when blood leukocytes are stimulated with RANK ligand and macrophage colony-stimulating factor (M-CSF) compared to control A20 expressing cells. These observations suggest that A20 may play a direct role in the regulation of RANK-induced osteoclastogenesis. However, the enhanced osteoclastogenesis may also be the result of the more general inflammatory phenotype of A20 deficient mice, since inflammatory cytokines such as TNF, IL-1 and IL-6 are known to promote osteoclastogenesis. To further address this, we here generated mice which specifically lack A20 in maturating osteoclasts, by crossing A20 floxed mice with mice expressing Cre under control of the

CathepsinK promotor (osteoclast-specific A20 knockout, $A20^{OC\text{-}KO}$). We could show that these mice spontaneously develop osteoporosis with a significant increase in the number of TRAP-positive osteoclasts present at the growth plate, but without the systemic inflammation as seen in $A20^{myel\text{-}KO}$ mice. We further showed that A20 deficiency leads to increased and prolonged activation of RANK-induced NF-κB signaling in osteoclasts. How A20 regulates RANK-induced signaling is, however, still not clear and requires further research.

Algemene samenvatting

Inflammatie, beter gekend als ontsteking, is een beschermende reactie van het lichaam als antwoord op de aanwezigheid van lichaamsvreemde stoffen, pathogenen of beschadigde cellen en weefsels. De ontstekingsreactie speelt een cruciale rol in het verwijderen van deze potentieel gevaarlijke stoffen en het induceren van een herstelreactie. Aanhoudende 'chronische' inflammatie kan echter leiden tot het ontwikkelen van auto-inflammatoire en auto-immuunziekten, en kan zelfs aanleiding geven tot het ontstaan van kanker. NF-κB eiwitten, een familie van transcriptiefactoren, zijn van cruciaal belang in de regulatie van onstekingsprocessen en immuunreacties, en verschillende cellulaire mechanismen zorgen ervoor dat NF-κB activatie gecontroleerd gebeurt om zo chronische inflammatie te voorkomen. In deze doctoraatsthesis lag de focus op het eiwit A20 (ook gekend als Tumor necrosis factor alpha-induced protein 3, TNFAIP3), één van de belangrijkste regulatorische eiwitten betrokken in NF-κB activatie en inflammatie. Genoomwijde associatie-studies hebben polymorfismen (zogenaamde 'single nucleotide polymorfismen', SNPs) geïdentificeerd in de *A20/TNFAIP3* locus, en deze gelinkt aan verschillende auto-inflammatoire en auto-immuunziekten waaronder reumatoïde artritis (RA), systemische lupus erythematosis (SLE) en inflammatoire darmziekten (IBD). Meer recent werden bij patiënten die lijden aan een zeldzaam auto-inflammatoir syndroom heterozygote mutaties gevonden in het *A20/TNFAIP3* gen, aanleiding gevend tot A20 haplo-insufficiëntie. Ook in verschillende B-cel lymfomen worden frequent bi-allelische somatische mutaties in *A20* gevonden. Genetische studies in muizen hebben de belangrijke rol van A20 in de regulatie van inflammatie bevestigd, maar het onderliggende mechanisme dat verklaart waarom A20 dit doet is nog onvolledig gekend. Het doel van deze doctoraatsthesis was dan ook het verder onderzoeken van de moleculaire mechanismen waarmee A20 inflammatie reguleert.

Het A20 eiwit bestaat uit een N-terminaal OTU domein en een C-terminaal deel met zeven 'zinc finger' (ZnF) domeinen. In het eerste deel van deze thesis hebben we de *in vivo* rol onderzocht van twee ZnF domeinen, namelijk het ZnF4 en ZnF7 domein die verantwoordelijk zijn voor binding van A20 aan respectievelijk K63- en M1-ubiquitine. Hiervoor werden nieuwe transgene muislijnen gemaakt met mutaties in het ZnF7 domein ($A20^{ZnF7}$) enerzijds, of in zowel het ZnF4 als het ZnF7 domein ($A20^{ZnF4ZnF7}$). In vroegere studies werd gesuggereerd dat A20 werkzaam is als een zogenaamd 'ubiquitin-editing' enzym, waarbij het NF-κB signalisatie reguleert via zijn deubiquitinerende en E3-ligase activiteiten gemedieerd via zijn respectievelijk OTU en ZnF4 domein. Muizen met mutaties in het OTU of ZnF4 domein ontwikkelen echter geen spontaan inflammatoir fenotype, in tegenstelling tot A20 knock-out muizen, wat suggereert dat de anti-inflammatoire activiteit van A20 *in vivo* niet bepaald wordt door deze enzymatische activiteiten. $A20^{ZnF7}$ muizen, waarvan het A20 eiwit niet

langer kan binden aan lineaire (M1) ubiquitine ketens, ontwikkelen echter wel spontaan een inflammatoire pathologie. Deze muizen hebben een verminderd lichaamsgewicht, ontwikkelen splenomegalie en lymfadenopathie, en vertonen verhoogde niveaus van inflammatoire cytokines in hun serum. Ook kan de aanwezigheid van weefselinflammatie zoals in lever worden aangetoond in $A20^{ZnF7}$ muizen. Injectie van een normaal subletale dosis TNF in $A20^{ZnF7}$ muizen veroorzaakt hypothermie en dood van de muizen, in tegenstelling tot controle muizen die resistent zijn aan dergelijke inflammatoire blootstelling. Mechanistisch hebben we aangetoond dat in afwezigheid van een functioneel ZnF7 domein, A20 niet langer gerekruteerd wordt naar het TNFR1 complex, waardoor het niveau aan lineaire ubiquitinatie in dit complex zeer drastisch wordt gereduceerd, wat op zijn beurt leidt tot instabiliteit van het complex en inductie van celdood. Het additioneel muteren van het ZnF4 domein in deze muizen ($A20^{ZnF4ZnF7}$ muizen), leidt tot het ontstaan van ernstige multi-orgaan inflammatie en perinatale dood van de muizen. Dit fenotype is identiek aan het fenotype van A20 deficiënte muizen, wat het cruciale belang aantoont van de beide ubiquitine-bindende domeinen van A20 voor zijn anti-inflammatoire activiteit *in vivo*.

In het tweede deel van deze thesis werd de rol van A20 in de ontwikkeling van artritis verder onderzocht. Vroeger onderzoek binnen onze onderzoeksgroep heeft aangetoond dat muizen die specifiek A20 ontberen in de myeloide cellen ($A20^{myel\text{-}KO}$), spontaan artritis ontwikkelen, en deze pathologie sterke gelijkenissen vertoont met reumatoïde artritis in de mens. Verder onderzoek heeft aangetoond dat verhoogde Nlrp3 inflammasoom activatie en IL-1β secretie aan de basis liggen van deze artritis. Echter, het precieze moleculaire mechanisme dat verklaart waarom A20 deficiëntie leidt tot een verhoogde activatie van het Nlrp3 inflammasoom is echter nog steeds niet duidelijk. In samenwerking met de onderzoeksgroep van Manolis Pasparakis (Universiteit van Keulen) hebben we kunnen aantonen dat de artritis in $A20^{myel\text{-}KO}$ muizen wordt voorkomen wanneer deze muizen werden ingekruist met RIPK3 deficiënte, MLKL deficiënte of RIPK1 kinase-dood (KD) transgene muizen. Verder *in vitro* onderzoek kon aantonen dat A20 de activatie van het Nlrp3 inflammasoom controleert door het voorkomen van macrofaag necroptose. Hierbij konden we verder aantonen dat het ZnF7 domein van A20 hierin een cruciale rol speelt, aangezien $A20^{ZnF7}$ muizen spontaan artritis ontwikkelen, vergelijkbaar met $A20^{myel\text{-}KO}$ muizen. LPS-gestimuleerde beenmerg-afgeleide macrofagen (BMDMs) afkomstig van $A20^{ZnF7}$ muizen stellen IL-1α en IL-1β vrij in het cel medium, waarbij IL-1α en IL-1β, in samenwerking met IL-18 en andere DAMPs die vrijgesteld worden door necrotische macrofagen, op hun beurt MyD88-afhankelijke pro-inflammatoire signalisatie mediëren in de synoviale fibroblasten, wat uiteindelijk resulteert in het ontstaan van artritis.

In het laatste deel van deze doctoraatsthesis hebben we de rol onderzocht van A20 in de regulatie van osteoclastogenese en RANK signalisatie. Vroeger onderzoek binnen onze onderzoeksgroep heeft immers aangetoond dat $A20^{myel\text{-}KO}$ muizen meer $CD115^{+}CD117^{+}$ osteoclast precursoren hebben en dat, *in vitro,* meer osteoclasten worden gevormd wanneer bloed leukocyten van $A20^{myel\text{-}KO}$ muizen worden gestimuleerd met RANK ligand en macrophage colony-stimulating factor (M-CSF) in vergelijking met culturen van controle muizen. Dit suggereert dat A20 betrokken zou kunnen zijn in de regulatie van osteoclastogenese en RANK signalisatie, doch de verhoogde osteoclastogenese in deze muizen zou ook het gevolg kunnen zijn van het inflammatoire fenotype van deze muizen, vermits is geweten dat inflammatoire cytokines zoals TNF, IL-1β en IL-6 osteoclastogenese kunnen stimuleren. Om dit verder te onderzoeken hebben we dan ook muizen gegenereerd die specifiek A20 ontberen in mature osteoclasten ($A20^{OC\text{-}KO}$), door het kruisen van A20 gefloxte muizen met muizen die Cre expresseren onder controle van de Cathepsine K (CtsK) promotor. We konden aantonen dat deze muizen spontaan osteoporose ontwikkelen met aanwezigheid van een groter aantal TRAP-positieve osteoclasten in hun botweefsel. Ook konden we aantonen dat *in vitro* stimulatie van BMDMs met RANK ligand aanleiding geeft tot meer en langere activatie van RANK signalisatie. Deze bevindingen wijzen dus inderdaad op een belangrijke functie van A20 in de regulatie van RANK signalisatie en osteoclastogenese. Hoe A20 precies RANK signalisatie reguleert is nog onduidelijk, en vergt bijkomend onderzoek.

Table of contents

List of abbreviations

A

ABIN	A20-binding inhibitor of NF-κB
ALR	AIM2-like receptor
AIM2	Absent in melanoma 2 (AIM2)
AP-1	Activator protein-1
aPKC	Atypical protein kinase C
ASC	Apoptosis-associated speck-like protein containing a CARD domain
Ash1l	Absent small or homeotic-like
ATP	Adenosine triphosphate

B

BAFFR	B cell activating factor receptor
BM	Bone marrow
BMDM	Bone marrow-derived macrophage
BRC	Bone remodeling compartment

C

CalcR	Calcitonin receptor
cIAP	Cellular inhibitor of apoptosis protein
COPD	Chronic obstructive pulmonary disease
CtsK	Cathepsin K
CYLD	Cylindromatosis

D

DAMPs	Damage-associated molecular patterns
DC-stamp	Dendrocyte expressed seven transmembrane protein
DISC	Death-inducing signaling complex
DRE	Downstream regulatory element
DREAM	Downstream regulatory element antagonist modulator
DSS	Dextran sodium sulfate
DUB	Deubiquitinating enzyme

E

EAE	Experimental autoimmune encephalomyelitis
EMT	Epithelial–mesenchymal transition
ERK	Extracellular signal–regulated kinase
ERRα	Estrogen-related receptor α

F

FADD	Fas-associated death domain

G

GWAS	Genome wide association studies

H

H&E	Hematoxylin and eosin
HOLI-1	Haem-oxidized IRP2 Ub ligase-1
HOIP	HOIL-1 interacting protein

I

IBD	Inflammatory bowel disease
IEC	Intestinal epithelial cell
IFN	Interferon
IKK	Inhibitor of κB kinase
IL	Interleukin
IL-1R	Interleukin-1 receptor
IRAK	Interleukin-1 receptor-associated kinase
IκB	Inhibitor of κB

J

JNK	c-Jun N-terminal kinase

K

KD	Kinase dead
KO	Knockout

L

LOF	Loss-of function
LPS	Lipopolysaccharide
LRR	Leucin-rich region
LTβ	Lymphotoxin-β
LTβR	Lymphotoxin-β receptor
LUBAC	Linear Ub chain assembly complex
LysM	Lysozyme M

M

M1	Linear ubiquitin
MALT1	Mucosa-associated lymphoid tissue lymphoma translocation protein 1
MAPK	Mitogen activated protein kinase
M-CSF	Macrophage colony-stimulating factor
miR	MicroRNA
MITF	Microphthalmia transcription factor
MK2	MAPK-activated protein kinase-2
MLKL	Mixed lineage kinase domain-likepseudokinase
MMP	Matrix metalloproteinase
MSC	Mesenchymal stem cell
MyD88	Myeloid differentiation primary response 88

N

NEMO	NF-κB essential modifier
NFATc1	Nuclear factor-activated T cells c1
NF-κB	Nuclear factor-κB
NIK	NF-κB-inducing kinase
NLS	Nuclear localization signal
NLR	Nucleotide oligomerization domain-like receptor
NO	Nitric oxide
NOD	Nucleotide oligomerization domain

O

OC-stamp	Osteoclast stimulatory transmembrane protein
OPC	Osteoclast precursor cells
OPG	Osteoprotegerin
OTU	Ovarian tumor
OTULIN	Ovarian tumor family linear chain deubiquitinase

P

PAMPs	Pathogen-associated molecular patterns
PI(3)K	Phosphatidylinositol 3-OH kinase
PRR	Pattern recognition receptor

R

RA	Rheumatoid arthritis
RANK	Receptor activator of NF-κB
RANKL	Receptor activator of NF-κB ligand
RHD	Rel homology domain
RIG	Retinoic acid-inducible gene
RIPK	Receptor-interacting protein
RLR	Retinoic acid-inducible gene-I-like receptor
RNF11	RING finger protein 11

S

$SCF^{\beta TRCP}$	Skp, Cullin, F-box containing complex, beta-transducin repeat containing protein
SHARPIN	Shank-associated RH domain-interacting protein
SLE	Systemic lupus erythematosus
SNP	Single-nucleotide polymorphism

T

TAB2	TGFβ-activated kinase 1 binding protein 2

TAD	Transcription transactivation domain
TAK1	TGFβ-activated kinase 1
TANK	TRAF family member-associated NF-κB activator
TAX1BP1	Tax1-binding protein 1
TBK1	TANK-binding kinase 1
TCR	T-cell receptor
TGF-β	Transforming growth factor beta
TIR	Toll/IL-1 receptor
TIRAP	Toll/interleukin-1 (IL-1) receptor adaptor protein
TLR	Toll-like receptor
TNF	Tumor necrosis factor
TNFAIP3	Tumor necrosis factor -α-induced protein 3
TNFR	Tumor necrosis factor receptor
TRADD	Tumor necrosis factor receptor –associated death domain protein
TRAF	Tumor necrosis factor receptor–associated factor
TRAM	TRIF-related adaptor molecule
TRAP	Tartrate-resistant acid phosphatase
TRIF	TIR-domain-containing adaptor protein inducing interferon-β

U

Ub	Ubiquitin
UBC13/H5c	Ubiquitin carrier protein 13/H5c
UBD	Ubiquitin-binding domain
USF-1	Upstream stimulatory factor 1

Z

ZnF	Zinc finger

Part I
Introduction

I. NF-κB signaling in inflammation and cell death

NF-κB signaling in inflammation and cell death

NF-κB signaling downstream of immune receptors

Inflammation is a protective response that is induced by the detection of pathogens or damaged cells through specific receptors, called pattern recognition receptors (PRRs). The PRRs comprise toll-like receptors (TLRs), Retinoic acid-inducible gene (RIG)-I-like receptors (RLRs), nucleotide oligomerization domain (NOD)-like receptors (NLRs) and C-type lectin receptors (CLRs). PRRs sense the presence of pathogen-associated molecular patterns (PAMPs), or damage-associated molecular patterns (DAMPs) released from damaged cells, initiating an inflammatory response through a multitude of intracellular signaling pathways[1,2]. Nuclear factor kappa B (NF-κB) signaling is a central pathway downstream of PRRs and plays a critical role in inflammatory signaling and immunity. Furthermore, NF-κB is also involved in cell survival, development, cell proliferation, differentiation and metabolism[3].

The NF-κB family of transcription factors consists of five members: RelA (p65), c-Rel, RelB and the precursor proteins p105 (NF-κB1) and p100 (NF-κB2) which are processed into p50 and p52, respectively. These proteins all share a N-terminal Rel homology domain (RHD), important for DNA binding and dimerization, and a nuclear localization signal (NLS). All NF-κB proteins, except p50 and p52, also contain a transcription transactivation domain (TAD) which enables them to initiate transcription. Upon activation, NF-κB family members form homo- or heterodimers to assemble functional transcription factors that bind to κB sites in the promotor of their target genes[3]. In resting conditions, however, NF-κB dimers are sequestered in the cytoplasm by binding to the inhibitor of κB (IκB) family of proteins which masks their NLS sequence preventing nuclear translocation and gene transcription[4].

Ubiquitination in NF-κB signaling

NF-κB signaling is tightly regulated by posttranslational modifications including ubiquitination, a process in which ubiquitin (Ub), a 76-amino-acid protein, is covalently attached to a target protein by the sequential action of 3 classes of enzymes: Ub-activating enzymes (E1), Ub-conjugating enzymes (E2) and Ub protein ligases (E3)[5]. Ubiquitin itself contains 7 lysine residues (K6, K11, K27, K29, K33, K48, and K63) which can be bound by another ubiquitin molecule, generating polyubiquitin chains of different linkage types. Also the amino-terminal methionine of ubiquitin can be bound by another ubiquitin molecule, forming linear ubiquitin chains (M1)[5]. The linear ubiquitin chain assembly complex (LUBAC), an E3 ubiquitin-ligase complex consisting of HOIP, HOIL-1 and SHARPIN, is the only

E3 ligase complex described that can form linear ubiquitin chains[6]. The role of LUBAC and linear ubiquitin in TNFR-signaling is described in more detail in chapter II of the introduction[7]. Different types of polyubiquitin chains mediate different effects, with K48, K63 and M1 chains being the most important in inflammatory signaling. K48 ubiquitination targets proteins for proteasomal degradation, while K63 and M1 chains mediate downstream signaling by facilitating low affinity binding of proteins containing a ubiquitin binding domain (UBD). More recently, also branched ubiquitin linkages have been described, consisting of mixed K63/M1 or K48/K63 chains, which facilitate downstream NF-κB signaling[9,10].

Two main signaling pathways are involved in the activation of NF-κB: the canonical (or classical) pathway and the non-canonical (or alternative) pathway. The canonical pathway is induced by several stimuli, including cytokine receptors, PRRs and B- and T- cell receptors[11]. A central process is the recruitment of 2 protein complexes, the TGFβ-activated kinase 1 (TAK1)-TAB2/3 complex which is recruited via the K63-binding affinity of TAB2/3 and the IκB kinase (IKK) complex, consisting of 2 kinase subunits, IKK1 and IKK2 (also known as IKKα and IKKβ), and a regulatory subunit, called NF-κB essential modulator (NEMO) which selectively binds M1 chains via its UBAN domain[12]. The activated IKK complex will phosphorylate IκB, thereby targeting it for ubiquitination by the Skp, Cullin, F-box containing, beta-transducin repeat containing protein ($SCF^{\beta TRCP}$) complex and subsequent proteasomal degradation. This releases the NF-κB dimers from their inhibitor, allowing their translocation to the nucleus to induce gene transcription[12]. Alternatively, NF-κB can be activated via non-canonical signaling, which is induced by a number of tumor necrosis factor receptor (TNFR) superfamily members including the lymphotoxin-β receptor (LTβR), the B cell activating factor receptor (BAFFR), CD40, the receptor activator for NF-κB (RANK) and TNFR2[13]. In steady-state conditions, NF-κB-inducing kinase (NIK) is in complex with TNFR-associated factor (TRAF) 3, TRAF2 and cellular inhibitor of apoptosis (cIAP) 1 and 2 proteins, where cIAP1/2 target NIK for proteasomal degradation via K48 ubiquitination, keeping levels of NIK very low. Upon receptor ligation, NIK is released from TRAF3, allowing it to phosphorylate and activate IKK1, which in turn mediates phosphorylation of p100, an IκB-like protein that predominantly binds the NF-κB family member RelB. Phosphorylation of p100 induces K48-mediated degradation of the C-terminal part of p100, generating p52, which together with RelB translocates to the nucleus to induce gene expression[13].

Finally, ubiquitination is a reversible process, and several deubiquitinating enzymes (DUBs), including A20, CYLD and OTULIN, have been described to negatively regulate NF-κB activation by cleaving conjugated ubiquitin chains from signaling proteins[14-17]. Although the importance of the DUB function of A20 for the regulation of inflammation has always been a matter of debate[18-21] (A20 is discussed in detail in chapter II), CYLD was shown to act as a DUB by removing both K63 and M1

chains, while OTULIN acts as a DUB specific for linear (M1) ubiquitin chains[22]. In conclusion, NF-κB signaling is regulated by the tight interplay between ubiquitin ligases, ubiquitin-binding proteins and deubiquitinases. Dysregulation of this interplay will lead to aberrant signaling and may induce the development of autoimmune and autoinflammatory disease[23]. As an example, patients which carry loss-of-function mutations in *HOIL1*, a component of the LUBAC complex responsible for linear ubiquitination, will suffer from both auto-inflammation and immunodeficiency[24]. Furthermore, loss-of-function mutations in the *A20* gene cause severe auto-inflammation[25], and single-nucleotide polymorphisms (SNPs) in or near *A20* have been linked to a variety of autoimmune and inflammatory diseases [7].

Inflammasomes

Next to the induction of inflammatory gene expression, a subset of cytosolic NLRs and ALRs (absent in melanoma 2 (AIM2)-like receptors) trigger the assembly of cytosolic multiprotein complexes called inflammasomes, important for the innate immune response[26]. In general, assembly of inflammasomes results in the proteolytical activation of Caspase-1, which in its turn processes pro-IL-1β and pro-IL-18 into mature cytokines. In addition, inflammasome assembly can induce pyroptosis, a lytic form of cell death, via which IL-1β , IL-18 and DAMPs such as IL-1α and HMGB1 are released[27]. Cleavage of Gasdermin D (GSDMD) by caspase-1 or -11 (or -1, -4 and -5 in human) releases an amino-terminal pore-forming GSDMD domain that oligomerizes and inserts in the plasma membrane, inducing membrane rupture and leakage of the cytosolic contents[28] (Figure 1).

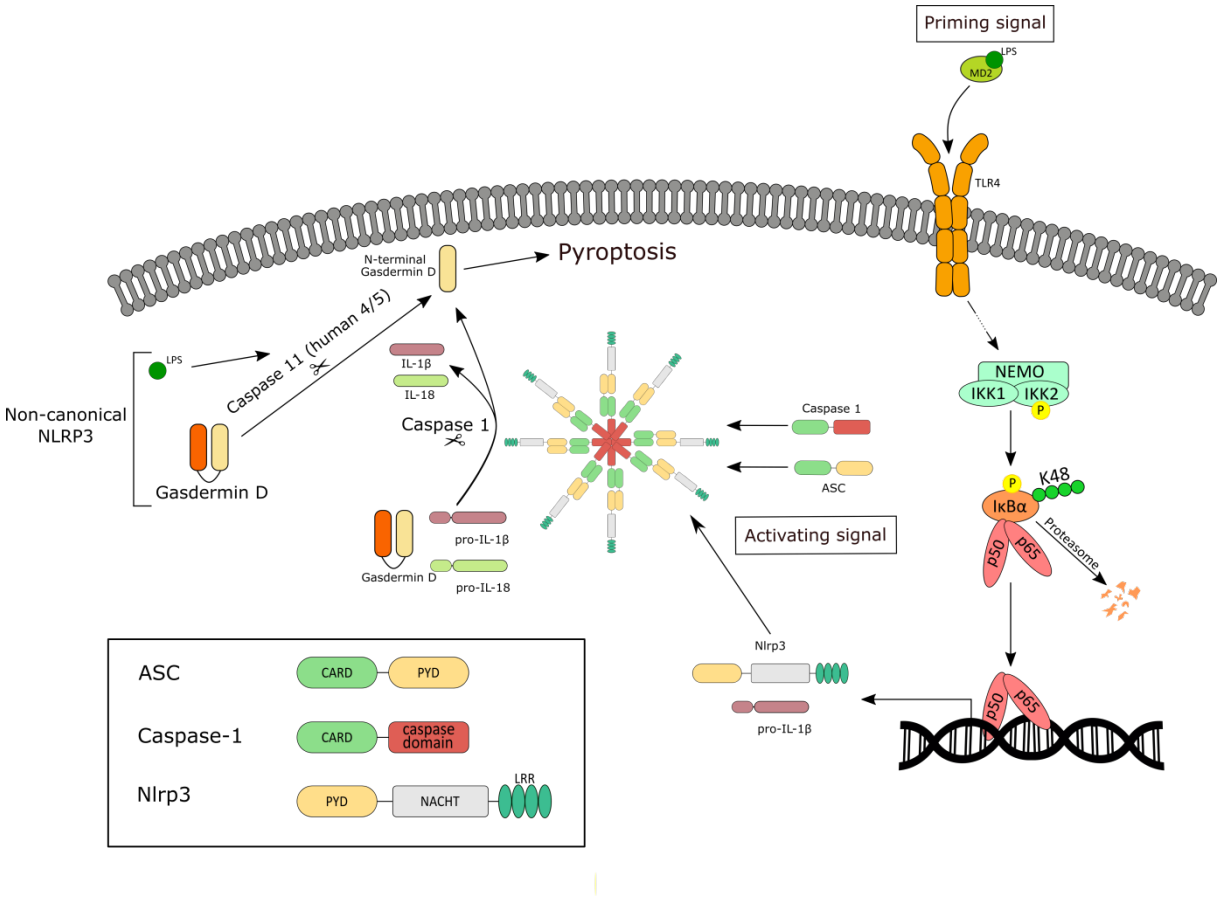

Fig. 1 NLRP3 inflammasome signaling. NLRP3 inflammasome activation requires a two-step mechanism. A priming signal (e.g. LPS-TLR4 signaling) induces the expression of NLRP3 and pro-IL-1β. The activating signal induces the formation of the inflammasome complex and the processing and activation of caspase-1, which processes pro-IL-1β and pro-IL-18 into mature cytokines. In addition, activated caspase-1 cleaves Gasdermin D and the N-terminal part translocates to the plasma membrane where it forms pores and induces pyroptotic cell death, allowing the release of IL-1β and IL-18. Alternatively, in the non-canonical NLRP3 inflammasome pathway, caspase-11 (or its human orthologs caspase-4 and -5) are activated by cytosolic LPS, inducing Gasdermin D cleavage and pyroptosis.

Several cytosolic receptor proteins have been shown to assemble into inflammasome complexes, including NLRP1, NLRP3 and NLRC4, which belong to the NLR family of receptors, as well as the proteins AIM2 and pyrin[26,27]. The best characterized inflammasome is the NLRP3 inflammasome, which is activated by a wide variety of bacterial, fungal and viral PAMPs, and DAMPS such as adenosine triphosphate (ATP), crystals and protein aggregates[26]. Activation of the NLRP3 inflammasome additionally requires an NF-κB mediated extracellular priming signal to transcriptionally upregulate the expression of NLRP3 and pro-IL-1β, e.g. via TLR signaling (Fig. 1). Upon sensing danger molecules, the NLRP3 proteins will oligomerize and recruit the adaptor protein apoptosis-associated speck like protein containing a caspase recruitment domain (ASC) via its pyrin domain (PYD), and pro-caspase 1 through its caspase 1 recruitment domain (CARD), thereby forming

the multiprotein inflammasome complex responsible for the activation of caspase-1 by proximity-induced autoprocessing[29]. Alternatively, cytosolic lipopolysaccharide (LPS) can induce the activation of caspase-11 (or caspase-4/5 in humans) which then initiates pyroptosis by cleaving GSDMD.Caspase-11 is however not capable of processing pro-IL-1β and pro-IL-18[27] (Fig. 1).

LPS-TLR4 and IL-1/IL-1R signaling

The TLR family of receptors are the best studied family of PRRs. These receptors are characterized by the presence of an extracellular leucin-rich region (LRR) and a cytoplasmatic Toll/IL-1 receptor (TIR) domain responsible for signal transduction[30]. Toll-Like Receptor 4 (TLR4) recognizes and binds LPS, a component of the bacterial membrane, activating downstream signaling. The interleukin-1 receptor (IL-1R) also contains a cytoplasmatic TIR domain and shares TIR-domain containing adaptor proteins with the TLR family for downstream signaling[31]. Binding of LPS or IL-1α/β to their cognate receptor, respectively TLR4 and IL-1R, induces receptor dimerization leading to the recruitment of myeloid differentiation primary response 88 (MyD88) via the adaptor molecule Toll/interleukin-1 (IL-1) receptor adaptor protein (TIRAP), also known as Mal. This will now recruit interleukin-1 receptor-associated kinase (IRAK) 4 which, upon activation by autophosphorylation, binds and phosphorylates IRAK1, which on its turn will recruit tumor necrosis factor receptor–associated factor 6 (TRAF6) into the complex. Autoubiquitination of TRAF6 with K63 chains forms a platform for the recruitment of the TAK1-TAB2/3 complex. Activated TAK1 subsequently phosphorylates and activates the IKK complex, inducing IKK2-mediated phosphorylation of IκBα, promoting its degradation, leading to the release and activation of NF-κB transcription factors. Furthermore, TAK1 can activate mitogen-activated protein kinase (MAPK) signaling pathways also inducing the expression of pro-inflammatory cytokines. In the MyD88-dependent pathway, MyD88 also recruits TRAF3, and proteasomal degradation of TRAF3, via cIAP1/2 mediated K48-ubiquitination, was shown to be crucial for activation of downstream MAPKs[32]. It is suggested that TRAF6 attaches K63 chains to cIAP1/2, thereby inducing cIAP1/2 K48 ligase activity[33]. Upon receptor endocytosis, TLR4 can also signal in a MyD88-independent way by recruiting TIR-domain-containing adaptor protein inducing interferon-β (TRIF; also known as TICAM1) via adaptor molecule TRIF-related adaptor molecule (TRAM; also known as TICAM2). TRIF will now recruit TRAF6 and Receptor-interacting protein kinase 1 (RIPK1) to the receptor complex, followed by K63-ubiquitination of TRAF6 and RIPK1 by pellino-1[34], facilitating TAK1 recruitment and the activation of NF-κB and MAPK signaling pathways. Alternatively, TRIF can recruit TRAF3, activating the non-canonical IKKs TRAM-binding kinase-1 (TBK1) and IKKε, resulting in the phosphorylation and activation of the transcription factor Interferon regulatory factor-3 (IRF3) to induce the expression of type I interferons (Fig. 2)[30,31,34-37]. In contrast to its role in MyD88-dependent

signaling, auto-ubiquitinated TRAF3 was shown to be required for the activation of IRF3[32]. The role of LUBAC and linear ubiquitin in TLR4/IL-1R signaling is still not clear. Sharpin deficiency results in impaired NF-κB activation and cytokine production, and K63-M1-hybrid chains can be detected upon activation of IL-1R or TLR1/2. How LUBAC is recruited as well as the identity of LUBAC targets are, however, still elusive[10,38,39].

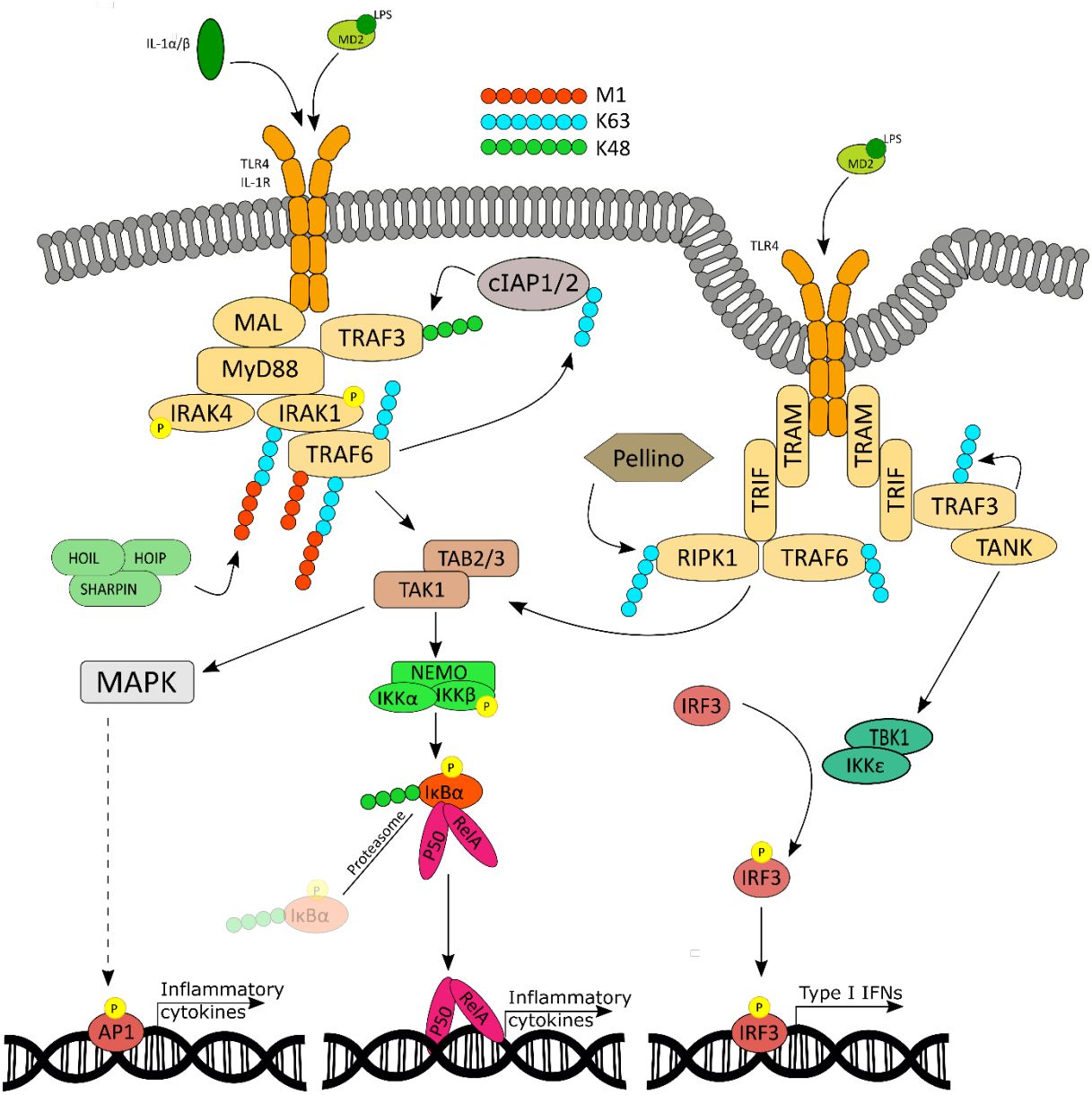

Fig. 2 TLR4/IL-1R signaling. Binding of IL-1 or LPS to its receptor IL-1R or TLR4 induces receptor dimerization and recruitment of several adaptors. MyD88-dependent and TRIF-dependent signaling induces TAK1 activation and subsequent activation of NF-κB and MAPK signaling, inducing the expression of proinflammatory cytokines. TLR4 induced TRIF-dependent signaling can also induce the expression of type I IFNs via IRF3 activation.

TNF-TNFR1 signaling

Detailed information on the TNF-TNFR1 pathway : see chapter II, review Martens and van Loo, “A20 at the crossroads of cell death, inflammation and autoimmunity”.

Cell death and its role in inflammation

Cell death has long been considered a consequence of sustained inflammation in many diseases, however recent studies identified cell death as a driver of inflammation. Apoptosis, which relies on the activation of the initiator caspases-8/10 or 9 and the downstream effector caspases-3 and -7, is considered a non-inflammatory form of cell death whereby the integrity of the plasma membrane is preserved and dying cells are removed by phagocytosis. Although, aberrant apoptosis in e.g. the intestinal epithelium results in intestinal barrier disruption, inducing systemic inflammation and lethality in mice[40]. In contrast, lytic forms of cell death, such as necroptosis and pyroptosis, are known to induce inflammation by the release of DAMPS[41,42]. Necroptosis is a lytic form of regulated cell death and depends on the activation of receptor interacting protein kinase-3 (RIPK3) and its substrate mixed lineage kinase like (MLKL). Upon phosphorylation by RIPK3, MLKL oligomerizes into a pore-forming complex that inserts in the plasma membrane and induces plasma membrane disruption, allowing the release of DAMPS (e.g. IL-1α) which can induce an inflammatory response. In normal conditions, caspase-8 prevents necroptosis and subsequent inflammation. Indeed, caspase-8 deficiency in mice results in embryonic lethality due to aberrant necroptosis, as was shown by the rescue of the phenotype of caspase-8 knockout mice in a RIPK3 or MLKL deficient background[43-45]. Pyroptosis is induced by GDSMD cleavage by caspase-1 or caspase-11 (human caspase-4/5), and the N-terminal part of GSDMD will oligomerize and form pores in the cell membrane allowing the release of IL-1β, IL-18 and DAMPS[28]. In conclusion, more and more evidence has shown that cell death is not only a consequence of inflammation, but can also be the driving force of inflammation in many inflammatory diseases.

References

1 Takeuchi, O. & Akira, S. Pattern recognition receptors and inflammation. *Cell* **140**, 805-820, doi:10.1016/j.cell.2010.01.022 (2010).

2 Newton, K. & Dixit, V. M. Signaling in innate immunity and inflammation. *Cold Spring Harb Perspect Biol* **4**, doi:10.1101/cshperspect.a006049 (2012).

3 Hayden, M. S. & Ghosh, S. NF-kappaB, the first quarter-century: remarkable progress and outstanding questions. *Genes Dev* **26**, 203-234, doi:10.1101/gad.183434.111 (2012).

4 Oeckinghaus, A., Hayden, M. S. & Ghosh, S. Crosstalk in NF-kappaB signaling pathways. *Nat Immunol* **12**, 695-708, doi:10.1038/ni.2065 (2011).

5 Chen, J. & Chen, Z. J. Regulation of NF-kappaB by ubiquitination. *Curr Opin Immunol* **25**, 4-12, doi:10.1016/j.coi.2012.12.005 (2013).

6 Spit, M., Rieser, E. & Walczak, H. Linear ubiquitination at a glance. *J Cell Sci* **132**, doi:10.1242/jcs.208512 (2019).

7 Martens, A. & van Loo, G. A20 at the Crossroads of Cell Death, Inflammation, and Autoimmunity. *Cold Spring Harb Perspect Biol*, doi:10.1101/cshperspect.a036418 (2019).

8 Wu, Y. *et al.* Ubiquitination regulation of inflammatory responses through NF-kappaB pathway. *Am J Transl Res* **10**, 881-891 (2018).

9 Ohtake, F., Saeki, Y., Ishido, S., Kanno, J. & Tanaka, K. The K48-K63 Branched Ubiquitin Chain Regulates NF-kappaB Signaling. *Mol Cell* **64**, 251-266, doi:10.1016/j.molcel.2016.09.014 (2016).

10 Emmerich, C. H. *et al.* Activation of the canonical IKK complex by K63/M1-linked hybrid ubiquitin chains. *Proc Natl Acad Sci U S A* **110**, 15247-15252, doi:10.1073/pnas.1314715110 (2013).

11 Liu, T., Zhang, L., Joo, D. & Sun, S. C. NF-kappaB signaling in inflammation. *Signal Transduct Target Ther* **2**, doi:10.1038/sigtrans.2017.23 (2017).

12 Zhang, Q., Lenardo, M. J. & Baltimore, D. 30 Years of NF-kappaB: A Blossoming of Relevance to Human Pathobiology. *Cell* **168**, 37-57, doi:10.1016/j.cell.2016.12.012 (2017).

13 Sun, S. C. The non-canonical NF-kappaB pathway in immunity and inflammation. *Nat Rev Immunol* **17**, 545-558, doi:10.1038/nri.2017.52 (2017).

14 Sun, S. C. Deubiquitylation and regulation of the immune response. *Nat Rev Immunol* **8**, 501-511, doi:10.1038/nri2337 (2008).

15 Fiil, B. K. *et al.* OTULIN restricts Met1-linked ubiquitination to control innate immune signaling. *Mol Cell* **50**, 818-830, doi:10.1016/j.molcel.2013.06.004 (2013).

16 Keusekotten, K. *et al.* OTULIN antagonizes LUBAC signaling by specifically hydrolyzing Met1-linked polyubiquitin. *Cell* **153**, 1312-1326, doi:10.1016/j.cell.2013.05.014 (2013).

17 Rivkin, E. *et al.* The linear ubiquitin-specific deubiquitinase gumby regulates angiogenesis. *Nature* **498**, 318-324, doi:10.1038/nature12296 (2013).

18 Wertz, I. E. *et al.* De-ubiquitination and ubiquitin ligase domains of A20 downregulate NF-kappaB signalling. *Nature* **430**, 694-699, doi:10.1038/nature02794 (2004).

19 Lu, T. T. *et al.* Dimerization and ubiquitin mediated recruitment of A20, a complex deubiquitinating enzyme. *Immunity* **38**, 896-905, doi:10.1016/j.immuni.2013.03.008 (2013).

20 De, A., Dainichi, T., Rathinam, C. V. & Ghosh, S. The deubiquitinase activity of A20 is dispensable for NF-kappaB signaling. *EMBO Rep* **15**, 775-783, doi:10.15252/embr.201338305 (2014).

21 Wertz, I. E. *et al.* Phosphorylation and linear ubiquitin direct A20 inhibition of inflammation. *Nature* **528**, 370-375, doi:10.1038/nature16165 (2015).

22 Lork, M., Verhelst, K. & Beyaert, R. CYLD, A20 and OTULIN deubiquitinases in NF-kappaB signaling and cell death: so similar, yet so different. *Cell Death Differ* **24**, 1172-1183, doi:10.1038/cdd.2017.46 (2017).

23 Hu, H. & Sun, S. C. Ubiquitin signaling in immune responses. *Cell Res* **26**, 457-483, doi:10.1038/cr.2016.40 (2016).

24 Boisson, B. *et al.* Immunodeficiency, autoinflammation and amylopectinosis in humans with inherited HOIL-1 and LUBAC deficiency. *Nat Immunol* **13**, 1178-1186, doi:10.1038/ni.2457 (2012).
25 Zhou, Q. *et al.* Loss-of-function mutations in TNFAIP3 leading to A20 haploinsufficiency cause an early-onset autoinflammatory disease. *Nat Genet* **48**, 67-73, doi:10.1038/ng.3459 (2016).
26 Lamkanfi, M. & Dixit, V. M. Mechanisms and functions of inflammasomes. *Cell* **157**, 1013-1022, doi:10.1016/j.cell.2014.04.007 (2014).
27 Broz, P. & Dixit, V. M. Inflammasomes: mechanism of assembly, regulation and signalling. *Nat Rev Immunol* **16**, 407-420, doi:10.1038/nri.2016.58 (2016).
28 Shi, J., Gao, W. & Shao, F. Pyroptosis: Gasdermin-Mediated Programmed Necrotic Cell Death. *Trends Biochem Sci* **42**, 245-254, doi:10.1016/j.tibs.2016.10.004 (2017).
29 Jo, E. K., Kim, J. K., Shin, D. M. & Sasakawa, C. Molecular mechanisms regulating NLRP3 inflammasome activation. *Cell Mol Immunol* **13**, 148-159, doi:10.1038/cmi.2015.95 (2016).
30 Kuzmich, N. N. *et al.* TLR4 Signaling Pathway Modulators as Potential Therapeutics in Inflammation and Sepsis. *Vaccines (Basel)* **5**, doi:10.3390/vaccines5040034 (2017).
31 Loiarro, M., Ruggiero, V. & Sette, C. Targeting TLR/IL-1R signalling in human diseases. *Mediators Inflamm* **2010**, 674363, doi:10.1155/2010/674363 (2010).
32 Tseng, P. H. *et al.* Different modes of ubiquitination of the adaptor TRAF3 selectively activate the expression of type I interferons and proinflammatory cytokines. *Nat Immunol* **11**, 70-75, doi:10.1038/ni.1819 (2010).
33 Hacker, H., Tseng, P. H. & Karin, M. Expanding TRAF function: TRAF3 as a tri-faced immune regulator. *Nat Rev Immunol* **11**, 457-468, doi:10.1038/nri2998 (2011).
34 Chang, M., Jin, W. & Sun, S. C. Peli1 facilitates TRIF-dependent Toll-like receptor signaling and proinflammatory cytokine production. *Nat Immunol* **10**, 1089-1095, doi:10.1038/ni.1777 (2009).
35 Wertz, I. E. & Dixit, V. M. Signaling to NF-kappaB: regulation by ubiquitination. *Cold Spring Harb Perspect Biol* **2**, a003350, doi:10.1101/cshperspect.a003350 (2010).
36 Lu, Y. C., Yeh, W. C. & Ohashi, P. S. LPS/TLR4 signal transduction pathway. *Cytokine* **42**, 145-151, doi:10.1016/j.cyto.2008.01.006 (2008).
37 Cohen, P. The TLR and IL-1 signalling network at a glance. *J Cell Sci* **127**, 2383-2390, doi:10.1242/jcs.149831 (2014).
38 Zinngrebe, J. & Walczak, H. TLRs Go Linear - On the Ubiquitin Edge. *Trends Mol Med* **23**, 296-309, doi:10.1016/j.molmed.2017.02.003 (2017).
39 Cohen, P. & Strickson, S. The role of hybrid ubiquitin chains in the MyD88 and other innate immune signalling pathways. *Cell Death Differ* **24**, 1153-1159, doi:10.1038/cdd.2017.17 (2017).
40 Vereecke, L. *et al.* Enterocyte-specific A20 deficiency sensitizes to tumor necrosis factor-induced toxicity and experimental colitis. *J Exp Med* **207**, 1513-1523, doi:10.1084/jem.20092474 (2010).
41 Gunther, C. *et al.* Caspase-8 regulates TNF-alpha-induced epithelial necroptosis and terminal ileitis. *Nature* **477**, 335-339, doi:10.1038/nature10400 (2011).
42 Welz, P. S. *et al.* FADD prevents RIP3-mediated epithelial cell necrosis and chronic intestinal inflammation. *Nature* **477**, 330-334, doi:10.1038/nature10273 (2011).
43 Kaiser, W. J. *et al.* RIP3 mediates the embryonic lethality of caspase-8-deficient mice. *Nature* **471**, 368-372, doi:10.1038/nature09857 (2011).
44 Oberst, A. *et al.* Catalytic activity of the caspase-8-FLIP(L) complex inhibits RIPK3-dependent necrosis. *Nature* **471**, 363-367, doi:10.1038/nature09852 (2011).
45 Alvarez-Diaz, S. *et al.* The Pseudokinase MLKL and the Kinase RIPK3 Have Distinct Roles in Autoimmune Disease Caused by Loss of Death-Receptor-Induced Apoptosis. *Immunity* **45**, 513-526, doi:10.1016/j.immuni.2016.07.016 (2016).

II. A20 at the Crossroads of Cell Death, inflammation and Autoimmunity

A20 at the Crossroads of Cell Death, Inflammation, and Autoimmunity

Arne Martens[1,2] and Geert van Loo[1,2]

[1]VIB Center for Inflammation Research, 9052 Ghent, Belgium

[2]Department of Biomedical Molecular Biology, Ghent University, 9052 Ghent, Belgium

Correspondence: geert.vanloo@irc.vib-ugent.be

Cold Spring Harbor Perspectives in Biology
www.cshperspectives.org

A20 is a potent anti-inflammatory protein, acting by inhibiting nuclear factor κB (NF-κB) signaling and inflammatory gene expression and/or by preventing cell death. Mutations in the *A20/TNFAIP3* gene have been associated with a plethora of inflammatory and autoimmune pathologies in humans and in mice. Although the anti-inflammatory role of A20 is well accepted, fundamental mechanistic questions regarding its mode of action remain unclear. Here, we review new findings that further clarify the molecular and cellular mechanisms by which A20 controls inflammatory signaling and cell death, and discuss new evidence for its involvement in inflammatory and autoimmune disease development.

Inflammation is a protective response to induce repair in conditions of cellular damage and stress. It involves activation of the nuclear factor κB (NF-κB) family of transcription factors leading to the expression of inflammatory cytokines and chemokines to establish an appropriate immune response. Activation of NF-κB also induces the expression of cell-survival genes to protect the cell from dying (Zhang et al. 2017). NF-κB signaling is tightly regulated at multiple levels and strongly depends on reversible modification of signaling proteins, with important roles for phosphorylation and ubiquitination. Ubiquitination is a posttranslational protein modification in which ubiquitin (Ub), a small 76-amino-acid protein, is covalently attached to lysine residues of target proteins by the stepwise activity of an E1 Ub-activating enzyme, E2 Ub-conjugating enzymes, and E3 Ub protein ligases. Each of the seven lysine residues (K6, K11, K27, K29, K33, K48, and K63) in Ub can themselves be bound to another Ub, leading to the formation of polyubiquitin chains on the target protein. Linear Ub chains (M1), in which Ub is bound via the amino-terminal methionine (M1) residue to another Ub, also happens, and has been shown to be crucially important for NF-κB signaling (Iwai and Tokunaga 2009). Depending on the type of chain, ubiquitination can target the modified protein for proteasomal degradation, or function as a scaffold for proteins that contain a Ub-binding domain (UBD) and mediate downstream signaling. Ubiquitination is reversed by deubiquitinating enzymes (DUBs) that cleave Ub chains from their substrate (Hrdinka and Gyrd-Hansen 2017). Hence, the ubiquitination of proteins, defined by the tight interplay between Ub

Editors: Kim Newton, James M. Murphy, and Edward A. Miao
Additional Perspectives on Cell Survival and Cell Death available at www.cshperspectives.org

Advanced Online Article. Cite this article as *Cold Spring Harb Perspect Biol* doi: 10.1101/cshperspect.a036418

Cold Spring Harbor Perspectives in Biology
www.cshperspectives.org

ligases, Ub-binding proteins, and DUBs, controls NF-κB signaling.

The importance of ubiquitination for the regulation of inflammatory signaling has been studied extensively for the prototype inflammatory pathway induced by the cytokine tumor necrosis factor (TNF) (Verhelst et al. 2011). Binding of TNF to its cognate receptor TNF receptor 1 (TNFR1) mediates NF-κB-dependent gene activation through assembly of a primary membrane-bound signaling complex known as complex I (Ting and Bertrand 2016). This complex is assembled through the recruitment of TNF receptor–associated death domain protein (TRADD), receptor-interacting protein 1 (RIPK1), TNF receptor–associated factor 2 (TRAF2) and/or TRAF5, and cellular inhibitor of apoptosis protein-1 (cIAP1) and cIAP2. cIAP1 and cIAP2 are E3 Ub ligases that on recruitment conjugate RIPK1 and cIAPs themselves with K63-linked polyubiquitin chains, which now serve as a platform for the recruitment of the linear Ub chain assembly complex (LUBAC), consisting of HOIP, HOIL1, and SHARPIN. As a consequence, LUBAC will conjugate several components of the TNFR1 complex with M1-linked chains, followed by the recruitment and activation of the TAB–TAK1 complex and the NEMO–IKK complex via their UBD domains (Haas et al. 2009). This allows TAK1 to phosphorylate and activate the IKK complex, the latter phosphorylating the inhibitor of κB α (IκBα), targeting it for proteasomal degradation. Degradation of IκBα releases NF-κB, which now translocates to the nucleus where it induces the expression of proinflammatory and cell-survival genes (Fig. 1; Zhang et al. 2017). Besides activating NF-κB and inducing inflammatory gene activation and cell survival, TNF can also induce the assembly of a cytosolic death-inducing signaling complex (DISC) composed of TRADD, Fas-associated death domain (FADD), and caspase-8 (complex IIa), or composed of RIPK1, FADD, and caspase-8 (complex IIb, also called the Ripoptosome). In conditions of caspase-8 inhibition, TNF can induce necroptosis by further recruitment of RIPK3 and mixed lineage kinase domain-like pseudokinase (MLKL) assembling the necrosome (Fig. 1; Pasparakis and Vandenabeele 2015; Ting and Bertrand 2016).

Deregulation of inflammatory NF-κB and cell-death signaling has been associated with several (auto)inflammatory diseases and cancer (Kondylis et al. 2017; Lork et al. 2017). Therefore, tight regulation of these pathways is required to avoid chronic inflammation and maintain tissue homeostasis. In this context, numerous (auto)regulatory mechanisms have been described (Renner and Schmitz 2009), and A20, CYLD, and OTULIN have been identified as key players in the negative regulation of NF-κB and cell death in response to TNF (Lork et al. 2017). In this review, we will discuss the molecular mechanisms by which A20 regulates NF-κB signaling and cell death, its own regulation, and our current knowledge on its involvement in inflammatory and autoimmune pathology.

A20 STRUCTURE AND MECHANISM OF NF-κB REGULATION

A20, also known as TNF-α-induced protein 3 (TNFAIP3), was first discovered as a primary response gene that is expressed on stimulation of human endothelial cells with TNF, protecting the cells from TNF-induced cell death (Dixit et al. 1990). Although A20 was initially characterized as an inhibitor of TNF-induced apoptosis, further studies identified A20 as a negative regulator of TNF-induced NF-κB activation, but also of NF-κB signaling downstream from the interleukin 1 receptor (IL-1R), pathogen recognition receptors (PRRs), NOD-like receptors (NLRs), T- and B-cell receptors, and CD40 (Opipari et al. 1990; Catrysse et al. 2014). The basal expression of A20 is low in most cell types, but is rapidly and transiently induced in inflammatory conditions through NF-κB-dependent transcription owing to the presence of two κB elements in the *A20* promotor region (Krikos et al. 1992). A20 thus behaves as a prototype negative feedback regulator of NF-κB signaling.

A20 has been characterized as a so-called "Ub-editing" enzyme that inhibits NF-κB signaling by interfering with the ubiquitination status of multiple NF-κB signaling proteins (Wertz et al. 2004). The A20 protein consists

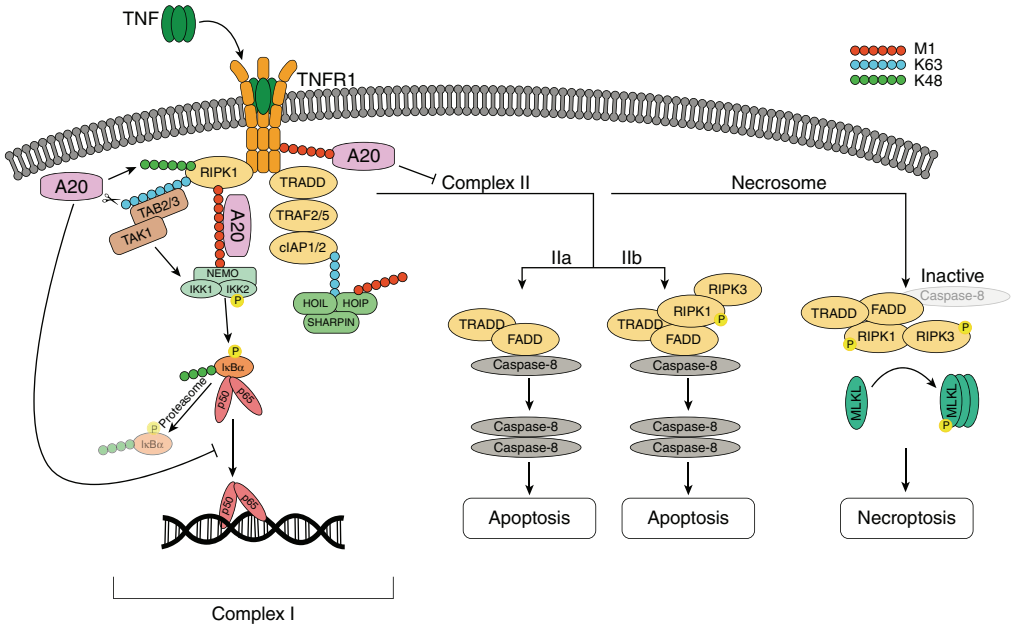

Figure 1. Tumor necrosis factor (TNF)-induced nuclear factor κB (NF-κB) signaling, apoptosis, and necroptosis. Binding of TNF to TNF receptor 1 (TNFR1) induces receptor trimerization that allows the recruitment of TNF receptor-associated death domain protein (TRADD) and receptor-interacting protein 1 (RIPK1). TRADD recruits TRAF2/5 and the E3 ubiquitin (Ub) ligases cIAP1 and cIAP2. cIAP1 and cIAP2 conjugate RIPK1 as well as themselves with K63-linked polyubiquitin chains, which serve as a platform for the recruitment of the LUBAC complex, consisting of HOIP, HOIL1, and SHARPIN. Linear Ub chain assembly complex (LUBAC) conjugates several components of the TNFR1 complex, including NEMO and RIPK1, with linear Ub chains (M1). The TAB2/3–TAK1 complex binds K63-linked chains on RIPK1, whereas the IKK complex is recruited via NEMO binding to M1-linked polyubiquitin. This allows TAK1 to phosphorylate and activate the IKK complex. On activation, IKK2 phosphorylates the inhibitor of κB α (IκBα), targeting IκBα for ubiquitination with K48-linked chains and proteasomal degradation. This releases the p50/p65 NF-κB dimer, which translocates to the nucleus where it induces the expression of NF-κB response genes. A20 is recruited to the TNFR1 signaling complex via M1-linked Ub, which binds to ZnF7. In addition, A20 has been shown to act as a deubiquitinating enzyme (DUB) that removes K63-linked polyubiquitin from different target proteins, including RIPK1 and NEMO. Furthermore, A20 has been shown to target RIPK1 and TNFR1 for proteasomal degradation through its ZnF4 E3 ligase activity. Binding of A20 to M1-linked polyubiquitin prevents downstream signaling by competing with other Ub-binding proteins and by preventing the degradation of M1-linked chains by CYLD (not shown). Loss of M1-linked chains destabilizes complex I and results in the formation of a cytosolic death-inducing signaling complex (DISC), consisting of TRADD, Fas-associated death domain (FADD), and caspase 8 (complex IIa) or RIPK1, FADD, and caspase-8 (complex IIb). Homodimerization and activation of caspase-8 leads to the activation of downstream executioner caspases 3 and 7 (not shown) and apoptotic cell death. If caspase-8 activity is compromised, RIPK1 associates with RIPK3 (the necrosome), which is activated by auto-phosphorylation. The activated necrosome recruits and activates MLKL inducing necroptotic cell death.

of an amino-terminal ovarian tumor (OTU) domain, which has DUB activity, and carboxy-terminal zinc finger (ZnF) domains, with the fourth ZnF domain shown to have Ub E3 ligase activity (Wertz et al. 2004). In addition, the ZnF4 domain was shown to act as a UBD for K63-linked polyubiquitin (Bosanac et al. 2010). More recently, the seventh ZnF (ZnF7) domain of A20 was shown to function as a UBD, but with high binding affinity for M1-linked Ub (Fig. 2; Tokunaga et al. 2012; Verhelst et al. 2012). The Ub editing function of A20 was first shown in

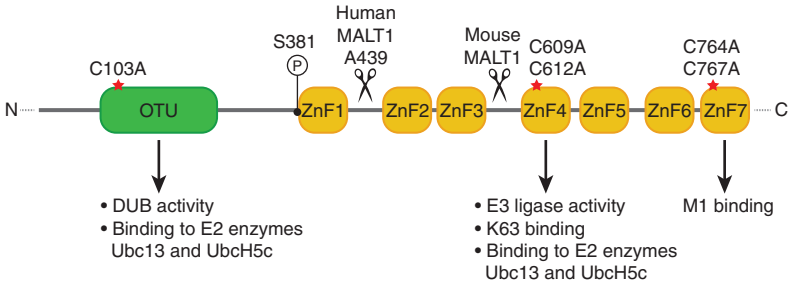

Figure 2. Domain structure of the A20 protein. The amino terminus of A20 contains an ovarian tumor (OTU) domain, which has deubiquitinating enzyme (DUB) activity relying on the catalytic residue Cys103. The carboxy-terminal part of A20 contains seven zinc finger (ZnF) domains. The fourth ZnF domain has K63-linked polyubiquitin-binding affinity and possesses E3 ubiquitin (Ub) ligase activity, whereas the seventh ZnF domain has strong binding affinity for linear (M1) Ub chains. IKK2-mediated phosphorylation of A20 at Ser381 enhances the DUB activity of A20 toward K63-linked polyubiquitin. MALT1 cleaves A20 at Ala439 in human, or between the third and fourth ZnF domains in mouse. Mutations that were introduced to generate OTU (C103A), ZnF4 (C609A, C612A), or ZnF7 (C764A, C767A) domain-specific mutant mice are depicted by red stars. Both the OTU and ZnF4 domains have been shown to bind to E2 enzymes Ubc13 and UbcH5c.

TNFR1 signaling. Using its tandem DUB-E3 ligase activities, A20 was shown to negatively regulate NF-κB signaling by replacing K63-linked chains on RIPK1 with K48-linked chains, which targeted RIPK1 for proteasomal degradation (Wertz et al. 2004). A20 was also shown to deubiquitinate TNFR1 and NEMO after TNF stimulation (Mauro et al. 2006; Wertz et al. 2015). This DUB activity of A20 was further shown to be promoted by IKK2-mediated phosphorylation of A20 at Ser381 (Fig. 2; Mauro et al. 2006; Wertz et al. 2015).

Besides its role in regulating TNF-induced NF-κB signaling, the DUB activity of A20 was shown to regulate TLR4- and NOD2-induced NF-κB activation by removing K63-linked chains from TRAF6 and RIPK2, respectively (Boone et al. 2004; Hitotsumatsu et al. 2008). Furthermore, A20 was shown to negatively regulate T-cell receptor (TCR)-induced NF-κB activation by deubiquitinating MALT1, thereby preventing the interaction between MALT1 and the IKK complex (Mauro et al. 2006; Duwel et al. 2009). Besides functioning as a DUB, A20 can also affect the ubiquitination of signaling mediators indirectly by interfering with the interaction between E2 and E3 enzymes, limiting polyubiquitin formation. In this context, A20 was shown to disrupt the interaction of TRAF6 with the E2 conjugating enzymes Ubc13 and UbcH5c in response to IL-1 and LPS stimulation. Similarly, on TNF stimulation, A20 was shown to prevent the association between Ubc13 and both cIAP1 and TRAF2 (Shembade et al. 2010).

Despite many reports claiming a crucial role of A20 as a DUB regulating NF-κB signaling, the physiological relevance of the deubiquitinase activity of A20 is still unclear. Recently, a number of transgenic mouse lines bearing a point mutation in the catalytic OTU domain (A20-C103A, $A20^{OTU}$ mice) to abrogate A20 DUB activity were generated (Lu et al. 2013; De et al. 2014; Wertz et al. 2015). These mice are grossly normal and do not develop the severe phenotype of A20-deficient mice, which die perinatally because of multiorgan inflammation and cachexia (Lee et al. 2000). However, $A20^{OTU}$ mice were shown to be sensitized to TNF and LPS treatment, and to dextran sodium sulfate (DSS)-induced colitis and experimental autoimmune encephalomyelitis (EAE) (Lu et al. 2013; Wertz et al. 2015). De and colleagues, however, did not observe sensitization of $A20^{OTU}$ mice to LPS-induced pathology, nor did they observe any difference in TNF- or LPS-induced NF-κB signaling or cell death in cells derived from these mice. They concluded that the DUB function of

Cold Spring Harbor Perspectives in Biology
www.cshperspectives.org

A20 is dispensable for inflammatory signaling in vivo (De et al. 2014). A20 transgenic mice with a mutation in the E3 ligase activity (A20-C609A/C612A, $A20^{ZnF4}$ mice) have also been generated, but these mice also develop normally without any spontaneous phenotype (Lu et al. 2013; Wertz et al. 2015). Mouse embryo fibroblasts isolated from $A20^{0TU}$ or $A20^{ZnF4}$ mice show increased K63-linked ubiquitination of RIPK1 and TNFR1, resulting in slightly increased mitogen-activated protein kinase (MAPK) and NF-κB signaling on TNF stimulation (Lu et al. 2013; Wertz et al. 2015). Together, these findings indicate that neither the DUB nor E3 ligase functions of A20 critically contribute to its anti-inflammatory function in vivo. Simultaneous inactivation of the OTU and ZnF4 domains may be required to fully abolish its function and phenocopy A20-deficient mice. However, recent in vitro and in vivo evidence indicates that ZnF7 of A20 plays a more prominent role. A20 was shown to impair IKK activation through a non-enzymatic mechanism based on its binding to polyubiquitin via ZnF7 (Skaug et al. 2011). Additional studies have shown that A20 recruitment to TNFR1 and NOD2-associated signaling complexes by binding of ZnF7 to LUBAC-generated M1-linked polyubiquitin is required to inhibit downstream NF-κB signaling (Iwai and Tokunaga 2009; Tokunaga et al. 2012; Verhelst et al. 2012; Draber et al. 2015). Recently, we generated mice bearing a mutation in A20 ZnF7 domain (A20-C764A/C767A, $A20^{ZnF7}$ mice) that abolishes its capacity to bind to M1-linked chains. These mice develop a spontaneous inflammatory arthritis and have reduced bodyweight and splenomegaly, showing an indispensable function for ZnF7 in A20-mediated suppression of inflammation in vivo (Polykratis et al. 2019). The ZnF7 mutation abolished the recruitment of A20 into the TNFR1 signaling complex, and reduced the amount of linear Ub chains within the complex (Draber et al. 2015; Polykratis et al. 2019). These observations indicate that A20 through its ZnF7 stabilizes M1 linkages in the TNFR1 signaling complex, shielding them from degradation by DUBs that are capable of cleaving linear Ub chains in signaling complexes. However, the spontaneous inflammatory phenotype of $A20^{ZnF7}$ mice is mild compared with the severe multiorgan inflammation and postnatal lethality seen in A20 knockout mice (Lee et al. 2000), suggesting that other domains also critically contribute to A20's anti-inflammatory function in vivo. Knockin mice with combined domain mutations may be required to fully inactivate A20 and phenocopy the A20 knockout.

A20 IN THE REGULATION OF CELL DEATH

In addition to its role in the regulation of NF-κB signaling, A20 also acts as a strong inhibitor of cell death in many cell types. Originally, A20 was identified as an inhibitor of TNF-induced apoptosis in endothelial cells (Dixit et al. 1990), but it can also limit apoptosis in thymocytes and fibroblasts (Lee et al. 2000), pancreatic β cells (Liuwantara et al. 2006; Catrysse et al. 2015; Fukaya et al. 2016), hepatocytes (Catrysse et al. 2016), and intestinal epithelial cells (IECs) (Vereecke et al. 2010, 2014; Kattah et al. 2018; Slowicka et al. 2019).

Besides dying from caspase-dependent apoptosis, cells can also undergo caspase-independent but RIPK3- and MLKL-dependent necroptosis (Fig. 1; Pasparakis and Vandenabeele 2015; Ting and Bertrand 2016). A20 has also been proposed as an inhibitor of necroptosis in some cell types. A20-deficient T cells were shown to be more susceptible to anti-CD3/CD28-induced cell death, independent of caspase activation but dependent on RIPK3 and the kinase activity of RIPK1 (Onizawa et al. 2015). In addition, RIPK3 deficiency or inhibition of RIPK1 could considerably delay the early postnatal lethality of A20 knockout mice (Onizawa et al. 2015; Newton et al. 2016). In contrast, MLKL deficiency could not rescue the early lethality of A20 knockout mice, questioning the role of necroptosis in the pathology of these mice (Newton et al. 2016). We recently showed that A20-deficient macrophages can die from RIPK1/RIPK3/MLKL-dependent necroptosis, causing inflammasome activation and arthritis development in myeloid-specific A20-deficient mice (Polykratis et al. 2019). Therefore, inhibi-

tion of necroptosis is a critical anti-inflammatory function of A20 in vivo.

Finally, in some cell types, A20 may have proapoptotic functions. A20-deficient B cells and dendritic cells were shown to be protected from Fas-mediated cell death, most likely owing to the up-regulation of NF-κB-dependent expression of antiapoptotic proteins such as Bcl-2 and Bcl-x (Tavares et al. 2010; Kool et al. 2011). A20 was also shown to sensitize smooth muscle cells to apoptosis through a mechanism depending on nitric oxide (NO) production (Patel et al. 2006).

Although it is clear that A20 is a key regulator of cell death, the mechanisms by which it does this are still incompletely understood. On activation of death receptors, A20 was shown to be recruited to the DISC, where it physically interacted with caspase-8. This interaction was suggested to prevent cullin3-mediated ubiquitination of caspase-8, inhibiting caspase-8 activation and apoptosis (Jin et al. 2009). Alternatively, A20 was shown to inhibit TNF-induced apoptosis by preventing the recruitment of RIPK1 and TRADD to TNFR1, thereby inhibiting the recruitment of FADD and caspase-8 (He and Ting 2002). A20 was also shown to inhibit TNF-induced c-jun amino-terminal kinase (JNK) activation and apoptosis by targeting upstream ASK1 for ubiquitination and proteasomal degradation (Won et al. 2010). In the context of its protective function against necroptosis, A20 was shown to restrict RIPK3 ubiquitination, preventing the formation of RIPK1–RIPK3 complexes and necroptosis induction (Onizawa et al. 2015).

Although these latter studies suggest that A20 acts as either a DUB or an E3 ligase, it is becoming more established that the nonenzymatic, polyubiquitin-binding function of A20 plays a prominent role in the regulation of cell death. A reduction of linear Ub chains within TNFR1 complex I was shown to promote cell death by inducing complex II assembly (Ikeda et al. 2011; Peltzer et al. 2014). The ZnF7 domain of A20 stabilizes linear Ub chains in complex I, inhibiting TNFR1-mediated cell death (Draber et al. 2015; Yamaguchi and Yamaguchi 2015). Hence, a mutation in the ZnF7 domain of A20 abolishes the recruitment of A20 and reduces the amount of linear Ub chains in TNFR1 complex I (Tokunaga et al. 2012; Draber et al. 2015; Polykratis et al. 2019). Interestingly, the binding of M1-linked chains by ZnF7 in A20 was shown to protect these chains from degradation by CYLD, thereby stabilizing complex I and preventing the formation of the DISC (Fig. 1; Draber et al. 2015).

MECHANISMS THAT REGULATE A20 ACTIVITY

A20 expression and function is under the control of several regulatory mechanisms, viz. transcriptional, posttranscriptional, and posttranslational. In most cell types, A20 expression levels are low at steady state, but are rapidly up-regulated in inflammatory conditions as a result of NF-κB activation (Krikos et al. 1992; Verstrepen et al. 2010). Different transcription factors work together to fine-tune the expression of A20 and the strength of NF-κB signaling. DREAM (downstream regulatory element antagonist modulator) has been shown to constitutively repress expression of A20 by binding to downstream regulatory elements (DREs) in the *A20* promoter, whereas upstream stimulatory factor 1 (USF1) has been shown to bind to the DRE-associated E-box domain in *A20* to activate its expression in response to an inflammatory stimulus (Amir-Zilberstein and Dikstein 2008; Tiruppathi et al. 2014). Also, the orphan nuclear estrogen-related receptor α (ERRα), a key metabolic regulator, has been shown to promote expression of A20 in mice (Yuk et al. 2015). ERRα binds to an Esrra consensus motif in the *A20* promoter, inducing expression of A20 and suppressing NF-κB signaling in LPS-stimulated macrophages (Yuk et al. 2015). Finally, the histone methyltransferase Ash1l (absent small or homeotic-like) was shown to enhance expression of A20 through H3K4 methylation of the *A20* promoter, suppressing inflammatory signaling (Xia et al. 2013).

T lymphocytes constitutively express high levels of A20, which are down-regulated on TCR activation and NF-κB induction (Tewari et al. 1995). Proteasomal degradation of A20,

as well as its cleavage by the paracaspase MALT1, contribute to the down-regulation of A20 following TCR stimulation (Coornaert et al. 2008; Duwel et al. 2009). Methylation of the *A20* promotor, preventing expression of A20 and stimulating constitutive NF-κB activation, has been observed in several types of lymphomas (Honma et al. 2009; Chanudet et al. 2010).

Expression of A20 is also regulated by several microRNAs (miRs). In diffuse large B-cell lymphomas, miR-125a and miR-125b were shown to down-regulate expression of A20, leading to constitutive activation of NF-κB, B-cell proliferation, and lymphomagenesis (Kim et al. 2012). miR-125-mediated inhibition of A20 has also been shown in lung infection and in chronic obstructive pulmonary disease (COPD) (Hsu et al. 2017). miR-19, miR-29, miR-221, and miR-let-7 are other miRNAs that have been shown to suppress A20, leading to enhanced NF-κB signaling and/or cell death (Wang et al. 2011; Gantier et al. 2012; Balkhi et al. 2013; Kumar et al. 2015; Langsch et al. 2016; Zhao et al. 2016).

A20 interacts with different partners to perform its regulatory functions. Multiple Ub-binding proteins have been described that bind to A20 and recruit it to its substrates. A20-binding inhibitor of NF-κB (ABIN1) was shown to recruit A20 to polyubiquitinated NEMO to remove Ub chains from NEMO (Heyninck et al. 1999; Mauro et al. 2006; Wagner et al. 2008). Tax1-binding protein 1 (TAX1BP1) negatively regulates NF-κB signaling by recruiting A20 to TRAF6 and RIPK1 (Shembade et al. 2007; Iha et al. 2008). Itch and RING finger protein 11 (RNF11) have been shown to function as subunits of an A20 Ub-editing complex to inhibit NF-κB signaling (Shembade et al. 2008, 2009).

The activity of A20 is also regulated by post-translational modifications. On receptor activation, A20 is phosphorylated at Ser381 by IKK2, increasing its inhibitory capacity (Hutti et al. 2007). Although A20 hydrolyzes K63-linked Ub chains in vivo via its OTU domain, recombinant A20 expressed in bacteria preferentially cleaves K48-linked chains in vitro (Komander and Barford 2008; Lin et al. 2008). The phosphorylation status of A20 appears to account for this discrepancy because phosphorylated A20 was shown to efficiently cleave K63-linked chains in vitro (Wertz et al. 2015). In T lymphocytes, A20 can be ubiquitinated by the E3 Ub ligase RNF114, thereby stabilizing A20 and restraining NF-κB responses (Rodriguez et al. 2014). In smooth muscle cells exposed to high glucose levels, A20 can be *O*-glycosylated and subsequently ubiquitinated and targeted for proteasomal degradation (Shrikhande et al. 2010). Finally, A20 is also regulated by reversible oxidation of the catalytic cysteine residue, modifying its activation state (Kulathu et al. 2013; Lee et al. 2013).

A20 AS A DISEASE SUSCEPTIBILITY GENE

Several single-nucleotide polymorphisms (SNPs) in or near the *A20* gene have been linked to a variety of autoimmune and inflammatory diseases, including systemic lupus erythematosus (SLE), rheumatoid arthritis, psoriasis, type 1 diabetes, Crohn's disease, celiac disease, coronary artery disease in type 2 diabetes, systemic sclerosis, and Sjogren's syndrome (Ma and Malynn 2012; Catrysse et al. 2014). Associations have also been reported for autoimmune hepatitis (de Boer et al. 2014) and primary biliary cirrhosis (Cordell et al. 2015). Most of these disease-associated variants are located in upstream or downstream noncoding regions or in intronic regions of the *A20* gene, possibly affecting the expression of A20 (Graham et al. 2008; Adrianto et al. 2011). Downstream SNPs can influence expression of A20 by affecting the function of cell- and activation-specific enhancers. For example, deletion of a downstream region containing four enhancers was shown to significantly reduce expression of A20, resulting in enhanced inflammatory responses (Sokhi et al. 2018). One of these enhancers harbors the TT > A variant that was linked to SLE susceptibility (Adrianto et al. 2011; Wang et al. 2013a). Deletion of this TT > A enhancer in mice induced spontaneous inflammatory arthritis, thereby establishing the importance of this enhancer in preventing inflammatory pathology and autoimmunity (Sokhi et al. 2018). Besides the many noncod-

ing variants, two SNPs have been identified in exon 3 of *A20* that induce nonsynonymous mutations (rs5029941/A125V and rs2230926/F127C) (Musone et al. 2008; Lodolce et al. 2010). These mutations are suggested to affect the DUB activity of A20, although this has not been evaluated in vivo.

Recently, whole-exome sequencing identified heterozygous loss-of-function mutations in the *A20/TNFAIP3* gene (A20 haploinsufficiency, HA20) of patients with a rare, early-onset autoinflammatory syndrome (Zhou et al. 2016). These nonsense and frameshift mutations are all localized in the DUB or the ZnF4 domains of A20, and the mutant proteins are likely unstable because A20 was not detected in cells from HA20 patients (Zhou et al. 2016). Patients' cells displayed increased NF-κB signaling, NLRP3 inflammasome activity, and increased expression of proinflammatory cytokines (Zhou et al. 2016). Several other cases of germline HA20 have since been identified in patients with early-onset autoimmune disease (Fig. 3; Table 1; Aeschlimann et al. 2018; Duncan et al. 2018). Overall, HA20 patients develop recurrent oral, genital, and/or gastrointestinal ulcers, musculoskeletal and gastrointestinal problems, episodic fever, and recurrent infections. However, disease severity is strongly patient-dependent, ranging from very mild disease to severe multiorgan inflammation, and treatment regimens need to be adjusted to disease severity (Aeschlimann et al. 2018).

Finally, *A20* has been identified as a tumor suppressor gene, because biallelic somatic mutations in *A20* are frequently observed in several B-cell lymphomas, including MALT lymphoma, Hodgkin's lymphoma, diffuse large B-cell lymphoma, and follicular lymphoma. These loss-of-function mutations are associated with constitutive NF-κB signaling and uncontrolled cell proliferation (Compagno et al. 2009; Honma et al. 2009; Kato et al. 2009; Novak et al. 2009; Schmitz et al. 2009; Okosun et al. 2014). Biallelic mutations in *A20* have also been identified in Sézary syndrome, an aggressive variant of cutaneous T-cell lymphoma (Braun et al. 2011). However, A20 has also been described as a tumor promotor, likely connected to its anti-apoptotic functions, and high levels of A20 have been detected in glioma (Guo et al. 2009), glioblastoma (Hjelmeland et al. 2010), and acute lymphoblastic leukemia (Chen et al. 2015). Furthermore, A20 was shown to be up-regulated in human basal-like breast cancers in which it promotes epithelial–mesenchymal transition (EMT) through monoubiquitination and nuclear stabilization of SNAIL1, a transcription factor that drives EMT (Lee et al. 2017).

TISSUE-SPECIFIC FUNCTIONS OF A20

A20 is an important anti-inflammatory protein that acts as a direct inhibitor of NF-κB signaling, or as an inhibitor of proinflammatory cell death. However, inflammatory signaling pathways and

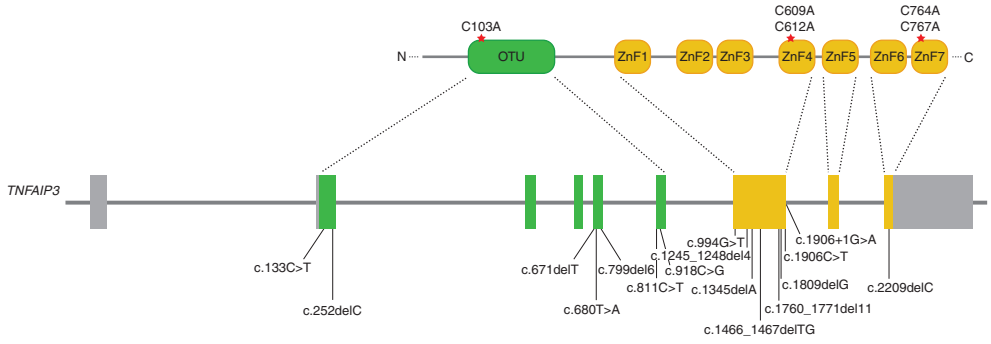

Figure 3. Schematic representation of the *TNFAIP3* gene indicating mutations causing A20 haploinsufficiency (HA20). Exons (1–9) are represented as rectangles. Exons encoding the ovarian tumor (OTU) domain are depicted in green and exons encoding the ZnF domains are depicted in orange; noncoding exons are shown in gray. HA20 mutations depicted in the figure are also listed in Table 1.

Table 1. Overview of identified HA20 mutations

cDNA alteration	Amino acid alteration	Domain	References
c.680T < A	p.Leu227*	Ovarian tumor (OTU)	Zhou et al. 2016; Aeschlimann et al. 2018
c.671delT	p.Phe224Ser*fs**4	OTU	
c.811C > T	p.Arg271*	OTU	
c.1809delG	p.Thr604Arg*fs**93	ZnF4	
c.918C > G	p.Tyr306*	OTU	
c.799delG	p.Pro268Leu*fs**19	OTU	
c.252delC	p.Trp85Gly*fs**11	OTU	Shigemura et al. 2016; Ohnishi et al. 2017;
c.133C > T	p.Arg45*	OTU	Takagi et al. 2017; Kadowaki et al. 2018
c.1760_1770del11	p.Ala588Val*fs**80	Between ZnF3-4	
c.1345delA	p.Asn449Thr*fs**28	Between ZnF1-2	
c.1906 + 1G > A	p.Phe637Glu*2	Between ZnF4-5	
c.2209delC	p.Gln737Ser*fs**79	ZnF6	
c.2088 + 5G > C	p.His636Glu*fs**55	ZnF4	
c.728G > A	p.Cys243Tyr	OTU	
c.1245-1248del4	p.Lys417Ser*fs**4	Between ZnF1-2	
c.994G > T	p.Glu332*	OTU	Berteau et al. 2019
c.1466_1467delTG	p.Val489Ala*fs**7	ZnF2	Duncan et al. 2018
c.1906C > T	p.His636*fs**1	ZnF4	Lawless et al. 2018

cell death are differentially regulated in different cell types; hence, A20 may have cell-specific contributions to prevent inflammation and disease pathogenesis. Because A20 knockout mice die prematurely because of severe multiorgan inflammation (Lee et al. 2000), conditional, lineage-specific knockout strategies are needed to unravel the tissue-specific functions of A20. Several tissue-specific A20-deficient mice have been generated in recent years that clearly show the importance of A20 in maintaining tissue homeostasis by regulating inflammatory responses and cell death (Table 2). In this section, we refer to a number of recent mouse studies that provide new information on the role of A20 in the prevention of cell death and its implications for inflammatory pathology.

Mice lacking A20 in their myeloid cells ($A20^{Myel\text{-}KO}$) develop spontaneous polyarthritis with many characteristics of human rheumatoid arthritis, including autoantibodies against type II collagen and rheumatoid arthritis–associated cytokines (Matmati et al. 2011). The arthritis phenotype in $A20^{Myel\text{-}KO}$ mice was shown to require IL-6 and TLR4-MyD88, but not TNF. Primary macrophages from these mice show sustained NF-κB activation in response to lipopolysaccharide (LPS), in agreement with a role for A20 as an inhibitor of NF-κB signaling (Matmati et al. 2011). A20-deficient macrophages also express higher levels of STAT1 and STAT1-dependent genes upon stimulation with interferon γ (IFN-γ) or IL-6. Inhibition of JAK-STAT signaling in vivo with the JAK inhibitor tofacitinib was shown to suppress the development of enthesitis in $A20^{Myel\text{-}KO}$ mice (De Wilde et al. 2017). Interestingly, myeloid A20 deficiency was also shown to promote osteoclastogenesis, suggesting a role for A20 in regulating receptor activator of the NF-κB (RANK)-induced NF-κB signaling. Further studies, preferably using osteoclast-specific A20 targeting, are needed to confirm a direct regulatory role of A20 in regulating osteoclastogenesis and bone formation.

Arthritis development in $A20^{Myel\text{-}KO}$ mice relies on activation of the Nlrp3 inflammasome and IL-1R signaling (Vande Walle et al. 2014). Thus, $A20^{Myel\text{-}KO}$ mice crossed into an Nlrp3-, caspase-1/11-, or IL-1R-deficient background no longer develop arthritis. Primary A20-deficient macrophages show enhanced Nlrp3 inflammasome-mediated caspase-1 activation, pyroptosis, and IL-1β secretion by soluble and

Table 2. Phenotypes of tissue-specific A20 knockout and A20 transgenic mice

Cell type	OE/KO	Phenotype	References
Myeloid cells	KO	Spontaneous severe destructive polyarthritis	Matmati et al. 2011; Vande Walle et al. 2014; De Wilde et al. 2017; Polykratis et al. 2019
	KO	Protected from influenza A virus infection	Maelfait et al. 2012
Dendritic cells	KO	Spontaneous colitis, IBD-associated arthritis	Hammer et al. 2011
	KO	Systemic autoimmunity resembling SLE	Kool et al. 2011
	KO	Multiorgan inflammation, hypersensitive to LPS	Xuan et al. 2015
B cells	KO	Development of autoimmune syndrome in older mice (autoreactive immunoglobulins, glomerular immunoglobulin deposits, ↑ germinal center B cells, B-cell resistance to Fas-mediated cell death)	Tavares et al. 2010; Chu et al. 2011; Hovelmeyer et al. 2011
T cells	KO	No spontaneous phenotype, ↓ iNKT cell numbers	Drennan et al. 2016
	KO	No spontaneous phenotype, protected from EAE	Onizawa et al. 2015
	KO	Lymphadenopathy but no detectable pathology, enhanced antitumor activity	Giordano et al. 2014
	KO	↑ Treg cell numbers	Fischer et al. 2017
HSC	KO	Loss of HSC quiescence causing anemia, lymphopenia, and postnatal lethality	Nakagawa et al. 2015
Mast cells	KO	Hypersensitive to allergic airway responses and collagen-induced arthritis	Heger et al. 2014
IEC	KO	No spontaneous pathology, enhanced susceptibility to DSS-induced colitis and to TNF toxicity	Vereecke et al. 2010; Kattah et al. 2018
	OE	Protected from LPS-induced barrier disruption	Kolodziej et al. 2011
	OE	Protected from DSS-induced IEC death and barrier disruption	Rhee et al. 2012
	OE	Hypersensitive to TNF-induced IEC death and systemic inflammation	Garcia-Carbonell et al. 2018
IEC + myeloid cells	KO	Spontaneous severe ileitis and colitis, colorectal cancer	Vereecke et al. 2014
Hepatocytes	KO	Chronic liver inflammation, enhanced sensitivity to TNF and LPS toxicity and to chemically and high fat diet–induced hepatocarcinogenesis	Catrysse et al. 2016
Keratinocytes		Keratinocyte hyperproliferation, ectodermal organ abnormalities, sensitized to experimental psoriasis, and atopic dermatitis	Lippens et al. 2011; Devos et al. 2019
Neurons	KO	No phenotype	McGuire et al. 2013
CNS progenitor cells	KO		
Microglia	KO	↑ Microglia numbers and microglia activation, hypersensitive LPS and EAE	Voet et al. 2018
Astrocytes	KO	Hypersensitive to EAE	Wang et al. 2013b
Airway epithelial cells	KO	Protected from influenza A virus infection, highly sensitive to allergic airway inflammation	Schuijs et al. 2015; Maelfait et al. 2016
Pancreatic β cells	KO	No phenotype	Liuwantara et al. 2006; Catrysse et al. 2015; Fukaya et al. 2016

OE, Overexpression; KO, knockout; IBD, inflammatory bowel disease; SLE, systemic lupus erythematosus; LPS, lipopolysaccharide; iNKT, invariant natural killer T cell; EAE, experimental autoimmune encephalomyelitis; HSC, hematopoietic stem cell; IEC, intestinal epithelial cell; DSS, dextran sodium sulfate; TNF, tumor necrosis factor.

crystalline Nlrp3 stimuli. Myeloid-specific ASC deficiency substantially ameliorated arthritis in $A20^{Myel\text{-}KO}$ mice, indicating that cell-intrinsic inflammasome activation in A20-deficient myeloid cells drives pathology (Polykratis et al. 2019). Although A20 was shown to regulate Nlrp3 inflammasome activation in vitro by negatively regulating NF-κB-dependent priming needed for optimal expression of pro-IL-1β and Nlrp3 (Vande Walle et al. 2014), inhibition of IKK/NF-κB signaling in A20-deficient myeloid cells was not sufficient to prevent arthritis development (Polykratis et al. 2019). Rather, regulation of cell death, and particularly of necroptosis, was identified as the key anti-inflammatory function of A20 in preventing the development of arthritis. Indeed, RIPK1/RIPK3/MLKL-dependent macrophage necroptosis was shown to induce inflammasome activation, IL-1β production, and arthritis development in $A20^{Myel\text{-}KO}$ mice (Polykratis et al. 2019). These data are supported by real-time single-cell imaging experiments, which show that IL-1β is secreted exclusively by dying A20-deficient macrophages. An earlier study had suggested that inflammasome activation and IL-1β release in A20-deficient macrophages occurs in the absence of cell death (Duong et al. 2015). A20 has also been shown to control microglia activation and neuroinflammation via regulation of Nlrp3 inflammasome activation (Voet et al. 2018). How A20 regulates Nlrp3 activation, and whether this is directly or indirectly preventing microglia cell death, needs further investigation.

An important prosurvival role for A20 has also been shown in IECs. Although IEC-specific A20 knockout mice ($A20^{IEC\text{-}KO}$) do not develop spontaneous disease, they are highly susceptible to DSS-induced colitis and are hypersensitive to a normally sublethal dose of TNF. IECs from $A20^{IEC\text{-}KO}$ mice are hypersensitive to apoptosis, leading to loss of intestinal barrier integrity and bacterial infiltration in $A20^{IEC\text{-}KO}$ mice (Vereecke et al. 2010). The antiapoptotic property of A20. in IECs was confirmed in transgenic mice with IEC-specific overexpression of A20. These mice are protected from DSS- and LPS-induced IEC apoptosis and loss of barrier function (Kolodziej et al. 2011; Rhee et al. 2012), but are highly susceptible to TNF-induced IEC apoptosis, intestinal damage, and systemic inflammation. The latter phenotype required RIPK1 and caspase-8, and was mediated by ZnF7 of A20 (Garcia-Carbonell et al. 2018). Thus, A20 binding to linear Ub appears to stabilize the Ripoptosome and potentiate its apoptosis-inducing activity (Garcia-Carbonell et al. 2018). Although $A20^{IEC\text{-}KO}$ mice do not develop a spontaneous intestinal phenotype (Vereecke et al. 2010; Kattah et al. 2018), mice lacking A20 in both IECs and myeloid cells develop severe ileitis and colitis, associated with epithelial apoptosis and hyperproliferation, which eventually leads to the development of colon cancer (Vereecke et al. 2014). Combined IEC-specific deletion of A20 and the A20-interacting protein ABIN1 also induces spontaneous intestinal inflammation and severe pathology because of the caspase-8 and RIPK1-dependent death of IECs (Kattah et al. 2018). Similarly, combined deletion of A20 and Atg16L1 in IECs induces spontaneous inflammatory bowel disease (IBD)-like pathology caused by IEC apoptosis (Slowicka et al. 2019). Interestingly, both ABIN-1 and Atg16L1 have been associated with IBD (Hampe et al. 2007; Rioux et al. 2007; Jostins et al. 2012) and have been shown to bind to A20 and to Ub (Wagner et al. 2008; Fujita et al. 2013; Slowicka et al. 2019). Collectively, these data suggest that inflammatory signaling and autophagy cooperatively control intestinal homeostasis by preventing the death of enterocytes that would compromise intestinal barrier integrity.

Finally, A20 was shown to have hepatoprotective activities. Hepatocyte-specific A20-deficient mice ($A20^{LPC\text{-}KO}$) spontaneously develop mild liver inflammation and steatosis, but succumb to a normally sublethal dose of TNF owing to excessive hepatocyte apoptosis. Moreover, chronic liver inflammation and enhanced hepatocyte apoptosis in $A20^{LPC\text{-}KO}$ mice increased their susceptibility to chemically and high fat diet–induced hepatocellular carcinoma development (Catrysse et al. 2016). A20 overexpression in liver has been shown to be protective in models of hepatectomy and acute toxic hepatitis, owing to antiapoptotic and anti-

inflammatory mechanisms (Arvelo et al. 2002; Ramsey et al. 2009; Damrauer et al. 2011; da Silva et al. 2013).

CONCLUDING REMARKS

A20 was identified nearly 30 years ago (Dixit et al. 1990; Opipari et al. 1990) and has emerged as a critical regulator of inflammatory signaling to preserve tissue immune homeostasis. Although inhibition of NF-κB activation has long been considered the key anti-inflammatory function of A20, it is becoming more evident that its role in preventing cell death is a major mechanism for suppressing inflammation. However, A20 may have different modes of action in different cell types given the phenotypes of different tissue-specific A20 knockout mice. NF-κB inhibitory activities, antiapoptotic functions, as well as antinecroptotic functions, and even proapoptotic functions have been identified in different cell types. Mechanistically, A20 has been proposed to function as a DUB, but the physiological relevance of its function as a DUB has been challenged by the finding that DUB-inactive A20 knockin mice do not develop spontaneous inflammatory disease. Recent evidence suggests that A20 mainly acts as a Ub-binding protein via its ZnF7 domain, which primarily recruits A20 into specific protein complexes to prevent downstream signaling. However, fine-tuning of signaling may require additional A20-specific activities, including A20 DUB activity. Generation of knockin mice with combined domain mutations will be essential to dissect the importance of and redundancies between the different functional domains of A20. Such studies will help to better understand the role of A20 in inflammation and immunity, which might help to develop new therapeutics for the treatment of disease.

ACKNOWLEDGMENTS

A.M. is supported by a grant from the Concerted Research Actions (GOA) of the Ghent University. Research in the G.v.L. laboratory is supported by research grants from the Research Foundation – Flanders (FWO), the Geneeskundige Stichting Koningin Elisabeth (GSKE), the CBC Banque Prize, the Charcot Foundation, the Belgian Foundation against Cancer, and Kom op tegen Kanker.

REFERENCES

Adrianto I, Wen F, Templeton A, Wiley G, King JB, Lessard CJ, Bates JS, Hu Y, Kelly JA, Kaufman KM, et al. 2011. Association of a functional variant downstream of *TNFAIP3* with systemic lupus erythematosus. *Nat Genet* **43:** 253–258. doi:10.1038/ng.766

Aeschlimann FA, Batu ED, Canna SW, Go E, Gül A, Hoffmann P, Leavis HL, Ozen S, Schwartz DM, Stone DL, et al. 2018. A20 haploinsufficiency (HA20): Clinical phenotypes and disease course of patients with a newly recognised NF-κB-mediated autoinflammatory disease. *Ann Rheum Dis* **77:** 728–735. doi:10.1136/annrheumdis-2017-212403

Amir-Zilberstein L, Dikstein R. 2008. Interplay between E-box and NF-κB in regulation of A20 gene by DRB sensitivity-inducing factor (DSIF). *J Biol Chem* **283:** 1317–1323. doi:10.1074/jbc.M706767200

Arvelo MB, Cooper JT, Longo C, Daniel S, Grey ST, Mahiou J, Czismadia E, Abu-Jawdeh G, Ferran C. 2002. A20 protects mice from D-galactosamine/lipopolysaccharide acute toxic lethal hepatitis. *Hepatology* **35:** 535–543. doi:10.1053/jhep.2002.31309

Balkhi MY, Iwenofu OH, Bakkar N, Ladner KJ, Chandler DS, Houghton PJ, London CA, Kraybill W, Perrotti D, Croce CM, et al. 2013. miR-29 acts as a decoy in sarcomas to protect the tumor suppressor A20 mRNA from degradation by HuR. *Sci Signal* **6:** ra63. doi:10.1126/scisignal.2004177

Berteau F, Rouvière B, Nau A, Le Berre R, Sarrabay G, Touitou I, de Moreuil C. 2019. A20 haploinsufficiency (HA20): Clinical phenotypes and disease course of patients with a newly recognised NF-κB-mediated autoinflammatory disease. *Ann Rheum Dis* **78:** e35. doi:10.1136/annrheumdis-2018-213347

Boone DL, Turer EE, Lee EG, Ahmad RC, Wheeler MT, Tsui C, Hurley P, Chien M, Chai S, Hitotsumatsu O, et al. 2004. The ubiquitin-modifying enzyme A20 is required for termination of Toll-like receptor responses. *Nat Immunol* **5:** 1052–1060. doi:10.1038/ni1110

Bosanac I, Wertz IE, Pan B, Yu C, Kusam S, Lam C, Phu L, Phung Q, Maurer B, Arnott D, et al. 2010. Ubiquitin binding to A20 ZnF4 is required for modulation of NF-κB signaling. *Mol Cell* **40:** 548–557. doi:10.1016/j.molcel.2010.10.009

Braun FC, Grabarczyk P, Möbs M, Braun FK, Eberle J, Beyer M, Sterry W, Busse F, Schroder J, Delin M, et al. 2011. Tumor suppressor TNFAIP3 (A20) is frequently deleted in Sézary syndrome. *Leukemia* **25:** 1494–1501. doi:10.1038/leu.2011.101

Catrysse L, Vereecke L, Beyaert R, van Loo G. 2014. A20 in inflammation and autoimmunity. *Trends Immunol* **35:** 22–31. doi:10.1016/j.it.2013.10.005

Catrysse L, Fukaya M, Sze M, Meyerovich K, Beyaert R, Cardozo AK, van Loo G. 2015. A20 deficiency sensitizes

pancreatic β cells to cytokine-induced apoptosis in vitro but does not influence type 1 diabetes development in vivo. *Cell Death Dis* **6:** e1918. doi:10.1038/cddis.2015.301

Catrysse L, Farhang Ghahremani M, Vereecke L, Youssef SA, McGuire C, Sze M, Weber A, Heikenwalder M, de Bruin A, Beyaert R, et al. 2016. A20 prevents chronic liver inflammation and cancer by protecting hepatocytes from death. *Cell Death Dis* **7:** e2250. doi:10.1038/cddis.2016.154

Chanudet E, Huang Y, Ichimura K, Dong G, Hamoudi RA, Radford J, Wotherspoon A, Isaacson PG, Ferry J, Du MQ. 2010. A20 is targeted by promoter methylation, deletion and inactivating mutation in MALT lymphoma. *Leukemia* **24:** 483–487. doi:10.1038/leu.2009.234

Chen S, Xing H, Li S, Yu J, Li H, Liu S, Tian Z, Tang K, Rao Q, Wang M, et al. 2015. Up-regulated A20 promotes proliferation, regulates cell cycle progression and induces chemotherapy resistance of acute lymphoblastic leukemia cells. *Leukemia Res* **39:** 976–983. doi:10.1016/j.leukres.2015.06.004

Chu Y, Vahl JC, Kumar D, Heger K, Bertossi A, Wojtowicz E, Soberon V, Schenten D, Mack B, Reutelshofer M, et al. 2011. B cells lacking the tumor suppressor TNFAIP3/A20 display impaired differentiation and hyperactivation and cause inflammation and autoimmunity in aged mice. *Blood* **117:** 2227–2236. doi:10.1182/blood-2010-09-306019

Compagno M, Lim WK, Grunn A, Nandula SV, Brahmachary M, Shen Q, Bertoni F, Ponzoni M, Scandurra M, Califano A, et al. 2009. Mutations of multiple genes cause deregulation of NF-κB in diffuse large B-cell lymphoma. *Nature* **459:** 717–721. doi:10.1038/nature07968

Coornaert B, Baens M, Heyninck K, Bekaert T, Haegman M, Staal J, Sun L, Chen ZJ, Marynen P, Beyaert R. 2008. T cell antigen receptor stimulation induces MALT1 paracaspase–mediated cleavage of the NF-κB inhibitor A20. *Nat Immunol* **9:** 263–271. doi:10.1038/ni1561

Cordell HJ, Han Y, Mells GF, Li Y, Hirschfield GM, Greene CS, Xie G, Juran BD, Zhu D, Qian DC, et al. 2015. International genome-wide meta-analysis identifies new primary biliary cirrhosis risk loci and targetable pathogenic pathways. *Nat Commun* **6:** 8019. doi:10.1038/ncomms9019

Damrauer SM, Studer P, da Silva CG, Longo CR, Ramsey HE, Csizmadia E, Shrikhande GV, Scali ST, Libermann TA, Bhasin MK, et al. 2011. A20 modulates lipid metabolism and energy production to promote liver regeneration. *PLoS ONE* **6:** e17715. doi:10.1371/journal.pone.0017715

da Silva CG, Studer P, Skroch M, Mahiou J, Minussi DC, Peterson CR, Wilson SW, Patel VI, Ma A, Csizmadia E, et al. 2013. A20 promotes liver regeneration by decreasing SOCS3 expression to enhance IL-6/STAT3 proliferative signals. *Hepatology* **57:** 2014–2025. doi:10.1002/hep.26197

De A, Dainichi T, Rathinam CV, Ghosh S. 2014. The deubiquitinase activity of A20 is dispensable for NF-κB signaling. *EMBO Rep* **15:** 775–783. doi:10.15252/embr.201338305

de Boer YS, van Gerven NM, Zwiers A, Verwer BJ, van Hoek B, van Erpecum KJ, Beuers U, van Buuren HR, Drenth JP, den Ouden JW, et al. 2014. Genome-wide association study identifies variants associated with autoimmune hepatitis type 1. *Gastroenterology* **147:** 443–452.e5. doi:10.1053/j.gastro.2014.04.022

Devos M, Mogilenko DA, Fleury S, Gilbert B, Becquart C, Quemener S, Dehondt H, Tougaard P, Staels B, Bachert C, et al. 2019. Keratinocyte expression of A20/TNFAIP3 controls skin inflammation associated with atopic dermatitis and psoriasis. *J Invest Dermatol* **139:** 135–145. doi:10.1016/j.jid.2018.06.191

De Wilde K, Martens A, Lambrecht S, Jacques P, Drennan MB, Debusschere K, Govindarajan S, Coudenys J, Verheugen E, Windels F, et al. 2017. A20 inhibition of STAT1 expression in myeloid cells: A novel endogenous regulatory mechanism preventing development of enthesitis. *Ann Rheum Dis* **76:** 585–592. doi:10.1136/annrheumdis-2016-209454

Dixit VM, Green S, Sarma V, Holzman LB, Wolf FW, O'Rourke K, Ward PA, Prochownik EV, Marks RM. 1990. Tumor necrosis factor-α induction of novel gene products in human endothelial cells including a macrophage-specific chemotaxin. *J Biol Chem* **265:** 2973–2978.

Draber P, Kupka S, Reichert M, Draberova H, Lafont E, de Miguel D, Spilgies L, Surinova S, Taraborrelli L, Hartwig T, et al. 2015. LUBAC-recruited CYLD and A20 regulate gene activation and cell death by exerting opposing effects on linear ubiquitin in signaling complexes. *Cell Rep* **13:** 2258–2272. doi:10.1016/j.celrep.2015.11.009

Drennan MB, Govindarajan S, Verheugen E, Coquet JM, Staal J, McGuire C, Taghon T, Leclercq G, Beyaert R, van Loo G, et al. 2016. NKT sublineage specification and survival requires the ubiquitin-modifying enzyme TNFAIP3/A20. *J Exp Med* **213:** 1973–1981. doi:10.1084/jem.20151065

Duncan CJA, Dinnigan E, Theobald R, Grainger A, Skelton AJ, Hussain R, Willet JDP, Swan DJ, Coxhead J, Thomas MF, et al. 2018. Early-onset autoimmune disease due to a heterozygous loss-of-function mutation in *TNFAIP3* (A20). *Ann Rheum Dis* **77:** 783–786. doi:10.1136/annrheumdis-2016-210944

Duong BH, Onizawa M, Oses-Prieto JA, Advincula R, Burlingame A, Malynn BA, Ma A. 2015. A20 restricts ubiquitination of pro-interleukin-1β protein complexes and suppresses NLRP3 inflammasome activity. *Immunity* **42:** 55–67. doi:10.1016/j.immuni.2014.12.031

Duwel M, Welteke V, Oeckinghaus A, Baens M, Kloo B, Ferch U, Darnay BG, Ruland J, Marynen P, Krappmann D. 2009. A20 negatively regulates T cell receptor signaling to NF-κB by cleaving Malt1 ubiquitin chains. *J Immunol* **182:** 7718–7728. doi:10.4049/jimmunol.0803313

Fischer JC, Otten V, Kober M, Drees C, Rosenbaum M, Schmickl M, Heidegger S, Beyaert R, van Loo G, Li XC, et al. 2017. A20 restrains thymic regulatory T cell development. *J Immunol* **199:** 2356–2365. doi:10.4049/jimmunol.1602102

Fujita N, Morita E, Itoh T, Tanaka A, Nakaoka M, Osada Y, Umemoto T, Saitoh T, Nakatogawa H, Kobayashi S, et al. 2013. Recruitment of the autophagic machinery to endosomes during infection is mediated by ubiquitin. *J Cell Biol* **203:** 115–128. doi:10.1083/jcb.201304188

Fukaya M, Brorsson CA, Meyerovich K, Catrysse L, Delaroche D, Vanzela EC, Ortis F, Beyaert R, Nielsen LB, Andersen ML, et al. 2016. A20 inhibits β-cell apoptosis

Cold Spring Harbor Perspectives in Biology
www.cshperspectives.org

by multiple mechanisms and Predicts residual β-cell function in type 1 diabetes. *Mol Endocrinol* **30:** 48–61. doi:10.1210/me.2015-1176

Gantier MP, Stunden HJ, McCoy CE, Behlke MA, Wang D, Kaparakis-Liaskos M, Sarvestani ST, Yang YH, Xu D, Corr SC, et al. 2012. A miR-19 regulon that controls NF-κB signaling. *Nucleic Acids Res* **40:** 8048–8058. doi:10.1093/nar/gks521

Garcia-Carbonell R, Wong J, Kim JY, Close LA, Boland BS, Wong TL, Harris PA, Ho SB, Das S, Ernst PB, et al. 2018. Elevated A20 promotes TNF-induced and RIPK1-dependent intestinal epithelial cell death. *Proc Natl Acad Sci* **115:** E9192–E9200. doi:10.1073/pnas.1810584115

Giordano M, Roncagalli R, Bourdely P, Chasson L, Buferne M, Yamasaki S, Beyaert R, van Loo G, Auphan-Anezin N, Schmitt-Verhulst AM, et al. 2014. The tumor necrosis factor α-induced protein 3 (TNFAIP3, A20) imposes a brake on antitumor activity of CD8 T cells. *Proc Natl Acad Sci* **111:** 11115–11120. doi:10.1073/pnas.1406259111

Graham RR, Cotsapas C, Davies L, Hackett R, Lessard CJ, Leon JM, Burtt NP, Guiducci C, Parkin M, Gates C, et al. 2008. Genetic variants near TNFAIP3 on 6q23 are associated with systemic lupus erythematosus. *Nat Genet* **40:** 1059–1061. doi:10.1038/ng.200

Guo Q, Dong H, Liu X, Wang C, Liu N, Zhang J, Li B, Cao W, Ding T, Yang Z, et al. 2009. A20 is overexpressed in glioma cells and may serve as a potential therapeutic target. *Exp Opin Ther Targets* **13:** 733–741. doi:10.1517/14728220903045018

Haas TL, Emmerich CH, Gerlach B, Schmukle AC, Cordier SM, Rieser E, Feltham R, Vince J, Warnken U, Wenger T, et al. 2009. Recruitment of the linear ubiquitin chain assembly complex stabilizes the TNF-R1 signaling complex and is required for TNF-mediated gene induction. *Mol Cell* **36:** 831–844. doi:10.1016/j.molcel.2009.10.013

Hammer GE, Turer EE, Taylor KE, Fang CJ, Advincula R, Oshima S, Barrera J, Huang EJ, Hou B, Malynn BA, et al. 2011. Expression of A20 by dendritic cells preserves immune homeostasis and prevents colitis and spondyloarthritis. *Nat Immunol* **12:** 1184–1193. doi:10.1038/ni.2135

Hampe J, Franke A, Rosenstiel P, Till A, Teuber M, Huse K, Albrecht M, Mayr G, De La Vega FM, Briggs J, et al. 2007. A genome-wide association scan of nonsynonymous SNPs identifies a susceptibility variant for Crohn disease in ATG16L1. *Nat Genet* **39:** 207–211. doi:10.1038/ng1954

He KL, Ting AT. 2002. A20 inhibits tumor necrosis factor (TNF) α–induced apoptosis by disrupting recruitment of TRADD and RIP to the TNF receptor 1 complex in Jurkat T cells. *Mol Cell Biol* **22:** 6034–6045. doi:10.1128/MCB.22.17.6034-6045.2002

Heger K, Fierens K, Vahl JC, Aszodi A, Peschke K, Schenten D, Hammad H, Beyaert R, Saur D, van Loo G, et al. 2014. A20-deficient mast cells exacerbate inflammatory responses in vivo. *PLoS Biol* **12:** e1001762. doi:10.1371/journal.pbio.1001762

Heyninck K, Denecker G, De Valck D, Fiers W, Beyaert R. 1999. Inhibition of tumor necrosis factor-induced necrotic cell death by the zinc finger protein A20. *Anticancer Res* **19:** 2863–2868. doi:10.1016/0014-5793(96)00283-9

Hitotsumatsu O, Ahmad RC, Tavares R, Wang M, Philpott D, Turer EE, Lee BL, Shiffin N, Advincula R, Malynn BA, et al. 2008. The ubiquitin-editing enzyme A20 restricts nucleotide-binding oligomerization domain containing 2-triggered signals. *Immunity* **28:** 381–390. doi:10.1016/j.immuni.2008.02.002

Hjelmeland AB, Wu Q, Wickman S, Eyler C, Heddleston J, Shi Q, Lathia JD, Macswords J, Lee J, McLendon RE, et al. 2010. Targeting A20 decreases glioma stem cell survival and tumor growth. *PLoS Biol* **8:** e1000319. doi:10.1371/journal.pbio.1000319

Honma K, Tsuzuki S, Nakagawa M, Tagawa H, Nakamura S, Morishima Y, Seto M. 2009. TNFAIP3/A20 functions as a novel tumor suppressor gene in several subtypes of non-Hodgkin lymphomas. *Blood* **114:** 2467–2475. doi:10.1182/blood-2008-12-194852

Hovelmeyer N, Reissig S, Xuan NT, Adams-Quack P, Lukas D, Nikolaev A, Schlüter D, Waisman A. 2011. A20 deficiency in B cells enhances B-cell proliferation and results in the development of autoantibodies. *Eur J Immunol* **41:** 595–601. doi:10.1002/eji.201041313

Hrdinka M, Gyrd-Hansen M. 2017. The Met1-linked ubiquitin machinery: Emerging themes of (de)regulation. *Mol Cell* **68:** 265–280. doi:10.1016/j.molcel.2017.09.001

Hsu AC, Dua K, Starkey MR, Haw TJ, Nair PM, Nichol K, Zammit N, Grey ST, Baines KJ, Foster PS, et al. 2017. MicroRNA-125a and -b inhibit A20 and MAVS to promote inflammation and impair antiviral response in COPD. *JCI Insight* **2:** e90443. doi:10.1172/jci.insight.90443

Hutti JE, Turk BE, Asara JM, Ma A, Cantley LC, Abbott DW. 2007. IκB kinase β phosphorylates the K63 deubiquitinase A20 to cause feedback inhibition of the NF-κB pathway. *Mol Cell Biol* **27:** 7451–7461. doi:10.1128/MCB.01101-07

Iha H, Peloponese JM, Verstrepen L, Zapart G, Ikeda F, Smith CD, Starost MF, Yedavalli V, Heyninck K, Dikic I, et al. 2008. Inflammatory cardiac valvulitis in TAX1BP1-deficient mice through selective NF-κB activation. *EMBO J* **27:** 629–641. doi:10.1038/emboj.2008.5

Ikeda F, Deribe YL, Skånland SS, Stieglitz B, Grabbe C, Franz-Wachtel M, van Wijk SJ, Goswami P, Nagy V, Terzic J, et al. 2011. SHARPIN forms a linear ubiquitin ligase complex regulating NF-κB activity and apoptosis. *Nature* **471:** 637–641. doi:10.1038/nature09814

Iwai K, Tokunaga F. 2009. Linear polyubiquitination: A new regulator of NF-κB activation. *EMBO Rep* **10:** 706–713. doi:10.1038/embor.2009.144

Jin Z, Li Y, Pitti R, Lawrence D, Pham VC, Lill JR, Ashkenazi A. 2009. Cullin3-based polyubiquitination and p62-dependent aggregation of caspase-8 mediate extrinsic apoptosis signaling. *Cell* **137:** 721–735. doi:10.1016/j.cell.2009.03.015

Jostins L, Ripke S, Weersma RK, Duerr RH, McGovern DP, Hui KY, Lee JC, Schumm LP, Sharma Y, Anderson CA, et al. 2012. Host–microbe interactions have shaped the genetic architecture of inflammatory bowel disease. *Nature* **491:** 119–124. doi:10.1038/nature11582

Kadowaki T, Ohnishi H, Kawamoto N, Hori T, Nishimura K, Kobayashi C, Shigemura T, Ogata S, Inoue Y, Kawai T, et al. 2018. Haploinsufficiency of A20 causes autoinflammatory and autoimmune disorders. *J Allergy Clin Immunol* **141:** 1485–1488.e11. doi:10.1016/j.jaci.2017.10.039

Kato M, Sanada M, Kato I, Sato Y, Takita J, Takeuchi K, Niwa A, Chen Y, Nakazaki K, Nomoto J, et al. 2009. Frequent

inactivation of A20 in B-cell lymphomas. *Nature* **459:** 712–716. doi:10.1038/nature07969

Kattah MG, Shao L, Rosli YY, Shimizu H, Whang MI, Advincula R, Achacoso P, Shah S, Duong BH, Onizawa M, et al. 2018. A20 and ABIN-1 synergistically preserve intestinal epithelial cell survival. *J Exp Med* **215:** 1839–1852. doi:10.1084/jem.20180198

Kim SW, Ramasamy K, Bouamar H, Lin AP, Jiang D, Aguiar RC. 2012. MicroRNAs miR-125a and miR-125b constitutively activate the NF-κB pathway by targeting the tumor necrosis factor α-induced protein 3 (TNFAIP3, A20). *Proc Natl Acad Sci* **109:** 7865–7870. doi:10.1073/pnas.1200081109

Kolodziej LE, Lodolce JP, Chang JE, Schneider JR, Grimm WA, Bartulis SJ, Zhu X, Messer JS, Murphy SF, Reddy N, et al. 2011. TNFAIP3 maintains intestinal barrier function and supports epithelial cell tight junctions. *PLoS ONE* **6:** e26352. doi:10.1371/journal.pone.0026352

Komander D, Barford D. 2008. Structure of the A20 OTU domain and mechanistic insights into deubiquitination. *Biochem J* **409:** 77–85. doi:10.1042/BJ20071399

Kondylis V, Kumari S, Vlantis K, Pasparakis M. 2017. The interplay of IKK, NF-κB and RIPK1 signaling in the regulation of cell death, tissue homeostasis and inflammation. *Immunol Rev* **277:** 113–127. doi:10.1111/imr.12550

Kool M, van Loo G, Waelput W, De Prijck S, Muskens F, Sze M, van Praet J, Branco-Madeira F, Janssens S, Reizis B, et al. 2011. The ubiquitin-editing protein A20 prevents dendritic cell activation, recognition of apoptotic cells, and systemic autoimmunity. *Immunity* **35:** 82–96. doi:10.1016/j.immuni.2011.05.013

Krikos A, Laherty CD, Dixit VM. 1992. Transcriptional activation of the tumor necrosis factor α-inducible zinc finger protein, A20, is mediated by kappa B elements. *J Biol Chem* **267:** 17971–17976.

Kulathu Y, Garcia FJ, Mevissen TE, Busch M, Arnaudo N, Carroll KS, Barford D, Komander D. 2013. Regulation of A20 and other OTU deubiquitinases by reversible oxidation. *Nat Commun* **4:** 1569. doi:10.1038/ncomms2567

Kumar M, Sahu SK, Kumar R, Subuddhi A, Maji RK, Jana K, Gupta P, Raffetseder J, Lerm M, Ghosh Z, et al. 2015. MicroRNA let-7 modulates the immune response to *Mycobacterium tuberculosis* infection via control of A20, an inhibitor of the NF-κB pathway. *Cell Host Microbe* **17:** 345–356. doi:10.1016/j.chom.2015.01.007

Langsch S, Baumgartner U, Haemmig S, Schlup C, Schäfer SC, Berezowska S, Rieger G, Dorn P, Tschan MP, Vassella E. 2016. miR-29b mediates NF-κB signaling in KRAS-induced non-small cell lung cancers. *Cancer Res* **76:** 4160–4169. doi:10.1158/0008-5472.CAN-15-2580

Lawless D, Pathak S, Scambler TE, Ouboussad L, Anwar R, Savic S. 2018. A case of adult-onset Still's disease caused by a novel splicing mutation in *TNFAIP3* successfully treated with tocilizumab. *Front Immunol* **9:** 1527. doi:10.3389/fimmu.2018.01527

Lee EG, Boone DL, Chai S, Libby SL, Chien M, Lodolce JP, Ma A. 2000. Failure to regulate TNF-induced NF-κB and cell death responses in A20-deficient mice. *Science* **289:** 2350–2354. doi:10.1126/science.289.5488.2350

Lee JG, Baek K, Soetandyo N, Ye Y. 2013. Reversible inactivation of deubiquitinases by reactive oxygen species in vitro and in cells. *Nat Commun* **4:** 1568. doi:10.1038/ncomms2532

Lee JH, Jung SM, Yang KM, Bae E, Ahn SG, Park JS, Seo D, Kim M, Ha J, Lee J, et al. 2017. A20 promotes metastasis of aggressive basal-like breast cancers through multi-mono-ubiquitylation of Snail1. *Nat Cell Biol* **19:** 1260–1273. doi:10.1038/ncb3609

Lin SC, Chung JY, Lamothe B, Rajashankar K, Lu M, Lo YC, Lam AY, Darnay BG, Wu H. 2008. Molecular basis for the unique deubiquitinating activity of the NF-κB inhibitor A20. *J Mol Biol* **376:** 526–540. doi:10.1016/j.jmb.2007.11.092

Lippens S, Lefebvre S, Gilbert B, Sze M, Devos M, Verhelst K, Vereecke L, McGuire C, Guerin C, Vandenabeele P, et al. 2011. Keratinocyte-specific ablation of the NF-κB regulatory protein A20 (TNFAIP3) reveals a role in the control of epidermal homeostasis. *Cell Death Differ* **18:** 1845–1853. doi:10.1038/cdd.2011.55

Liuwantara D, Elliot M, Smith MW, Yam AO, Walters SN, Marino E, McShea A, Grey ST. 2006. Nuclear factor-κB regulates β-cell death: A critical role for A20 in β-cell protection. *Diabetes* **55:** 2491–2501. doi:10.2337/db06-0142

Lodolce JP, Kolodziej LE, Rhee L, Kariuki SN, Franek BS, McGreal NM, Logsdon MF, Bartulis SJ, Perera MA, Ellis NA, et al. 2010. African-derived genetic polymorphisms in *TNFAIP3* mediate risk for autoimmunity. *J Immunol* **184:** 7001–7009. doi:10.4049/jimmunol.1000324

Lork M, Verhelst K, Beyaert R. 2017. CYLD, A20 and OTULIN deubiquitinases in NF-κB signaling and cell death: So similar, yet so different. *Cell Death Differ* **24:** 1172–1183. doi:10.1038/cdd.2017.46

Lu TT, Onizawa M, Hammer GE, Turer EE, Yin Q, Damko E, Agelidis A, Shifrin N, Advincula R, Barrera J, et al. 2013. Dimerization and ubiquitin mediated recruitment of A20, a complex deubiquitinating enzyme. *Immunity* **38:** 896–905. doi:10.1016/j.immuni.2013.03.008

Ma A, Malynn BA. 2012. A20: linking a complex regulator of ubiquitylation to immunity and human disease. *Nat Rev Immunol* **12:** 774–785. doi:10.1038/nri3313

Maelfait J, Roose K, Bogaert P, Sze M, Saelens X, Pasparakis M, Carpentier I, van Loo G, Beyaert R. 2012. A20 (*Tnfaip3*) deficiency in myeloid cells protects against influenza A virus infection. *PLoS Pathog* **8:** e1002570. doi:10.1371/journal.ppat.1002570

Maelfait J, Roose K, Vereecke L, McGuire C, Sze M, Schuijs MJ, Willart M, Ibanez LI, Hammad H, Lambrecht BN, et al. 2016. A20 deficiency in lung epithelial cells protects against influenza A virus infection. *PLoS Pathog* **12:** e1005410. doi:10.1371/journal.ppat.1005410

Matmati M, Jacques P, Maelfait J, Verheugen E, Kool M, Sze M, Geboes L, Louagie E, McGuire C, Vereecke L, et al. 2011. A20 (*TNFAIP3*) deficiency in myeloid cells triggers erosive polyarthritis resembling rheumatoid arthritis. *Nat Genet* **43:** 908–912. doi:10.1038/ng.874

Mauro C, Pacifico F, Lavorgna A, Mellone S, Iannetti A, Acquaviva R, Formisano S, Vito P, Leonardi A. 2006. ABIN-1 binds to NEMO/IKKγ and co-operates with A20 in inhibiting NF-κB. *J Biol Chem* **281:** 18482–18488. doi:10.1074/jbc.M601502200

McGuire C, Rahman M, Schwaninger M, Beyaert R, van Loo G. 2013. The ubiquitin editing enzyme A20 (TNFAIP3) is

Cold Spring Harbor Perspectives in Biology
www.cshperspectives.org

upregulated during permanent middle cerebral artery occlusion but does not influence disease outcome. *Cell Death Dis* **4:** e531. doi:10.1038/cddis.2013.55

Musone SL, Taylor KE, Lu TT, Nititham J, Ferreira RC, Ortmann W, Shifrin N, Petri MA, Kamboh MI, Manzi S, et al. 2008. Multiple polymorphisms in the *TNFAIP3* region are independently associated with systemic lupus erythematosus. *Nat Genet* **40:** 1062–1064. doi:10.1038/ng.202

Nakagawa MM, Thummar K, Mandelbaum J, Pasqualucci L, Rathinam CV. 2015. Lack of the ubiquitin-editing enzyme A20 results in loss of hematopoietic stem cell quiescence. *J Exp Med* **212:** 203–216. doi:10.1084/jem.20132544

Newton K, Dugger DL, Maltzman A, Greve JM, Hedehus M, Martin-McNulty B, Carano RA, Cao TC, van Bruggen N, Bernstein L, et al. 2016. RIPK3 deficiency or catalytically inactive RIPK1 provides greater benefit than MLKL deficiency in mouse models of inflammation and tissue injury. *Cell Death Differ* **23:** 1565–1576. doi:10.1038/cdd.2016.46

Novak U, Rinaldi A, Kwee I, Nandula SV, Rancoita PM, Compagno M, Cerri M, Rossi D, Murty VV, Zucca E, et al. 2009. The NF-κB negative regulator *TNFAIP3* (A20) is inactivated by somatic mutations and genomic deletions in marginal zone lymphomas. *Blood* **113:** 4918–4921. doi:10.1182/blood-2008-08-174110

Ohnishi H, Kawamoto N, Seishima M, Ohara O, Fukao T. 2017. A Japanese family case with juvenile onset Behçet's disease caused by *TNFAIP3* mutation. *Allergol Int* **66:** 146–148. doi:10.1016/j.alit.2016.06.006

Okosun J, Bödör C, Wang J, Araf S, Yang CY, Pan C, Boller S, Cittaro D, Bozek M, Iqbal S, et al. 2014. Integrated genomic analysis identifies recurrent mutations and evolution patterns driving the initiation and progression of follicular lymphoma. *Nat Genet* **46:** 176–181. doi:10.1038/ng.2856

Onizawa M, Oshima S, Schulze-Topphoff U, Oses-Prieto JA, Lu T, Tavares R, Prodhomme T, Duong B, Whang MI, Advincula R, et al. 2015. The ubiquitin-modifying enzyme A20 restricts ubiquitination of the kinase RIPK3 and protects cells from necroptosis. *Nat Immunol* **16:** 618–627. doi:10.1038/ni.3172

Opipari AW Jr, Boguski MS, Dixit VM. 1990. The A20 cDNA induced by tumor necrosis factor α encodes a novel type of zinc finger protein. *J Biol Chem* **265:** 14705–14708.

Pasparakis M, Vandenabeele P. 2015. Necroptosis and its role in inflammation. *Nature* **517:** 311–320. doi:10.1038/nature14191

Patel VI, Daniel S, Longo CR, Shrikhande GV, Scali ST, Czismadia E, Groft CM, Shukri T, Motley-Dore C, Ramsey HE, et al. 2006. A20, a modulator of smooth muscle cell proliferation and apoptosis, prevents and induces regression of neointimal hyperplasia. *FASEB J* **20:** 1418–1430. doi:10.1096/fj.05-4981com

Peltzer N, Rieser E, Taraborrelli L, Draber P, Darding M, Pernaute B, Shimizu Y, Sarr A, Draberova H, Montinaro A, et al. 2014. HOIP deficiency causes embryonic lethality by aberrant TNFR1-mediated endothelial cell death. *Cell Rep* **9:** 153–165. doi:10.1016/j.celrep.2014.08.066

Polykratis A, Martens A, Eren RO, Shirasaki Y, Yamagishi M, Yamaguchi Y, Uemura S, Miura M, Holzmann B, Kollias G, et al. 2019. A20 prevents inflammasome-dependent arthritis by inhibiting macrophage necroptosis through its ZnF7 ubiquitin-binding domain. *Nat Cell Biol* **21:** 731–742. doi:10.1038/s41556-019-0324-3

Ramsey HE, Da Silva CG, Longo CR, Csizmadia E, Studer P, Patel VI, Damrauer SM, Siracuse JJ, Daniel S, Ferran C. 2009. A20 protects mice from lethal liver ischemia/reperfusion injury by increasing peroxisome proliferator-activated receptor- α expression. *Liver Transpl* **15:** 1613–1621. doi:10.1002/lt.21879

Renner F, Schmitz ML. 2009. Autoregulatory feedback loops terminating the NF-κB response. *Trends Biochem Sci* **34:** 128–135. doi:10.1016/j.tibs.2008.12.003

Rhee L, Murphy SF, Kolodziej LE, Grimm WA, Weber CR, Lodolce JP, Chang JE, Bartulis SJ, Messer JS, Schneider JR, et al. 2012. Expression of TNFAIP3 in intestinal epithelial cells protects from DSS- but not TNBS-induced colitis. *Am J Physiol Gastrointest Liver Physiol* **303:** G220–G227. doi:10.1152/ajpgi.00077.2012

Rioux JD, Xavier RJ, Taylor KD, Silverberg MS, Goyette P, Huett A, Green T, Kuballa P, Barmada MM, Datta LW, et al. 2007. Genome-wide association study identifies new susceptibility loci for Crohn disease and implicates autophagy in disease pathogenesis. *Nat Genet* **39:** 596–604. doi:10.1038/ng2032

Rodriguez MS, Egana I, Lopitz-Otsoa F, Aillet F, Lopez-Mato MP, Dorronsoro A, Lobato-Gil S, Sutherland JD, Barrio R, Trigueros C, et al. 2014. The RING ubiquitin E3 RNF114 interacts with A20 and modulates NF-κB activity and T-cell activation. *Cell Death Dis* **5:** e1399. doi:10.1038/cddis.2014.366

Schmitz R, Hansmann ML, Bohle V, Martin-Subero JI, Hartmann S, Mechtersheimer G, Klapper W, Vater I, Giefing M, Gesk S, et al. 2009. *TNFAIP3* (A20) is a tumor suppressor gene in Hodgkin lymphoma and primary mediastinal B cell lymphoma. *J Exp Med* **206:** 981–989. doi:10.1084/jem.20090528

Schuijs MJ, Willart MA, Vergote K, Gras D, Deswarte K, Ege MJ, Madeira FB, Beyaert R, van Loo G, Bracher F, et al. 2015. Farm dust and endotoxin protect against allergy through A20 induction in lung epithelial cells. *Science* **349:** 1106–1110. doi:10.1126/science.aac6623

Shembade N, Harhaj NS, Liebl DJ, Harhaj EW. 2007. Essential role for TAX1BP1 in the termination of TNF-α-, IL-1- and LPS-mediated NF-κB and JNK signaling. *EMBO J* **26:** 3910–3922. doi:10.1038/sj.emboj.7601823

Shembade N, Harhaj NS, Parvatiyar K, Copeland NG, Jenkins NA, Matesic LE, Harhaj EW. 2008. The E3 ligase Itch negatively regulates inflammatory signaling pathways by controlling the function of the ubiquitin-editing enzyme A20. *Nat Immunol* **9:** 254–262. doi:10.1038/ni1563

Shembade N, Parvatiyar K, Harhaj NS, Harhaj EW. 2009. The ubiquitin-editing enzyme A20 requires RNF11 to downregulate NF-κB signalling. *EMBO J* **28:** 513–522. doi:10.1038/emboj.2008.285

Shembade N, Ma A, Harhaj EW. 2010. Inhibition of NF-κB signaling by A20 through disruption of ubiquitin enzyme complexes. *Science* **327:** 1135–1139. doi:10.1126/science.1182364

Shigemura T, Kaneko N, Kobayashi N, Kobayashi K, Takeuchi Y, Nakano N, Masumoto J, Agematsu K. 2016. Novel heterozygous C243Y A20/TNFAIP3 gene mutation is re-

sponsible for chronic inflammation in autosomal-dominant Behçet's disease. *RMD Open* **2:** e000223. doi:10.1136/rmdopen-2015-000223

Shrikhande GV, Scali ST, da Silva CG, Damrauer SM, Csizmadia E, Putheti P, Matthey M, Arjoon R, Patel R, Siracuse JJ, et al. 2010. *O*-glycosylation regulates ubiquitination and degradation of the anti-inflammatory protein A20 to accelerate atherosclerosis in diabetic ApoE-null mice. *PLoS ONE* **5:** e14240. doi:10.1371/journal.pone.0014240

Skaug B, Chen J, Du F, He J, Ma A, Chen ZJ. 2011. Direct, noncatalytic mechanism of IKK inhibition by A20. *Mol Cell* **44:** 559–571. doi:10.1016/j.molcel.2011.09.015

Slowicka K, Serramito-Gómez I, Boada Romero E, Martens A, Sze M, Petta I, Vikkula HK, dR R, Parthoens E, Lippens S, et al. 2019. Physical and functional interaction between A20 and ATG16L1-WD40 domain in the control of intestinal homeostasis. *Nat Commun* **10:** 1834. doi:10.1038/s41467-019-09667-z

Sokhi UK, Liber MP, Frye L, Park S, Kang K, Pannellini T, Zhao B, Norinsky R, Ivashkiv LB, Gong S. 2018. Dissection and function of autoimmunity-associated *TNFAIP3* (A20) gene enhancers in humanized mouse models. *Nat Commun* **9:** 658. doi:10.1038/s41467-018-03081-7

Takagi M, Ogata S, Ueno H, Yoshida K, Yeh T, Hoshino A, Piao J, Yamashita M, Nanya M, Okano T, et al. 2017. Haploinsufficiency of *TNFAIP3* (A20) by germline mutation is involved in autoimmune lymphoproliferative syndrome. *J Allergy Clin Immunol* **139:** 1914–1922. doi:10.1016/j.jaci.2016.09.038

Tavares RM, Turer EE, Liu CL, Advincula R, Scapini P, Rhee L, Barrera J, Lowell CA, Utz PJ, Malynn BA, et al. 2010. The ubiquitin modifying enzyme A20 restricts B cell survival and prevents autoimmunity. *Immunity* **33:** 181–191. doi:10.1016/j.immuni.2010.07.017

Tewari M, Wolf FW, Seldin MF, O'Shea KS, Dixit VM, Turka LA. 1995. Lymphoid expression and regulation of A20, an inhibitor of programmed cell death. *J Immunol* **154:** 1699–1706.

Ting AT, Bertrand MJM. 2016. More to life than NF-κB in TNFR1 signaling. *Trends Immunol* **37:** 535–545. doi:10.1016/j.it.2016.06.002

Tiruppathi C, Soni D, Wang DM, Xue J, Singh V, Thippegowda PB, Cheppudira BP, Mishra RK, Debroy A, Qian Z, et al. 2014. The transcription factor DREAM represses the deubiquitinase A20 and mediates inflammation. *Nat Immunol* **15:** 239–247. doi:10.1038/ni.2823

Tokunaga F, Nishimasu H, Ishitani R, Goto E, Noguchi T, Mio K, Kamei K, Ma A, Iwai K, Nureki O. 2012. Specific recognition of linear polyubiquitin by A20 zinc finger 7 is involved in NF-κB regulation. *EMBO J* **31:** 3856–3870. doi:10.1038/emboj.2012.241

Vande Walle L, Van Opdenbosch N, Jacques P, Fossoul A, Verheugen E, Vogel P, Beyaert R, Elewaut D, Kanneganti TD, van Loo G, et al. 2014. Negative regulation of the NLRP3 inflammasome by A20 protects against arthritis. *Nature* **512:** 69–73. doi:10.1038/nature13322

Vereecke L, Sze M, McGuire C, Rogiers B, Chu Y, Schmidt-Supprian M, Pasparakis M, Beyaert R, van Loo G. 2010. Enterocyte-specific A20 deficiency sensitizes to tumor necrosis factor-induced toxicity and experimental colitis. *J Exp Med* **207:** 1513–1523. doi:10.1084/jem.20092474

Vereecke L, Vieira-Silva S, Billiet T, van Es JH, McGuire C, Slowicka K, Sze M, van den Born M, De Hertogh G, Clevers H, et al. 2014. A20 controls intestinal homeostasis through cell-specific activities. *Nat Commun* **5:** 5103. doi:10.1038/ncomms6103

Verhelst K, Carpentier I, Beyaert R. 2011. Regulation of TNF-induced NF-κB activation by different cytoplasmic ubiquitination events. *Cytokine Growth Factor Rev* **22:** 277–286. doi:10.1016/j.cytogfr.2011.11.002

Verhelst K, Carpentier I, Kreike M, Meloni L, Verstrepen L, Kensche T, Dikic I, Beyaert R. 2012. A20 inhibits LUBAC-mediated NF-κB activation by binding linear polyubiquitin chains via its zinc finger 7. *EMBO J* **31:** 3845–3855. doi:10.1038/emboj.2012.240

Verstrepen L, Verhelst K, van Loo G, Carpentier I, Ley SC, Beyaert R. 2010. Expression, biological activities and mechanisms of action of A20 (*TNFAIP3*). *Biochem Pharmacol* **80:** 2009–2020. doi:10.1016/j.bcp.2010.06.044

Voet S, McGuire C, Hagemeyer N, Martens A, Schroeder A, Wieghofer P, Daems C, Staszewski O, Vande Walle L, Jordao MJC, et al. 2018. A20 critically controls microglia activation and inhibits inflammasome-dependent neuroinflammation. *Nat Commun* **9:** 2036. doi:10.1038/s41467-018-04376-5

Wagner S, Carpentier I, Rogov V, Kreike M, Ikeda F, Löhr F, Wu CJ, Ashwell JD, Dötsch V, Dikic I, et al. 2008. Ubiquitin binding mediates the NF-κB inhibitory potential of ABIN proteins. *Oncogene* **27:** 3739–3745. doi:10.1038/sj.onc.1211042

Wang CM, Wang Y, Fan CG, Xu FF, Sun WS, Liu YG, Jia JH. 2011. miR-29c targets *TNFAIP3*, inhibits cell proliferation and induces apoptosis in hepatitis B virus-related hepatocellular carcinoma. *Biochem Biophys Res Commun* **411:** 586–592. doi:10.1016/j.bbrc.2011.06.191

Wang S, Wen F, Wiley GB, Kinter MT, Gaffney PM. 2013a. An enhancer element harboring variants associated with systemic lupus erythematosus engages the *TNFAIP3* promoter to influence A20 expression. *PLoS Genet* **9:** e1003750. doi:10.1371/journal.pgen.1003750

Wang X, Deckert M, Xuan NT, Nishanth G, Just S, Waisman A, Naumann M, Schlüter D. 2013b. Astrocytic A20 ameliorates experimental autoimmune encephalomyelitis by inhibiting NF-κB- and STAT1-dependent chemokine production in astrocytes. *Acta Neuropathol* **126:** 711–724. doi:10.1007/s00401-013-1183-9

Wertz IE, O'Rourke KM, Zhou H, Eby M, Aravind L, Seshagiri S, Wu P, Wiesmann C, Baker R, Boone DL, et al. 2004. De-ubiquitination and ubiquitin ligase domains of A20 downregulate NF-κB signalling. *Nature* **430:** 694–699. doi:10.1038/nature02794

Wertz IE, Newton K, Seshasayee D, Kusam S, Lam C, Zhang J, Popovych N, Helgason E, Schoeffler A, Jeet S, et al. 2015. Phosphorylation and linear ubiquitin direct A20 inhibition of inflammation. *Nature* **528:** 370–375. doi:10.1038/nature16165

Won M, Park KA, Byun HS, Sohn KC, Kim YR, Jeon J, Hong JH, Park J, Seok JH, Kim JM, et al. 2010. Novel anti-apoptotic mechanism of A20 through targeting ASK1 to suppress TNF-induced JNK activation. *Cell Death Differ* **17:** 1830–1841. doi:10.1038/cdd.2010.47

Xia M, Liu J, Wu X, Liu S, Li G, Han C, Song L, Li Z, Wang Q, Wang J, et al. 2013. Histone methyltransferase Ash1l suppresses interleukin-6 production and inflammatory autoimmune diseases by inducing the ubiquitin-editing enzyme A20. *Immunity* **39:** 470–481. doi:10.1016/j.immuni.2013.08.016

Xuan NT, Wang X, Nishanth G, Waisman A, Borucki K, Isermann B, Naumann M, Deckert M, Schlüter D. 2015. A20 expression in dendritic cells protects mice from LPS-induced mortality. *Eur J Immunol* **45:** 818–828. doi:10.1002/eji.201444795

Yamaguchi N, Yamaguchi N. 2015. The seventh zinc finger motif of A20 is required for the suppression of TNF-α-induced apoptosis. *FEBS Lett* **589:** 1369–1375. doi:10.1016/j.febslet.2015.04.022

Yuk JM, Kim TS, Kim SY, Lee HM, Han J, Dufour CR, Kim JK, Jin HS, Yang CS, Park KS, et al. 2015. Orphan nuclear receptor ERRα controls macrophage metabolic signaling and A20 Expression to negatively regulate TLR-induced inflammation. *Immunity* **43:** 80–91. doi:10.1016/j.immuni.2015.07.003

Zhang Q, Lenardo MJ, Baltimore D. 2017. 30 years of NF-κB: A blossoming of relevance to human pathobiology. *Cell* **168:** 37–57. doi:10.1016/j.cell.2016.12.012

Zhao D, Zhuang N, Ding Y, Kang Y, Shi L. 2016. MiR-221 activates the NF-κB pathway by targeting A20. *Biochem Biophys Res Commun* **472:** 11–18. doi:10.1016/j.bbrc.2015.11.009

Zhou Q, Wang H, Schwartz DM, Stoffels M, Park YH, Zhang Y, Yang D, Demirkaya E, Takeuchi M, Tsai WL, et al. 2016. Loss-of-function mutations in *TNFAIP3* leading to A20 haploinsufficiency cause an early-onset autoinflammatory disease. *Nat Genet* **48:** 67–73. doi:10.1038/ng.3459

Addendum: A20 phosphorylation controls A20 function

INFLAMMATORY RESPONSE

A20 phosphorylation controls A20 function

A new study has identified various previously unknown mutations in the genes encoding human and mouse A20 that affect its phosphorylation and its function as an inhibitor of the transcription factor NF-κB, with implications for immunity and inflammatory disease.

Arne Martens and Geert van Loo

Inflammation is a protective response for resistance to infections and the induction of repair in conditions of damage and stress. However, excessive inflammatory responses can lead to chronic inflammation, tissue damage and the development of disease, indicative of the need for tight control of inflammatory processes.

One of the key molecules that regulate inflammatory signaling via the transcription factor NF-κB is A20, and mutations in the gene encoding A20 (*TNFAIP3*) have been identified in patients with inflammatory or autoimmune diseases[1]. In this issue of *Nature Immunology*, Zammit et al. demonstrate how different newly discovered *TNFAIP3* alleles encoding A20 variants can modulate, to different degrees, the phosphorylation of A20, with graded effects on NF-κB responses, microbial tolerance and immunity[2].

A20 has been characterized as a 'ubiquitin-editing' enzyme that inhibits the activation of NF-κB by changing the ubiquitination status of NF-κB signaling proteins through the presence (in A20) of an amino-terminal ovarian tumor (OTU) domain with deubiquitinase (DUB) activity, and of a carboxy-terminal zinc-finger domain with E3 ligase activity and ubiquitin-binding properties[1,3].

A20's own activity is under the control of several regulatory mechanisms, including phosphorylation. In inflammatory conditions, A20 is phosphorylated at Ser381 by the NF-κB-activating kinase IKK2, which increases its inhibitory capacity[4]. Indeed, when phosphorylated, A20 has been shown to more efficiently cleave ubiquitin chains and suppress inflammatory signaling, which illustrates the importance of its phosphorylation for its DUB activity[5].

In their study, Zammit et al. describe three new A20 variants, each with a different alteration in the OTU domain that affects the phosphorylation and activation of A20 to a different degree[2] (Fig. 1). First, they identify the allele encoding the A20 variant consisting of the T108A and I207L substitutions (collectively called 'T108A/I207L' here) through whole-genome sequencing of healthy subjects of Maori and Pacific Islander ancestry. This A20 variant turns out to be frequent among people of Island Southeast Asia and Oceania who acquired part of their genome from Denisova hominins, archaic humans who migrated from Siberia (from the so-called 'Denisova Cave' in the Altai Mountains) through Asia to settle in the islands of Southeast Asia and Oceania. The Denisovan T108A/I207L variant is associated with enhanced expression of NF-kB response genes after stimulation of carrier peripheral blood mononuclear cells with the cytokine TNF, indicative of a (partial) loss of function of A20 as an inhibitor of NF-κB. The second A20 OTU variant, I325N, is identified in an N-ethyl-N-nitrosourea–mutagenized mouse strain with an increased frequency of activated and/or memory and regulatory T cells. Immune cells from these mice show increased activation of NF-κB, and I325N macrophages produce more inflammatory cytokines after being stimulated with lipopolysaccharide in vitro. The third OTU domain mutant, C243Y, was identified, through whole-exome sequencing, in a Japanese family with a history of Behcet's disease and was shown to affect proper regulation of NF-κB, which led to enhanced production of inflammatory cytokines[6].

Next, Zammit et al. introduce the human *TNFAIP3* alleles encoding the A20 variants I207L and C243Y into mice via CRISPR-Cas9 gene editing for functional studies[2]. In agreement with the human condition, mice homozygous for the allele encoding

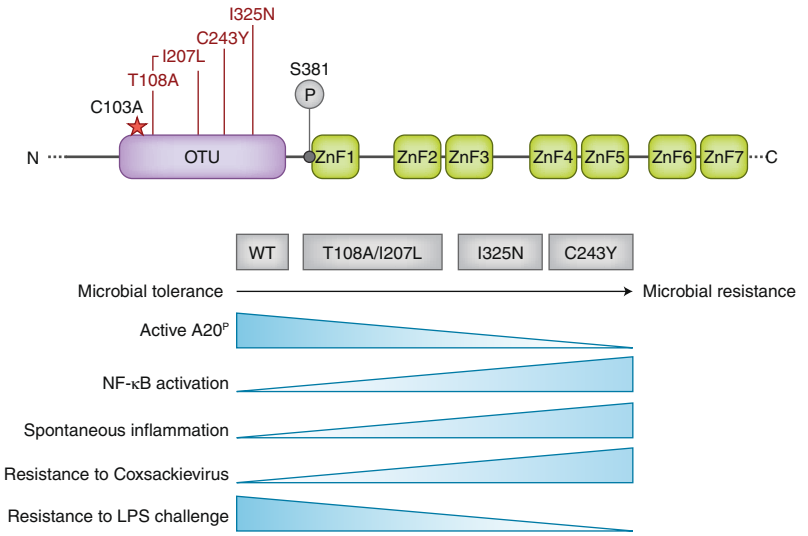

Fig. 1 | Newly discovered A20 variants that affect phosphorylation of A20, NF-κB signaling, microbial tolerance and immunity. a, A20 and the mutant variants (top left) of its OTU domain (purple), including the C103A variant of the OTU catalytic residue, and the T108A, I207L, C243Y and I325N variants (encoded by missense mutations) identified by Zammit et al.[2], as well as the Ser381 (S381) IKK2 phosphorylation site (P), and seven zinc-finger domains (ZnF1–ZnF7; green). **b**, Increased immunity versus increased pathogenicity in wild-type mice (WT) and mice bearing the A20 variants (above plot) described by Zammit et al.[2], as well as other effects of the variants (left margin). A20^{P}, phosphorylated A20; LPS, lipopolysaccharide.

the I207L Denisovan mutant (C57BL/6 mice already have the mutation encoding T108A) develop normally without overt signs of disease, while mice homozygous for the allele encoding C243Y are runted, display severe signs of inflammatory pathology in different organs and often die prematurely. Mice homozygous for the allele encoding I325N seem to be healthy but have reduced body weight compared with that of wild-type mice and display low-grade inflammation in multiple organs, consistent with reduced control of NF-κB signaling.

None of the three mutants have altered expression or stability of A20, in contrast to the recently identified nonsense and frameshift HA20 mutations that probably generate unstable proteins, since A20 expression could not be detected in cells from patients with such mutations[7]. However, the three mutations identified affect, to different degrees, the phosphorylation status of A20 protein, which leads to varying loss of Ser381 phosphorylation: mild (T108A/I207L), intermediate (I325N) or severe and almost complete (C243Y). The graded effect of the different variants on the phosphorylation status of A20 consequently causes a graded reduction in A20's function and its control of NF-κB.

An interesting observation from Zammit et al. is the difference in microbial tolerance among mice bearing each of the three alleles[2]. In contrast to mice expressing the wild-type allele, which all die, I207L mice are substantially protected from infection with a normally lethal dose of coxsackievirus, and I325N and C243Y mice are fully protected from this. The graded reduction in A20 phosphorylation among the three A20-mutant mouse strains (I207L < I325N < C243Y) enhances their protective immunity to viral infection. In an experimental model of septic shock, however, the opposite is shown, with I325N and C243Y mice demonstrating greater mortality than Denisovan or wild-type mice after a challenge with lipopolysaccharide. Similarly, I325N mice are highly sensitive to infection with a mouse variant of smallpox. Beyond the difference in microbial tolerance, I325N mice are also more prone to develop autoimmunity in a model of autoimmune diabetes than are wild-type mice. This shows that the outcome of alterations in the microbial resistance–microbial tolerance balance can be beneficial or detrimental, depending on the context (Fig. 1). Collectively, these data demonstrate how differences in the amount of A20 phosphorylation have a serious effect on immunity and microbial tolerance in different environmental conditions and suggest that specific alleles encoding A20 may have been critical in the genetic selection of indigenous populations.

Despite many reports claiming that A20 acts as a DUB, transgenic mouse lines expressing the OTU protease-dead C103A variant show minimal differences in NF-κB signaling and do not develop spontaneous inflammatory pathology[5,8,9]. This study demonstrates that the three newly identified OTU A20 variants, which diminish A20 phosphorylation to different degrees, have a much greater effect on NF-κB inhibition, immunity and microbial tolerance than does the catalytic C103A variant. This supports the conclusion that A20's function is critically regulated by phosphorylation and suggests that phosphorylation-mediated activation of A20 also has an effect on other activities of A20 beyond its DUB function. However, additional studies are needed to fully understand how phosphorylation regulates the activation of A20, as well as to identify the involvement of other phosphorylation sites or mechanisms whereby A20 is regulated. Finally, although inhibition of NF-κB's activation has long been considered the key anti-inflammatory function of A20, it is becoming more and more evident that its role in preventing cell death is a major mechanism of suppressing inflammation. Published evidence has demonstrated that the non-enzymatic, ubiquitin-binding function of A20 has a predominant role in this[10,11]. Further studies should investigate how the A20 variants described in this study act in the context of cell death and should asses the importance of the phosphorylation of A20 at Ser381 or other sites for its cytoprotective functions. Such studies will generate new insights in the molecular mechanisms behind pathologies associated with impaired A20 function and may lead to better therapies for such diseases. ❐

Arne Martens[1,2] and Geert van Loo[1,2*]

[1]*VIB Center for Inflammation Research, Ghent, Belgium.* [2]*Department of Biomedical Molecular Biology, Ghent University, Ghent, Belgium.*
**e-mail: geert.vanloo@irc.vib-ugent.be*

Published online: 18 September 2019
https://doi.org/10.1038/s41590-019-0481-3

References

1. Martens, A. & van Loo, G. *Cold Spring Harb. Perspect. Biol.* https://doi.org/10.1101/cshperspect.a036418 (2019).
2. Zammit, N. et al. *Nat. Immunol.* https://doi.org/10.1038/s41590-019-0492-0 (2019).
3. Wertz, I. E. et al. *Nature* **430**, 694–699 (2004).
4. Hutti, J. E. et al. *Mol. Cell. Biol.* **27**, 7451–7461 (2007).
5. Wertz, I. E. et al. *Nature* **528**, 370–375 (2015).
6. Shigemura, T. et al. *RMD Open* **2**, e000223 (2016).
7. Zhou, Q. et al. *Nat. Genet.* **48**, 67–73 (2016).
8. Lu, T. T. et al. *Immunity* **38**, 896–905 (2013).
9. De, A., Dainichi, T., Rathinam, C. V. & Ghosh, S. *EMBO Rep.* **15**, 775–783 (2014).
10. Draber, P. et al. *Cell Reports* **13**, 2258–2272 (2015).
11. Polykratis, A. et al. *Nat. Cell Biol.* **21**, 731–742 (2019).

Competing interests

The authors declare no competing interests.

PROTEIN EVOLUTION

Too much can be as bad as too little

Transcription-factor paralogs are not equivalent and serve distinct roles in immune cells. Analysis of the RUNX family of transcription factors reveals insights into the non-redundant roles of RUNX1 and RUNX3.

Wooseok Seo and Ichiro Taniuchi

Stronger binding to motif sequences in DNA by distinct paralogs within a transcription-factor family is not always better, as weak DNA-binding interactions can nevertheless have important biological functions. In this issue of *Nature Immunology*, Bruno et al. assess transcription factors of RUNX ('RUNT-related') family that are expressed in cells of the immune system and reveal that RUNX proteins differ in their regulatory strength (and, hence, their functional activity) and report how this evolution of varying 'strength' serves a biological role[1].

III. Osteoclasts in health and disease

Osteoclasts in health and disease

Bone homeostasis

The human skeleton consists of bone, a connective tissue of which the main function is to provide structural support to the body and to protect vital internal organs, including the bone marrow. Next to this, bone functions as a metabolic organ assuring homeostasis by serving as a reservoir for calcium, phosphate and growth factors[1]. Two distinct types of bone can be distinguished : the cortical bone consisting of mineralized hardened bone providing strength, and the spongy trabecular bone found in the axial skeleton and at the end of long bones[2]. Bone is a highly dynamic organ which is constantly broken down, a process called 'bone resorption', and reformed by a process called 'bone remodeling'. This is a highly regulated process that requires the "coupling" of bone resorption and bone formation to maintain bone homeostasis. Perturbations in this balance result in low bone density, a disease called osteoporosis, or in too dense bones, known as osteopetrosis[3].

Bone cells and their role in remodeling

Four distinct types of bone cells that play an important role in bone remodeling have been described: osteocytes, osteoblasts, bone lining cells and osteoclasts[4,5]. Osteocytes are a highly abundant cell type distributed in the bone matrix that act as mechanosensors and are important regulators of the bone remodeling process [4-6]. Bone lining cells are flat-shaped mature osteoblasts that are in a quiescent state and line the bone surface as a monolayer. The exact functions of these cells are still not completely understood[5]. Osteoblasts are mononucleated cells derived from mesenchymal stem cells (MSC) that are responsible for the formation of bone mineral matrix by producing osteoid, an organic matrix consisting largely of type I collagen[5]. Finally, osteoclasts are the bone resorbing cells. These are multinucleated cells that differentiate from the monocyte/macrophage lineage under influence of two critical factors, namely macrophage colony-stimulating factor (M-CSF) and receptor activator of NF-κB (RANK) ligand (RANKL)[5].

Bone remodeling, replacing old bone with new bone, takes place in micro-scale in the so called bone remodeling compartment (BRC). The BRC is a highly vascularized closed compartment, delineated by a canopy of bone lining cells, which brings osteoclasts and osteoblasts in close proximity to support "coupling"[4,7](Fig. 1). A cycle of bone remodeling consists of four major stages. It starts with the initiation or activation stage where osteocytes induce the detachment of bone lining cells from the

surface to form a canopy and recruit osteoclast precursors cells (OPC) from the circulation, which will then differentiate into mature bone resorbing osteoclasts. This is followed by a resorption phase where osteoclasts brake down bone matrix, releasing several factors form the matrix that couple bone degradation to bone reformation to prevent a change in bone mass after each cycle. This phase ends with a process of osteoclast apoptosis. During the bone formation stage, osteoblasts differentiate from MSCs, get activated and produce osteoid to fill the gaps formed by bone resorption. Finally, during the termination phase, new bone matrix is formed by the mineralization of the osteoid. Osteoblast are removed via apoptosis, differentiate into bone lining cells, or are captured in the newly formed matrix and differentiate into osteocytes [4,7].

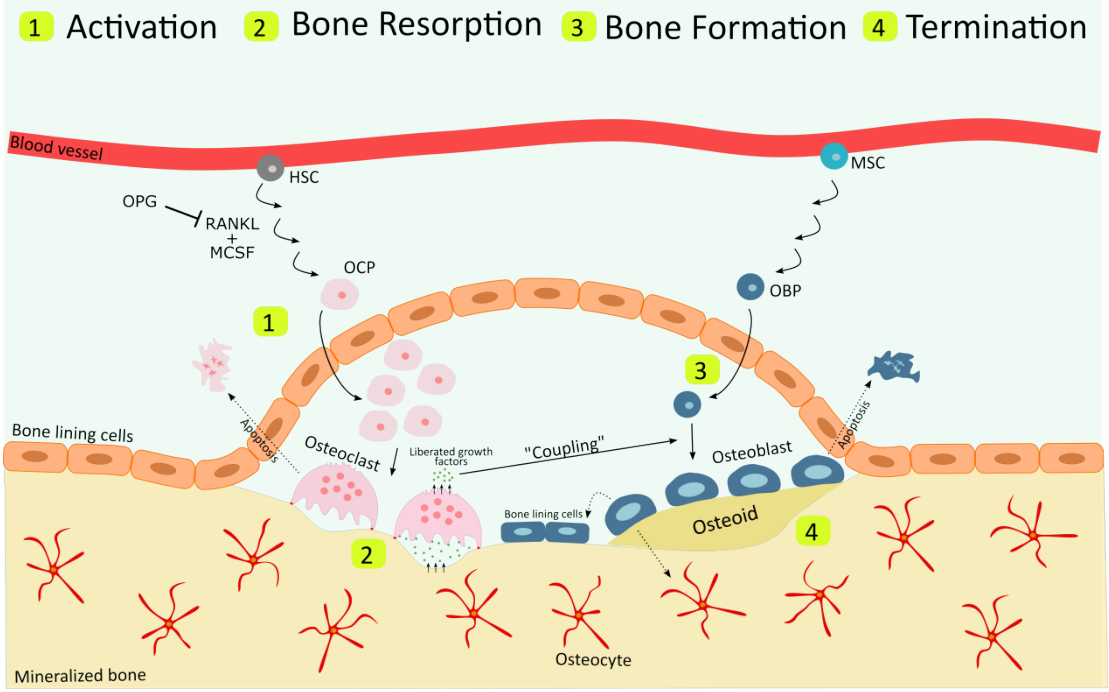

Fig. 1 The bone remodeling compartment. Different stages of the bone remodeling cycle. 1) The activation stage initiated by osteocyte signaling. Bone lining cells detach from the bone surface and form a canopy to which OCPs are recruited to form mature multinucleated osteoclasts. 2) The bone resorption stage, during which osteoclasts degrade bone matrix, releasing several factors from the matrix that couple bone degradation to bone reformation. Bone resorption is ended by osteoclast apoptosis. 3) The bone formation stage, where osteoblast are differentiated from MSC and are recruited to the bone surface where they produce osteoid. 4) The termination phase, where new bone matrix is formed by the mineralization of osteoid. Osteoblasts are removed via apoptosis, differentiate into bone lining cells or are captured in the newly formed matrix and differentiate into osteocytes. HSC, Hematopoietic stem cell; MSC, Mesenchymal stem cell; OCP, Osteoclast precursor; OBP, Osteoblast precursor.

Osteoclasts

Osteoclasts are multinucleated cells formed by the fusion of osteoclast precursors derived from the monocyte/macrophage lineage. These cells have an irregular shape in which distinct membrane

areas can be delineated (Fig. 2). Activated osteoclasts adhere to the bone surface and form tightly sealed resorption pits. These resorption pits are formed by a circular outer membrane domain in the osteoclasts, called the sealing zone, that is formed by podosomes mainly consisting of actin microfilaments, actin binding proteins, adhesion proteins and integrins. This structure is also known as the actin ring[8,9]. Within the sealing zone, the membrane, called the ruffled border, consists of membrane expansions that are responsible for the trafficking of protons and proteases into the resorption pit to degrade the bone matrix[8,9]. Finally, the degraded matrix products are taken up by the osteoclast via endocytosis and are released into the vascular system through the functional secretory domain (FSD), the membrane located at the opposite site of the ruffled borded[8,9] (Fig. 2).

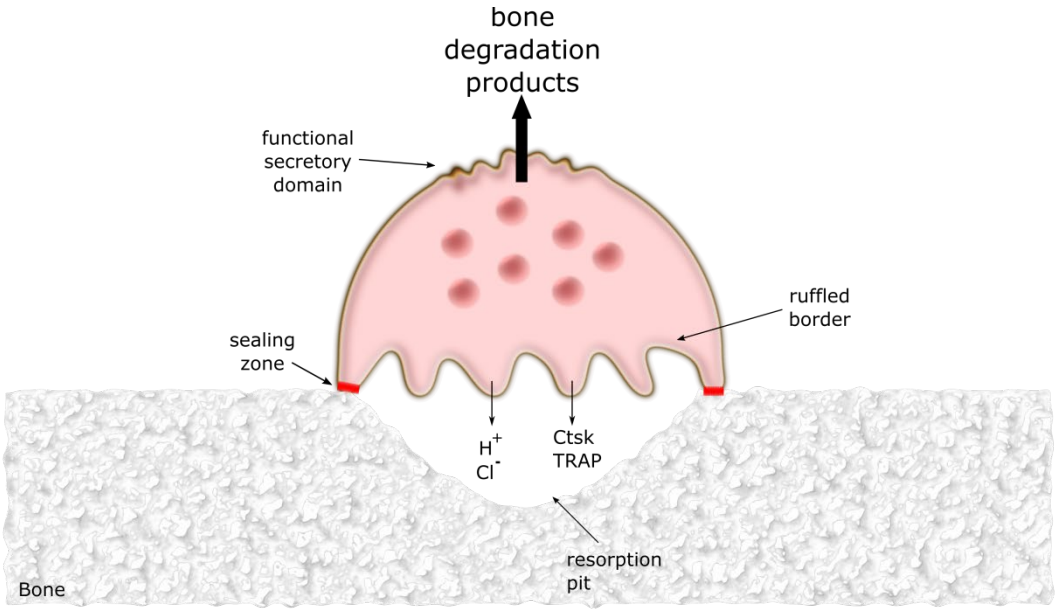

Fig. 2 Bone resorbing osteoclast. Schematic overview of a mature multinucleated osteoclast attached to the bone surface via the sealing zone, forming a tightly sealed resorption pit. Osteoclasts acidify the resorption pit by the release of protons (H^+) to demineralize the inorganic matrix, and by the secretion of Cl^- to neutralize the H^+ release. Lytic enzymes, cathepsin-K (Ctsk) and tartrate-resistant acid phosphatase (TRAP), are also secreted via the ruffled border to degrade the organic matrix. Bone degradation products are taken up by endocytosis and released via the functional secretory domain (FSD) into the vascular system.

Bone consists of both inorganic (primarily hydroxyapatite) and organic (primarily type I collagen) material. Osteoclasts acidify the resorption pit through the release of protons (H^+), to demineralize the bone matrix and expose the organic content. Next, also lytic enzymes, of which tartrate-resistant acid phosphatase (TRAP) and cathepsin K (CtsK) are the most important, are secreted into the resorption pit to degrade the organic matrix[4,10].

Osteoclastogenesis depends on M-CSF and RANKL, two critical factors that are sufficient to induce osteoclast differentiation *in vitro*[11]. Binding of M-CSF to its cognate receptor c-Fms stimulates

osteoclast precursor proliferation and survival, and is important in mature osteoclasts for cytoskeletal reorganization and osteoclast motility[12]. M-CSF is produced by different cell types, of which osteoblasts and stromal cells are the most important ones in the context of osteoclastogenesis[4]. Next to M-CSF, also RANKL is critically important for osteoclastogenesis, and RANK deficient mice do not have mature osteoclasts and develop osteopetrosis[13]. RANK expression on the surface of osteoclast precursors is induced by M-CSF. Several cell types express RANKL in the context of bone remodeling, including stromal cells, osteoblasts, osteocytes, B cells and T cells[4]. Binding of RANKL to its receptor RANK activates several downstream signaling pathways, eventually leading to the expression of osteoclast-specific genes important for osteoclast differentiation, activation and bone degradation[10]. Osteoclastogenesis is also regulated by osteoprotegerin (OPG), a soluble protein expressed by osteoblasts and stromal cells that blocks osteoclast differentiation and activation by acting as a decoy receptor for RANKL thereby competing with RANK[14]. Strictly regulated expression of RANKL and OPG is therefore important to keep proper bone homeostasis.

RANK signaling in osteoclastogenesis

Since RANK, a member of the tumor necrosis factor (TNF) receptor (TNFR) superfamily, does not contain intrinsic enzymatic activity, it requires the recruitment of adaptor molecules to facilitate downstream signaling and induce gene expression[15]. Upon binding of RANKL to RANK, various TNFR-associated factors (TRAFs) are recruited to the cytoplasmic tail of RANK, including TRAF2, TRAF5 and TRAF6. However, only deletion of TRAF6 in mice results in the absence of mature osteoclasts and the development of osteopetrosis[16], while deletion of TRAF2 or TRAF5 only results in minor effects on osteoclastogenesis *in vitro*[17,18]. Recruitment of TRAF6 to the ligated RANK receptor rapidly induces the activation of several downstream signaling pathways, eventually leading to the activation of the transcription factors nuclear factor-κB (NF-κB) and activator protein-1 (AP-1) (Fig. 3). Canonical NF-κB is activated through the recruitment and activation of the TAK1 (TGFβ-activated kinase 1)-TAB2 (TAK1 binding protein 2) complex, which in its turn activates the inhibitor of κB (IκB) kinase (IKK) complex by phosphorylation of IKKβ, leading to the degradation of IκBa, releasing the p50/p65 NF-κB dimer[19,20]. Alternatively, the IKK complex can be activated through the p62-mediated recruitment of the atypical protein kinase C (aPKC), which has been shown to be important for induced but not basal osteoclastogenesis[21]. Binding of RANKL to RANK can also activate signaling through the non-canonical NF-κB pathway, involving NF-κB-inducing kinase (NIK) and IKKα, inducing the expression of osteoclast-specific genes. However, while OCPs from $NIK^{-/-}$ or $IKK\alpha^{-/-}$ mice do not form osteoclasts *in vitro* upon RANKL stimulation, mice deficient for NIK, p100, RelB or IKKα do not develop an osteopetrosis phenotype nor show a reduction in the number of osteoclasts, indicating that non-

canonical signaling is important for the induced osteoclastogenesis but not the basal osteoclastogenesis[19] (Fig. 3).

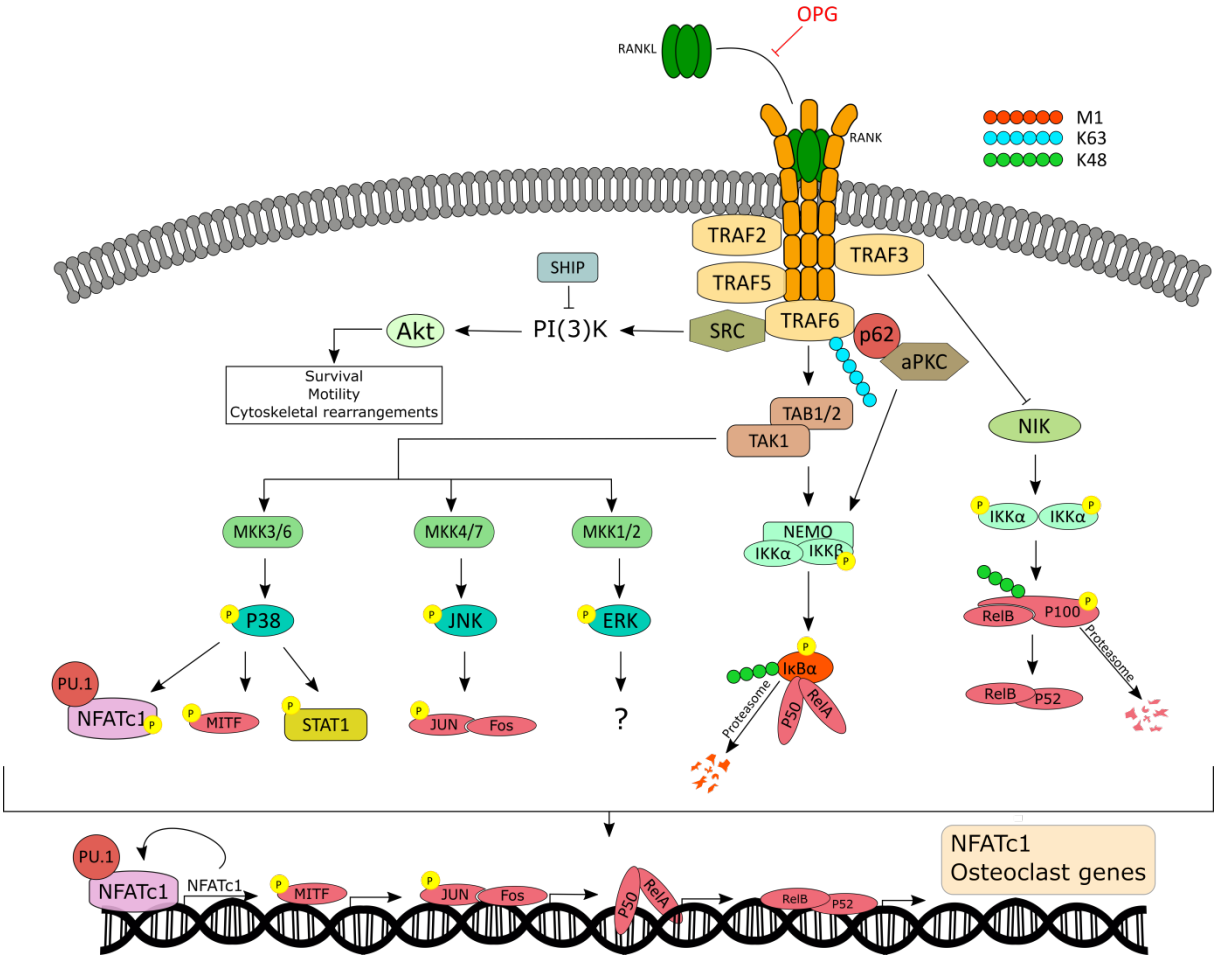

Fig. 3 RANK-induced signaling important for osteoclastogenesis. Binding of RANKL to its cognate receptor RANK induces the recruitment of several adaptor molecules of which TRAF6 is the central player, activating several downstream signaling pathways involving the activation of NF-κB, MAP kinases and the PI(3)K/AKT pathway This induces the expression of the master regulator of osteoclastogenesis, NFATc1, and initiates expression of osteoclast-specific genes important for osteoclastogenesis.

Also members of the mitogen activated protein kinase (MAPK) family, c-Jun N-terminal kinase (JNK), p38 and extracellular signal–regulated kinase (ERK) 1/2 play an important role in osteoclastogenesis downstream of RANK[3]. Activation of these kinases relies on the recruitment of TRAF6 to the RANK receptor. JNK, activated through the RANK-TRAF6-TAK1-MKK4/7 axis, phosphorylates the Jun component of the AP-1 transcription factor, inducing the expression of osteoclast-specific genes[22]. p38, phosphorylated and activated through the RANK-TRAF6-TAK1-MKK3/6 axis, directly phosphorylates and activates the transcription factors nuclear factor-activated T cells c1 (NFATc1) and microphthalmia transcription factor (MITF, important for the differentiation of osteoclasts)[22-24].

Furthermore, p38 was shown to directly promote NF-κB transcriptional activity by phosphorylating the p65 subunit of NF-κB[25]. Finally, p38 also directly phosphorylates STAT1, important for the adhesion and migration of osteoclasts, and MAPK-activated protein kinase-2 (MK2), critical for the expression of genes responsible for OPC fusion, including osteoclast stimulatory transmembrane protein (OC-stamp) and dendrocyte expressed seven transmembrane protein (DC-stamp)[22]. Although ERK1/2 is activated upon RANKL stimulation and has been shown to promote osteoclastogenesis, it is still not clear how ERK is involved in RANK signaling. However, ERK is important for M-CSF-induced signaling and directly phosphorylates MITF and Fos[26,27] (Fig. 3).

Finally, TRAF6 also recruits Src to the receptor, allowing downstream signaling through phosphatidylinositol 3-OH kinase (PI(3)K) and the serine/threonine protein kinase AKT. PI(3)K and AKT are important for cell survival, cytoskeletal rearrangements and osteoclast motility, and mutation of the *c-src* proto-oncogene results in the development of osteopetrosis in mice. PI(3)K signaling is negatively regulated by SHIP, a lipid phosphatase, and SHIP deficiency results in increased numbers of osteoclasts and in the development of severe osteoporosis in mice [3,10] (Fig. 3).

Several osteoclast-specific genes, critical for osteoclast differentiation, are expressed via activation of the transcription factors NF-κB and AP-1. However, the main downstream target of RANK signaling is the so called "master regulator of osteoclast differentiation", NFATc1, a transcription factor responsible for the expression of critical osteoclast genes such as TRAP, cathepsin K and the calcitonin receptor (CalcR)[28], while RANK-induced transcription factors c-Fos, p65/p50 NF-κB and AP-1 are mainly important for the expression of NFATc1[29].

Inflammation and osteoclasts

Several inflammatory cytokines, including TNF, interleukin (IL)-1 and IL-6 have a stimulatory effect on osteoclast differentiation *in vitro* and promote bone resorption in the presence of RANKL *in vivo*. RANKL, TNF, IL-1 and IL-6 share common downstream signaling pathways and might therefore act synergistically to induce osteoclastogenesis[3]. Elevated levels of inflammatory cytokines are found in rheumatoid arthritis (RA) patients, where bone loss can be detected at the sites of (peri)-articular inflammation[30]. IL-6 alone or in cooperation with TNF can indirectly induce osteoclastogenesis by upregulating the expression of RANKL by synovial fibroblasts[31]. This is important in the context of RA, since mice lacking RANKL specifically in the synovial fibroblasts are greatly protected from a model of inflammatory arthritis[32]. TNF directly stimulates osteoclastogenesis by stimulating OPC proliferation and by promoting osteoclast differentiation in presence of permissive levels of RANKL[33,34]. In absence of RANKL, TNF/IL-6 can induce mature functional osteoclasts *in vitro*[35]. Also IL-1 can induce

differentiation of multinucleated bone-resorbing osteoclasts from OCPs *in vitro* in the absence of osteoblasts/stromal cells[36].

NF-κB signaling is heavily regulated by reversible ubiquitination and several deubiquitinating enzymes (DUBs), including A20, cylindromatosis (CYLD) and OTULIN, have been shown to critically regulate NF-κB signaling downstream of several immune receptors, including TNF and IL-1. CYLD has also been shown to negatively regulate RANK-induced NF-κB signaling and osteoclastogenesis, and CYLD knockout mice were shown to develop severe osteoporosis. Upon RANK activation, CYLD is recruited to TRAF6 via interaction with the adaptor protein p62[37]. No other DUBs regulating RANK-induced signaling have been characterized so far. However, mice that lack A20 in their myeloid cells ($A20^{myel\text{-}KO}$) develop spontaneous erosive polyarthritis that resembles human RA, and blood leukocytes from these mice show significantly increased osteoclastogenesis in the presence of RANKL *in vitro*[38]. This suggests that the enhanced osteoclastogenesis observed in $A20^{myel\text{-}KO}$ is due to the presence of increased levels of inflammatory cytokines, or is a direct consequence of the lack of control on RANK signaling and osteoclastogenesis in the absence of A20. To study the specific role of A20 in the direct regulation of RANK-induced osteoclastogenesis, osteoclast-specific deletion of A20 will be needed.

References

1 Clarke, B. Normal bone anatomy and physiology. *Clin J Am Soc Nephrol* **3 Suppl 3**, S131-139, doi:10.2215/CJN.04151206 (2008).

2 Zaidi, M. Skeletal remodeling in health and disease. *Nat Med* **13**, 791-801, doi:10.1038/nm1593 (2007).

3 Wada, T., Nakashima, T., Hiroshi, N. & Penninger, J. M. RANKL-RANK signaling in osteoclastogenesis and bone disease. *Trends Mol Med* **12**, 17-25, doi:10.1016/j.molmed.2005.11.007 (2006).

4 Feng, X. & Teitelbaum, S. L. Osteoclasts: New Insights. *Bone Res* **1**, 11-26, doi:10.4248/BR201301003 (2013).

5 Florencio-Silva, R., Sasso, G. R., Sasso-Cerri, E., Simoes, M. J. & Cerri, P. S. Biology of Bone Tissue: Structure, Function, and Factors That Influence Bone Cells. *Biomed Res Int* **2015**, 421746, doi:10.1155/2015/421746 (2015).

6 Goldring, S. R. The osteocyte: key player in regulating bone turnover. *RMD Open* **1**, e000049, doi:10.1136/rmdopen-2015-000049 (2015).

7 Kenkre, J. S. & Bassett, J. The bone remodelling cycle. *Ann Clin Biochem* **55**, 308-327, doi:10.1177/0004563218759371 (2018).

8 Cappariello, A., Maurizi, A., Veeriah, V. & Teti, A. The Great Beauty of the osteoclast. *Arch Biochem Biophys* **558**, 70-78, doi:10.1016/j.abb.2014.06.017 (2014).

9 Itzstein, C., Coxon, F. P. & Rogers, M. J. The regulation of osteoclast function and bone resorption by small GTPases. *Small GTPases* **2**, 117-130, doi:10.4161/sgtp.2.3.16453 (2011).

10 Boyle, W. J., Simonet, W. S. & Lacey, D. L. Osteoclast differentiation and activation. *Nature* **423**, 337-342, doi:10.1038/nature01658 (2003).

11 Quinn, J. M., Elliott, J., Gillespie, M. T. & Martin, T. J. A combination of osteoclast differentiation factor and macrophage-colony stimulating factor is sufficient for both human and mouse osteoclast formation in vitro. *Endocrinology* **139**, 4424-4427, doi:10.1210/endo.139.10.6331 (1998).

12 Teitelbaum, S. L. & Ross, F. P. Genetic regulation of osteoclast development and function. *Nat Rev Genet* **4**, 638-649, doi:10.1038/nrg1122 (2003).

13 Dougall, W. C. *et al.* RANK is essential for osteoclast and lymph node development. *Genes Dev* **13**, 2412-2424, doi:10.1101/gad.13.18.2412 (1999).

14 Udagawa, N. *et al.* Osteoprotegerin produced by osteoblasts is an important regulator in osteoclast development and function. *Endocrinology* **141**, 3478-3484, doi:10.1210/endo.141.9.7634 (2000).

15 Park, J. H., Lee, N. K. & Lee, S. Y. Current Understanding of RANK Signaling in Osteoclast Differentiation and Maturation. *Mol Cells* **40**, 706-713, doi:10.14348/molcells.2017.0225 (2017).

16 Lomaga, M. A. *et al.* TRAF6 deficiency results in osteopetrosis and defective interleukin-1, CD40, and LPS signaling. *Genes Dev* **13**, 1015-1024, doi:10.1101/gad.13.8.1015 (1999).

17 Kanazawa, K., Azuma, Y., Nakano, H. & Kudo, A. TRAF5 functions in both RANKL- and TNFalpha-induced osteoclastogenesis. *J Bone Miner Res* **18**, 443-450, doi:10.1359/jbmr.2003.18.3.443 (2003).

18 Kanazawa, K. & Kudo, A. TRAF2 is essential for TNF-alpha-induced osteoclastogenesis. *J Bone Miner Res* **20**, 840-847, doi:10.1359/JBMR.041225 (2005).

19 Boyce, B. F., Xiu, Y., Li, J., Xing, L. & Yao, Z. NF-kappaB-Mediated Regulation of Osteoclastogenesis. *Endocrinol Metab (Seoul)* **30**, 35-44, doi:10.3803/EnM.2015.30.1.35 (2015).

20 Mizukami, J. *et al.* Receptor activator of NF-kappaB ligand (RANKL) activates TAK1 mitogen-activated protein kinase kinase kinase through a signaling complex containing RANK, TAB2, and TRAF6. *Mol Cell Biol* **22**, 992-1000, doi:10.1128/mcb.22.4.992-1000.2002 (2002).

21 Duran, A. *et al.* The atypical PKC-interacting protein p62 is an important mediator of RANK-activated osteoclastogenesis. *Dev Cell* **6**, 303-309 (2004).
22 Lee, K., Seo, I., Choi, M. H. & Jeong, D. Roles of Mitogen-Activated Protein Kinases in Osteoclast Biology. *Int J Mol Sci* **19**, doi:10.3390/ijms19103004 (2018).
23 Matsumoto, M. *et al.* Essential role of p38 mitogen-activated protein kinase in cathepsin K gene expression during osteoclastogenesis through association of NFATc1 and PU.1. *J Biol Chem* **279**, 45969-45979, doi:10.1074/jbc.M408795200 (2004).
24 Mansky, K. C., Sankar, U., Han, J. & Ostrowski, M. C. Microphthalmia transcription factor is a target of the p38 MAPK pathway in response to receptor activator of NF-kappa B ligand signaling. *J Biol Chem* **277**, 11077-11083, doi:10.1074/jbc.M111696200 (2002).
25 Huang, H. *et al.* Osteoclast differentiation requires TAK1 and MKK6 for NFATc1 induction and NF-kappaB transactivation by RANKL. *Cell Death Differ* **13**, 1879-1891, doi:10.1038/sj.cdd.4401882 (2006).
26 Weilbaecher, K. N. *et al.* Linkage of M-CSF signaling to Mitf, TFE3, and the osteoclast defect in Mitf(mi/mi) mice. *Mol Cell* **8**, 749-758 (2001).
27 Wagner, E. F. & Matsuo, K. Signalling in osteoclasts and the role of Fos/AP1 proteins. *Ann Rheum Dis* **62 Suppl 2**, ii83-85, doi:10.1136/ard.62.suppl_2.ii83 (2003).
28 Takayanagi, H. *et al.* Induction and activation of the transcription factor NFATc1 (NFAT2) integrate RANKL signaling in terminal differentiation of osteoclasts. *Dev Cell* **3**, 889-901 (2002).
29 Kim, J. H. & Kim, N. Regulation of NFATc1 in Osteoclast Differentiation. *J Bone Metab* **21**, 233-241, doi:10.11005/jbm.2014.21.4.233 (2014).
30 Coury, F., Peyruchaud, O. & Machuca-Gayet, I. Osteoimmunology of Bone Loss in Inflammatory Rheumatic Diseases. *Front Immunol* **10**, 679, doi:10.3389/fimmu.2019.00679 (2019).
31 Hashizume, M., Hayakawa, N. & Mihara, M. IL-6 trans-signalling directly induces RANKL on fibroblast-like synovial cells and is involved in RANKL induction by TNF-alpha and IL-17. *Rheumatology (Oxford)* **47**, 1635-1640, doi:10.1093/rheumatology/ken363 (2008).
32 Danks, L. *et al.* RANKL expressed on synovial fibroblasts is primarily responsible for bone erosions during joint inflammation. *Ann Rheum Dis* **75**, 1187-1195, doi:10.1136/annrheumdis-2014-207137 (2016).
33 Yao, Z. *et al.* Tumor necrosis factor-alpha increases circulating osteoclast precursor numbers by promoting their proliferation and differentiation in the bone marrow through up-regulation of c-Fms expression. *J Biol Chem* **281**, 11846-11855, doi:10.1074/jbc.M512624200 (2006).
34 Lam, J. *et al.* TNF-alpha induces osteoclastogenesis by direct stimulation of macrophages exposed to permissive levels of RANK ligand. *J Clin Invest* **106**, 1481-1488, doi:10.1172/JCI11176 (2000).
35 O'Brien, W. *et al.* RANK-Independent Osteoclast Formation and Bone Erosion in Inflammatory Arthritis. *Arthritis Rheumatol* **68**, 2889-2900, doi:10.1002/art.39837 (2016).
36 Jimi, E. *et al.* Interleukin 1 induces multinucleation and bone-resorbing activity of osteoclasts in the absence of osteoblasts/stromal cells. *Exp Cell Res* **247**, 84-93, doi:10.1006/excr.1998.4320 (1999).
37 Jin, W. *et al.* Deubiquitinating enzyme CYLD negatively regulates RANK signaling and osteoclastogenesis in mice. *J Clin Invest* **118**, 1858-1866, doi:10.1172/JCI34257 (2008).
38 Matmati, M. *et al.* A20 (TNFAIP3) deficiency in myeloid cells triggers erosive polyarthritis resembling rheumatoid arthritis. *Nat Genet* **43**, 908-912, doi:10.1038/ng.874 (2011).

Part II
Aim and objectives

Aims and objectives

NF-κB signaling is essential in immunity, inflammation and development, and dysregulation of NF-κB-dependent gene expression contributes to a variety of (auto-)inflammatory and autoimmune diseases, and eventually cancer[1,2]. Therefore tight regulation of NF-κB signaling is needed to maintain tissue homeostasis and prevent the development of inflammatory pathology. Several (auto)regulatory mechanisms are known to control inflammatory pathways[3]. One critical regulator of NF-κB activation is A20, a protein that is rapidly induced in inflammatory conditions[4].

A20 is a potent anti-inflammatory protein, acting by inhibiting NF-κB signaling and inflammatory gene expression and/or by preventing cell death. Genome-wide association studies (GWAS) have identified single nucleotide polymorphisms (SNPs) in or around the *A20/TNFAIP3* locus, identifying A20 as a disease susceptibility gene for a variety of human inflammatory and autoimmune diseases, including rheumatoid arthritis (RA), systemic lupus erythematosus (SLE) and inflammatory bowel disease (IBD)[5,6]. More recently, in patients with an early-onset autoinflammatory syndrome, heterozygous loss-of-function mutations in the *A20/TNFAIP3* gene have been identified[7-9]. Experimental studies in mice have confirmed the important anti-inflammatory role of A20. Mice deficient for A20 die perinatally due to severe multi-organ inflammation, and tissue-specific deletion of A20 demonstrated the importance of A20 in preventing cell death and inflammation in order to maintain tissue homeostasis. Together, these data illustrate the important function of A20 in the regulation of inflammatory signaling and cell death, however, the *in vivo* mechanisms by which A20 performs these functions still remain elusive.

While *in vitro* experiments have shown that A20 regulates NF-κB signaling by removing ubiquitin chains via the DUB activity of its OTU-domain and targets proteins for ubiquitination and subsequent degradation via the E3 ligase activity of its ZnF4 domain [10], transgenic mouse lines abrogating *in vivo* the DUB activity or the E3 ligase activity do not develop spontaneous disease, questioning the *in vivo* importance of these functions[11-13]. However *in vitro* studies have shown that the ZnF7 domain of A20, which binds to linear ubiquitin chains, is critical for the recruitment of A20 to TNFR1 and NOD2 receptor complexes, and prevents NF-κB signaling and cell death in a non-enzymatic way [14-17].

The main aim of this PhD thesis was to further understand the molecular mechanisms by which A20 regulates inflammation and cell death *in vivo*. Therefore, we generated mice with disruptive point mutations in the ZnF7 domain of A20 abrogating its capacity to bind linear ubiquitin. In parallel, we generated mice with mutations in both the ZnF4 and ZnF7 domains of A20, also preventing the binding of A20 to K63-specific ubiquitin. These mice and cells thereof were used to challenge the

hypothesis that A20 prevents inflammation in a non-catalytic way by acting as a ubiquitin-binding protein.

Next to its role in inflammatory signaling, A20 was previously demonstrated to control non-inflammatory developmental signaling pathways. In this context, epidermis-specific A20 deficient mice were shown to develop ectodermal organ abnormalities due to dysregulated NF-κB signaling induced by the activation of Ectodysplasin A receptor (EDAR) signaling[18]. Myeloid-specific A20 deficient mice develop spontaneous polyarthritis resembling human rheumatoid arthritis[19]. Interestingly, these mice have increased numbers of osteoclast precursors and form more TRAP-positive multinucleated osteoclast from leukocytes stimulated with RANKL *in vitro*, suggesting a role for A20 in regulating RANK-induced NF-κB signaling[19]. This enhanced osteoclastogenesis may, however, also result from the more general inflammatory condition of myeloid-specific A20 deficient mice, since inflammatory cytokines are known to promote osteoclastogenesis[20,21]. To investigate the direct role of A20 in regulating osteoclastogenesis, we have generated osteoclast-specific A20 deficient mice. *In vivo* and *in vitro* analyses of these mice and cells thereof were used to demonstrate a direct regulatory role of A20 in the regulation of RANK-induced osteoclastogenesis and bone homeostasis *in vivo*.

References

1 Kondylis, V., Kumari, S., Vlantis, K. & Pasparakis, M. The interplay of IKK, NF-kappaB and RIPK1 signaling in the regulation of cell death, tissue homeostasis and inflammation. *Immunol Rev* **277**, 113-127, doi:10.1111/imr.12550 (2017).

2 Lork, M., Verhelst, K. & Beyaert, R. CYLD, A20 and OTULIN deubiquitinases in NF-kappaB signaling and cell death: so similar, yet so different. *Cell Death Differ* **24**, 1172-1183, doi:10.1038/cdd.2017.46 (2017).

3 Renner, F. & Schmitz, M. L. Autoregulatory feedback loops terminating the NF-kappaB response. *Trends Biochem Sci* **34**, 128-135, doi:10.1016/j.tibs.2008.12.003 (2009).

4 Verstrepen, L. *et al.* Expression, biological activities and mechanisms of action of A20 (TNFAIP3). *Biochem Pharmacol* **80**, 2009-2020, doi:10.1016/j.bcp.2010.06.044 (2010).

5 Ma, A. & Malynn, B. A. A20: linking a complex regulator of ubiquitylation to immunity and human disease. *Nat Rev Immunol* **12**, 774-785, doi:10.1038/nri3313 (2012).

6 Catrysse, L. *et al.* A20 prevents chronic liver inflammation and cancer by protecting hepatocytes from death. *Cell Death Dis* **7**, e2250, doi:10.1038/cddis.2016.154 (2016).

7 Zhou, Q. *et al.* Loss-of-function mutations in TNFAIP3 leading to A20 haploinsufficiency cause an early-onset autoinflammatory disease. *Nat Genet* **48**, 67-73, doi:10.1038/ng.3459 (2016).

8 Aeschlimann, F. A. *et al.* A20 haploinsufficiency (HA20): clinical phenotypes and disease course of patients with a newly recognised NF-kB-mediated autoinflammatory disease. *Ann Rheum Dis* **77**, 728-735, doi:10.1136/annrheumdis-2017-212403 (2018).

9 Duncan, C. J. A. *et al.* Early-onset autoimmune disease due to a heterozygous loss-of-function mutation in TNFAIP3 (A20). *Ann Rheum Dis* **77**, 783-786, doi:10.1136/annrheumdis-2016-210944 (2018).

10 Wertz, I. E. *et al.* De-ubiquitination and ubiquitin ligase domains of A20 downregulate NF-kappaB signalling. *Nature* **430**, 694-699, doi:10.1038/nature02794 (2004).

11 Lu, T. T. *et al.* Dimerization and ubiquitin mediated recruitment of A20, a complex deubiquitinating enzyme. *Immunity* **38**, 896-905, doi:10.1016/j.immuni.2013.03.008 (2013).

12 De, A., Dainichi, T., Rathinam, C. V. & Ghosh, S. The deubiquitinase activity of A20 is dispensable for NF-kappaB signaling. *EMBO Rep* **15**, 775-783, doi:10.15252/embr.201338305 (2014).

13 Wertz, I. E. *et al.* Phosphorylation and linear ubiquitin direct A20 inhibition of inflammation. *Nature* **528**, 370-375, doi:10.1038/nature16165 (2015).

14 Skaug, B. *et al.* Direct, noncatalytic mechanism of IKK inhibition by A20. *Mol Cell* **44**, 559-571, doi:10.1016/j.molcel.2011.09.015 (2011).

15 Verhelst, K. *et al.* A20 inhibits LUBAC-mediated NF-kappaB activation by binding linear polyubiquitin chains via its zinc finger 7. *EMBO J* **31**, 3845-3855, doi:10.1038/emboj.2012.240 (2012).

16 Draber, P. *et al.* LUBAC-Recruited CYLD and A20 Regulate Gene Activation and Cell Death by Exerting Opposing Effects on Linear Ubiquitin in Signaling Complexes. *Cell Rep* **13**, 2258-2272, doi:10.1016/j.celrep.2015.11.009 (2015).

17 Tokunaga, F. *et al.* Specific recognition of linear polyubiquitin by A20 zinc finger 7 is involved in NF-kappaB regulation. *EMBO J* **31**, 3856-3870, doi:10.1038/emboj.2012.241 (2012).

18 Lippens, S. *et al.* Keratinocyte-specific ablation of the NF-kappaB regulatory protein A20 (TNFAIP3) reveals a role in the control of epidermal homeostasis. *Cell Death Differ* **18**, 1845-1853, doi:10.1038/cdd.2011.55 (2011).

19 Matmati, M. *et al.* A20 (TNFAIP3) deficiency in myeloid cells triggers erosive polyarthritis resembling rheumatoid arthritis. *Nat Genet* **43**, 908-912, doi:10.1038/ng.874 (2011).

20 Lam, J. *et al.* TNF-alpha induces osteoclastogenesis by direct stimulation of macrophages exposed to permissive levels of RANK ligand. *J Clin Invest* **106**, 1481-1488, doi:10.1172/JCI11176 (2000).

21 Dai, J. *et al.* Chronic alcohol ingestion induces osteoclastogenesis and bone loss through IL-6 in mice. *J Clin Invest* **106**, 887-895, doi:10.1172/JCI10483 (2000).

Part III
Results

I. Two distinct ubiquitin-binding motifs in A20 mediate its anti-inflammatory and cell-protective activities

Arne Martens[1,2], Dario Priem[1,2], Esther Hoste[1,2], Jessica Vetters[1,3], Sofie Rennen[1,3], Leen Catrysse[1,2], Sofie Voet[1,2], Laura Deelen[1,2], Mozes Sze[1,2], Hanna Vikkula[1,2], Karolina Slowicka[1,2], Tino Hochepied[1,2], Kalliopi Iliaki[4], Andy Wullaert[1,2,3], Sophie Janssens[1,3], Mohamed Lamkanfi[1,3,5], Rudi Beyaert[1,2], Marietta Armaka[4], Mathieu JM Bertrand[1,2] and Geert van Loo[1,2]

1. VIB Center for Inflammation Research, B-9052 Ghent, Belgium.
2. Department of Biomedical Molecular Biology, Ghent University, B-9052 Ghent, Belgium.
3. Department of Internal Medicine and Pediatrics, Ghent University, Ghent, Belgium.
4. Biomedical Sciences Research Center 'Alexander Fleming', G-16672 Vari, Greece
5. Janssen Immunosciences, World without Disease Accelerator, Pharmaceutical Companies of Johnson & Johnson, B-2340 Beerse, Belgium

Manuscript accepted for publication in *Nature Immunology*

Author contributions

A.M., D.P., E.H., J.V., S.R., L.C., S.V., L.D., M.S., H.V., K.S. and K.I. performed the experiments. A.M., D.P., E.H., J.V., S.R., L.C., S.V., T.H., A.W., M.L., M.A., R.B., M.B. and G.v.L. analysed the data. G.v.L. provided ideas and coordinated the project. A.M. and G.v.L. wrote the manuscript.

Two distinct ubiquitin-binding motifs in A20 mediate its anti-inflammatory and cell- protective activities

Abstract

Protein ubiquitination regulates protein stability and modulates the composition of signaling complexes. A20 is a negative regulator of inflammatory signaling, but the molecular mechanisms involved are ill-understood. Here, we generated *Tnfaip3* gene-targeted A20 mutant mice bearing inactivating mutations in the zinc finger 7 (ZnF7) and ZnF4 ubiquitin-binding domains, revealing that binding to polyubiquitin is essential for A20 to suppress inflammatory disease. We demonstrate that a functional ZnF7 domain was required for recruiting A20 to the tumor necrosis factor receptor 1 (TNFR1) signaling complex and to suppress inflammatory signaling and cell death. The combined inactivation of ZnF4 and ZnF7 phenocopied the postnatal lethality and severe multi-organ inflammation of A20-deficient mice. Conditional tissue-specific expression of mutant A20 further revealed the key role of ubiquitin-binding in myeloid and intestinal epithelial cells. Collectively, these results demonstrate that the anti-inflammatory and cytoprotective functions of A20 are largely dependent on its ubiquitin-binding properties.

Main

A20, also referred to as Tumor Necrosis Factor alpha-induced protein 3 (TNFAIP3), has been implicated in diverse inflammatory diseases, and has been shown to act by repressing inflammatory NF-κB signaling and by promoting cell survival [1,2]. A20 is thought to act as a 'ubiquitin-editing' enzyme that inhibits NF-κB signaling by modulating the ubiquitination status of specific signaling proteins through the combined action of its deubiquitinase (DUB) activity and its E3 ubiquitin ligase activity that promotes K48-linked polyubiquitination and proteasomal degradation of its targets following tumor necrosis factor receptor 1 (TNFR1) activation [3]. However, transgenic mouse strains with inactivating mutations in A20's DUB or E3 ligase domains are grossly normal and do not develop spontaneous disease [4-6], in sharp contrast to the systemic inflammatory and perinatal lethality seen in A20-deficient mice [7]. These studies challenged the notion that A20 primarily acts via a 'ubiquitin editing' mechanism to suppress inflammation *in vivo*. Other studies suggest that the 7th zinc finger domain of A20 competes with the IκB kinase (IKK) adaptor protein NEMO for binding to linear (M1) ubiquitin chains generated by the linear ubiquitin chain assembly complex (LUBAC) to repress TNF-induced NF-κB signaling *in vitro* [8-10]. However, the physiological role of A20's ZnF7 domain is not known.

To determine the physiological role of the ZnF7 domain of A20 *in vivo*, we generated *Tnfaip3* gene-targeted A20 mutant mice carrying two cysteine to alanine point mutations in the ZnF7 motif - C764A and C767A (hereafter referred to as $A20^{ZnF7}$) (Extended Data Fig. 1a), which was previously shown to abrogate A20's ability to bind to linear polyubiquitin chains [8,10,11]. Homozygous $A20^{ZnF7/ZnF7}$ knock-in mice, derived from interbred $A20^{ZnF7/+}$ mice, were born with expected Mendelian frequency and did not display perinatal lethality (Extended Data Fig. 1b). This phenotype contrasts markedly with *Tnfaip3*$^{-/-}$ mice that, in our mouse facility, develop perinatal cachexia and die before weaning age (data not shown). However, all $A20^{ZnF7/ZnF7}$ knock-in mice had severely reduced body weight (Fig. 1a, Extended Data Fig. 1c) and only rarely produced offspring. Macroscopic and histological examination of young $A20^{ZnF7/ZnF7}$ mice revealed splenomegaly and lymphadenopathy (Extended Data Fig. 1d), paw swelling with absence of nails (Extended Data Fig. 1e), bone erosion (Extended Data Fig. 1f) and joint inflammation (Extended Data Fig. 1g), as previously shown [11], but also inflammation and immune cell infiltration in other tissues such as in the liver (Fig. 1b). Staining for cleaved caspase-3 revealed the presence of numerous apoptotic cells in $A20^{ZnF7/ZnF7}$ livers but not in control livers (Fig. 1c, d), suggesting that $A20^{ZnF7}$ expression sensitized hepatocytes to apoptosis. This can be due to a direct role for the ZnF7 domain in preventing hepatocyte apoptosis, or indirectly due to the increased levels of cytotoxic cytokines. In agreement with the observed phenotype, $A20^{ZnF7/ZnF7}$ knock-in mice had high serum concentrations of the inflammatory cytokines TNF and interleukin 6 (IL-6, Fig. 1e). Flow

cytometric analyses of spleen tissue from 20 week-old mice revealed that A20$^{ZnF7/ZnF7}$ knock-in mice had increased numbers of myeloid cells but reduced numbers of B cells, T cells and natural killer (NK) cells, demonstrating that A20's ZnF7 domain regulates immune homeostasis (Fig. 1f, Extended Data Fig. 2). Finally, in agreement with the increased TNF concentrations detected in their serum, A20$^{ZnF7/ZnF7}$ myeloid cells displayed enhanced amounts of intracellular TNF (Fig. 1g).

Cachexia and premature lethality in A20-deficient mice were shown to be promoted by MyD88-mediated pro-inflammatory responses in the absence of A20 [12]. To address the role of MyD88-dependent signaling in the inflammatory pathology of A20$^{ZnF7/ZnF7}$ mice, these mice were crossed with *Myd88*$^{-/-}$ animals. As described recently [11], deletion of *Myd88* in A20$^{ZnF7/ZnF7}$ mice partly restored body weight (Extended Data Fig. 3a, b) and A20$^{ZnF7/ZnF7}$ *Myd88*$^{-/-}$ mice were partly protected from developing spontaneous tissue inflammation, as shown by reduced inflammation in liver (Extended Data Fig. 3c) and absence of swollen toes and ankles (Extended Data Fig. 3d). Inflammatory cytokine concentrations in serum of A20$^{ZnF7/ZnF7}$*Myd88*$^{-/-}$ mice were, however, elevated compared to control animals (Extended Data Fig. 3e). Together, these data demonstrate that MyD88-dependent mechanisms contribute to the local inflammatory pathology in the absence of ZnF7-dependent A20 functions, while more systemic inflammation is unaffected.

The role of A20 ZnF7 in regulating inflammation was further evaluated by examining the sensitivity of A20$^{ZnF7/ZnF7}$ mice to TNF *in vivo*. Indeed, an important anti-inflammatory and cytoprotective role for A20 has been demonstrated in intestinal epithelial cells (IECs), and IEC-specific A20-deficient mice (A20$^{IEC\text{-}KO}$) were previously shown to die from a challenge with a normally sublethal dose of TNF [13]. In contrast to the control mice, which all survived and only showed a modest drop in body temperature in the first hours after TNF injection, A20$^{ZnF7/ZnF7}$ mice displayed typical symptoms associated with TNF toxicity, including hypothermia and severe diarrhea, and all died within 3 h after TNF injection (Fig. 1h). A20$^{ZnF7/ZnF7}$ mice displayed severe damage of the small intestine, showing extensive epithelial destruction and presence of numerous cleaved caspase-3 positive apoptotic IECs, in contrast to control littermates which maintained tissue integrity without showing epithelial cell apoptosis. Next to the damage of the intestinal tissue, massive apoptosis could be detected in liver tissue of A20$^{ZnF7/ZnF7}$ mice upon exposure to TNF (Fig. 1i). Together, these data establish that A20's ZnF7 motif is essential to restrict inflammatory responses *in vivo*.

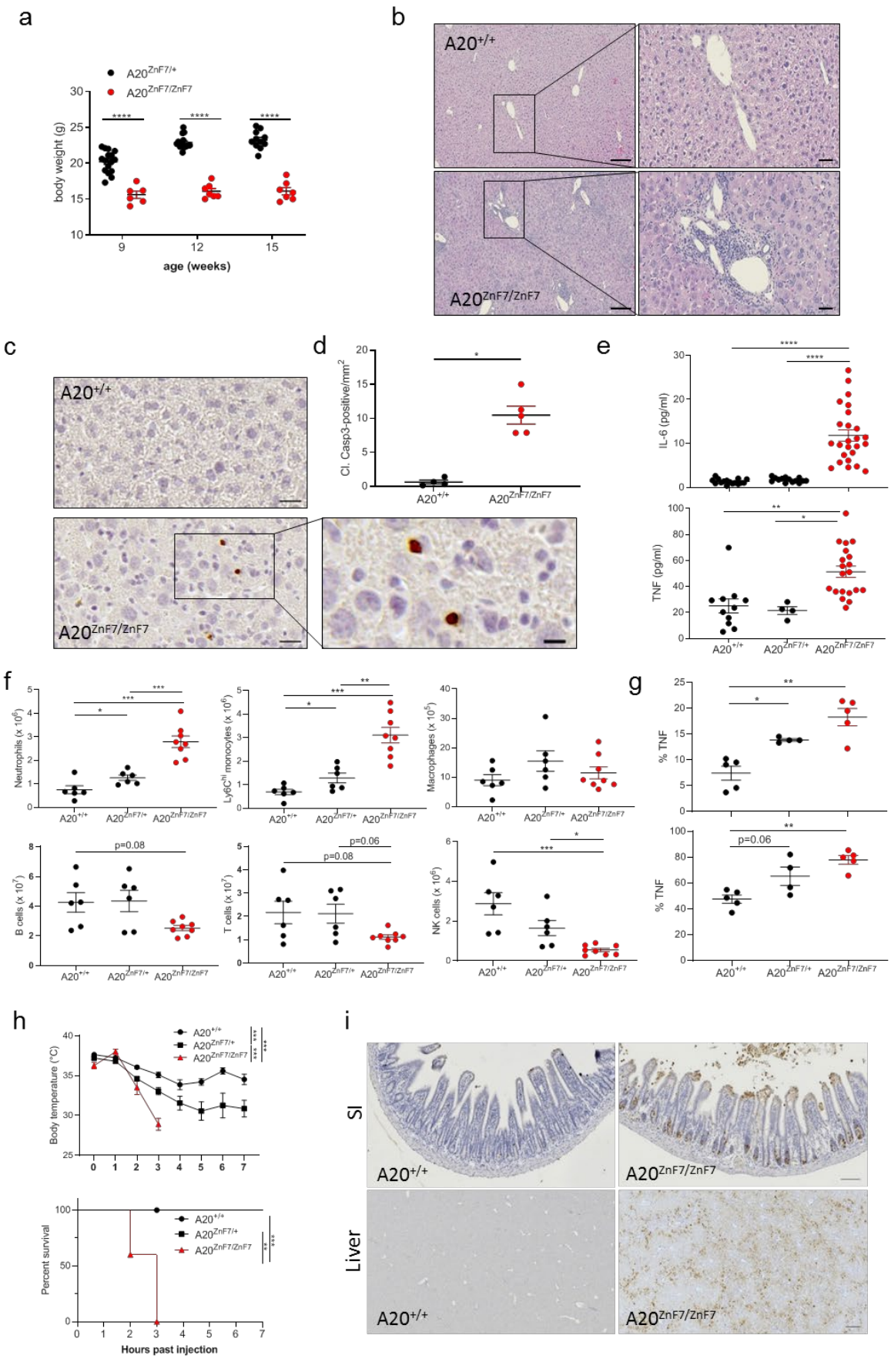
a
A20ZnF7/+
A20ZnF7/ZnF7
body weight (g)
age (weeks)
b
A20+/+
A20ZnF7/ZnF7
c
A20+/+
A20ZnF7/ZnF7
d
Cl. Casp3-positive/mm2
e
IL-6 (pg/ml)
TNF (pg/ml)
f
Neutrophils (x 10^6)
Ly6Chi monocytes (x 10^6)
Macrophages (x 10^5)
B cells (x 10^7)
T cells (x 10^7)
NK cells (x 10^6)
p=0.08
p=0.06
g
% TNF
h
Body temperature (°C)
Percent survival
Hours past injection
i
SI
Liver

Figure 1. A20$^{ZnF7/ZnF7}$ knock-in mice develop spontaneous inflammatory pathology and are sensitized to TNF induced toxicity. (a) Bodyweight of A20$^{ZnF7/+}$ and A20$^{ZnF7/ZnF7}$ mice in function of time. Each dot represents a biologically independent mouse (9 week-old mice: A20$^{ZnF7/+}$, n=16; A20$^{ZnF7/ZnF7}$, n=6; 12 week-old mice: A20$^{ZnF7/+}$, n=15; A20$^{ZnF7/ZnF7}$, n=7; 15week-old mice: A20$^{ZnF7/+}$, n=11; A20$^{ZnF7/ZnF7}$, n=7). Data are expressed as mean ± SEM. **** represents p<0.0001 (parametric two-way ANOVA between indicated genotypes). **(b)** Representative hematoxylin-eosin-stained sections of liver from 28-week-old control (A20$^{+/+}$) and A20$^{ZnF7/ZnF7}$ littermates. Scale bar, 200 μm and 50 μm (insert). Picture representative for at least 5 biologically independent mice per group. **(c-d)** Immunohistochemistry for cleaved caspase 3 on liver sections from A20$^{ZnF7/ZnF7}$ mice and control (A20$^{+/+}$) littermates (c), and number of cleaved caspase 3-positive cells per mm^2 (A20$^{ZnF7/ZnF7}$, n=5 biologically independent samples; A20$^{+/+}$, n=4 biologically independent samples) (d). Pictures shown are representative for 5 biologically independent mice per group. Scale bar, 20 μm (insert, 10 μm) Data are expressed as mean ± SEM. * represents p=0.0159 (Two-sided non-parametric Mann Whitney test between indicated genotypes). **(e)** Levels of IL-6 and TNF in serum of control (A20$^{+/+}$), A20$^{ZnF7/+}$ and A20$^{ZnF7/ZnF7}$ mice at the age between 15 and 30 weeks. Each dot represents a biologically independent mouse (IL-6: A20$^{+/+}$, n=16; A20$^{ZnF7/+}$, n=14; A20$^{ZnF7/ZnF7}$, n=25; TNF: A20$^{+/+}$, n=11; A20$^{ZnF7/+}$, n=4; A20$^{ZnF7/ZnF7}$, n=20). Data are expressed as mean ± SEM. *, ** and **** represent p=0.0133, p=0.0014 and p<0.0001 respectively (parametric one-way ANOVA between indicated genotypes). **(f)** Absolute cell numbers of indicated immune cell populations in the spleens of A20$^{+/+}$, A20$^{ZnF7/+}$ and A20$^{ZnF7/ZnF7}$ mice, as measured by flow cytometry. Each dot represents a biologically independent mouse (A20$^{+/+}$, n=6; A20$^{ZnF7/+}$, n=6; A20$^{ZnF7/ZnF7}$, n=8). Data are expressed as mean ± SEM. *, **, *** represents p < 0.05, p < 0.01 and p < 0.001 (Two-sided non-parametric Mann-Whitney test between indicated genotypes). **(g)** Splenocytes isolated from A20$^{+/+}$, A20$^{ZnF7/+}$ and A20$^{ZnF7/ZnF7}$ mice were incubated for 4 hours in the presence of protein transport inhibitors to assess intracellular TNF production by flow cytometry. Bar graphs represent percentage TNF that is produced within total macrophage (top) and Ly6C^{hi} monocyte (bottom) populations. Each dot represents a biologically independent mouse (A20$^{+/+}$, n=5; A20$^{ZnF7/+}$, n=4; A20$^{ZnF7/ZnF7}$, n=5). Data are expressed as mean ± SEM. * and ** represent p < 0.05 and p < 0.01 respectively (Two-sided non-parametric Mann-Whitney test between indicated genotypes). **(h)** Body temperature and survival of A20$^{ZnF7/ZnF7}$ mice and control littermates injected with recombinant mTNF (i.p., 5 μg / 20 g of bodyweight), in function of time (A20$^{+/+}$, n=7; A20$^{ZnF7/+}$, n=5; A20$^{ZnF7/ZnF7}$, n=5 mice). Data are expressed as mean ± SEM. p < ** and *** represent p<0.01, p<0.001, respectively (body temperature, REML analysis and survival, two-sided mantel-cox test). **(i)** Cleaved caspase 3 staining on sections from small intestine (SI) and liver from control (A20$^{+/+}$) and A20$^{ZnF7/ZnF7}$ mice. Scale bar, 200 μm (liver) and 100 μm (SI). Pictures shown are representative for 5 biologically independent mice per group.

Consistent with the essential role of A20 as a negative feedback regulator of inducible NF-κB–dependent gene expression, cultured mouse embryonic fibroblasts (MEFs) from A20$^{ZnF7/ZnF7}$ knock-in mice demonstrated increased TNF-induced NF-κB signaling, as reflected by earlier phosphorylation and sustained degradation of the NF-κB inhibitory molecule IκBα, and enhanced IL-6 production upon TNF stimulation compared to wild-type MEFs (Fig. 2a, b). Also cultured bone marrow-derived macrophages (BMDMs) from A20$^{ZnF7/ZnF7}$ knock-in mice showed sustained degradation of IκBα and expressed and produced increased amounts of cytokines than control BMDMs in response to lipopolysaccharide (LPS) and TNF (Fig. 2c,d, Extended Data Fig. 4). In agreement with the reported role of A20 ZnF7 in binding M1 ubiquitin chains[8-10], A20 recruitment to the TNFR1 complex was severely impaired upon stimulation of A20$^{ZnF7/ZnF7}$ BMDMs with Flag-tagged TNF, similar to what is

observed in A20-deficient BMDMs (Fig. 2e). Absence of A20 at the membrane-bound signaling complex (known as complex I) was also associated with reduced abundance of M1 chains in the TNFR1 signaling complex I (Fig. 2f), which is consistent with the reported role of A20 recruitment in protecting M1 chains from degradation[9,14]. Mutation of ZnF7 did not prevent the recruitment of RIPK1 and TRADD adaptor proteins to the TNFR1 complex (Fig. 2f). Destabilization of complex I by reduced M1 ubiquitination favored formation of the death-inducing complex II and activation of an apoptotic caspase cascade (Fig. 2g, h), as previously reported[9,14].

We previously demonstrated that mice with a myeloid-restricted deficiency in A20 spontaneously develop polyarthritis caused by myeloid cell necroptosis, NLRP3 inflammasome hyperactivation and IL-1 receptor (IL-1R) signaling [11,15,16]. In agreement, $A20^{ZnF7/ZnF7}$ BMDMs showed significantly enhanced NLRP3 inflammasome-mediated caspase-1 activation, pyroptosis and IL-1β and IL-18 secretion upon stimulation with LPS and ATP (Fig. 2i-k). Together, these data illustrate the importance of the ZnF7 domain of A20 for preserving TNFR1 receptor complex integrity, and preventing cell death, inflammasome activation and inflammation.

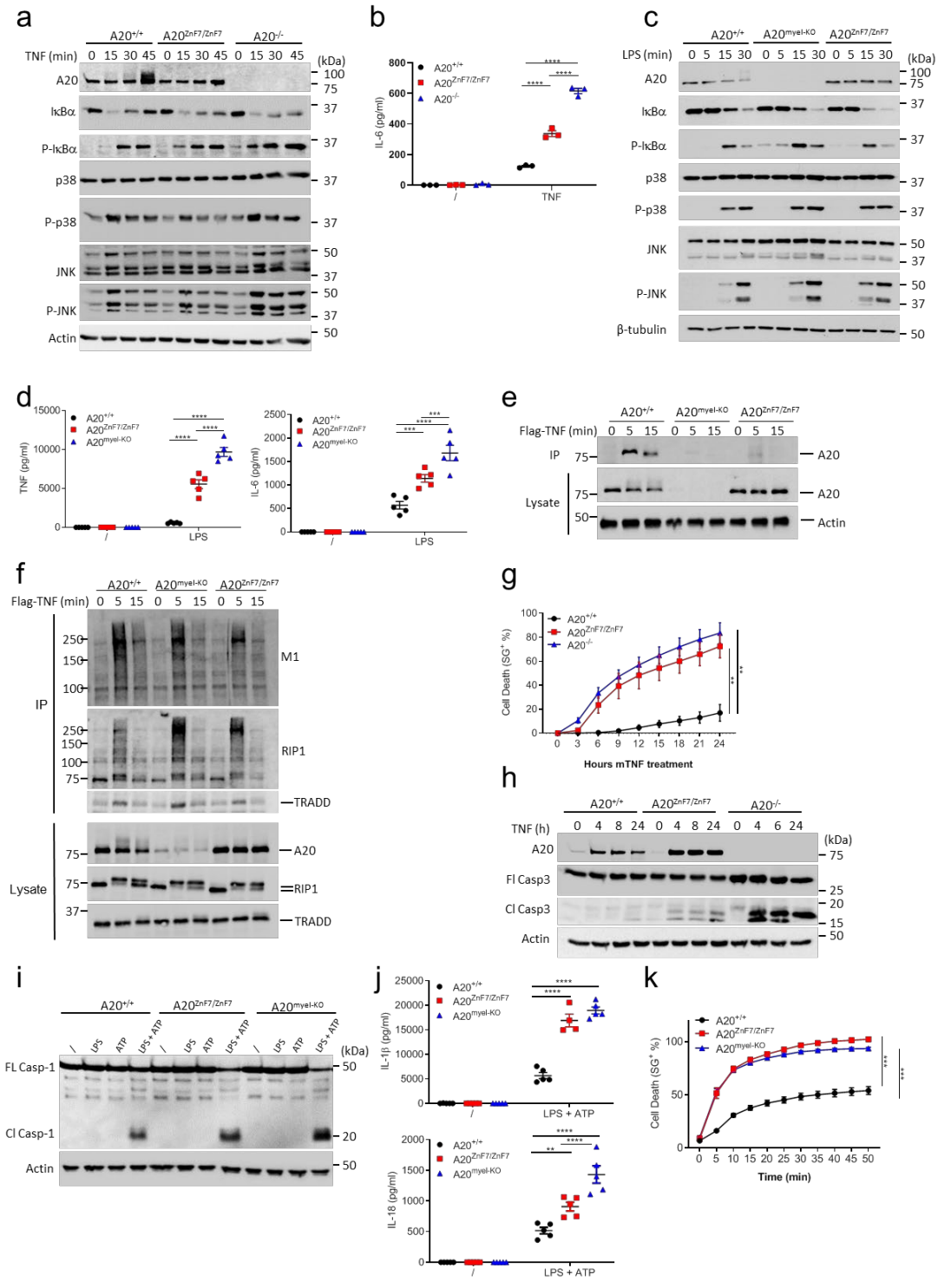

Figure 2. ZnF7 is critical for A20-mediated suppression of inflammatory signaling and cell death. (a) Western blot analysis of whole cell lysates from $A20^{+/+}$, $A20^{ZnF7/ZnF7}$ and $A20^{-/-}$ MEF cells stimulated with TNF for the indicated time periods**.** Actin is shown as a loading control. Figure representative for 3 independent experiments. **(b)** IL-6 secretion by control $A20^{+/+}$, $A20^{ZnF7/ZnF7}$ and $A20^{-/-}$ MEF cells, either or not stimulated with TNF for 4 h ($A20^{+/+}$, n=3; $A20^{ZnF7/ZnF7}$, n=3; $A20^{-/-}$, n=3 independent cell cultures). **** represents p<0.0001 (parametric two-way ANOVA between indicated genotypes). Data are expressed as mean ± SEM. **(c)** Western blot analysis of whole cell lysates from $A20^{+/+}$, $A20^{ZnF7/ZnF7}$ and $A20^{myel\text{-}KO}$ BMDMs stimulated with LPS as indicated**.** β-tubulin is shown as a loading control. Figure representative for 3 independent experiments. **(d)** TNF and IL-6 secretion by BMDMs

isolated from control $A20^{+/+}$ (n=5), $A20^{ZnF7/ZnF7}$(n=5) and $A20^{myel\text{-}KO}$ (n=5) mice, either or not stimulated with LPS for 6 h. *** and **** represent p<0.001 and p<0.0001 respectively (parametric two-way ANOVA between indicated genotypes). Data are expressed as mean ± SEM. **(e)** TNFR1 pulldown assay in BMDMs isolated from $A20^{+/+}$, $A20^{myel\text{-}KO}$ and $A20^{ZnF7/ZnF7}$ mice after stimulation with Flag-TNF (1 μg/ml) for the indicated time periods, and immunoprecipitation of the TNFR1 complex with anti-Flag beads in presence of USP2 (24 μg/ml) and immunoblot for A20. Actin is shown as a loading control. Figure representative for 3 independent experiments. **(f)** TNFR1 pulldown on BMDMs isolated from $A20^{+/+}$, $A20^{myel\text{-}KO}$ and $A20^{ZnF7/ZnF7}$ mice stimulated with Flag-TNF (1 μg/ml) for the indicated time periods, and immunoprecipitation of the TNFR1 complex using anti-Flag beads and immunoblotted for A20, RIPK1, TRADD and M1. Figure representative for 3 independent experiments. **(g)** Cell death induction in $A20^{+/+}$, $A20^{ZnF7/ZnF7}$ and $A20^{-/-}$ MEFs stimulated with mouse TNF, in function of time as measured by SytoxGreen (SG+) positivity. Data are expressed as mean ± SEM, and representative of 3 independent experiments ($A20^{+/+}$, n=3; $A20^{ZnF7/ZnF7}$, n=3; $A20^{myel\text{-}KO}$, n=3 independent cell cultures). ** represents p<0.01 (RELM analysis) **(h)** Western blot analysis for expression of A20, full-length (FL) and cleaved (Cl) caspase-3 in $A20^{+/+}$, $A20^{ZnF7/ZnF7}$ and $A20^{-/-}$ MEFs stimulated with mouse TNF for the indicated time points. Actin is shown as loading control. Figure representative for 3 independent experiments **(i)** Immunoblot for procaspase-1 and cleaved caspase-1 (p20) in BMDMs from $A20^{+/+}$, $A20^{ZnF7/ZnF7}$ and $A20^{myel\text{-}KO}$ either or not stimulated with LPS and/or ATP. Actin is shown as loading control. Data are representative of three independent experiments. **(j)** IL1β and IL18 secretion by BMDMs isolated from $A20^{+/+}$ (n=5), $A20^{ZnF7/ZnF7}$ (n=5) and $A20^{myel\text{-}KO}$ (n=5) mice either or not stimulated with LPS and ATP. Data represent the mean ± SEM.**, **** represent p<0.01 and p<0.0001, respectively (parametric two-way ANOVA between indicated genotypes). **(k)** Pyroptosis induction in BMDMs from $A20^{+/+}$ (n=5), $A20^{ZnF7/ZnF7}$ (n=5) and $A20^{myel\text{-}KO}$ (n=5) mice stimulated with LPS and ATP, as measured by Sytox Green (SG) uptake. Data are presented as mean ± SEM and are representative of three independent experiments. *** represents p<0.001 (RELM analysis).

Although $A20^{ZnF7/ZnF7}$ mice develop a spontaneous inflammatory phenotype, they do not fully recapitulate the phenotype of *Tnfaip3*$^{-/-}$ mice that develop severe multi-organ inflammation and cachexia and die in the first weeks after birth. This observation suggests that A20 exerts additional protective functions independent of its ZnF7 linear ubiquitin binding activity. In this respect, the ZnF4 domain of A20 has been demonstrated to bind K63-linked polyubiquitin, and mutations in the A20 ZnF4 ubiquitin-binding interface were shown to result in slightly impaired regulation of NF-κB signaling [4,17]. Gene-targeted mice mutated in the A20 ZnF4 domain, however, did not develop spontaneous pathology[4,6]. To clarify the physiological role of A20's ZnF4 domain in suppressing inflammation, we introduced two cysteine to alanine point mutations in the ZnF4 motif – C609A and C612A – of $A20^{ZnF7}$ mice, generating mice with combined inactivation of the K63 polyubiquitin binding ZnF4 and M1 polyubiquitin binding ZnF7 domains (hereafter referred to as $A20^{ZnF4ZnF7}$ mice) (Extended Data Fig. 5a). Heterozygous $A20^{ZnF4ZnF7/+}$ mice had a normal appearance without evidence of clinical pathology. In contrast, although $A20^{ZnF4ZnF7/ZnF4ZnF7}$ mice were born at normal frequencies, they were severely runted and none of these animals survived past weaning age (Table 1, Extended data Fig. 5b). Gross and histological examination of tissues of 2-week-old $A20^{ZnF4ZnF7/ZnF4ZnF7}$ mice revealed severe inflammation in multiple organs, including intestine, liver, and skin (Fig. 3a, b), and

cleaved caspase 3-positive cells were detected in livers of A20$^{ZnF4ZnF7/ZnF4ZnF7}$ mice, indicative of spontaneous liver cell apoptosis (Fig. 3c, d). In addition, systemic inflammation in A20$^{ZnF4ZnF7/ZnF4ZnF7}$ mice was also evident from the detection of high serum concentrations of the inflammatory cytokines TNF and IL-6 (Fig. 3e).

A20$^{ZnF4ZnF7/ZnF4ZnF7}$ mice in a MyD88-deficient background did not die in the first postnatal weeks as is the case with A20$^{ZnF4ZnF7/ZnF4ZnF7}$ mice (Extended Data Fig. 5c) and did not develop the severe tissue pathology as seen in MyD88-sufficient controls (Fig. 3f). However, these mice still failed to thrive, presented with severely reduced bodyweight and did not survive beyond 20 weeks of age (Fig 3g). Although 15 week-old A20$^{ZnF4ZnF7/ZnF4ZnF7}$*Myd88*$^{-/-}$ did not display pronounced swelling of ankles and toes (Fig. 3h), histological examination still revealed inflammation in liver tissue of these mice (Fig. 3i). These results demonstrate that MyD88 drives dysregulated homeostatic TLR signals in the absence of ZnF4 and ZnF7-dependent A20 functions in young mice, whereas MyD88-independent inflammatory signaling contributed to pathology at older age.

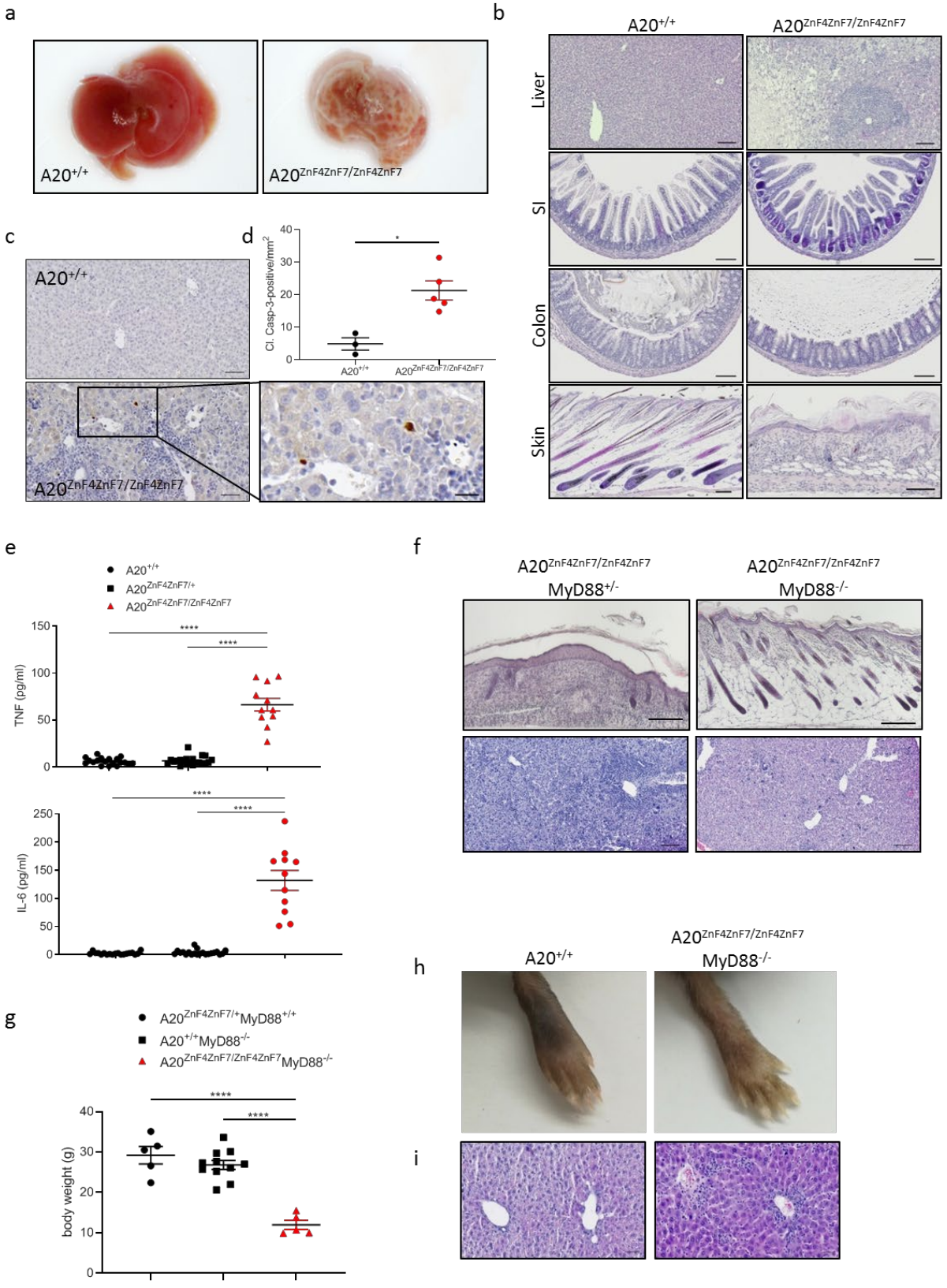

Figure 3. A20$^{ZnF4ZnF7/ZnF4ZnF7}$ knock-in mice phenocopy A20 knockout mice. (a) Gross appearance of livers of 2-week old control A20$^{+/+}$, A20$^{ZnF4ZnF7/+}$ and A20$^{ZnF4ZnF7/ZnF4ZnF7}$ mice. Note pale acellular regions in A20$^{ZnF4ZnF7/ZnF4ZnF7}$ livers. Picture representative for 3 biologically independent mice. **(b)** Representative hematoxylin-eosin-stained sections from 2-week old control A20$^{+/+}$, A20$^{ZnF4ZnF7/+}$ and

$A20^{ZnF4ZnF7/ZnF4ZnF7}$ intestine (small intestine and colon), liver and skin. Note severe inflammation in all $A20^{ZnF4ZnF7/ZnF4ZnF7}$ tissue sections. Scale bar, 100 µm. Pictures representative for 3 biologically independent mice. **(c)** Immunostaining for cleaved caspase 3 on liver sections from 2-week old control $A20^{+/+}$ and $A20^{ZnF4ZnF7/ZnF4ZnF7}$ mice. Pictures representative for 3 biologically independent mice. Scale bars, 50 µm (insert, 20 µm). **(d)** Quantification of cleaved caspase 3-positive cells in sections from the liver of 2-week old control $A20^{+/+}$and $A20^{ZnF4ZnF7/ZnF4ZnF7}$ mice. Number of cleaved caspase 3-positive cells per mm^2 is shown ($A20^{ZnF4ZnF7/ZnF4ZnF7}$, n= 5; $A20^{+/+}$, n=3 mice) Data are expressed as mean ± SEM. Each dot represents an individual mouse. *, p=0.036 (two-sided non-parametric Mann Whitney test between indicated genotypes). **(e)** Levels of IL-6 and TNF in serum of control $A20^{+/+}$, $A20^{ZnF4ZnF7/+}$ and $A20^{ZnF4ZnF7/ZnF4ZnF7}$ mice at the age of 2 weeks. Each dot represents a biologically independent mouse ($A20^{+/+}$, n=19; $A20^{ZnF4ZnF7/+}$, n=21; $A20^{ZnF4ZnF7/ZnF4ZnF7}$, n=11). Data are expressed as mean ± SEM. ****, p<0.0001 (parametric one-way ANOVA between indicated genotypes). **(f)** Representative hematoxylin-eosin-stained sections from liver and skin tissue of 2 week-old $A20^{ZnF4ZnF7/ZnF4ZnF7}MyD88^{-/-}$ mice and $A20^{ZnF4ZnF7/ZnF4ZnF7}MyD88^{+/-}$ littermates. Scale bar, 100 µm. Pictures representative for 3 biologically independent mice. **(g)** Bodyweight of 15-week old $A20^{ZnF4ZnF7/ZnF4ZnF7}MyD88^{-/-}$ mice compared to control mice. Data are expressed as mean ± SEM. Each dot represents a biologically independent mouse ($A20^{ZnF4ZnF7/+}MyD88^{+/+}$, n=5; $A20^{+/+}MyD88^{-/-}$, n=11; $A20^{ZnF4ZnF7/ZnF4ZnF7}MyD88^{-/-}$, n=5). **** represents p<0.0001 (parametric one-way ANOVA between indicated genotypes). **(h)** Representative pictures of hindpaws of 15 week-old $A20^{ZnF4ZnF7/ZnF4ZnF7}MyD88^{-/-}$ mice and control wild-type mice. **(i)** Representative hematoxylin-eosin-stained liver sections from 15 week-old $A20^{ZnF4ZnF7/ZnF4ZnF7}MyD88^{-/-}$ mice and control wild-type mice (scale bars, 50µm). Pictures representative for 3 biologically independent mice. Mark that $A20^{ZnF4ZnF7/ZnF4ZnF7}$ could not be used as control mice in Fig. 3g-i since these mice do not survive beyond the age of 3 weeks.

Because $A20^{ZnF4ZnF7/ZnF4ZnF7}$ mice are not viable, we next developed mice with a conditional 'floxed' allele of *Tnfaip3*, allowing tissue-specific expression of the ZnF4 and ZnF7 mutations through expression of a Cre recombinase (Extended data Fig. 6a). Mice homozygous for the loxP-flanked $Tnfaip3^{ZnF4ZnF7}$ allele expressed normal amounts of A20 and developed normally (data not shown). General deletion of the loxP-flanked $Tnfaip3^{ZnF4ZnF7}$ alleles through expression of a ubiquitous Cre recombinase triggered severe pathology and postnatal lethality, reminiscent of our observations in $A20^{ZnF4ZnF7/ZnF4ZnF7}$ mice (Fig. 4a and Extended Data Fig. 6b). To test if myeloid-specific $Tnfaip3^{ZnF4ZnF7/ZnF4ZnF7}$ mice ($Tnfaip3^{ZnF4ZnF7/ZnF4ZnF7}$*LysM*-Cre) also developed spontaneous arthritis as seen in myeloid-specific A20-deficient mice [11,15,16], we crossed loxP-flanked $Tnfaip3^{ZnF4ZnF7}$ mice with *LysM*-Cre mice. Indeed, $Tnfaip3^{ZnF4ZnF7/ZnF4ZnF7}$*LysM*-Cre mice developed a progressive polyarthritis, characterized by immune cell infiltration, cartilage destruction indicated by decreased proteoglycan staining with toluidine blue, and bone erosion with increased osteoclast activity detected by tartrate-resistant acid phosphatase (TRAP) staining (Fig. 4b-e and Extended Data Fig. 6c). Myeloid-specific $Tnfaip3^{ZnF4ZnF7/ZnF4ZnF7}$ mice also had significantly higher serum concentrations of the inflammatory cytokines TNF and IL-6 compared to control littermate mice (Fig. 4f). In line with these *in vivo* observations, cultured BMDMs from $Tnfaip3^{ZnF4ZnF7/ZnF4ZnF7}$*LysM*-Cre mice produced significantly more

cytokines upon stimulation with LPS compared to control BMDMs (Fig. 4g), consistent with the role of A20 as a negative feedback regulator of inducible NF-κB–dependent gene expression.

To investigate the consequence of mutant A20^{ZnF4ZnF7} expression in intestinal epithelial cells (IECs), we generated IEC-specific *Tnfaip3*$^{ZnF4ZnF7/ZnF4ZnF7}$ mice by crossing loxP-flanked *Tnfaip3*^{ZnF4ZnF7} mice with villin-Cre mice (*Tnfaip3*$^{ZnF4ZnF7/ZnF4ZnF7}$*Vil1*-Cre), and challenged these animals with a normally sublethal dose of TNF. As expected, control littermates all survived and only showed a modest drop in body temperature. In contrast, and as previously demonstrated in IEC-specific A20-deficient mice [13], IEC-specific *Tnfaip3*$^{ZnF4ZnF7/ZnF4ZnF7}$ mice displayed typical symptoms associated with TNF toxicity, including hypothermia and severe diarrhea, and all died between 5 and 10 h after injection due to the TNF-induced apoptosis of A20 mutant IECs (Fig. 4h-j). Finally, IEC-specific *Tnfaip3*$^{ZnF4ZnF7/ZnF4ZnF7}$ mice and control littermates were evaluated in the model of dextran sodium sulfate (DSS)-induced colitis. Mice were subjected to 1.5 % DSS in drinking water for 5 days and monitored daily for clinical pathology. Compared with control mice, IEC-*Tnfaip3*$^{ZnF4ZnF7/ZnF4ZnF7}$ mice showed increased susceptibility to DSS-induced colitis, similar to what had been shown with IEC-specific A20-deficient mice [13] (Extended Data Fig. 6d). In agreement, IEC-*Tnfaip3*$^{ZnF4ZnF7/ZnF4ZnF7}$ mice showed more pronounced loss of intestinal barrier integrity after 5 days of DSS compared to the control group (Extended Data Fig. 6e). Unchallenged mice, however, did no show spontaneous barrier permeability (Extended Data Fig. 6e).

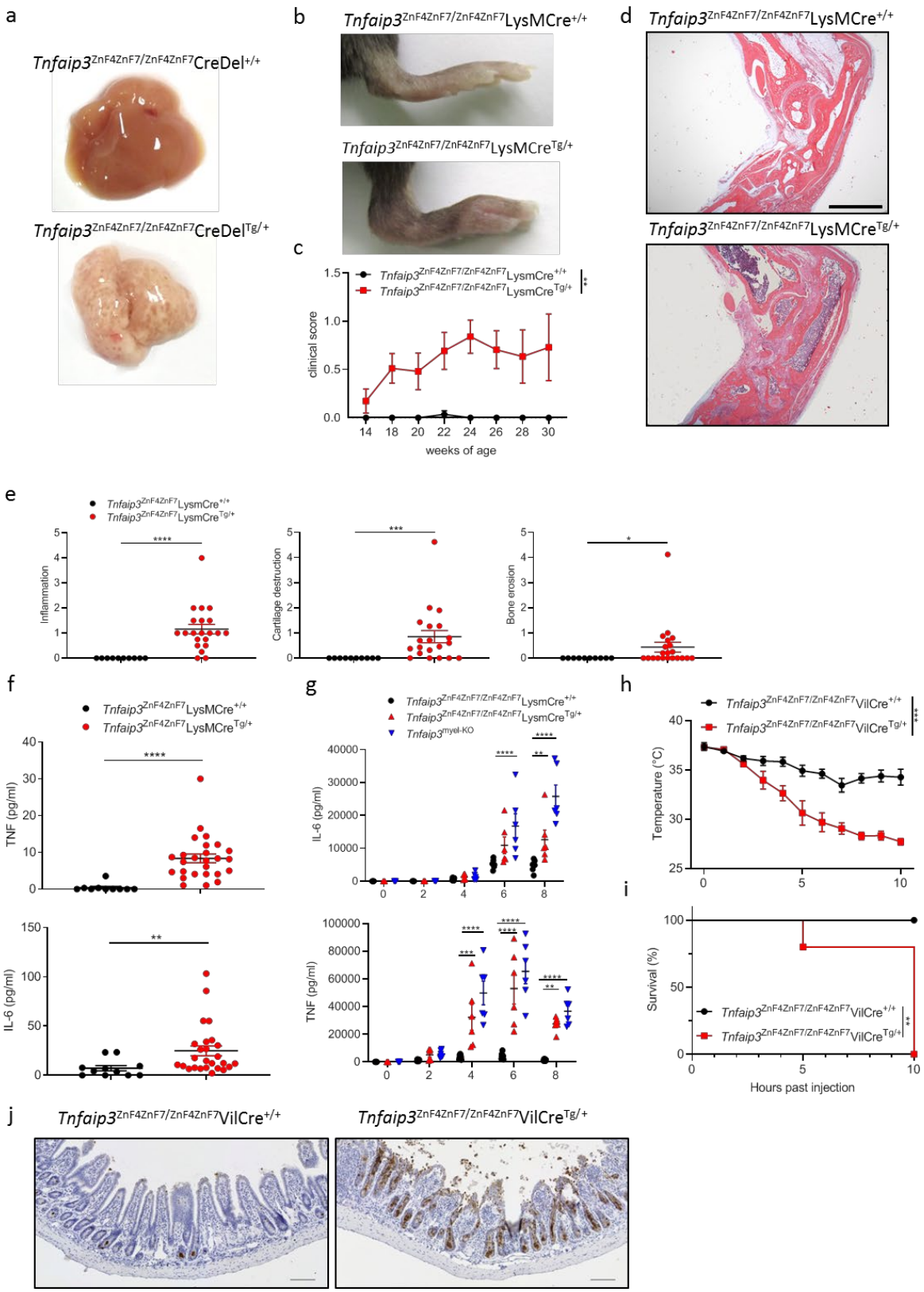

Figure 4. Tissue-specific A20^{ZnF4ZnF7} expression phenocopies tissue-specific A20 deficiency. (a) Gross appearance of livers of 2-week old control (*Tnfaip3*$^{ZnF4ZnF7/ZnF4ZnF7}$CreDel$^{+/+}$) and *Tnfaip3*$^{ZnF4ZnF7/ZnF4ZnF7}$CreDel$^{Tg/+}$ littermate mice. Note pale acellular regions in *Tnfaip3*$^{ZnF4ZnF7/ZnF4ZnF7}$CreDel$^{Tg/+}$ livers. **(b)** Representative picture of the hind paws of 32 week-old control (*Tnfaip3*$^{ZnF4ZnF7/ZnF4ZnF7}$LysMCre$^{+/+}$) and *Tnfaip3*$^{ZnF4ZnF7/ZnF4ZnF7}$LysMCre$^{Tg/+}$ littermate mice. **(c)**

Biweekly clinical arthritis scores of the ankles of control (*Tnfaip3*$^{ZnF4ZnF7/ZnF4ZnF7}$LysMCre$^{+/+}$) and *Tnfaip3*$^{ZnF4ZnF7/ZnF4ZnF7}$LysMCre$^{Tg/+}$ littermate mice (*Tnfaip3*$^{ZnF4ZnF7/ZnF4ZnF7}$LysMCre$^{+/+}$, n=6-15 mice per age, *Tnfaip3*$^{ZnF4ZnF7/ZnF4ZnF7}$LysMCre$^{Tg/+}$, n=12-25 mice per age). Data are expressed as mean ± SEM. ** represents p=0.002 (REML analysis) **(d)** Histological images of H&E-stained ankle joints of mice with the indicated genotypes. Pictures representative for 5 biologicaly independent mice. **(e)** Graphs depicting histological scores for inflammation, bone erosion and cartilage destruction in mice with the indicated genotypes (28-33 weeks). Dots in the graphs indicate individual mice (*Tnfaip3*$^{ZnF4ZnF7/ZnF4ZnF7}$LysMCre$^{+/+}$, n=10; *Tnfaip3*$^{ZnF4ZnF7/ZnF4ZnF7}$LysMCre$^{Tg/+}$, n=21). Data are expressed as mean ± SEM. *, *** and **** represent p=0.0141, p=0.0003 and p<0.0001 respectively (Two-sided non-parametric Mann-Whitney test between indicated genotypes). **(f)** Levels of IL-6 and TNF in serum of control (*Tnfaip3*$^{ZnF4ZnF7/ZnF4ZnF7}$LysMCre$^{+/+}$) and *Tnfaip3*$^{ZnF4ZnF7/ZnF4ZnF7}$LysMCre$^{Tg/+}$ mice at the age of 30-40 weeks. Each dot represents a biologically independent mouse (*Tnfaip3*$^{ZnF4ZnF7/ZnF4ZnF7}$LysMCre$^{+/+}$, n=11, *Tnfaip3*$^{ZnF4ZnF7/ZnF4ZnF7}$LysMCre$^{Tg/+}$, n=27). Data are expressed as mean ± SEM. ** and **** represent p=0.0017 and p<0.0001 respectively (Two-sided non-parametric Mann-Whitney test between indicated genotypes). **(g)** TNF and IL-6 secretion by BMDMs isolated from control (*Tnfaip3*$^{ZnF4ZnF7/ZnF4ZnF7}$LysMCre$^{+/+}$**,** n=6), *Tnfaip3*$^{ZnF4ZnF7/ZnF4ZnF7}$LysMCre$^{Tg/+}$ (n=6) and A20$^{myel\text{-}KO}$ (n=6) littermate mice stimulated with LPS for the indicated time points. Data are expressed as mean ± SEM. **, *** and **** represent p<0.01, p<0.001 and p<0.0001 respectively (parametric two-way ANOVA between indicated genotypes at each time point). **(h-j)** *Tnfaip3*$^{ZnF4ZnF7/ZnF4ZnF7}$villinCre$^{Tg/+}$ (n=5) and control (*Tnfaip3*$^{ZnF4ZnF7/ZnF4ZnF7}$villinCre$^{+/+}$**,** n=6) littermate mice were injected i.p. with 5 µg recombinant mouse TNF per 20 g of bodyweight. Body temperature (h, mean ± SEM, *** represents p<0.001, REML analysis) and survival (i, ** represents p=0.0018, Two-sided mantel-cox test) in function of time. **(j)** Representative cleaved caspase 3-specific staining on sections of small intestine of mice with the indicated genotypes 5 h past TNF injection. Scale bar, 100µm.

In conclusion, we have demonstrated that A20 acts primarily as an ubiquitin-binding protein via both its ZnF4 and ZnF7 domains to suppress pro-inflammatory signaling. Upon TNFR1 and TLR4 activation, A20 is recruited to the receptor complexes through binding to linear ubiquitin chains via its ZnF7 in order to stabilize the respective signaling complexes and dampen downstream inflammatory signaling. We further show that A20's anti-inflammatory activity also relies on its K63 ubiquitin-binding ZnF4 domain, and mice lacking both functional ZnF4 and ZnF7 domains phenocopy A20-deficient mice in that they die perinatally due to severe multi organ inflammation. Together, our observations suggest a mainly non-enzymatic role for A20 in suppressing inflammation by allowing its recruitment and the stabilization of ubiquitin chains in the receptor complex. However, A20's DUB function may still be important in the downstream regulation of signaling. More studies, however, are needed to further investigate this.

Multiple genetic studies over the past ten years have associated *TNFAIP3* polymorphisms to diverse human inflammatory and autoimmune diseases[2]. These disease-associated variants are mostly located in upstream or downstream non-coding regions or in intronic regions of the *TNFAIP3* gene, which may affect the expression of A20 possibly by interfering with the function of cell- and activation-specific enhancers [18-21]. Also loss-of-function mutations and deletions in *TNFAIP3* have

been identified, especially in patients with B cell lymphomas [22-24]. The majority of these *TNFAIP3* mutations concern frameshift and premature stop codon mutations preventing the synthesis or compromising the ubiquitin-binding ability of the C-terminal ZnF7 domain [8,22-24]. Furthermore, A20 haploinsufficiency has recently been shown to cause a severe early-onset autoinflammatory disease, and peripheral blood monocytes isolated from these patients show severely reduced A20 expression [25]. Our findings presented here suggest that these mutations may cause a polyubiquitin-binding defect, that in these patients may be sufficient to affect homeostatic regulation of NF-κB signaling and cell death.

Materials and Methods

***Mice*.** For the generation of gene-targeted A20-ZnF7 mice, Cas9 mRNA (Sigma) and protein (VIB Protein Service Facility, Ghent) together with a 151 bp single-stranded repair template (IDT) containing the homologous sequence around the mutations and two short guide RNAs (sgRNAs, Synthego) targeting the ZnF7 domain of the murine *Tnfaip3* gene were microinjected into the pronucleus of zygotes obtained from C57BL/6J mice. Embryos were overnight incubated in KSOM medium and transferred the next day to foster mothers via oviduct transfer. sgRNA1: 5'-AGCCATACATCTGCTTGAACTGG-3'; sgRNA2: 5'-ATTGCAGTAACCATTACACTTGG-3'; ssDNA oligonucleotides used as repair template containing two Cys-to-Ala point-mutations [TGC>GCC (C764A); TGC>GCT (C767A)] and two silent mutations [GCC>GCT (A758); TAC>TAT (Y768)] to avoid re-editing after recombination: 5'-GCCTGAAGAGCCCCCTAAACAGCGCTGCCGGGCCCCTGCTTGTGATCACTTTGGCAATGCTAAGTGTAATGGT TACGCCAATGAGGCTTATCAGTTCAAGCAGATGTATGGCTAAGTGCGAACACATTGACAGGTCCAGCAAGAAG GAGCC-3'. For the generation of A20-ZnF4/ZnF7 knockin mice, Cas9 protein together with a donor vector containing ~1 kb 5' and 3' homologous arms around the Cys-to-Ala mutations [TGC>GCC (C609A); TGT>GCT (C612A); TGC>GCC (C764A); TGC>GCC (C767A)] and two synonymous mutations [TCC>TCA (S577); TAC>TAT (Y768)], and two sgRNAs (sgRNA1: 5'- CTCCTGGAGTCCGTGCAGCCTGG-3'; sgRNA2: 5'-AGCCATACATCTGCTTGAACTGG-3') targeting the ZnF4 and ZnF7 domain of the murine A20 gene were microinjected into the pronucleus of zygotes obtained from C57BL/6 mice. Conditional LoxP-flanked A20-ZnF4/ZnF7 knockin alleles were generated through homologous recombination in C57BL/6 ES cells. A neomycin resistance cassette flanked with RoxP sites was introduced after the last exon (exon 9) of the *Tnfaip3* gene. Exons 6-9 and the neo cassette are flanked with LoxP sites. At the 3' of the loxP flanked region we introduced a mutated exon 6-9 containing the ZnF4 (C609A/C612A) and ZnF7 (C764A/C767A) mutations. In *Tnfaip3*^{ZnF4ZnF7} floxed mice the neomycine cassette has been removed by Dre-mediated recombination. Cre-mediated recombination excises the LoxP-flanked fragment containing the wild-type exons 6-9, resulting in the expression of the mutated exons 6-9. Mice with conditional LoxP-flanked *Tnfaip3*^{ZnF4ZnF7} alleles were crossed with the *LysM*-Cre[26] or *Vil1*-Cre transgenic lines[27]. *Myd88*$^{-/-}$ mice were previously described[28]. Mice were housed in individually ventilated cages at the VIB Center for Inflammation Research, in a specific pathogen-free animal facility. All experiments on mice were conducted according to institutional, national and European animal regulations. Animal protocols were approved by the ethics committee of Ghent University.

Histological analysis of tissue sections. Liver, spleen, small intestine, colon, skin and joint sections were fixed in 4% paraformaldehyde for hematoxylin and eosin or immunostaining, or in Carnoy fixative (60% methanol, 30% chloroform, 10% glacial acetic acid) for Alcian Blue/Periodic Acid (AB/PAS) staining. Samples were dehydrated, embedded in paraffin, sectioned at 4 μm and examined by light microscopy. Bright-field microscopy was done using an Axio Scan.Z1 (Zeiss). For joint pathology, formalin-fixed, EDTA-decalcified, paraffin-embedded mouse tissue specimens were sectioned and stained with hematoxylin and eosin, Toluidine Blue and TRAP [Leukocyte Acid Phosphatase Kit; Sigma-Aldrich]. H&E-, Toluidine Blue- and TRAP-stained joint sections were semi-quantitatively and blindly evaluated for the following parameters: synovial inflammation/ hyperplasia (scale of 0–5), cartilage erosion (scale of 0–5), and bone loss (scale of 0–5) as described[29].

Isolation and immortalization of mouse embryonic fibroblasts. 12.5 dpc embryos from $A20^{ZnF7/+}$ or $A20^{ZnF4ZnF7/+}$ matings were isolated and mouse embryonic fibroblasts (MEFs) were prepared. MEFs were immortalized through serial passaging and frozen in liquid nitrogen. Confluent cells were stimulated with 20 ng/ml recombinant mouse TNF, after which cells were lysed for immunoblotting or quantitative real-time PCR.

Isolation of bone marrow-derived macrophages. BMDMs were obtained from bone marrow cells flushed from mouse femurs and tibia with ice-cold sterile RPMI medium, and cultured in RPMI 1640 supplemented with 40 ng/ml recombinant mouse M-CSF, 10% FCS, 1% penicillin/streptavidin and glutamine. Fresh M-CSF was added on day 3 and medium was refreshed on day 5. On day 7 cells were seeded and stimulated with 20 ng/ml ultrapure LPS (*Escherichia coli* 0111:B4 strain, InvivoGen) or 20 ng/ml ultrapure LPS (*E. coli* 0111:B4 strain, Invivogen) for 3 h followed by 5 mM ATP (Sigma-Aldrich) for 20 min for NLRP3 activation.

Cytokine detection. Cytokine concentrations in culture medium were determined by magnetic bead-based multiplex assay using Luminex technology (Bio-Rad), IL-1β ELISA (Affymetrix eBioscience), IL-18 ELISA (Biotechne - R & D Syst. Eur.), according to the manufacturers' instructions.

Immunoprecipitation studies. BMDMs were stimulated with human Flag–TNF (1 μg/ml) (VIB Protein Service Facility) as indicated. Cells were lysed in NP40 buffer (150 mM NaCl, 1% NP40, 10% glycerol and 10 mM Tris–HCl pH 8) and FLAG pulldown was performed using M2 beads (Sigma). The TNF-R1 signaling complex was eluted from beads using 3×FLAG peptide (Sigma) as described in the manufacturer's instructions. For USP2 and PPase treatment, the beads were incubated with 24 μg ml−1 USP2 (Enzo Life Sciences) and 8 U μl−1 λPPase (NEB) for 30 min at 37 °C before FLAG peptide elution.

Cell death assay. For cell death analysis in MEFs, cells were seeded the day before at 1 × 10 ^{4} per well in triplicates in a 96-well plate. The next day, cells were stimulated with the indicated concentration of mTNF in the presence of 2.5 μM SytoxGreen (Invitrogen). SytoxGreen intensity was measured at intervals of one hour using a Fluostar Omega fluorescence plate reader, with an excitation filter of 485 nm and an emission filter of 520 nm, gains set at 1, 100, 20 flashes per well and orbital averaging with a diameter of 3 mm. For pyroptosis assay in BMDMs, cells were seeded the day before at 2.5 x 10^4 per well in triplicates in a 96-well plate. The next day, cells were stimulated with the indicated concentration of LPS and ATP in the presence of 0.25 μM SytoxGreen (Molecular probes). SytoxGreen intensity was measured at intervals of 5 min, for a total of 1 h, using a Incucyte device (EssenbioScience). Percentage of cell death was calculated as (induced fluorescence − background fluorescence)/(maximum fluorescence − background fluorescence) × 100. The maximal fluorescence is obtained by full permeabilization of the cells by using Triton X-100 at a final concentration of 0.1 %. All cell death data are presented as mean ± SEM of n (indicated in the figure) independent experiments, unless stated otherwise.

Immunoblot analysis. Cells and tissue extracts were prepared in E1A lysis buffer (250 mM NaCl, 50 mM Tris pH 7.4, 0.1% NP-40) containing a complete protease inhibitor cocktail (1:25) (Roche) and centrifuged for 10 min at 14,000 rpm in a microcentrifuge at 4°C or were directly lysed in 2× Laemlli buffer. For cleaved Caspase 1 immunoblotting, cell lysates and culture supernatants were incubated with cell lysis buffer (20 mM Tris HCl pH 7.4, 200 mM NaCl, 1% NP-40) and denatured in Laemmli buffer. Supernatants were separated by SDS-polyacrylamide gel electrophoresis (PAGE), transferred to nitrocellulose and immunodetected with anti-IκBα (Santa Cruz Biotechnology, Inc., sc-371), anti-phospho-IκBα (Cell Signaling, CST9246), anti-A20 (Santa Cruz Biotechnology, Inc., sc-166692), anti-p38 (Cell Signaling, CST9212), anti-phospho-p38 (Cell Signaling, CST9215), anti-Caspase3 (Cell Signaling, CST9662), anti-SAPK/JNK (Cell Signaling, CST9252), anti-phospho-SAPK/JNK (Cell Signaling, CST4668), anti-caspase-1 (Adipogen, AG-20B-0042), anti-β-tubulin (Sigma-Aldrich, T4026) and anti-β-actin (Santa Cruz Biotechnology, Inc., sc-47778) antibodies.

In vivo TNF toxicity. Mice were injected i.p. with a sublethal dose of mouse TNF (5 μg mouse TNF/20 g mouse). *E. coli*-expressed recombinant mTNF was produced and purified to homogeneity in our laboratory, and endotoxin levels did not exceed 1 ng/mg protein. Body temperature and survival were monitored every hour. In a separate experiment, mice were euthanized after 2 h (A20^{ZnF7}) or 5 h (*Tnfaip3*$^{ZnF4ZnF7/ZnF4ZnF7}$*Vil1*-Cre) for histological analysis.

Induction of DSS-induced colitis and clinical score. Acute colitis was induced by addition of 1.5 % dextran sodium sulphate (DSS, 36–50 kDa; MP Biomedicals) to the drinking water for 5 days. Body

weight, stool consistency and fecal blood were determined daily. Fecal blood was determined using Hemoccult SENSA (Beckman Coulter) analysis. The baseline clinical score was determined on day 0. In brief, no weight loss was scored as 0, weight loss of 1–5 % from baseline as 1, 5–10 % as 2, 10–20 % as 3, and >20 % as 4. For bleeding, a score of 0 was assigned for no blood, 2 for positive hemoccult, and 4 for gross bleeding. For stool consistency, a score of 0 was assigned for well-formed pellets, pasty and semi-formed stools were scored as 2, and liquid stools as 4. The average of these 3 scores was used as total clinical score, ranging from 0 (healthy) to 4 (maximal colitis).

FITC–dextran intestinal permeability assay. Intestinal permeability was assessed by oral gavage of FITC–dextran (MW: 3000-5000, Sigma). Mice were administered 12 mg of FITC-dextran per 20 g body weight in sterile PBS by oral gavage. After 4 h, blood was collected from the facial vein, and FITC–dextran concentrations were measured in 50 μl of serum by fluorometry (485 nm). Mice were anesthetized during blood collection. Serial dilutions of FITC–dextran in PBS were used each time to generate a standard curve and serum from PBS-gavaged mice was used as blanks.

Clinical scoring for arthritis development. The severity of arthritis was assessed using a visual scoring system. Mice were scored every two weeks for development of peripheral arthritis. A score ranging from 0 to 3 was assigned to each paw, with 0 being normal, 0.5 being swelling of one or more toes, 1 being mild swelling of the wrist and/or ankle or carpus and/or tarsus, 2 being moderate swelling of the wrist and/or ankle or carpus and/or tarsus or mild swelling of both, and 3 being severe swelling of the entire paw.

Quantitative real-time PCR. Total RNA was isolated using TRIzol reagent (Invitrogen) and Aurum Total RNA Isolation Mini Kit (Biorad), according to manufacturer's instructions. Synthesis of cDNA was performed using iScript cDNA synthesis kit (BioRad) according to the manufacturer's instructions. cDNA was amplified on quantitative PCR in a total volume of 5 μl with SensiFAST SYBR® No-ROX Kit (Bioline) and specific primers on a LightCycler 480 (Roche). The reactions were performed in triplicates. The following mouse-specific primers were used: *Rpl13a* forward, 5'-CCTGCTGCTCTCAAGGTT-3'; *Rpl13a* reverse, 5'-TGGTTGTCACTGCCTGGTACTT-3'; *Rpl13a* forward, 5'-AGTGTTGGATACAGGCCAGAC-3'; *Rpl13a* reverse, 5'-CGTGATTCAAATCCCTGAAGT-3'; *Tnf* forward, 5'-ACCCTGGTATGAGCCCATATAC-3'; *Tnf* reverse, 5'-ACACCCATTCCCTTCACAGAG-3'*; Il1b* forward, 5'-CACCTCACAAGCAGAGCACAAG-3'; *Il1b* reverse, 5'-GCATTAGAAACAGTCCAGCCCATAC-3'; *Il6* forward, 5'-GAGGATACCACTCCCAACAGACC-3'; *Il6* reverse, 5'-AAGTGCATCATCGTTGTTCATACA-3'; *Il18* forward, 5'-CAGGCCTGACATCTTCTGCAA-3'; *Il18* reverse, 5'-TCTGACATGGCAGCCATTGT-3'.

Flow cytometry. Spleens were isolated and processed to a single-cell suspension. 5×10^6 splenocytes were stained with a combination of the following fluorochrome- or biotin-labeled monoclonal

antibodies: CD3 (Thermo Fisher Scientific, 145-2c11 or 17A2), CD4 (BD Biosciences, GK1.5), CD8 (Thermo Fisher Scientific, 53-6.7), CD11b (BD Biosciences, M1/70), CD11c (Thermo Fisher Scientific, N418), CD16/32 (Bioceros, 2.4G2), CD19 (Thermo Fisher Scientific, 1D3), CD62L (BD Biosciences, MEL-14), CD64 (BioLegend, X54-5/7.1), F4/80 (BioLegend, BM8), Ly6C (Thermo Fisher Scientific, HK1.4), Ly6G (BD Biosciences, 1A8), NK1.1 (BD Biosciences, PK136), SiglecF (BD Biosciences, E50-2440), and TNF (BD Biosciences, MP6-XT22). Intracellular staining for TNF was performed with the Foxp3 kit (eBioscience, 00-5523-00). Cell viability was measured using an eFluor 506 (eBioscience, 65-0866-18) or eFluor780 (eBioscience, 65-0865-14) fixable viability dye. Absolute cell counts were determined by use of 123 count ebeads (eBioscience, 01-1234-42). Samples were measured on a FACS Fortessa 5 laser or BD FACSymphony (BD Biosciences) and data were analyzed using FlowJo.

Ex vivo cytokine production. To assess intracellular TNF production, 5×10^6 splenocytes were cultured in DMEM (Gibco) supplemented with 10% FCS (Bodinco) in the presence of monensin (420701, BioLegend) and brefeldinA (420601, Biolegend) and incubated 3.5 h at 37°C.

Statistics. Results are expressed as the mean ± SEM or mean ± SD, as indicated in figure legend. Statistical significance between experimental groups was assessed using a nonparametric Mann–Whitney U-statistical test. Statistical significance between multiple groups was assessed using either one- or two-way ANOVA with Tukey correction for multiple comparison. Comparison of 2 or more groups over time was analysed as longitudinal data (repeated measurements over time) using the residual maximum likelihood (REML) as implemented in Genstat v19[30]. Briefly, a linear mixed model (random terms underlined) of the form response = μ + genotype + time + genotype.time + subject.time was fitted to the longitudinal data. The term subject.time represents the residual error term with dependent errors because the repeated measurements are taken repeatedly from the same subjects, causing correlations among observations. Times of measurement were set as equally spaced, and the best correlation model was selected based on the Aikake Information Coefficient (AIC). Significance of genotype effects over time (i.e. genotype.time) and changes in differences between genotype effects over time were assessed by an approximate F-test, of which the denominator degrees of freedom were calculated using algebraic derivatives as implemented in Genstat v19[30].

Data availability statement. All data supporting the findings of this study are available from the corresponding author on reasonable request.

ACKNOWLEDGEMENTS

We thank D. Huyghebaert, L. Bellen and D. Vanhede for animal care and A. Fossoul and M. Gennadi for excellent technical assistance. We also thank the InfrafrontierGR infrastructure (ERDF and NSRF 2007-2013 and 2014-2020) for providing histology and mCT facilities. A. Martens is supported by a grant from the “Concerted Research Actions” (GOA) of the Ghent University. Research in the G. van Loo lab is supported by research grants from the FWO, the “Geneeskundige Stichting Koningin Elisabeth” (GSKE), the CBC Banque Prize, the Charcot Foundation, the “Belgian Foundation against Cancer”, “Kom op tegen Kanker”, and the GOA of the Ghent University. M.A. lab is supported by a startup grant from the Stavros Niarchos Foundation donation to BSRC “Al. Fleming.

COMPETING FINANCIAL INTERESTS

M.L. is an employee of Janssen Pharmaceutica. All authors declare that they have no conflict of interest.

AUTHOR CONTRIBUTIONS

A.M., D.P., E.H., J.V., S.R., L.C., S.V., L.D., M.S., H.V., K.S., T.H. and K.I. performed the experiments. A.M., D.P., E.H., J.V., L.C., S.V., A.W., S.J., M.L., R.B., M.A., M.J.M.B. and G.v.L. analyzed the data. G.v.L. provided ideas and coordinated the project. A.M. and G.v.L. wrote the manuscript.

References

1 Catrysse, L., Vereecke, L., Beyaert, R. & van Loo, G. A20 in inflammation and autoimmunity. *Trends Immunol* **35**, 22-31, doi:10.1016/j.it.2013.10.005 (2014).

2 Martens, A. & van Loo, G. A20 at the Crossroads of Cell Death, Inflammation, and Autoimmunity. *Cold Spring Harb Perspect Biol*, doi:10.1101/cshperspect.a036418 (2019).

3 Wertz, I. E. *et al.* De-ubiquitination and ubiquitin ligase domains of A20 downregulate NF-kappaB signalling. *Nature* **430**, 694-699, doi:10.1038/nature02794 (2004).

4 Lu, T. T. *et al.* Dimerization and ubiquitin mediated recruitment of A20, a complex deubiquitinating enzyme. *Immunity* **38**, 896-905, doi:10.1016/j.immuni.2013.03.008 (2013).

5 De, A., Dainichi, T., Rathinam, C. V. & Ghosh, S. The deubiquitinase activity of A20 is dispensable for NF-kappaB signaling. *EMBO Rep* **15**, 775-783, doi:10.15252/embr.201338305 (2014).

6 Wertz, I. E. *et al.* Phosphorylation and linear ubiquitin direct A20 inhibition of inflammation. *Nature* **528**, 370-375, doi:10.1038/nature16165 (2015).

7 Lee, E. G. *et al.* Failure to regulate TNF-induced NF-kappaB and cell death responses in A20-deficient mice. *Science* **289**, 2350-2354, doi:10.1126/science.289.5488.2350 (2000).

8 Tokunaga, F. *et al.* Specific recognition of linear polyubiquitin by A20 zinc finger 7 is involved in NF-kappaB regulation. *EMBO J* **31**, 3856-3870, doi:10.1038/emboj.2012.241 (2012).

9 Draber, P. *et al.* LUBAC-Recruited CYLD and A20 Regulate Gene Activation and Cell Death by Exerting Opposing Effects on Linear Ubiquitin in Signaling Complexes. *Cell Rep* **13**, 2258-2272, doi:10.1016/j.celrep.2015.11.009 (2015).

10 Verhelst, K. *et al.* A20 inhibits LUBAC-mediated NF-kappaB activation by binding linear polyubiquitin chains via its zinc finger 7. *EMBO J* **31**, 3845-3855, doi:10.1038/emboj.2012.240 (2012).

11 Polykratis, A. *et al.* A20 prevents inflammasome-dependent arthritis by inhibiting macrophage necroptosis through its ZnF7 ubiquitin-binding domain. *Nat Cell Biol* **21**, 731-742, doi:10.1038/s41556-019-0324-3 (2019).

12 Turer, E. E. *et al.* Homeostatic MyD88-dependent signals cause lethal inflamMation in the absence of A20. *J Exp Med* **205**, 451-464, doi:10.1084/jem.20071108 (2008).

13 Vereecke, L. *et al.* Enterocyte-specific A20 deficiency sensitizes to tumor necrosis factor-induced toxicity and experimental colitis. *The Journal of experimental medicine* **207**, 1513-1523, doi:10.1084/jem.20092474 (2010).

14 Priem, D. *et al.* A20 protects cells from TNF-induced apoptosis through linear ubiquitin-dependent and -independent mechanisms. *Cell Death Dis* **10**, 692, doi:10.1038/s41419-019-1937-y (2019).

15 Matmati, M. *et al.* A20 (TNFAIP3) deficiency in myeloid cells triggers erosive polyarthritis resembling rheumatoid arthritis. *Nat Genet* **43**, 908-912, doi:10.1038/ng.874 (2011).

16 Vande Walle, L. *et al.* Negative regulation of the NLRP3 inflammasome by A20 protects against arthritis. *Nature* **512**, 69-73, doi:10.1038/nature13322 (2014).

17 Bosanac, I. *et al.* Ubiquitin binding to A20 ZnF4 is required for modulation of NF-kappaB signaling. *Mol Cell* **40**, 548-557, doi:10.1016/j.molcel.2010.10.009 (2010).

18 Graham, R. R. *et al.* Genetic variants near TNFAIP3 on 6q23 are associated with systemic lupus erythematosus. *Nat Genet* **40**, 1059-1061, doi:10.1038/ng.200 (2008).

19 Adrianto, I. *et al.* Association of a functional variant downstream of TNFAIP3 with systemic lupus erythematosus. *Nature genetics* **43**, 253-258, doi:10.1038/ng.766 (2011).

20 Sokhi, U. K. *et al.* Dissection and function of autoimmunity-associated TNFAIP3 (A20) gene enhancers in humanized mouse models. *Nat Commun* **9**, 658, doi:10.1038/s41467-018-03081-7 (2018).

21 Wang, S., Wen, F., Wiley, G. B., Kinter, M. T. & Gaffney, P. M. An enhancer element harboring variants associated with systemic lupus erythematosus engages the TNFAIP3 promoter to

influence A20 expression. *PLoS Genet* **9**, e1003750, doi:10.1371/journal.pgen.1003750 (2013).
22 Compagno, M. *et al.* Mutations of multiple genes cause deregulation of NF-kappaB in diffuse large B-cell lymphoma. *Nature* **459**, 717-721, doi:10.1038/nature07968 (2009).
23 Kato, M. *et al.* Frequent inactivation of A20 in B-cell lymphomas. *Nature* **459**, 712-716, doi:10.1038/nature07969 (2009).
24 Schmitz, R. *et al.* TNFAIP3 (A20) is a tumor suppressor gene in Hodgkin lymphoma and primary mediastinal B cell lymphoma. *J Exp Med* **206**, 981-989, doi:10.1084/jem.20090528 (2009).
25 Zhou, Q. *et al.* Loss-of-function mutations in TNFAIP3 leading to A20 haploinsufficiency cause an early-onset autoinflammatory disease. *Nat Genet* **48**, 67-73, doi:10.1038/ng.3459 (2016).
26 Clausen, B. E., Burkhardt, C., Reith, W., Renkawitz, R. & Forster, I. Conditional gene targeting in macrophages and granulocytes using LysMcre mice. *Transgenic Res* **8**, 265-277 (1999).
27 Madison, B. B. *et al.* Cis elements of the villin gene control expression in restricted domains of the vertical (crypt) and horizontal (duodenum, cecum) axes of the intestine. *J Biol Chem* **277**, 33275-33283, doi:10.1074/jbc.M204935200 (2002).
28 Adachi, O. *et al.* Targeted disruption of the MyD88 gene results in loss of IL-1- and IL-18-mediated function. *Immunity* **9**, 143-150 (1998).
29 Armaka, M., Ospelt, C., Pasparakis, M. & Kollias, G. The p55TNFR-IKK2-Ripk3 axis orchestrates arthritis by regulating death and inflammatory pathways in synovial fibroblasts. *Nat Commun* **9**, 618, doi:10.1038/s41467-018-02935-4 (2018).
30 Baird, D., Murray, D., Payne, R. & Soutar, D. An Introduction to GenStat for Windows (19th Edition). *Genstat* **Vol. 19** (2017).

Tables

Table 1 : Birth and survival rates of control $A20^{+/+}$, $A20^{ZnF4ZnF7/+}$ and $A20^{ZnF4ZnF7/ZnF4ZnF7}$ offspring from $A20^{ZnF4ZnF7/+}$ x $A20^{ZnF4ZnF7/+}$ breeding couples.

Genotype	Expected	Observed (at birth)	Observed (at weaning)
$A20^{+/+}$	25 % (20)	18	18
$A20^{ZnF4ZnF7/+}$	50 % (40)	46	46
$A20^{ZnF4ZnF7/ZnF4ZnF7}$	25 % (20)	16	0
Total (observed)	100 % (52)	52	64

Supplementary Figures

a

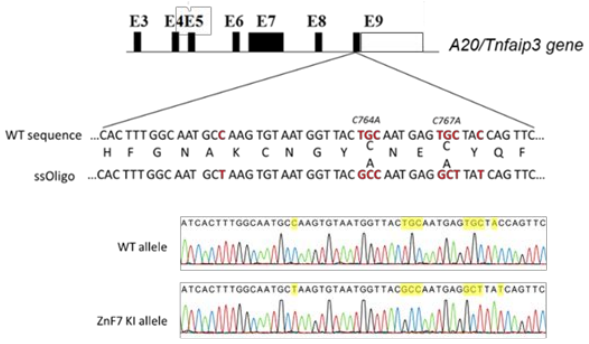

b

Genotype	Expected	Observed (at birth)	Observed (at weaning)
$A20^{+/+}$	25 % (41)	41	41
$A20^{ZnF7/+}$	50 % (83)	82	82
$A20^{ZnF7/ZnF7}$	25 % (41)	43	43
Total (observed)	100 % (166)	166	166

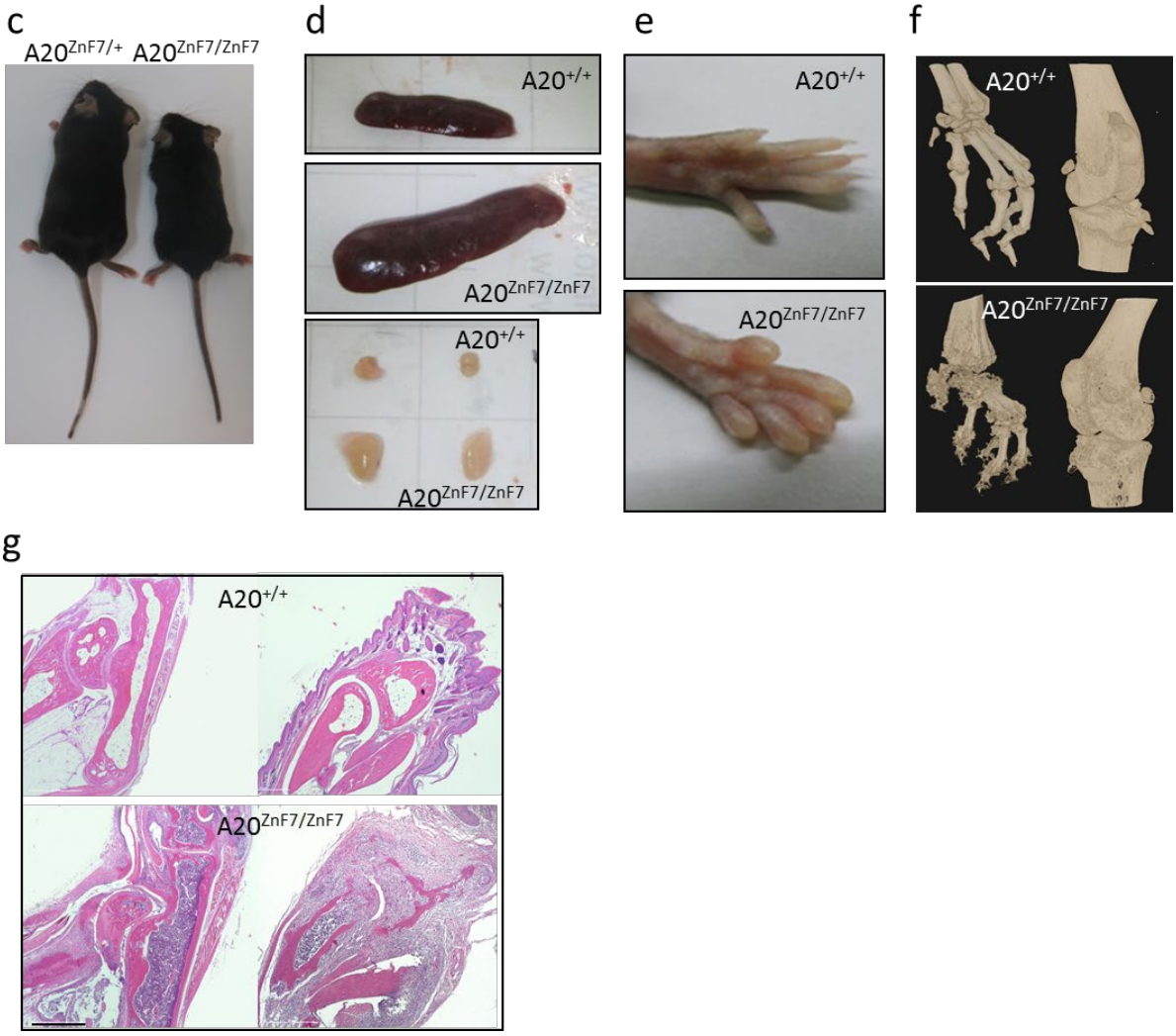

g

Extended Data Figure 1. $A20^{ZnF7}$ knock-in mice. (a) Schematic depiction of the *A20/Tnfaip3* locus indicating the sequence of the single stranded oligonucleotide used for mutating the ZnF7 domain that was introduced by pronuclear injection into mouse zygotes, and sequencing result of the wild-type (WT) and of the targeted ZnF7 knock-in allele. Boxes indicate exons 3 to 9 (E3–E9). **(b)** Birth and survival rates of control ($A20^{+/+}$), $A20^{ZnF7/+}$ and $A20^{ZnF7/ZnF7}$ offspring from $A20^{ZnF7/+}$ x $A20^{ZnF7/+}$ breeding couples. **(c)** Gross appearance of $A20^{ZnF7/+}$ and $A20^{ZnF7/ZnF7}$ mice. **(d)** Representative pictures of spleen and inguinal lymph nodes from 28-week-old control ($A20^{+/+}$) and $A20^{ZnF7/ZnF7}$ littermate mice. **(e)** Representative pictures of hindpaws of 15-week-old control ($A20^{+/+}$) and $A20^{ZnF7/ZnF7}$ littermates,

showing extensive swelling of the toes of the A20$^{ZnF7/ZnF7}$ mice. **(f)** Representative micro-CT pictures of hindpaws (left) and knees (right) of 28-week-old control (A20$^{+/+}$) and A20$^{ZnF7/ZnF7}$ littermates. **(g)** Representative hematoxylin-eosin-stained histological images of ankle joints (left) and toes (right) from 28-week-old control (A20$^{+/+}$) and A20$^{ZnF7/ZnF7}$ littermates. Scale bar, 500 µm.

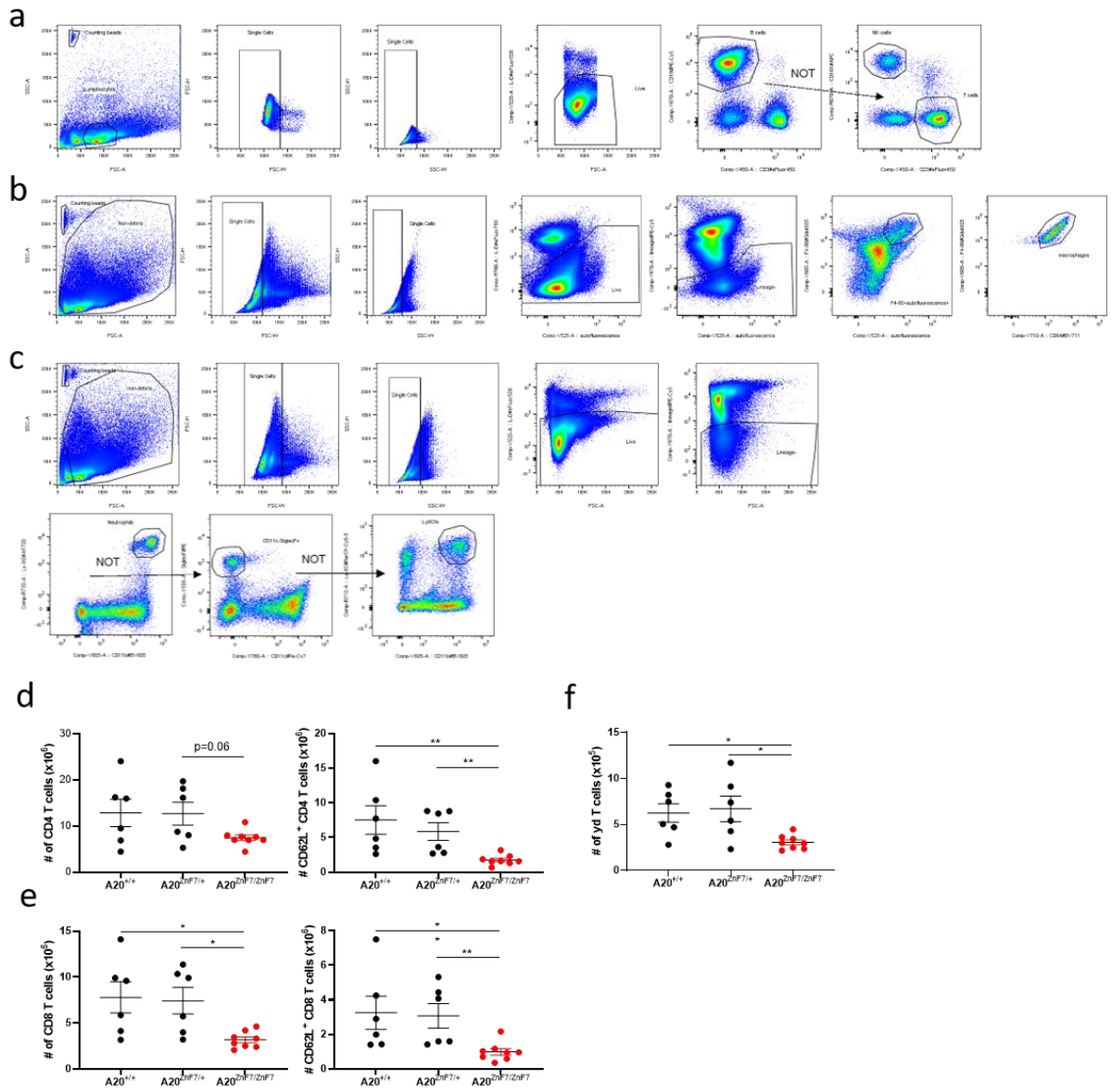

Extended Data Figure 2. FACS immunophenotyping of spleen of control and A20^{ZnF7} mice. (a-c) General gating strategy as applied for immune cell populations described in Figure 1g. (a) Lymphocytes, singlets, live, CD3$^-$CD19$^+$ (B cells), CD3$^+$CD19$^-$ (T cells) and CD3$^-$CD19$^-$ NK1.1$^+$ (NK cells); (b) non-debris, singlets, live, lineage$^-$ (CD3$^-$CD19$^-$NK1.1$^-$), F4/80$^+$, CD64$^+$ and autofluorescent; (c) non-debris, singlets, live, lineage$^-$, Ly6G$^+$CD11b$^+$ (neutrophils) and Ly6G$^-$SiglecF$^-$Ly6C^{hi}CD11b+ (monocytes). FSC: forward scatter, SSC: side scatter, A: Area, H: height, W: width, L/D: live/dead. **(d-f)** Bar graphs representing absolute numbers of total (left) and naive (right) CD4 T cells (d), total (left) and naive (right) CD8 T cells (e) and γd T cells (f) as measured by flow cytometry in the spleens of A20$^{+/+}$, A20$^{ZnF/+}$ and A20$^{ZnF7/ZnF7}$ animals. Data are expressed as mean ± SEM. *, ** represent $p < 0.05$ and $p < 0.01$ (Two-sided non-parametric Mann-Whitney test between indicated genotypes).

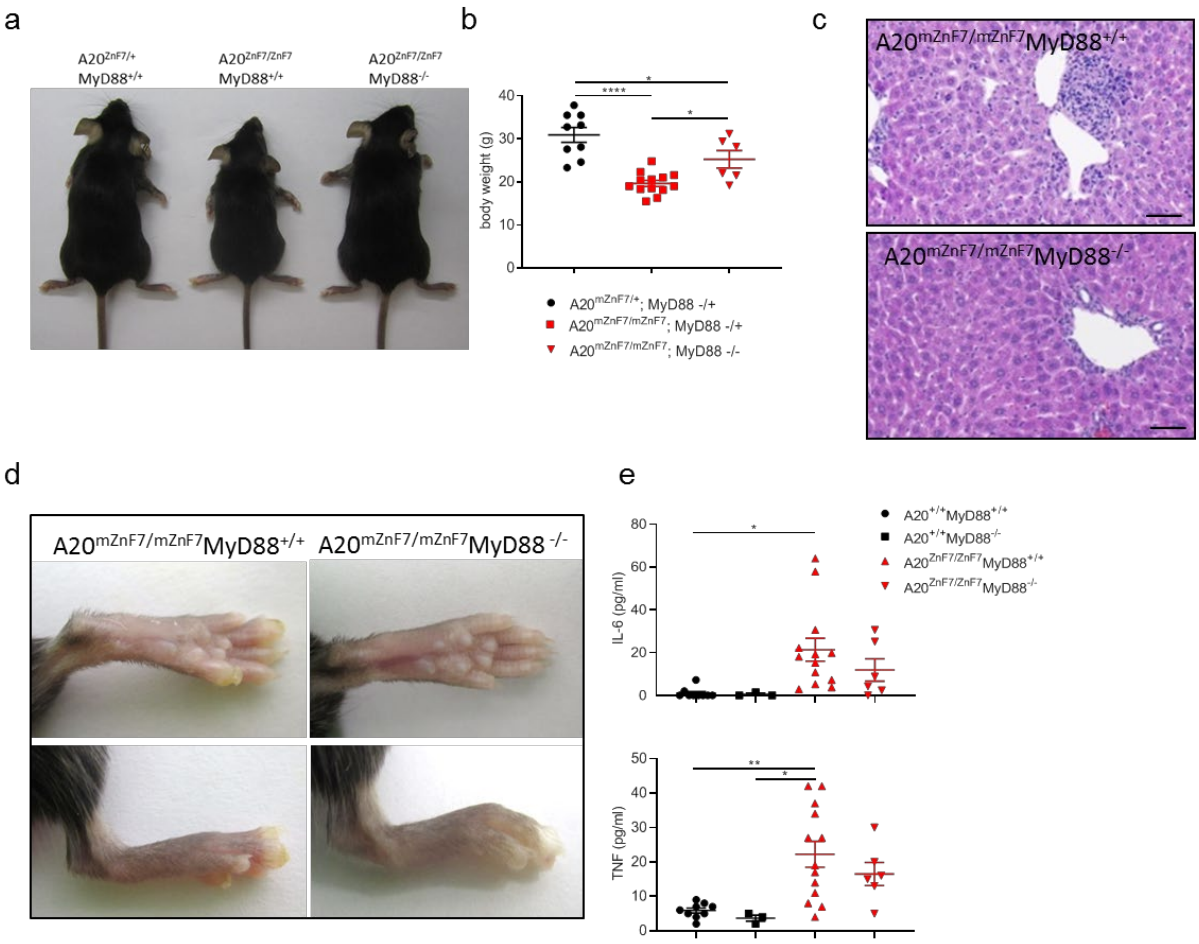

Extended Data Figure 3. MyD88-dependent mechanisms contribute to the local inflammatory pathology in A20^{ZnF7} mice (a-b) Gross appearance (a) and bodyweight (b) of of 10 week-old A20$^{ZnF7/+}$MyD88$^{+/-}$, A20$^{ZnF7/ZnF7}$MyD88$^{+/-}$ and A20$^{ZnF7/ZnF7}$ MyD88$^{-/-}$ mice. Each dot represents a biologically independent mouse (A20$^{ZnF7/+}$MyD88$^{+/-}$, n=9; A20$^{ZnF7/ZnF7}$MyD88$^{+/+}$, n=13 and A20$^{ZnF7/ZnF7}$ MyD88$^{-/-}$, n=6). Data are expressed as mean ± SEM. * and **** represent p<0.05 and p<0.0001, respectively (parametric two-way ANOVA between indicated genotypes). **(c)** Representative hematoxylin-eosin-stained sections of liver from 18-week-old A20$^{ZnF7/ZnF7}$MyD88$^{+/+}$ and A20$^{ZnF7/ZnF7}$MyD88$^{-/-}$ littermates. Scale bar, 50 µm. Picture representative for 3 biologically independent mice. **(d)** Representative pictures of hindpaws of 10-week-old A20$^{ZnF7/ZnF7}$MyD88$^{+/+}$ and A20$^{ZnF7/ZnF7}$MyD88$^{-/-}$ littermates. Pictures representative for 3 biologically independent mice **(e)** Levels of IL-6 and TNF in serum of A20$^{+/+}$MyD88$^{+/+}$, A20$^{+/+}$MyD88$^{-/-}$, A20$^{ZnF7/ZnF7}$MyD88$^{+/+}$ and A20$^{ZnF7/ZnF7}$MyD88$^{-/-}$ mice. Each dot represents a biologically independent mouse (A20$^{+/+}$MyD88$^{+/+}$, n=9; A20$^{+/+}$MyD88$^{-/-}$, n=3; A20$^{ZnF7/ZnF7}$MyD88$^{+/+}$, n=13 and A20$^{ZnF7/ZnF7}$MyD88$^{-/-}$, n=6). Data are expressed as mean ± SEM. *, ** represent p<0.05 and p=0.0033 respectively (parametric one-way ANOVA between indicated genotypes).

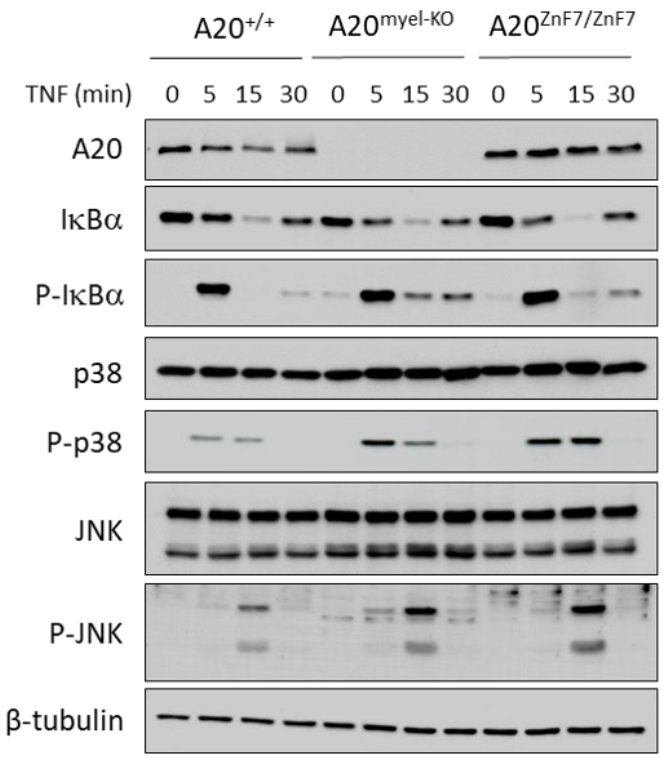

Extended Data Figure 4. ZnF7 is critical for A20-mediated suppression of inflammatory signaling. Western blot analysis of whole cell lysates from $A20^{+/+}$, $A20^{ZnF7/ZnF7}$ and $A20^{myel\text{-}KO}$ BMDMs stimulated with TNF as indicated**.** β-tubulin is shown as a loading control. Figure representative for 3 independent experiments.

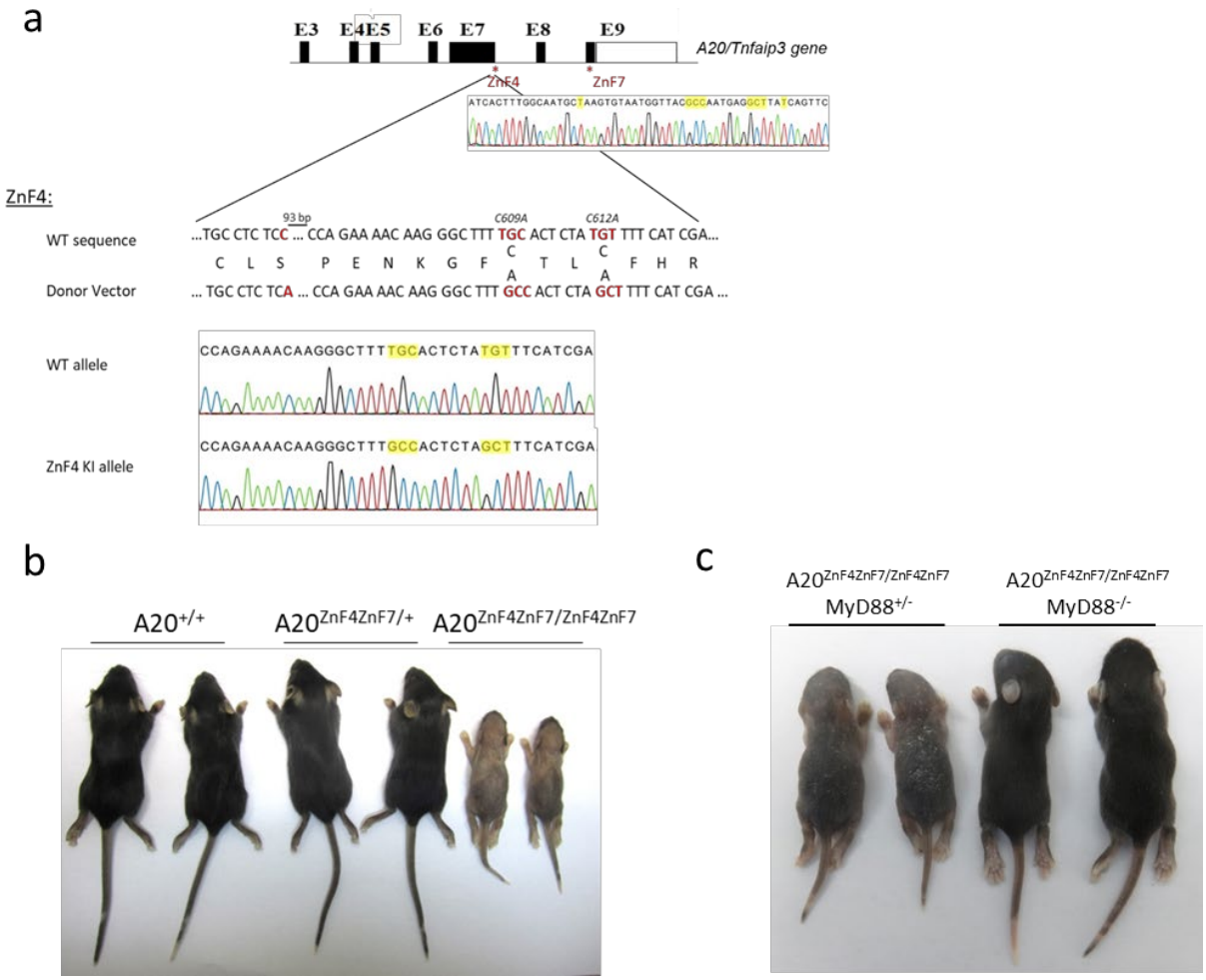

Extended Data Figure 5. A20^{ZnF4ZnF7} knock-in mice. (a) Schematic depiction of the *A20/Tnfaip3* locus indicating the position of ZnF4 and ZnF7 mutations. Boxes indicate exons 3 to 9 (E3–E9). Sequences of the donor vector, containing ~1kb 5' and 3' homologous arms around the Cys-to-Ala mutations used for mutating the ZnF4 and ZnF7 domains, that were introduced by pronuclear injection into mouse zygotes. Sequencing result of the wild-type (WT) allele and of the targeted ZnF4 and ZnF7 knock-in alleles. **(b)** Gross appearance of 2-week old control (A20$^{+/+}$), A20$^{ZnF4ZnF7/+}$ and A20$^{ZnF4ZnF7/ZnF4ZnF7}$ mice. **(c)** Gross appearance of 2-week old A20$^{ZnF4ZnF7/ZnF4ZnF7}$MyD88$^{-/-}$ mice compared to A20$^{ZnF4ZnF7/ZnF4ZnF7}$MyD88$^{+/-}$mice.

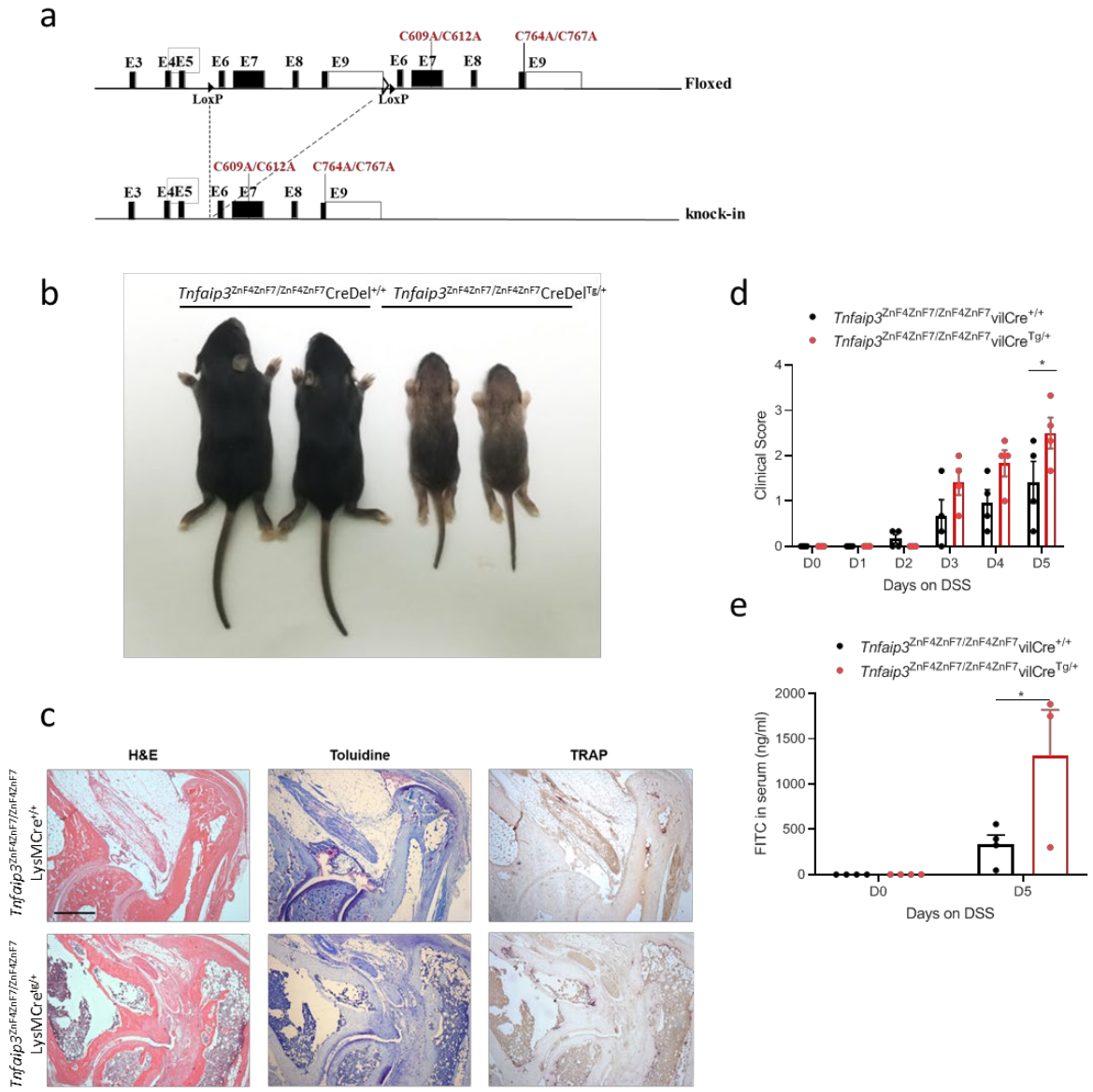

Extended Data Figure 6. Conditional 'floxed' A20$^{ZnF4/ZnF7}$ knock-in mice. (a) Targeting scheme showing the LoxP-flanked (Floxed) and knock-in A20 alleles. Boxes indicate exons 3 to 9 (E3-E9). LoxP sites are indicated by arrowheads. **(b)** Gross appearance of 2 week-old control (*Tnfaip3*$^{ZnF4ZnF7/ZnF4ZnF7}$CreDel$^{+/+}$) and *Tnfaip3*$^{ZnF4ZnF7/ZnF4ZnF7}$CreDel$^{Tg/+}$ littermate mice. **(c)** Representative histological images of ankle joints from 30-week-old littermate mice with the indicated genotypes. Bone erosion was detected by tartrate-resistant acid phosphatase (TRAP) staining of osteoclast activity, and cartilage destruction was assessed by proteoglycan staining with toluidine blue. H/E, haematoxylin and eosin. Scale bar: 500 µm. Pictures representative for 5 biologically independent mice. **(d)** Clinical score, based on loss in body weight, stool consistency, and presence of fecal blood, of 30 week-old *Tnfaip3*$^{ZnF4ZnF7/ZnF4ZnF7}$vilCre$^{Tg/+}$ (n=4) and control (*Tnfaip3*$^{ZnF4ZnF7/ZnF4ZnF7}$vilCre$^{+/+}$**,** n=4) littermate mice treated with 1.5 % DSS. The experiment was stopped at day 5 since *Tnfaip3*$^{ZnF4ZnF7/ZnF4ZnF7}$vilCre$^{Tg/+}$ started dying. Data are expressed as mean ± SEM. * represents p=0.0204 (2-way ANOVA with Sidak's multiple comparison) **(e)** Intestinal permeability assay using FITC-labelled dextran in 30-week-old *Tnfaip3*$^{ZnF4ZnF7/ZnF4ZnF7}$vilCre$^{Tg/+}$ (n=4) and control (*Tnfaip3*$^{ZnF4ZnF7/ZnF4ZnF7}$vilCre$^{+/+}$**,** n=4) mice before and after 5 days of DSS treatment. Data are expressed as mean ± SEM. * represents p=0.0143 (2-way ANOVA with Sidak's multiple comparison.

II. A20 prevents inflammasome-dependent arthritis by inhibiting macrophage necroptosis through its ZnF7 ubiquitin-binding domain

Apostolos Polykratis[1,11], Arne Martens[2,3,11], Remzi Onur Eren[1,11], Yoshitaka Shirasaki[4,5], Mai Yamagishi[5], Yoshifumi Yamaguchi[6,7], Sotaro Uemura[5], Masayuki Miura[6], Bernhard Holzmann[8], George Kollias[9,10], Marietta Armaka[9,12], Geert van Loo[2,3,12] and Manolis Pasparakis[1,12]

1. Institute for Genetics, Cologne Excellence Cluster on Cellular Stress Responses in Aging-Associated Diseases (CECAD) and Center for Molecular Medicine (CMMC), University of Cologne, Cologne, Germany.
2. VIB Center for Inflammation Research, Ghent, Belgium.
3. Department of Biomedical Molecular Biology, Ghent University, Ghent, Belgium.
4. JST PRESTO, Tokyo, Japan.
5. Department of Biological Sciences, Graduate School of Science, The University of Tokyo, Tokyo, Japan.
6. Department of Genetics, Graduate School of Pharmaceutical Science, The University of Tokyo, Tokyo, Japan.
7. Institute of Low Temperature Science, Hokkaido University, Sapporo, Japan.
8. Department of Surgery, School of Medicine, Technical University of Munich, Munich,Germany.
9. Biomedical Sciences Research Center 'Alexander Fleming', Vari, Greece.
10. Department of Physiology, Medical School, National and Kapodistrian University of Athens, Athens, Greece.
11. These authors contributed equally: Apostolos Polykratis, Arne Martens, Remzi Onur Eren.
12. These authors jointly supervised this work

Author contributions

A.P., G.v.L., M.A. and M.P. conceived the study and designed the experiments. A.P., A.M., R.O.E., Y.S., M.Y., Y.Y. and M.A. performed and analysed the experiments. B.H. provided the mice. Y.Y., S.U., M.M., G.K., M.A., G.v.L. and M.P. supervised the experiments. A.P., M.A., G.v.L. and M.P. interpreted the data and wrote the paper.

A20 prevents inflammasome-dependent arthritis by inhibiting macrophage necroptosis through its ZnF7 ubiquitin-binding domain

This publication is the result of a collaboration with the lab of prof. Manolis Pasparakis (University of Cologne). My contribution is figure 7, figure 8, supplementary figure 5, supplementary figure 6 and supplementary figure 7. Furthermore, some additional crosses were set up of which the results are not included in the manuscript (see addendum).

nature cell biology

ARTICLES

https://doi.org/10.1038/s41556-019-0324-3

A20 prevents inflammasome-dependent arthritis by inhibiting macrophage necroptosis through its ZnF7 ubiquitin-binding domain

Apostolos Polykratis[1,11], Arne Martens[2,3,11], Remzi Onur Eren[1,11], Yoshitaka Shirasaki[4,5], Mai Yamagishi[5], Yoshifumi Yamaguchi[6,7], Sotaro Uemura[5], Masayuki Miura[6], Bernhard Holzmann[8], George Kollias[9,10], Marietta Armaka[9,12], Geert van Loo[2,3,12*] and Manolis Pasparakis[1,12*]

Deficiency in the deubiquitinating enzyme A20 causes severe inflammation in mice, and impaired A20 function is associated with human inflammatory diseases. A20 has been implicated in negatively regulating NF-κB signalling, cell death and inflammasome activation; however, the mechanisms by which A20 inhibits inflammation in vivo remain poorly understood. Genetic studies in mice revealed that its deubiquitinase activity is not essential for A20 anti-inflammatory function. Here we show that A20 prevents inflammasome-dependent arthritis by inhibiting macrophage necroptosis and that this function depends on its zinc finger 7 (ZnF7). We provide genetic evidence that RIPK1 kinase-dependent, RIPK3–MLKL-mediated necroptosis drives inflammasome activation in A20-deficient macrophages and causes inflammatory arthritis in mice. Single-cell imaging revealed that RIPK3-dependent death caused inflammasome-dependent IL-1β release from lipopolysaccharide-stimulated A20-deficient macrophages. Importantly, mutation of the A20 ZnF7 ubiquitin binding domain caused arthritis in mice, arguing that ZnF7-dependent inhibition of necroptosis is critical for A20 anti-inflammatory function in vivo.

A20 (also known as TNF inducible protein 3, TNFAIP3) is a deubiquitinating enzyme with critical anti-inflammatory functions. Genome wide association studies have identified *A20* as a susceptibility gene in several human inflammatory and autoimmune diseases, including psoriasis, systemic lupus erythematosus, Crohn's disease and rheumatoid arthritis (reviewed in refs. [1–4]). Moreover, mutations in the *A20* gene have been identified in B cell lymphoma patients[5–8]. More recently, *A20* haploinsufficiency was identified as the cause of early-onset autoinflammatory and autoimmune conditions[9–13]. Studies in genetic mouse models support a key role for A20 as an inhibitor of inflammation. Depending on the genetic background, A20-deficient mice die perinatally or in the first weeks of life due to severe lethal multi-organ inflammation[14–16]. In addition, tissue-specific A20 deficiency sensitizes mice to inflammatory and autoimmune pathologies[17–26]. Although its important anti-inflammatory role in both humans and mice is indisputable, the mechanisms by which A20 suppresses inflammation in vivo remain poorly understood.

Inhibition of NF-κB activation is considered the primary anti-inflammatory function of A20 (refs. [1,2,27,28]). In addition, A20 was also suggested to inhibit necroptosis by deubiquitinating receptor interacting protein kinase 3 (RIPK3)[15]. Although RIPK3 deficiency prolonged the survival of *A20*-knockout mice, mixed lineage kinase-like (MLKL) deficiency did not have any protective effects, arguing against a role for necroptosis in the pathology caused by A20 deficiency[15,16]. Degradation of lysine 63 (K63)-linked ubiquitin chains by A20 is considered important for the inhibition of inflammation by preventing the ubiquitin-dependent recruitment of the inhibitor of NF-κB kinase (IKK) and transforming growth factor beta-activating kinase 1 (TAK1) signalling complexes to upstream receptors[1,2,27–29]. In addition, the ZnF4 domain of A20 was proposed to limit tumour necrosis factor receptor 1 (TNFR1) signalling by mediating K48-linked ubiquitination of RIPK1[29]. However, knock-in mice expressing A20 with mutated catalytic ovarian tumour or ZnF4 domains did not develop spontaneous inflammatory pathology, arguing that ubiquitin-chain degradation and ZnF4-dependent functions are not essential for the A20-mediated suppression of inflammation in vivo[28,30,31]. The capacity to bind to ubiquitin chains through its ZnF domains 4 and 7 has also been implicated in A20 function[32–36]. In particular, the ZnF7 of A20 was implicated in regulating TNFR1 signalling by binding specifically to linear ubiquitin chains[28,37] and inhibiting TNFR1-mediated apoptosis and necroptosis[35,37]. However, the in vivo function of the A20 ZnF7 remains unknown.

We showed previously that mice with myeloid-cell-specific A20 deficiency ($A20^{MYC\text{-}KO}$) spontaneously develop inflammatory joint pathology resembling rheumatoid arthritis[23]. Arthritis development in $A20^{MYC\text{-}KO}$ mice requires NLR family pyrin domain containing

[1]Institute for Genetics, Cologne Excellence Cluster on Cellular Stress Responses in Aging-Associated Diseases (CECAD) and Center for Molecular Medicine, University of Cologne, Cologne, Germany. [2]VIB Center for Inflammation Research, Ghent, Belgium. [3]Department of Biomedical Molecular Biology, Ghent University, Ghent, Belgium. [4]Precursory Research for Embryonic Science and Technology, Japan Science and Technology Agency, Tokyo, Japan. [5]Department of Biological Sciences, Graduate School of Science, The University of Tokyo, Tokyo, Japan. [6]Department of Genetics, Graduate School of Pharmaceutical Science, The University of Tokyo, Tokyo, Japan. [7]Institute of Low Temperature Science, Hokkaido University, Sapporo, Japan. [8]Department of Surgery, School of Medicine, Technical University of Munich, Munich, Germany. [9]Biomedical Sciences Research Center 'Alexander Fleming', Vari, Greece. [10]Department of Physiology, Medical School, National and Kapodistrian University of Athens, Athens, Greece. [11]These authors contributed equally: Apostolos Polykratis, Arne Martens, Remzi Onur Eren. [12]These authors jointly supervised this work: Marietta Armaka, Geert van Loo, Manolis Pasparakis. *e-mail: geert.vanloo@irc.vib-ugent.be; pasparakis@uni-koeln.de

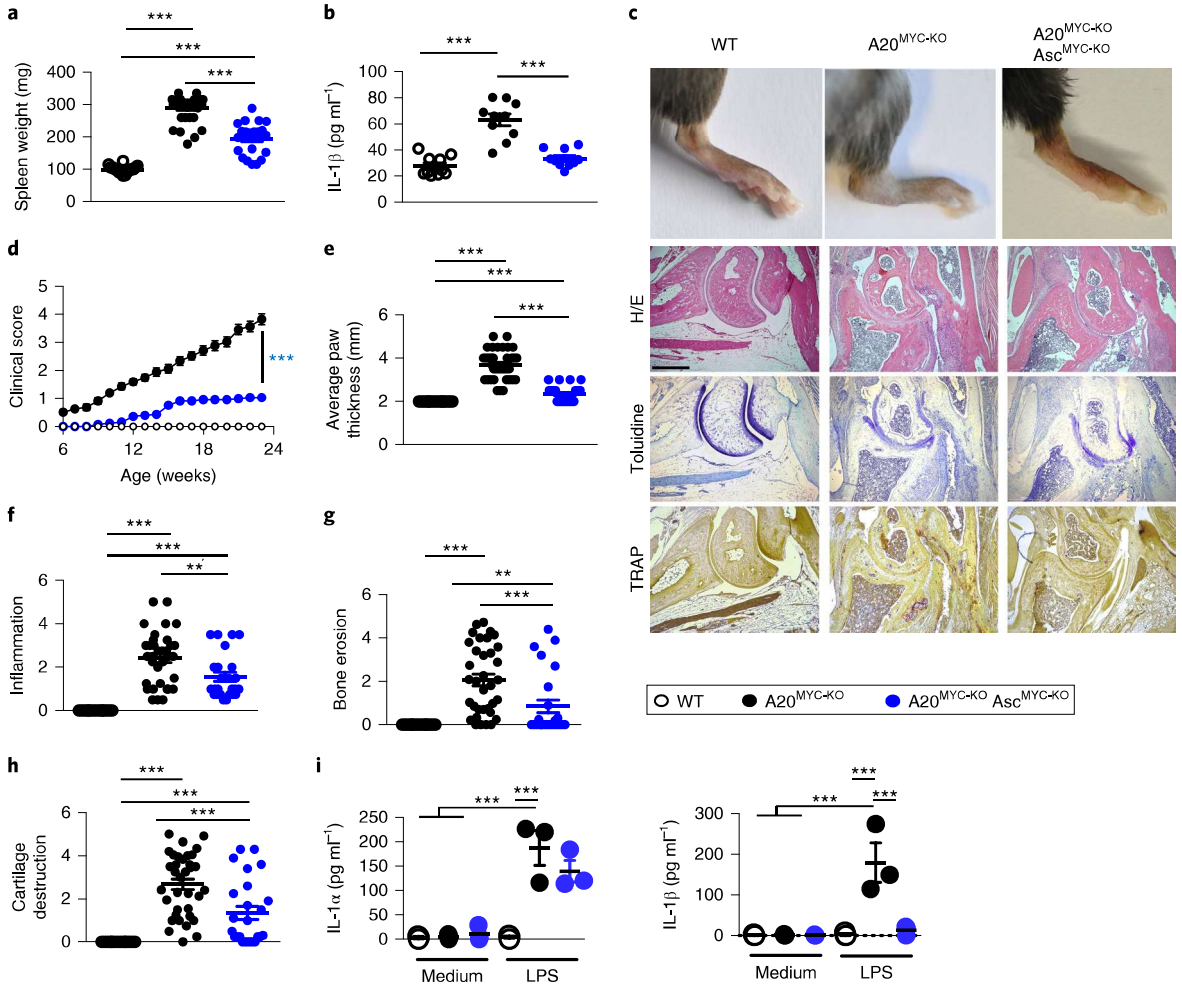

Fig. 1 | Myeloid-cell-specific *ASC* knockout inhibits arthritis development in A20^{MYC-KO} mice. a, Spleen weight of mice with the indicated genotypes. **b**, Serum IL-1β levels in mice with the indicated genotypes ($n=10$ mice per genotype). **c**, Representative macroscopic and histological images of the ankle joints of mice with the indicated genotypes. Bone erosion was detected by tartrate-resistant acid phosphatase (TRAP; bottom) staining of osteoclast activity, and cartilage destruction was assessed by proteoglycan staining with toluidine blue (middle). H/E, haematoxylin and eosin. Scale bar, 500 µm. **d–h**, Weekly clinical scores (**d**), average thicknesses of the rear paws at the ankle area (**e**), as well as the histological scores for inflammation (**f**), bone erosion (**g**) and cartilage destruction (**h**) of mice with the indicated genotypes. Spleen weight, paw thickness and joint histology were analysed at the age of 23–27 weeks (wild-type (WT), $n=16$; A20^{MYC-KO}, $n=35$ and A20^{MYC-KO} Asc^{MYC-KO}, $n=25$ mice for **a**,**c–h**). **i**, Levels of IL-1β (right) and IL-1α (left) released in the supernatants of BMDMs stimulated for 24 h with 1 µg ml^{-1} ultrapure LPS. The graphs show the pooled results of three independent experiments performed at different times with one independent isolation of macrophages from the indicated genotypes per experiment. The mean ± s.e.m. is shown for each group of mice in all graphs. $^{*}P<0.05$; $^{**}P<0.01$ and $^{***}P<0.001$; non-parametric Mann–Whitney test between the indicated genotypes for **a**,**b**,**e–h**, two-way analysis of variance (ANOVA) test with Bonferroni correction for **d** and one-way ANOVA with Bonferroni correction for **i**. All of the statistical tests are two-tailed. The raw data are provided in Supplementary Table 3. The legend in **g** applies to **a**,**b**,**d–i**.

3 (NLRP3), caspase-1 and interleukin 1 receptor (IL-1R1) signalling, suggesting that the regulation of inflammasome activation is a key anti-inflammatory function of A20[23,38]. However, the mechanisms by which A20 limits inflammasome activation remain poorly understood. Excessive inflammasome priming through impaired A20-dependent negative regulation of NF-κB-mediated expression of NLRP3 and pro-IL-1β was suggested to contribute to inflammasome hyperactivation and arthritis development based on in vitro studies using macrophages from A20^{MYC-KO} mice[38]. In addition, A20 was reported to negatively regulate the ubiquitination of pro-IL-1β as well as components of the NLRP3–Caspase-1 inflammasome in a RIPK3-dependent, but cell death-independent manner, suggesting that A20 directly regulates inflammasome activity by deubiquitination[39]. Therefore, the pathways that are controlled by A20 and are critical for the inhibition of inflammation in vivo as well as the functional domains of A20 that regulate these activities remain elusive.

Here we provide genetic and biochemical evidence that A20 prevents inflammasome activation and arthritis pathology indirectly by inhibiting macrophage necroptosis. Moreover, we show that knock-in mice expressing A20 with mutated ZnF7 develop spontaneous arthritis, revealing an indispensable function of ZnF7-mediated binding to linear ubiquitin chains in the A20-mediated suppression of inflammation in vivo. Together, these results identify the inhibition of necroptosis as a critical anti-inflammatory function of A20 in vivo and suggest that necroptosis inhibitors could be effective for the treatment of arthritis and other inflammatory pathologies associated with impaired A20 activity.

Results

Inflammasome activation in myeloid cells causes arthritis in A20^{MYC-KO} mice. A20^{MYC-KO} mice spontaneously develop inflammatory joint pathology resembling rheumatoid arthritis, which is

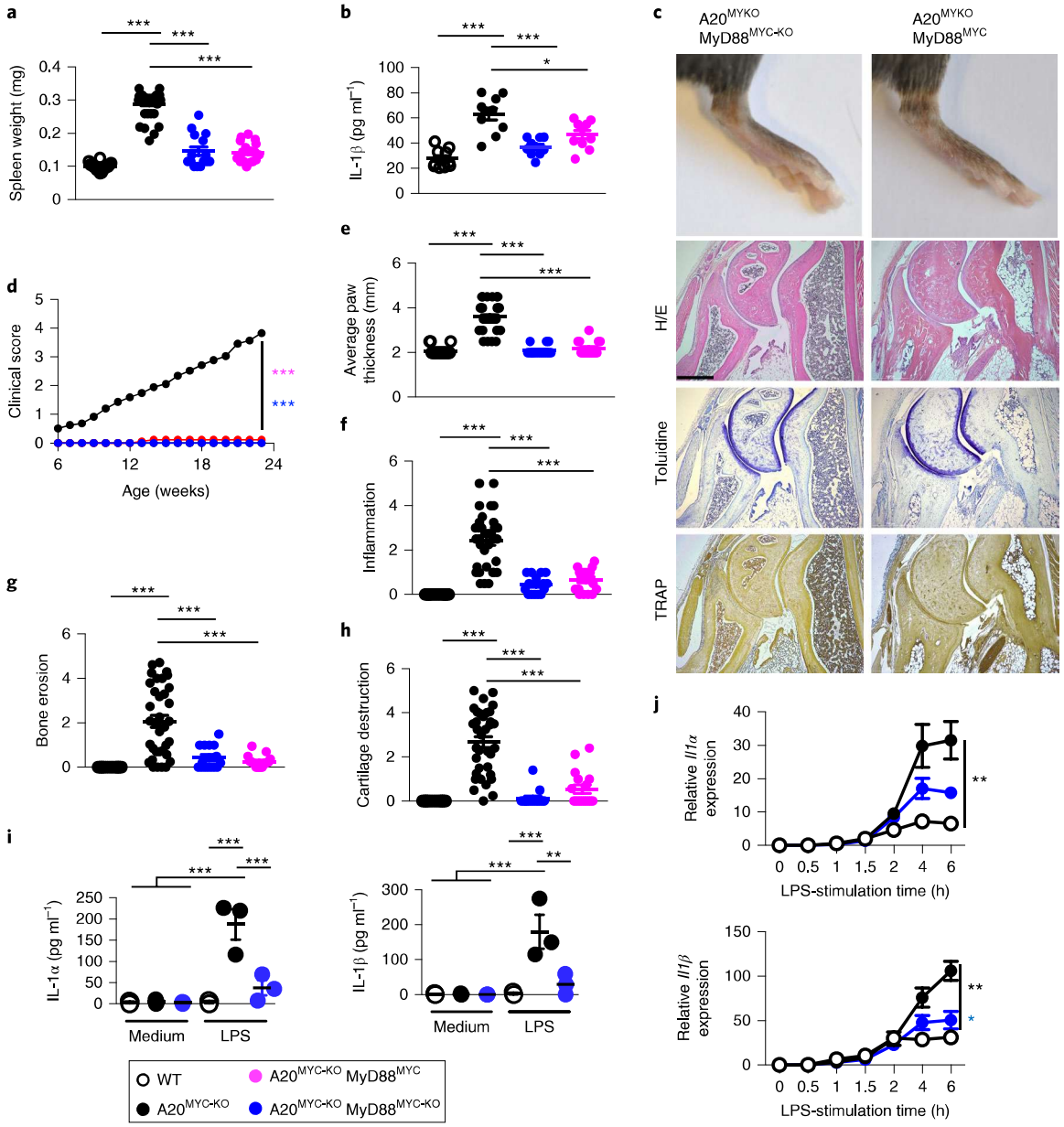

Fig. 2 | MyD88-dependent signalling in both myeloid and non-myeloid cells is required for spontaneous arthritis development in A20^{MYC-KO} mice. **a**, Spleen weight of mice with the indicated genotypes. **b**, Serum IL-1β levels in mice with the indicated genotypes ($n=10$ mice per genotype). **c**, Representative macroscopic and histological images of the ankle joints of mice with the indicated genotypes. Scale bar, 500 µm. **d–h**, Weekly clinical scores (**d**), average thicknesses of the rear paws at the ankle area (**e**), as well as histological scores for inflammation (**f**), bone erosion (**g**) and cartilage destruction (**h**) of mice with the indicated genotypes. Spleen weight, paw thickness and joint histology were analysed at the age of 23–27 weeks, WT and A20^{MYC-KO} data are the same as those in Fig. 1 and are included for comparison (WT, $n=16$; A20^{MYC-KO}, $n=35$; A20^{MYC-KO} MyD88^{MYC-KO}, $n=15$ and A20^{MYC-KO} MyD8^{8MYC}, $n=17$ mice for **a**,**c–h**). **i**, Levels of IL-1β (right) and IL-1α (left) released in the supernatants of BMDMs stimulated for 24 h with 1 µg ml^{-1} ultrapure LPS. The graphs show the pooled results of three independent experiments performed at different times with one independent isolation of macrophages from the indicated genotypes per experiment. **j**, Expression levels of *Il1β* (bottom) and *Il1α* (top) mRNA in macrophages stimulated with 20 ng ml^{-1} LPS. The graphs show the result of one experiment performed with three independent isolations of BMDMs with the indicated genotypes. The mean ± s.e.m. is shown for each group of mice in all graphs. *$P<0.05$, **$P<0.01$ and ***$P<0.001$; non-parametric Mann–Whitney test between the indicated genotypes for **a**,**b**,**e–h**, two-way ANOVA with Bonferroni correction for **d**,**j** and one-way ANOVA with Bonferroni correction for **i**. All of the statistical tests are two-tailed. The raw data are provided in Supplementary Table 3. The legend in **i** applies to **a**,**b**,**d–j**.

characterised by immune cell infiltration, bone erosion and cartilage destruction, and show splenomegaly and elevated numbers of blood monocytes and neutrophils[23] (Fig. 1a–c and Supplementary Fig. 1a). We showed previously that crossing A20^{MYC-KO} mice with *Nlpr3*$^{-/-}$, *Casp1/11*$^{-/-}$ or *Il-1r1*$^{-/-}$ mice strongly ameliorated arthritis development, suggesting that NLRP3 inflammasome-mediated IL-1β production drives the pathology[23,38]. To assess whether cell-intrinsic inflammasome activation in A20-deficient myeloid cells drives arthritis, we generated mice lacking both A20 and apoptosis-associated speck-like protein containing CARD (ASC), an adaptor required for the recruitment and activation of caspase-1 downstream of NLRP3[40], specifically in myeloid cells. The ablation of ASC

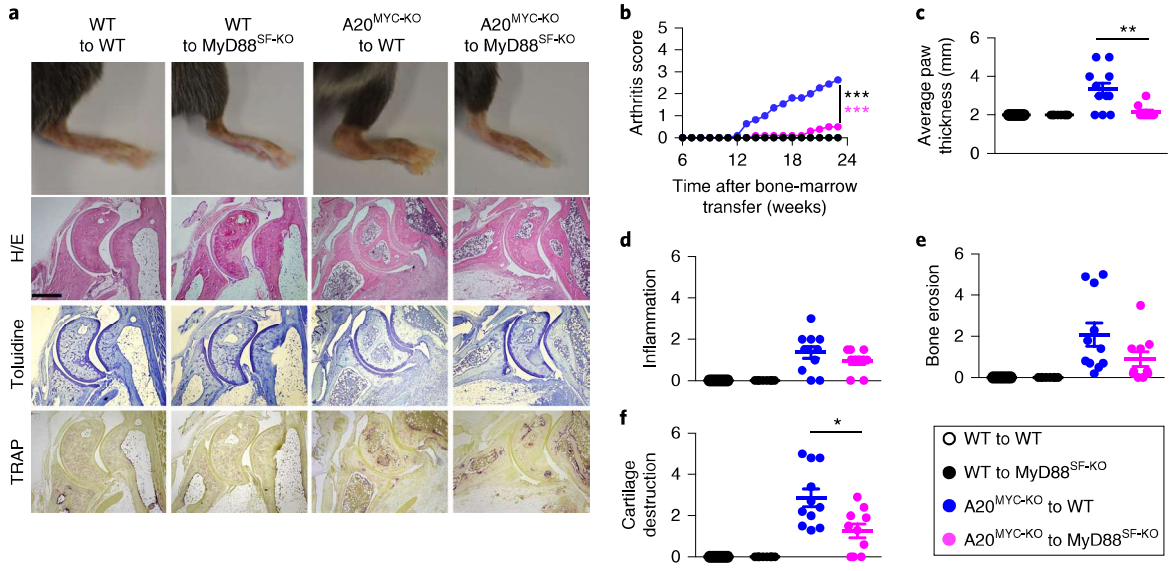

Fig. 3 | Synovial-fibroblast-specific MyD88-dependent signalling contributes to the spontaneous development of arthritis in A20$^{MYC\text{-}KO}$ mice. **a**, Representative macroscopic and histological images of the ankle joints of mice with the indicated genotypes. Scale bar, 500 µm. **b–f**, Weekly clinical scores (**b**), average thicknesses of the rear paws at the ankle area (**c**), as well as the histological scores for inflammation (**d**), bone erosion (**e**) and cartilage destruction (**f**) of mice with the indicated genotypes. Paw thickness and joint histology were analysed 25 weeks after bone marrow transfer. The dots in the graphs indicate individual mice (WT to WT, $n=7$; WT to MyD88$^{SF\text{-}KO}$, $n=8$; A20$^{MYC\text{-}KO}$ to WT, $n=11$ and A20$^{MYC\text{-}KO}$ to MyD88$^{SF\text{-}KO}$, $n=10$ mice for **a–f**). The mean ± s.e.m. is shown for each group of mice in all graphs. $^{*}P<0.05$ and $^{**}P<0.01$; non-parametric Mann–Whitney test between indicated genotypes for **c–f** and two-way ANOVA with Bonferroni correction for **b**. All of the statistical tests are two-tailed. The raw data are provided in Supplementary Table 3. The legend in **f** applies to **b–f**.

reduced the levels of IL-1β, IL-18 and TNF in the serum and ameliorated splenomegaly in A20$^{MYC\text{-}KO}$ mice (Fig. 1a,b and Supplementary Fig. 1b). Myeloid-specific ASC deficiency also substantially reduced arthritis severity but could not fully prevent joint inflammation or bone and cartilage damage (Fig. 1c–h). Lipopolysaccharide (LPS) stimulation triggered ASC-dependent IL-1β release from A20-deficient bone-marrow-derived macrophages (BMDMs) as shown previously[39] but also caused ASC-independent IL-1α release (Fig. 1i), suggesting that inflammasome-independent IL-1α production could also contribute to the development of arthritis.

Arthritis development in A20$^{MYC\text{-}KO}$ mice depends on MyD88 signalling in both myeloid and non-myeloid cells. We previously showed that MyD88 deficiency prevents the development of arthritis, splenomegaly and myeloid cell expansion in A20$^{MYC\text{-}KO}$ mice[23]. To investigate the relative contribution of MyD88 signalling in myeloid and non-myeloid cells, we employed a dual approach. First, we generated mice lacking both A20 and MyD88 in myeloid cells (A20$^{MYC\text{-}KO}$ MyD88$^{MYC\text{-}KO}$) and found that myeloid-cell-specific MyD88 ablation prevented arthritis, suppressed splenomegaly and myeloid cell expansion, normalized IL-1β and reduced TNF levels, but did not significantly affect IL-18, IL-6 and MCP-1 production in A20$^{MYC\text{-}KO}$ mice (Fig. 2a–h and Supplementary Fig. 1c,d). MyD88 deficiency also strongly reduced the LPS-induced release of IL-1β and IL-1α from A20-deficient BMDMs, which correlated with reduced transcription of *Il1β* and *Il1α* messenger RNA (Fig. 2i,j). To assess the role of MyD88 in non-myeloid cells, we employed *Myd88*^{LSL} mice carrying *Myd88* alleles containing a loxP-flanked transcriptional stop cassette in intron 1 that do not express MyD88 unless the loxP-flanked stop cassette is excised by Cre recombinase[41]. By intercrossing A20$^{MYC\text{-}KO}$ mice with *Myd88*^{LSL} animals we obtained mice with myeloid cells that lack A20 but express MyD88, whereas non-myeloid cells express A20 but lack MyD88 (A20$^{MYC\text{-}KO}$ MyD88^{MYC}). MyD88 deficiency in non-myeloid cells did not inhibit monocytosis but partly reduced neutrophilia and strongly suppressed splenomegaly in A20$^{MYC\text{-}KO}$ mice (Fig. 2a and Supplementary Fig. 1c). Importantly, A20$^{MYC\text{-}KO}$ MyD88^{MYC} mice were protected from arthritis and had reduced levels of IL-1β, IL-18, TNF and IL-6 in the serum (Fig. 2b–h and Supplementary Fig. 1d). Therefore, MyD88 acts in both myeloid and non-myeloid cells to induce the pathogenesis of inflammatory arthritis in A20$^{MYC\text{-}KO}$ mice.

MyD88-dependent signalling in synovial fibroblasts contributes to the development of arthritis in A20$^{MYC\text{-}KO}$ mice. MyD88 signalling in myeloid cells probably regulates arthritis development by inducing the expression of IL-1β and IL-1α; however, it is unclear how MyD88 acts in non-myeloid cells to drive arthritis in A20$^{MYC\text{-}KO}$ mice. We postulated that MyD88 acts downstream of the IL-1 receptor in synovial fibroblasts, which are activated by IL-1 and mediate the inflammation and destruction of joint tissue by producing metalloproteases and inflammatory cytokines[42,43] to drive arthritis pathogenesis. We therefore generated mice lacking MyD88 in synovial fibroblasts (MyD88$^{SF\text{-}KO}$) by crossing *Myd88*$^{FL/FL}$ mice with Col6a1Cre transgenic mice[44]. Synovial fibroblasts from MyD88$^{SF\text{-}KO}$ mice showed impaired NF-κB and mitogen-activated protein kinase (MAPK) activation and a strongly reduced expression of cytokines and metalloproteinases in response to stimulation with either LPS or IL-1β (Supplementary Fig. 2a–c). To address the role of MyD88 in synovial fibroblasts in the development of arthritis, we reconstituted lethally irradiated MyD88$^{SF\text{-}KO}$ as well as control *Myd88*$^{FL/FL}$ mice with bone marrow from A20$^{MYC\text{-}KO}$ or littermate *A20*$^{FL/FL}$ mice. MyD88$^{SF\text{-}KO}$ recipients that received the A20$^{MYC\text{-}KO}$ bone marrow showed reduced arthritis and splenomegaly compared with the wild-type recipients, whereas monocytosis and neutrophilia were not affected (Fig. 3 and Supplementary Fig. 2d). MyD88 acts downstream of toll-like receptors (TLRs) as well as IL-1 family receptors. Our earlier work provided evidence that both TLR4 and IL-1R signalling are important for the pathogenesis of arthritis in A20$^{MYC\text{-}KO}$ mice[23]. We found that the synovial-fibroblast-specific knockout of TLR4 did not affect arthritis and splenomegaly induced by reconstitution

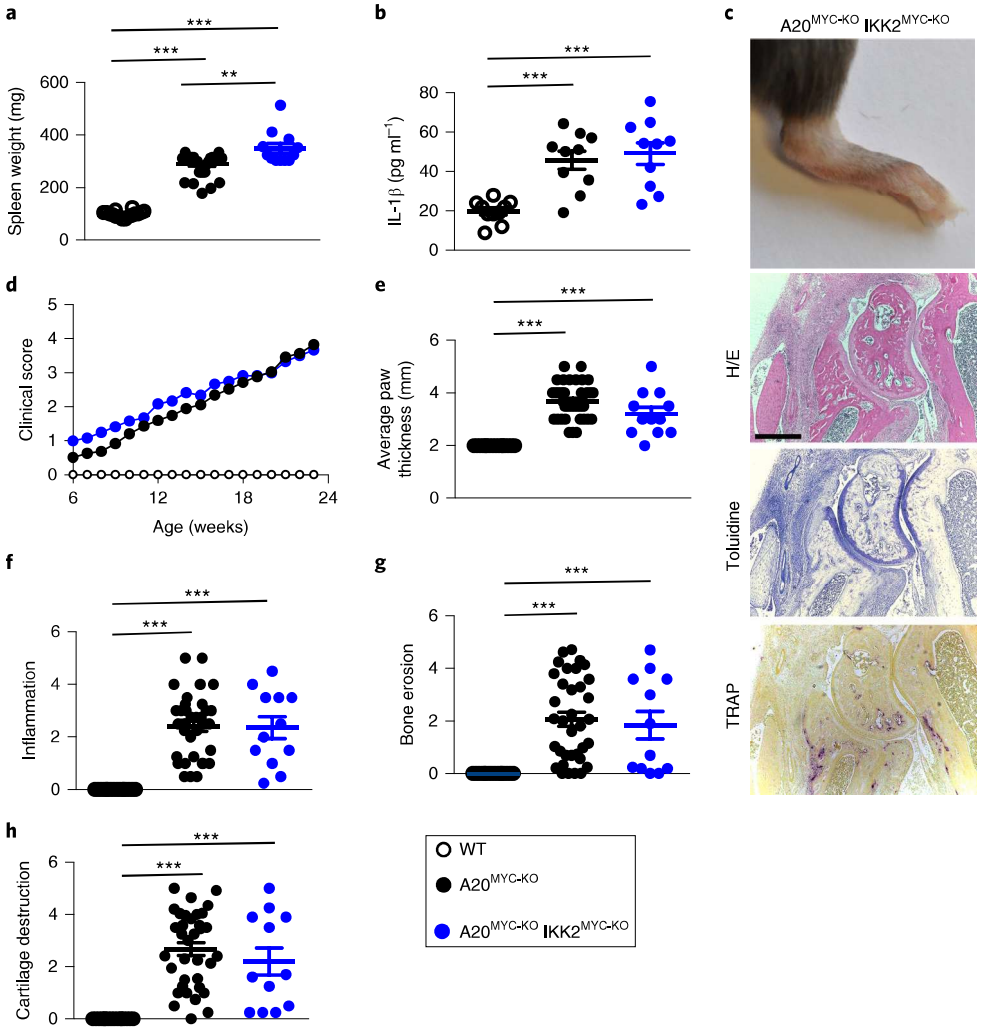

Fig. 4 | IKK2 deficiency in myeloid cells does not inhibit the development of arthritis in A20$^{MYC\text{-}KO}$ mice. a, Spleen weight of mice with the indicated genotypes. **b**, Serum IL-1β levels in mice with the indicated genotypes ($n=10$ mice per genotype). **c**, Representative macroscopic and histological images of the ankle joints of mice with the indicated genotypes. Scale bar, 500 µm. **d–h**, Weekly clinical scores (**d**), average thicknesses of the rear paws at the ankle area (**e**), as well as histological scores for inflammation (**f**), bone erosion (**g**) and cartilage destruction (**h**) of the mice with the indicated genotypes. Spleen weight, paw thickness and joint histology were analysed at the age of 23–27 weeks, WT and A20$^{MYC\text{-}KO}$ data are the same as those in Fig. 1 and are included for comparison (WT, $n=16$; A20$^{MYC\text{-}KO}$, $n=35$ and A20$^{MYC\text{-}KO}$ IKK2$^{MYC\text{-}KO}$, $n=12$ mice for **a**,**c–h**). The mean ± s.e.m. is shown for each group of mice in all graphs. ***$P<0.001$; non-parametric Mann–Whitney test between the indicated genotypes for **a**,**b**,**e–h** and two-way ANOVA with Bonferroni correction for **d**. All of the statistical tests are two-tailed. The raw data are provided in Supplementary Table 3. The legend in **h** applies to **a**,**b**,**d–h**.

with bone marrow from A20$^{MYC\text{-}KO}$ mice (Supplementary Fig. 3), further supporting that MyD88 acts downstream of IL-1R in synovial fibroblasts. Collectively, these results argue that the activation of arthritogenic MyD88-dependent signalling in synovial fibroblasts of A20$^{MYC\text{-}KO}$ animals occurs downstream of IL-1R activation induced by IL-1β and IL-1α released by A20-deficient macrophages.

Myeloid-cell-specific IKK2 deficiency does not prevent arthritis in A20$^{MYC\text{-}KO}$ mice. Inhibition of NF-κB activation is considered the main anti-inflammatory function of A20[1,2,27,28]. To address the role of NF-κB, we generated mice lacking both A20 and IKK2/IKKβ in myeloid cells. The A20$^{MYC\text{-}KO}$ IKK2$^{MYC\text{-}KO}$ mice exhibited similar spleen size, serum IL-1β levels and inflammatory joint pathology to A20$^{MYC\text{-}KO}$ animals, showing that NF-κB inhibition by IKK2 knockout in myeloid cells was not sufficient to suppress inflammation caused by A20 deficiency (Fig. 4). These results argue that the NF-κB-independent functions of A20 in myeloid cells are critical for preventing inflammation in vivo.

RIPK1–RIPK3–MLKL-dependent necroptosis drives arthritis development in A20$^{MYC\text{-}KO}$ mice. In addition to inhibiting NF-κB, A20 has been implicated in the regulation of RIPK3-dependent signalling[15,39]. We therefore generated A20$^{MYC\text{-}KO}$ *Ripk3*$^{-/-}$ mice and found that RIPK3 deficiency prevented arthritis development (Fig. 5). RIPK3 induces MLKL-dependent necroptosis but can also promote apoptosis and has been proposed to regulate inflammation independently of cell death[45]. To specifically address the role of necroptosis, we generated A20$^{MYC\text{-}KO}$ *Mlkl*$^{-/-}$ mice and found that they were also strongly protected from arthritis (Fig. 5). Inhibition of RIPK1 kinase activity has been shown to efficiently block necroptosis downstream of many receptors, including death receptors and TLRs[46]. To assess the role of RIPK1 kinase activity, we crossed A20$^{MYC\text{-}KO}$ mice with *Ripk1*$^{D138N/D138N}$ knock-in mice[47] that express kinase-inactive RIPK1. A lack of RIPK1 kinase activity protected A20$^{MYC\text{-}KO}$ mice from the development of arthritis to a similar extent as RIPK3 or MLKL deficiency (Fig. 5). A lack of RIPK1 kinase activity as well as RIPK3 or MLKL deficiency also

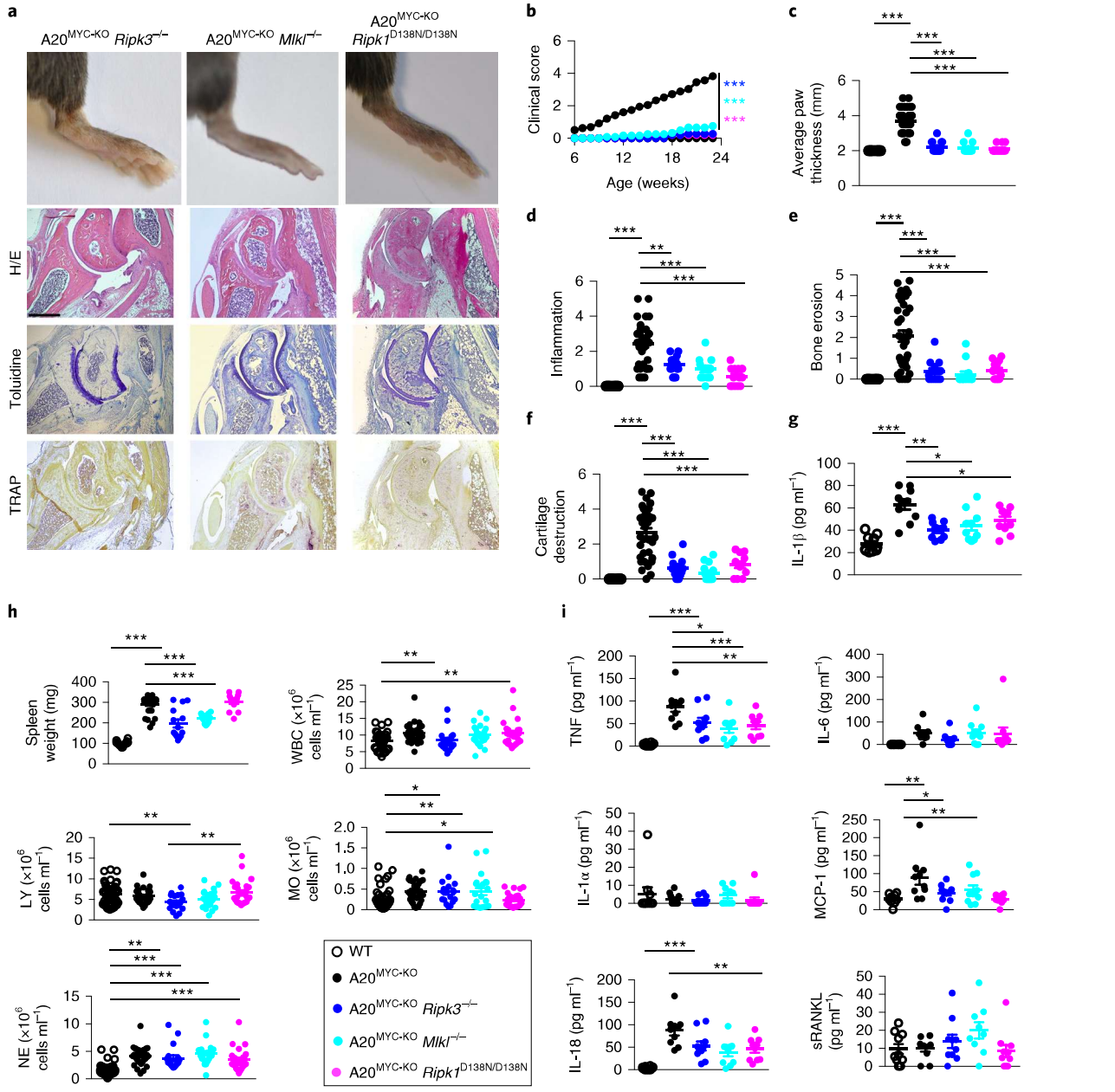

Fig. 5 | Necroptosis contributes to the spontaneous development of arthritis in A20^{MYC-KO} mice. a, Representative macroscopic and histological images of the ankle joints of mice with the indicated genotypes. Scale bar, 500 μm. **b–f**, Weekly clinical scores (**b**), average thicknesses of the rear paws at the ankle area (**c**), as well as the histological scores for inflammation (**d**), bone erosion (**e**) and cartilage destruction (**f**) of mice with the indicated genotypes. Spleen weight, paw thickness and joint histology were analysed at the age of 23–27 weeks. The WT and A20^{MYC-KO} data are the same as those in Fig. 1 and were included for comparison (WT, $n=16$; A20^{MYC-KO}, $n=35$; A20^{MYC-KO} *Ripk3*$^{-/-}$, $n=14$; A20^{MYC-KO} *Mlkl*$^{-/-}$, $n=12$ and A20^{MYC-KO} *Ripk1*$^{D138N/D138N}$, $n=14$ mice for **a–f**). **g**, Serum IL-1β levels in mice with the indicated genotypes ($n=10$ mice per genotype). **h**, Number of white blood cells (WBC), lymphocytes (LY), monocytes (MO) and neutrophils (NE) in the peripheral blood of mice with the indicated genotypes. The WT and A20^{MYC-KO} mice are the same as those in Supplementary Fig. 1 and are included for comparison (WT, $n=54$; A20^{MYC-KO}, $n=33$; A20^{MYC-KO} *Ripk3*$^{-/-}$, $n=18$; A20^{MYC-KO} *Mlkl*$^{-/-}$, $n=22$ and A20^{MYC-KO} *Ripk1*$^{D138N/D138N}$, $n=26$ mice). **i**, Levels of the indicated cytokines and chemokines in the serum of mice with the indicated genotypes ($n=10$ mice per genotype, excepting for IL-18 A20^{MYC-KO} *Ripk3*$^{-/-}$, where $n=9$ mice). The dots in the graphs indicate individual mice. The mean ± s.e.m. is also shown for each group of mice in all graphs. $^{*}P<0.05$, $^{**}P<0.01$ and $^{***}P<0.001$; non-parametric Mann–Whitney test between the indicated genotypes for **c–g** and two-way ANOVA with Bonferroni correction for **b**. All of the statistical tests are two-tailed. The raw data are provided in Supplementary Table 3. The legend in **h** applies to **b–i**.

reduced the levels of IL-1β and TNF in the serum of A20^{MYC-KO} mice (Fig. 5). However, splenomegaly was largely dependent on RIPK3–MLKL-mediated necroptosis but independent of RIPK1 kinase activity, whereas monocytosis was dependent on RIPK1 kinase activity but not RIPK3–MLKL (Fig. 5). Together, these results reveal a critical role of RIPK1–RIPK3–MLKL-dependent necroptosis in driving the pathogenesis of inflammatory arthritis in A20^{MYC-KO} mice.

RIPK3-dependent cell death is required for IL-1β and IL-1α release by LPS-stimulated *A20*-knockout macrophages. Our genetic studies showed that RIPK1–RIPK3–MLKL-induced

necroptosis drives IL-1β release in vivo and arthritis development in A20$^{MYC\text{-}KO}$ mice. To address how RIPK1, RIPK3 and MLKL regulate the release of IL-1β from A20-deficient myeloid cells, we studied the responses of BMDMs from the different mouse lines. Neither a deficiency of RIPK3 or MLKL nor a lack of RIPK1 kinase activity affected the LPS- or TNF-induced activation of NF-κB and MAPK signalling as well as the mRNA expression of inflammatory mediators in A20-deficient BMDMs (Supplementary Fig. 4), which suggests that RIPK1, RIPK3 and MLKL do not act by regulating NF-κB-mediated inflammatory gene transcription in A20-deficient macrophages.

RIPK3 deficiency prevented the LPS-induced release of processed IL-1β from A20-deficient BMDMs (Fig. 6a,b), as shown previously[39]. Interestingly, RIPK3 deficiency also prevented the inflammasome-independent release of IL-1α, which requires breach of the plasma membrane as, for example, during necrotic cell death[48]. These results suggest that RIPK3 might regulate the LPS-induced release of IL-1β and IL-1α from A20-deficient macrophages by triggering cell death. MLKL deficiency reduced the LPS-induced production of IL-1β and IL-1α by *A20*-knockout BMDMs, although it could not fully prevent the release of these cytokines as observed in RIPK3-deficient cells (Fig. 6a,b). The pan-caspase inhibitor z-VAD-fmk inhibited the release of IL-1β from A20-deficient BMDMs, probably due to the inhibition of caspase-1-dependent pro-IL-1β processing, whereas IL-1α was still produced by these cells albeit to somewhat reduced levels (Fig. 6b). However, z-VAD-fmk fully prevented the release of IL-1α from macrophages lacking both A20 and MLKL (Fig. 6b), suggesting that caspase-dependent cell death drives the production of IL-1α from A20-deficient macrophages when MLKL-dependent necroptosis is blocked. Interestingly, the inhibition of RIPK1 kinase activity—either genetically in A20$^{MYC\text{-}KO}$ *Ripk1*$^{D138N/D138N}$ BMDMs or pharmacologically by Necrostatin-1s—did not inhibit the LPS-induced release of IL-1β and IL-1α from A20-deficient macrophages (Fig. 6a,b), which suggests that RIPK1 kinase activity is dispensable for the production of these cytokines under in vitro stimulation conditions. Together, these results suggest that MLKL-dependent necroptosis contributes to both the inflammasome-dependent release of IL-1β and the inflammasome-independent production of IL-1α by A20-deficient macrophages.

Previous work suggested that RIPK3 regulates the LPS-induced IL-1β release by A20-deficient macrophages independently of cell death[39]. However, one caveat of assessing cell death using biochemical assays such as LDH release is that these methodologies are not sensitive enough to detect the death of a small fraction of the cells. Based on our results above, we reasoned that IL-1β could be released by a small fraction of dying A20-deficient macrophages. To test this hypothesis, we employed a newly developed methodology that allows the simultaneous dynamic real-time imaging of cell death and IL-1β release at the single-cell level[49,50]. The BMDMs from wild-type, A20$^{MYC\text{-}KO}$ and A20$^{MYC\text{-}KO}$ *Ripk3*$^{-/-}$ mice seeded on a microwell device were stimulated with LPS, and cell death and IL-1β secretion were measured at single-cell resolution using total internal reflection fluorescent microscopy. As shown in Fig. 6c, a considerable fraction of dying A20-deficient BMDMs secreted IL-1β, whereas surviving cells did not secrete the cytokine. Moreover, RIPK3 deficiency strongly suppressed both cell death and IL-1β release in LPS-stimulated *A20*-knockout macrophages (Fig. 6c,d). We then used a modified protocol that allows the concurrent detection of the release of both IL-1α and IL-1β as well as cell death and found that both cytokines were secreted simultaneously from the dying cells in the majority of cases (Fig. 6e). Therefore, the LPS-induced release of IL-1β, and also IL-1α, from A20-deficient macrophages requires RIPK3-dependent cell death.

ZnF7 is essential for A20-mediated inhibition of inflammation. Knock-in mice expressing A20 with mutations in its catalytic ovarian tumour domain or its ZnF4 domain did not develop spontaneous inflammatory pathology[28,30,31], suggesting that other domains are essential for the inhibition of inflammation in vivo. The ZnF7 of A20 has been shown to play an important role in both the inhibition of NF-κB activation and cell death downstream of TNFR1 in cell-line-reconstitution experiments[32,35,37], but its role in the regulation of inflammation in vivo has not been studied. We therefore generated knock-in mice expressing A20 with a mutated ZnF7 domain by mutating the cysteine residues 764 and 767 to alanines (C764A and C767A; hereafter referred to as mZnF7; Supplementary Fig. 5a). These mutations abrogate the ability of A20 to bind to polyubiquitin chains[32]. Homozygous *A20*$^{mZnF7/mZnF7}$ mice were born at a Mendelian ratio and did not show the early postnatal lethality observed in *A20*$^{-/-}$ mice but had reduced body weight and developed symmetric swellings in their ankles, wrists and toes that became obvious from the age of five weeks (Fig. 7a,c). *A20*$^{mZnF7/mZnF7}$ mice showed splenomegaly similar to A20$^{MYC\text{-}KO}$ mice (Fig. 7b). Ex vivo micro-computed tomography analyses of the hind and fore paws revealed erosions and new bone formation in the joints of the *A20*$^{mZnF7/mZnF7}$ mice—indicative of inflammatory bone remodelling—similar to the A20$^{MYC\text{-}KO}$ animals (Fig. 7d and Supplementary Fig. 5b). In addition, the *A20*$^{mZnF7/mZnF7}$ mice showed severe erosions of all distal phalanges and nails (Supplementary Fig. 5c), which is suggestive of a dactylitis-like phenotype characterized by the formation of pannus tissue and destruction of the nail bed and the underlying distal phalanx. Histological analysis of the ankle joints revealed clear signs of inflammatory arthritis manifesting a persisting synovitis evolving into pannus and leading to apparent proteoglycan degradation in articular cartilage, as this is exhibited through the loss of toluidine blue staining, as well as activation of osteo-resorptive processes in the adjacent bone (Fig. 7e–h). Therefore, *A20*$^{mZnF7/mZnF7}$ mice developed progressive inflammatory joint pathology, although the overall severity of the arthritis observed in the ankles of these animals was generally milder compared with age-matched A20$^{MYC\text{-}KO}$ mice. Increased neutrophil infiltration was observed in the joints of A20$^{MYC\text{-}KO}$ mice compared with *A20*$^{mZnF7/mZnF7}$ mice (Supplementary Fig. 6), which could account for the accelerated development and progression of arthritis in the A20$^{MYC\text{-}KO}$ mice[51]. In addition, *A20*$^{mZnF7/mZnF7}$ mice developed severe inflammation in their distal toe joints, which was never observed in the A20$^{MYC\text{-}KO}$ animals, suggesting that non-myeloid-cell-dependent mechanisms account for this pathology. We then assessed whether MyD88-dependent signalling also drives arthritis development in *A20*$^{mZnF7/mZnF7}$ mice, as is seen in the A20$^{MYC\text{-}KO}$ animals. As shown in Supplementary Fig. 7, MyD88 deficiency partly restored the reduced body weight and splenomegaly but fully prevented the development of arthritis and dactylitis in the *A20*$^{mZnF7/mZnF7}$ mice, showing that MyD88-dependent mechanisms drive arthritis development in the absence of ZnF7-dependent A20 functions, similarly to A20$^{MYC\text{-}KO}$ mice. Together, these results showed that the ZnF7 has a critical indispensable in vivo function for the A20-mediated repression of joint inflammation.

LPS stimulation induced the release of processed IL-1β as well as IL-1α in *A20*$^{mZnF7/mZnF7}$ BMDMs, although at lower levels compared with *A20*-knockout cells (Fig. 8a,b). The ZnF7 has been implicated in facilitating the recruitment of A20 to the TNFR1 signalling complex by binding linear ubiquitin chains[37]. Indeed, FLAG–TNF immunoprecipitation experiments showed that ZnF7 mutation almost completely prevented the recruitment of A20 to complex I (Fig. 8c). Immunoblot analysis of FLAG–TNF immunoprecipitates with anti-RIPK1 antibodies revealed the efficient recruitment and ubiquitination of RIPK1 in complex I in *A20*$^{mZnF7/mZnF7}$ as well as A20-deficient BMDMs (Fig. 8d). However, immunoblotting with antibodies that specifically recognize M1-linked ubiquitin chains revealed a strong reduction in linear ubiquitin chains in complex I in both *A20*$^{mZnF7/mZnF7}$ and A20-deficient BMDMs compared with

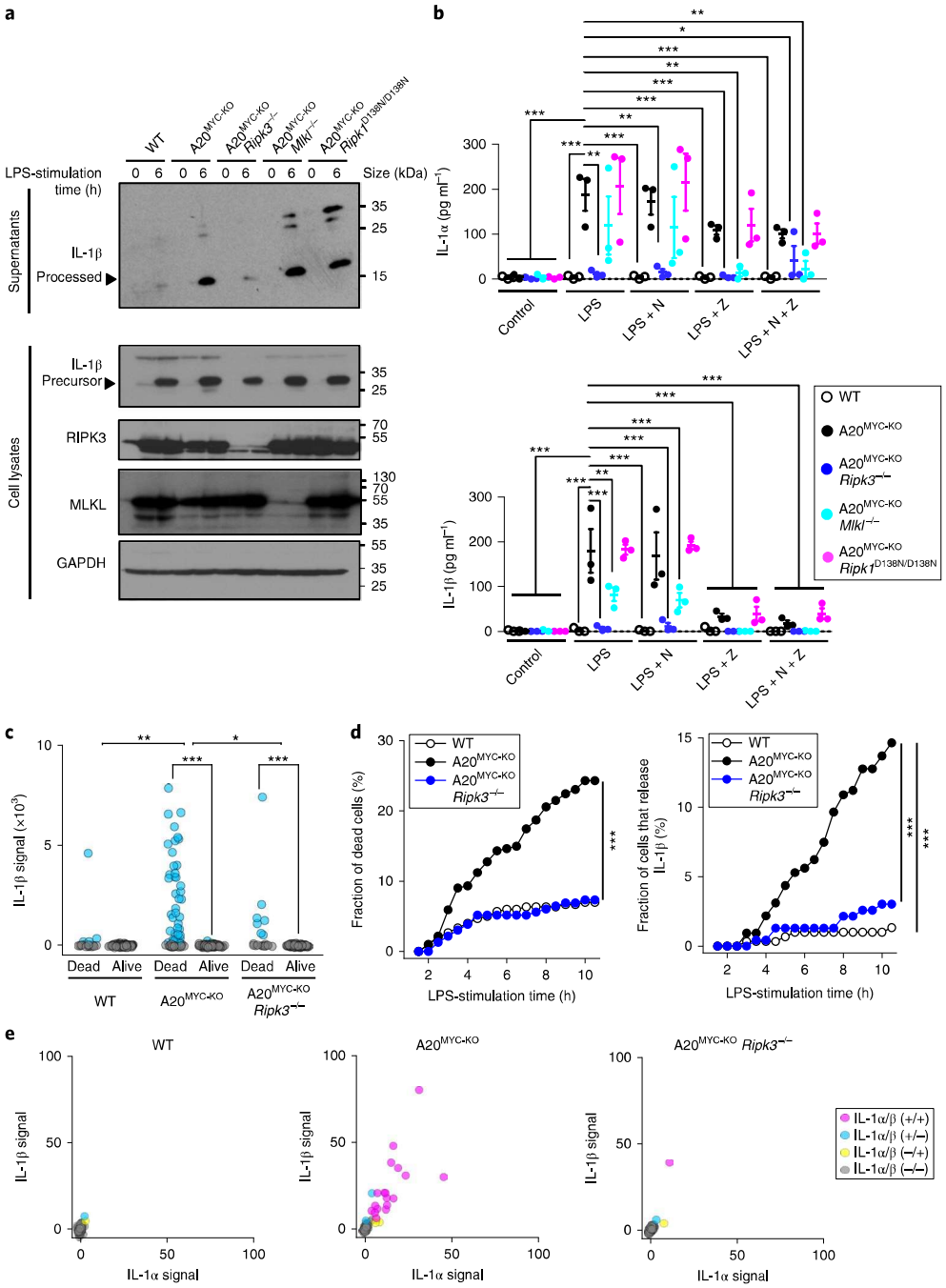

Fig. 6 | RIPK3-dependent necroptosis and apoptosis trigger LPS-induced IL-1β and IL-1α secretion from A20-deficient macrophages. a, BMDMs with the indicated genotypes were stimulated with 1 μg ml^{-1} LPS, and the indicated proteins were analysed in cell culture supernatants or cell lysates by immunoblotting. Representative data from one of three independent experiments are shown. **b**, Levels of IL-1β (bottom) and IL-1α (top) released into the supernatants of BMDMs from mice with the indicated genotypes stimulated for 24 h with 1 μg ml^{-1} ultrapure LPS in combination with Necrostatin-1s (N) or z-VAD-fmk (Z), as indicated. The graphs show the pooled results of three independent experiments performed at different times with one independent isolation of macrophages from the indicated genotypes per experiment. The mean ± s.e.m. is shown for each group of mice in both graphs. **c**, Representation of the signal intensity of IL-1β secreted from single cells (classified according to cell viability) analysed in BMDMs with the indicated genotypes stimulated with 2 μg ml^{-1} crude LPS for 10 h. Blue circles indicate IL-1β signal positive and gray circles indicate IL-1β signal negative, individual cells. **d**, Fraction of dead cells (left) or cells that released IL-1β (right) over time in the BMDMs from mice with the indicated genotypes stimulated with 2 μg ml^{-1} crude LPS. **e**, Representations of the signal intensities of IL-1β and IL-1α secreted from single cells, analysed in BMDMs with the indicated genotypes stimulated with 1 μg ml^{-1} ultrapure LPS for 12 h. The secretion signals of IL-1α/IL-1β (+/+) cells in A20^{MYC-KO} were moderately correlated, with Pearson's $r = 0.68$, $P < 0.001$. Data are representative of three independent experiments. $^{*}P < 0.05$, $^{**}P < 0.01$ and $^{***}P < 0.001$; two-way ANOVA with Bonferroni correction between the indicated genotypes in **b**; non-parametric Mann–Whitney test between cells that were dead and alive in the individual genotypes and between the indicated genotypes with $q < 0.05$, Benjamini–Hochberg procedure in **c**; Kaplan–Meier method with the log-rank test between the indicated genotypes in **d**. All of the statistical tests are two-tailed. The raw data are provided in Supplementary Table 3 and unprocessed immunoblots are provided in Supplementary Fig. 9.

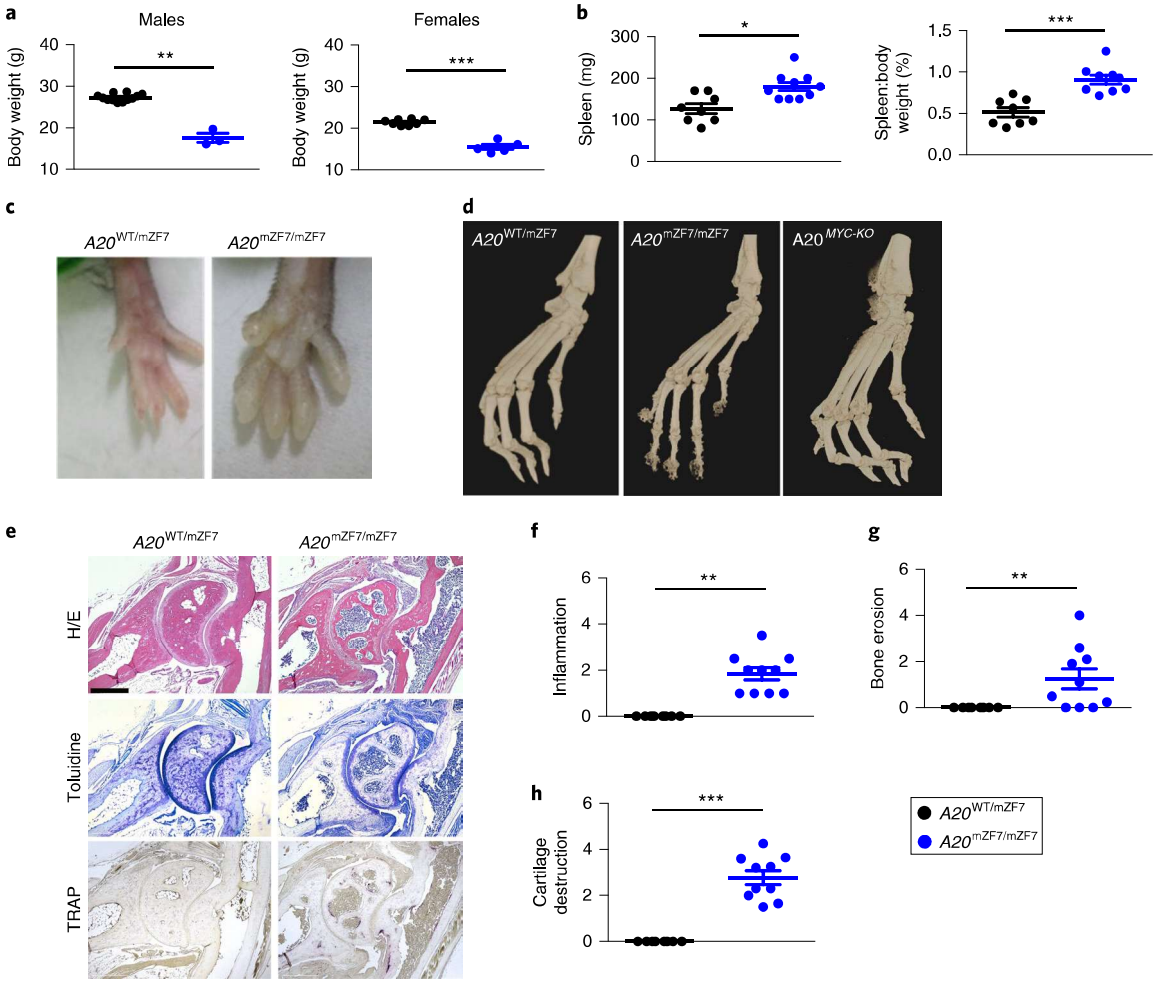

Fig. 7 | ZnF7 is essential for the A20-mediated inhibition of inflammation. a, Body weight of nine-week-old male and female $A20^{WT/mZnF7}$ and $A20^{mZnF7/mZnF7}$ mice (male $A20^{WT/mZnF7}$, $n=12$; male $A20^{mZnF7/mZnF7}$, $n=3$; female $A20^{WT/mZnF7}$, $n=8$ and female $A20^{mZnF7/mZnF7}$, $n=5$ mice). **b**, Spleen weight (left) and spleen:body weight ratio (right) in 28-week-old $A20^{WT/mZnF7}$ and $A20^{mZnF7/mZnF7}$ littermate mice ($A20^{WT/mZnF7}$, $n=8$ and $A20^{mZnF7/mZnF7}$, $n=10$ mice). **c**, Representative images of the hind paws of 28-week-old $A20^{WT/mZnF7}$ and $A20^{mZnF7/mZnF7}$ littermates, showing extensive swelling of the toes of the $A20^{mZnF7/mZnF7}$ mice. **d**, Representative micro-computed tomography images of the hind paws of 28-week-old $A20^{WT/mZnF7}$ ($n=7$ mice) and $A20^{mZnF7/mZnF7}$ ($n=10$ mice) littermates in comparison to age-matched $A20^{MYC-KO}$ mice. **e**, Representative histological images of the ankle joints of 28-week-old littermate mice with the indicated genotypes. Scale bar, 500 µm. **f–h**, Histological scores for inflammation (**f**), bone erosion (**g**) and cartilage destruction (**h**) of mice with the indicated genotypes ($A20^{WT/mZnF7}$, $n=8$ and $A20^{mZnF7/mZnF7}$, $n=10$ mice). The dots in the graphs indicate individual mice. The mean ± s.e.m. is also shown for each group of mice in all graphs. $^*P<0.05$, $^{**}P<0.01$ and $^{***}P<0.001$; non-parametric Mann–Whitney test between the indicated genotypes. All of the statistical tests are two-tailed. The raw data are provided in Supplementary Table 3. The legend in **h** applies to **a**,**b**,**f–h**.

wild-type BMDMs, which is consistent with the concept that A20 binding stabilises linear ubiquitin chains probably by preventing their degradation by other deubiquitinating enzymes[37]. Therefore, ZnF7 mutation abolishes the recruitment of A20 and reduces the amount of linear ubiquitin chains in the TNFR1 signalling complex.

Discussion

Multiple studies have established A20 as a key regulator of inflammation in animal models[3,8–10,12,14,15,17–27,38,39] and human patients[6–13], but the molecular mechanisms and the functional domains of A20 that are critical to the prevention of inflammation in vivo have remained elusive. Our results showing that mice expressing A20 with mutated ZnF7 spontaneously develop inflammatory joint pathology identify ZnF7-dependent binding to linear ubiquitin chains as a critical function of A20, which is indispensable to the inhibition of inflammation in vivo. However, the spontaneous inflammatory pathology that develops in $A20^{mZnF7/mZnF7}$ mice is mild compared with the severe inflammation causing early postnatal lethality in *A20*-knockout animals[14], suggesting that other domains of A20 also critically contribute to its in vivo anti-inflammatory function. The generation of knock-in mice with combined domain mutations, which could not be included in this study due to time limitations, will be important to dissect redundancies between the different functional domains of A20.

Inhibition of NF-κB activation is considered a key anti-inflammatory function of A20[2,27], whereas its role in preventing cell death has received little attention as a possible mechanism to suppress inflammation. Surprisingly, the inhibition of IKK/NF-κB signalling in A20-deficient myeloid cells was not sufficient to prevent arthritis development. Instead, our results identified the regulation of necroptosis as a critical anti-inflammatory function of A20 that is important to prevent the development of arthritis in mice. RIPK1–RIPK3–MLKL-dependent necroptosis was required for inflammasome activation, IL-1β production and arthritis development in $A20^{MYC-KO}$ mice, thus providing evidence that A20 suppresses inflammasome activation in vivo indirectly by inhibiting necroptosis.

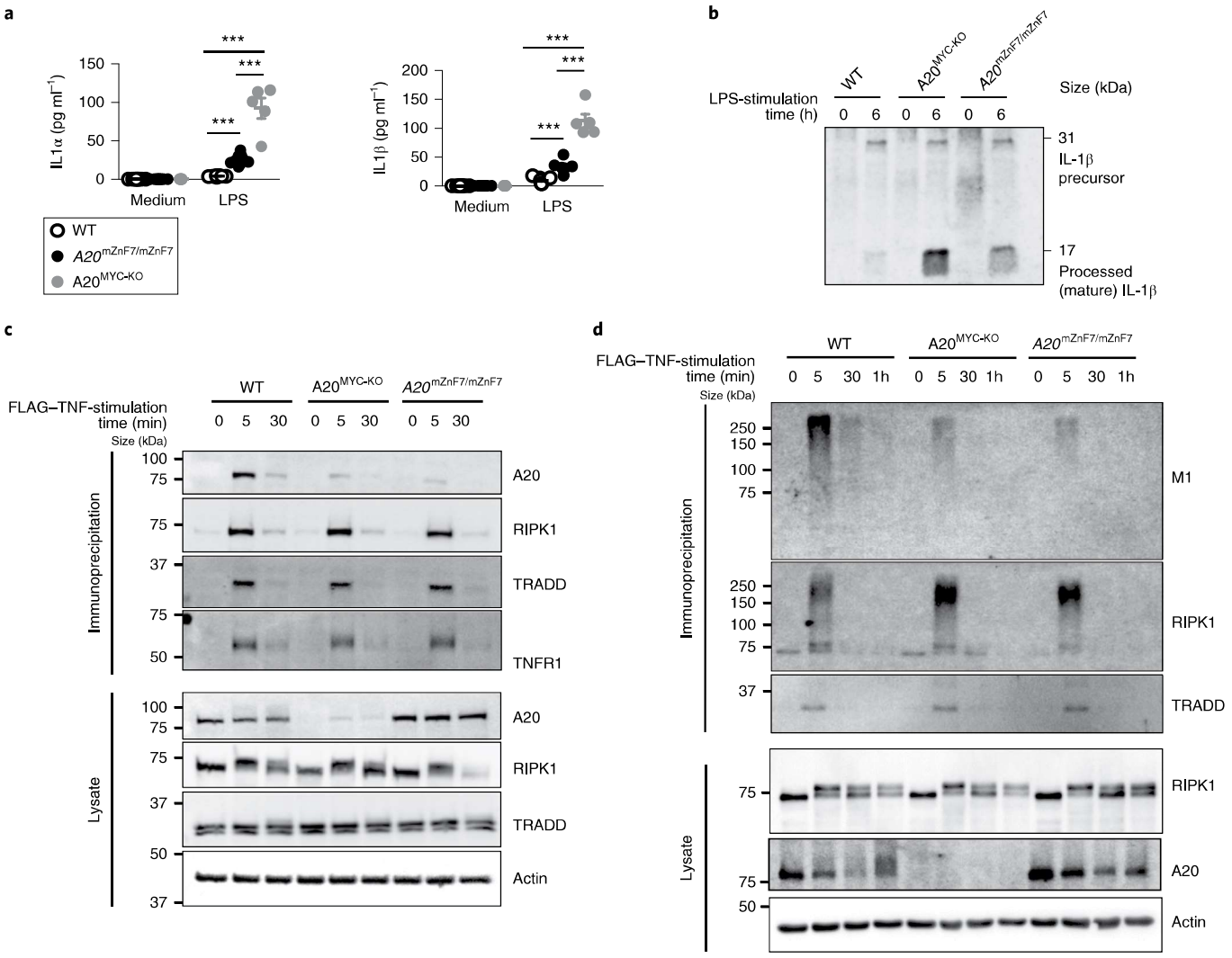

Fig. 8 | ZnF7 is critical for the A20-mediated suppression of LPS-induced IL-1β and IL-1α secretion, and the recruitment of A20 to the TNFR1 signalling complex. a, IL-1α (left) and IL-1β (right) protein levels in the supernatants of BMDMs from WT ($n=10$), *A20*$^{mZnF7/mZnF7}$ ($n=10$) and A20^{MYC-KO} ($n=5$) mice stimulated with LPS (1 μg ml^{-1}) for 6 h. The mean ± s.e.m. is shown for each group of mice in both graphs. $^{*}P<0.05$, $^{**}P<0.01$ and $^{***}P<0.001$; two-way ANOVA with Bonferroni correction between the indicated genotypes. All of the statistical tests are two-tailed. **b**, Immunoblot showing pro-IL-1β (31 kDa) and mature IL-1β (17 kDa) protein levels in the supernatants of BMDMs from WT, *A20*$^{mZnF7/mZnF7}$ and A20^{MYC-KO} mice stimulated with LPS (1 μg ml^{-1}) for 6 h. **c**, BMDMs from WT, *A20*$^{mZnF7/mZnF7}$ and A20^{MYC-KO} mice were stimulated with FLAG–TNF (1 μg ml^{-1}) for the indicated time periods. The TNF-R1 signalling complex was subsequently immunoprecipitated using α-FLAG beads in the presence of USP2 (24 μg ml^{-1}) and λPPase (8 U μl^{-1}), and immunoblotted for A20, RIPK1, TRADD and TNFR1. **d**, BMDMs from WT, *A20*$^{mZnF7/mZnF7}$ and A20^{MYC-KO} mice were stimulated with FLAG–TNF (1 μg ml^{-1}) for the indicated time periods. The TNF-R1 signalling complex was immunoprecipitated using α-FLAG beads and immunoblotted for RIPK1 and linear ubiquitin (M1) and TRADD. The data shown are representative of three independent experiments. The raw data are provided in Supplementary Table 3.

Plasma-membrane permeabilization by MLKL probably triggers NLRP3 inflammasome activation by inducing potassium efflux[52]. Although an earlier study suggested that LPS induces IL-1β secretion in *A20*-knockout macrophages in the absence of cell death[39], our single-cell imaging experiments demonstrated that IL-1β, as well as IL-1α, are secreted exclusively by a small number of dying *A20*-deficient macrophages. A deficiency in ASC could prevent IL-1β but not IL-1α release from *A20*-knockout macrophages, providing additional evidence that necroptosis and not pyroptosis drives the death of these cells in response to LPS stimulation. Our results also question earlier reports arguing that RIPK3 regulates inflammasome activation and IL-1β release independently of cell death[53,54]. Re-evaluation of these results using dynamic real-time imaging of cell death and IL-1β release at a single-cell level will be required to clarify whether RIPK3-dependent IL-1β secretion occurs independently of cell death. MLKL deficiency was as efficient as RIPK3 knockout in preventing IL-1β release and arthritis in vivo in A20^{MYC-KO} mice but only partly reduced LPS-induced IL-1β production from *A20*-knockout macrophages in vitro. IL-1α and IL-1β release could be prevented by z-VAD-fmk in *A20* and *Mlkl* double-deficient BMDMs, suggesting that caspase-dependent cell death drives the release of these cytokines in the absence of MLKL. It is probable that secondary necrosis of apoptotic *A20* and *Mlkl* double-deficient macrophages is responsible for the release of IL-1β and IL-1α in vitro, whereas these cells may be rapidly cleared by phagocytes in vivo thus preventing secondary necrosis. Our work also identified synovial fibroblasts as the key effector cells that respond to IL-1 family cytokines secreted by the A20-deficient myeloid cells in the joints, further driving the inflammatory response leading to the development of arthritis (Supplementary Fig. 8).

RIPK3 deficiency or inhibition of RIPK1 kinase activity considerably delayed the early postnatal lethality of *A20*$^{-/-}$ mice[15,16]; however, MLKL knockout did not show any protective effects[16]. Therefore, A20 deficiency in non-myeloid cells causes inflammation by inducing necroptosis-independent functions of RIPK1 and RIPK3. Both RIPK1 and RIPK3 can induce apoptosis but have also been reported to exert cell-death-independent pro-inflammatory functions[45]. Apoptosis of A20-deficient epithelial or stromal cells probably contributes to systemic inflammation in *A20*$^{-/-}$ mice as shown in conditional *A20*-knockout animals[18,22,25]. Unequivocal assessment of the role of cell death in the pathology caused by systemic A20 deficiency will require the combined inhibition of both FADD/Caspase-8-mediated apoptosis and MLKL-dependent necroptosis.

The ligands and receptors triggering necroptosis of A20-deficient macrophages in vivo are not known at present. Although TNFR1 deficiency did not prevent arthritis in A20$^{MYC\text{-}KO}$ animals[23], we cannot exclude that TNFR1 could contribute to necroptosis of A20-deficient macrophages in vivo in a redundant fashion with other upstream pathways, such as TRIF-dependent TLR3/TLR4 signalling or type I and type II interferon receptor signalling. TLR4 could act in a dual fashion, providing a MyD88-dependent 'priming' signal inducing the transcriptional upregulation of inflammasome components as well as IL-1α and IL-1β, and in parallel activating necroptosis directly via TRIF or indirectly by autocrine TNF production.

Together, our findings demonstrate that the regulation of macrophage necroptosis is a key in vivo anti-inflammatory function of A20. In addition, our results identify macrophage necroptosis as a potent in vivo trigger of inflammasome activation and arthritis development, suggesting that necroptosis and perhaps other mechanisms causing plasma membrane permeabilization of 'primed' myeloid cells could contribute to inflammasome-associated pathologies. Inhibitors of necroptosis—such as RIPK1 inhibitors, for example—could therefore prove effective in the treatment of chronic inflammatory diseases associated with impaired A20 function as well as inflammasome activation.

Online content

Any methods, additional references, Nature Research reporting summaries, source data, statements of code and data availability and associated accession codes are available at https://doi.org/10.1038/s41556-019-0324-3.

Received: 30 May 2018; Accepted: 29 March 2019;
Published online: 13 May 2019

References

1. Lork, M., Verhelst, K. & Beyaert, R. CYLD, A20 and OTULIN deubiquitinases in NF-κB signaling and cell death: so similar, yet so different. *Cell Death Differ.* **24**, 1172–1183 (2017).
2. Ma, A. & Malynn, B. A. A20: linking a complex regulator of ubiquitylation to immunity and human disease. *Nat. Rev. Immunol.* **12**, 774–785 (2012).
3. Das, T., Chen, Z., Hendriks, R. W. & Kool, M. A20/tumor necrosis factor α-induced protein 3 in immune cells controls development of autoinflammation and autoimmunity: lessons from mouse models. *Front. Immunol.* **9**, 104 (2018).
4. Vereecke, L., Beyaert, R. & van Loo, G. Genetic relationships between A20/TNFAIP3, chronic inflammation and autoimmune disease. *Biochem. Soc. Trans.* **39**, 1086–1091 (2011).
5. Novak, U. et al. The NF-κB negative regulator *TNFAIP3* (A20) is inactivated by somatic mutations and genomic deletions in marginal zone lymphomas. *Blood* **113**, 4918–4921 (2009).
6. Kato, M. et al. Frequent inactivation of A20 in B-cell lymphomas. *Nature* **459**, 712–716 (2009).
7. Schmitz, R. et al. *TNFAIP3* (A20) is a tumor suppressor gene in Hodgkin lymphoma and primary mediastinal B cell lymphoma. *J. Exp. Med.* **206**, 981–989 (2009).
8. Compagno, M. et al. Mutations of multiple genes cause deregulation of NF-κB in diffuse large B-cell lymphoma. *Nature* **459**, 717–721 (2009).
9. Aeschlimann, F. A. et al. A20 haploinsufficiency (HA20): clinical phenotypes and disease course of patients with a newly recognised NF-kB-mediated autoinflammatory disease. *Ann. Rheum. Dis.* **77**, 728–735 (2018).
10. Duncan, C. J. A. et al. Early-onset autoimmune disease due to a heterozygous loss-of-function mutation in *TNFAIP3* (A20). *Ann. Rheum. Dis.* **77**, 783–786 (2018).
11. Kadowaki, T. et al. Haploinsufficiency of *A20* causes autoinflammatory and autoimmune disorders. *J. Allergy Clin. Immunol.* **141**, 1485–1488 (2018).
12. Takagi, M. et al. Haploinsufficiency of *TNFAIP3* (A20) by germline mutation is involved in autoimmune lymphoproliferative syndrome. *J. Allergy Clin. Immunol.* **139**, 1914–1922 (2017).
13. Zhou, Q. et al. Loss-of-function mutations in *TNFAIP3* leading to A20 haploinsufficiency cause an early-onset autoinflammatory disease. *Nat. Genet.* **48**, 67–73 (2016).
14. Lee, E. G. et al. Failure to regulate TNF-induced NF-κB and cell death responses in A20-deficient mice. *Science* **289**, 2350–2354 (2000).
15. Onizawa, M. et al. The ubiquitin-modifying enzyme A20 restricts ubiquitination of the kinase RIPK3 and protects cells from necroptosis. *Nat. Immunol.* **16**, 618–627 (2015).
16. Newton, K. et al. RIPK3 deficiency or catalytically inactive RIPK1 provides greater benefit than MLKL deficiency in mouse models of inflammation and tissue injury. *Cell Death Differ.* **23**, 1565–1576 (2016).
17. Tavares, R. M. et al. The ubiquitin modifying enzyme A20 restricts B cell survival and prevents autoimmunity. *Immunity* **33**, 181–191 (2010).
18. Vereecke, L. et al. Enterocyte-specific A20 deficiency sensitizes to tumor necrosis factor-induced toxicity and experimental colitis. *J. Exp. Med.* **207**, 1513–1523 (2010).
19. Chu, Y. et al. B cells lacking the tumor suppressor TNFAIP3/A20 display impaired differentiation and hyperactivation and cause inflammation and autoimmunity in aged mice. *Blood* **117**, 2227–2236 (2011).
20. Hammer, G. E. et al. Expression of A20 by dendritic cells preserves immune homeostasis and prevents colitis and spondyloarthritis. *Nat. Immunol.* **12**, 1184–1193 (2011).
21. Kool, M. et al. The ubiquitin-editing protein A20 prevents dendritic cell activation, recognition of apoptotic cells, and systemic autoimmunity. *Immunity* **35**, 82–96 (2011).
22. Lippens, S. et al. Keratinocyte-specific ablation of the NF-κB regulatory protein A20 (TNFAIP3) reveals a role in the control of epidermal homeostasis. *Cell Death Differ.* **18**, 1845–1853 (2011).
23. Matmati, M. et al. A20 (TNFAIP3) deficiency in myeloid cells triggers erosive polyarthritis resembling rheumatoid arthritis. *Nat. Genet.* **43**, 908–912 (2011).
24. Heger, K. et al. A20-deficient mast cells exacerbate inflammatory responses in vivo. *PLoS Biol.* **12**, e1001762 (2014).
25. Catrysse, L. et al. A20 prevents chronic liver inflammation and cancer by protecting hepatocytes from death. *Cell Death Dis.* **7**, e2250 (2016).
26. Voet, S. et al. A20 critically controls microglia activation and inhibits inflammasome-dependent neuroinflammation. *Nat. Commun.* **9**, 2036 (2018).
27. Catrysse, L., Vereecke, L., Beyaert, R. & van Loo, G. A20 in inflammation and autoimmunity. *Trends Immunol.* **35**, 22–31 (2014).
28. Wertz, I. E. et al. Phosphorylation and linear ubiquitin direct A20 inhibition of inflammation. *Nature* **528**, 370–375 (2015).
29. Wertz, I. E. et al. De-ubiquitination and ubiquitin ligase domains of A20 downregulate NF-κB signalling. *Nature* **430**, 694–699 (2004).
30. Lu, T. T. et al. Dimerization and ubiquitin mediated recruitment of A20, a complex deubiquitinating enzyme. *Immunity* **38**, 896–905 (2013).
31. De, A., Dainichi, T., Rathinam, C. V. & Ghosh, S. The deubiquitinase activity of A20 is dispensable for NF-κB signaling. *EMBO Rep.* **15**, 775–783 (2014).
32. Skaug, B. et al. Direct, noncatalytic mechanism of IKK inhibition by A20. *Mol. Cell* **44**, 559–571 (2011).
33. Tokunaga, F. et al. Specific recognition of linear polyubiquitin by A20 zinc finger 7 is involved in NF-κB regulation. *EMBO J.* **31**, 3856–3870 (2012).
34. Verhelst, K. et al. A20 inhibits LUBAC-mediated NF-κB activation by binding linear polyubiquitin chains via its zinc finger 7. *EMBO J.* **31**, 3845–3855 (2012).
35. Yamaguchi, N. & Yamaguchi, N. The seventh zinc finger motif of A20 is required for the suppression of TNF-α-induced apoptosis. *FEBS Lett.* **589**, 1369–1375 (2015).
36. Bosanac, I. et al. Ubiquitin binding to A20 ZnF4 is required for modulation of NF-κB signaling. *Mol. Cell* **40**, 548–557 (2010).
37. Draber, P. et al. LUBAC-recruited CYLD and A20 regulate gene activation and cell death by exerting opposing effects on linear ubiquitin in signaling complexes. *Cell Rep.* **13**, 2258–2272 (2015).
38. Vande Walle, L. et al. Negative regulation of the NLRP3 inflammasome by A20 protects against arthritis. *Nature* **512**, 69–73 (2014).
39. Duong, B. H. et al. A20 restricts ubiquitination of pro-interleukin-1β protein complexes and suppresses NLRP3 inflammasome activity. *Immunity* **42**, 55–67 (2015).

40. Lamkanfi, M. & Dixit, V. M. Mechanisms and functions of inflammasomes. *Cell* **157**, 1013–1022 (2014).
41. Gais, P. et al. Cutting edge: divergent cell-specific functions of MyD88 for inflammatory responses and organ injury in septic peritonitis. *J. Immunol.* **188**, 5833–5837 (2012).
42. McInnes, I. B. & Schett, G. The pathogenesis of rheumatoid arthritis. *N. Engl. J. Med.* **365**, 2205–2219 (2011).
43. Smolen, J. S., Aletaha, D. & McInnes, I. B. Rheumatoid arthritis. *Lancet* **388**, 2023–2038 (2016).
44. Armaka, M. et al. Mesenchymal cell targeting by TNF as a common pathogenic principle in chronic inflammatory joint and intestinal diseases. *J. Exp. Med.* **205**, 331–337 (2008).
45. Moriwaki, K. & Chan, F. K. The inflammatory signal adaptor RIPK3: functions beyond necroptosis. *Int. Rev. Cell Mol. Biol.* **328**, 253–275 (2017).
46. Pasparakis, M. & Vandenabeele, P. Necroptosis and its role in inflammation. *Nature* **517**, 311–320 (2015).
47. Polykratis, A. et al. Cutting edge: RIPK1 kinase inactive mice are viable and protected from TNF-induced necroptosis in vivo. *J. Immunol.* **193**, 1539–1543 (2014).
48. Garlanda, C., Dinarello, C. A. & Mantovani, A. The interleukin-1 family: back to the future. *Immunity* **39**, 1003–1018 (2013).
49. Liu, T. et al. Single-cell imaging of caspase-1 dynamics reveals an all-or-none inflammasome signaling response. *Cell Rep.* **8**, 974–982 (2014).
50. Shirasaki, Y. et al. Real-time single-cell imaging of protein secretion. *Sci. Rep.* **4**, 4736 (2014).
51. Wright, H. L., Moots, R. J. & Edwards, S. W. The multifactorial role of neutrophils in rheumatoid arthritis. *Nat. Rev. Rheumatol.* **10**, 593–601 (2014).
52. Conos, S. A. et al. Active MLKL triggers the NLRP3 inflammasome in a cell-intrinsic manner. *Proc. Natl Acad. Sci. USA* **114**, E961–E969 (2017).
53. Kang, T. B., Yang, S. H., Toth, B., Kovalenko, A. & Wallach, D. Caspase-8 blocks kinase RIPK3-mediated activation of the NLRP3 inflammasome. *Immunity* **38**, 27–40 (2013).
54. Vince, J. E. et al. Inhibitor of apoptosis proteins limit RIP3 kinase-dependent interleukin-1 activation. *Immunity* **36**, 215–227 (2012).

Acknowledgements

We are grateful to J. Buchholz, C. Uthoff-Hachenberg, E. Mahlberg, B. Kühnel, E. Stade, T. Liu, B. Yao, K. Igarashi, M. Sze, L. Bellen, S. Lalos, P. Athanasakis and A. Kateveni for their excellent technical assistance, and T. Hochepied for help with the generation of $A20^{mZnf7/mZnf7}$ mice. We also thank D. Hackam for providing $Tlr4^{LPS/LPS}$ mice, V. Dixit and Genentech for providing $Ripk3^{-/-}$ mice, G. Vassilopoulos for providing access to microscope facilities and the InfrafrontierGR infrastructure (NSRF 2007–2013 and NSRF 2014–2020) for providing the mouse hosting and micro-computed tomography facilities. This work was supported by funding from the European Research Council (ERC grant nos AdG 323040 and 787826 to M.P.; grant no. AdG 340217 to G.K.), the Greek GSRT project INNATE FIBLROBLAST to G.K. (ERC06, co-financed by the ESF and NSRF 2007–2013), the European Commission (FP7 grant 'Masterswitch' 223404 to M.P. and G.K.), JSPS KAKENHI (grant no. JP16H06385 to M.M., JP26110005 to Y.Y., and JP15H01366 and JP17H05496 to Y.S.), JST PRESTO (grant no. JP17940748 to Y.S.), and the Japan Agency for Medical Research and Development (grant nos JP17gm0610004 and JP18gm5010001 to M.M.). The research in the G.v.L. lab is supported by research grants from the FWO, 'Geneeskundige Stichting Koningin Elisabeth' (GSKE), CBC Banque Prize, the Charcot Foundation, the 'Belgian Foundation against Cancer' and 'Kom op tegen Kanker'. A.M. is supported by a grant from the 'Concerted Research Actions' (GOA) of the Ghent University. Research in the M.A. lab is supported by a startup grant from the Stavros Niarchos Foundation donation to BSRC 'Alexander Fleming'. M.A. and G.K. also acknowledge support of this work by project MIS 5002562 funded by NSRF 2014–2020, co-financed by Greece and the European Union (ERDF). R.O.E. was supported by a postdoctoral fellowship from the Alexander von Humboldt foundation.

Author contributions

A.P., G.v.L., M.A. and M.P. conceived the study and designed the experiments. A.P., A.M., R.O.E., Y.S., M.Y., Y.Y. and M.A. performed and analysed the experiments. B.H. provided the mice. Y.Y., S.U., M.M., G.K., M.A., G.v.L. and M.P. supervised the experiments. A.P., M.A., G.v.L. and M.P. interpreted the data and wrote the paper.

Competing interests

M.P. received consulting and speaker fees from Genentech, GSK and Boehringer.

Additional information

Supplementary information is available for this paper at https://doi.org/10.1038/s41556-019-0324-3.

Reprints and permissions information is available at www.nature.com/reprints.

Correspondence and requests for materials should be addressed to G.v. or M.P.

Publisher's note: Springer Nature remains neutral with regard to jurisdictional claims in published maps and institutional affiliations.

Methods

Mice. Mice with conditional loxP-flanked *A20* (ref. [23]), *Ikk2* (ref. [55]), *Myd88* (ref. [56]), *Asc* (ref. [57]) and *Tlr4* (ref. [58]) alleles as well as *Myd88*^{lSL} (ref. [41]) mice were crossed with the LysMCre[59] or Col6a1Cre transgenic lines[44], as well as with *Ripk3*$^{-/-}$ (ref. [60]), *Mlkl*$^{-/-}$ (ref. [61]) and *Ripk1*$^{D138N/D138N}$ (ref. [47]) mice. The following combinations of alleles were used in the study: *A20*$^{FL/FL}$ *LysMCre* (A20^{MYC-KO}), *A20*$^{FL/FL}$ *Asc*$^{FL/FL}$ *LysMCre* (A20^{MYC-KO} ASC^{MYC-KO}), *A20*$^{FL/FL}$ *MyD88*$^{FL/FL}$ *LysMCre* (A20^{MYC-KO} Myd88^{MYC-KO}), *A20*$^{FL/FL}$ *MyD88*$^{lSL/lSL}$ *LysMCre* (A20^{MYC-KO} Myd88^{MYC}), *A20*$^{FL/FL}$ *Ikk2*$^{FL/FL}$ *LysMCre* (A20^{MYC-KO} IKK2^{MYC-KO}), *A20*$^{FL/FL}$ *LysMCre Ripk3*$^{-/-}$ (A20^{MYC-KO} *Ripk3*$^{-/-}$), *A20*$^{FL/FL}$ *LysMCre Mlkl*$^{-/-}$ (A20^{MYC-KO} *Mlkl*$^{-/-}$), *A20*$^{FL/FL}$ *LysMCre Ripk1*$^{D138N/D138N}$ (A20^{MYC-KO} *Ripk1*$^{D138N/D138N}$), *MyD88*$^{FL/FL}$ *Col6a1Cre* (Myd88^{SF-KO}) and *Tlr4*$^{FL/FL}$ *Col6a1Cre* (TLR4^{SF-KO}). *A20*$^{mZnF7/mZnF7}$ mice were crossed with *MyD88*$^{-/-}$(ref. [62]) mice. All of the mice were maintained in the C57Bl/6 background. The mice were maintained at the specific-pathogen free animal facilities of the Institute for Genetics and CECAD Research Center, BSRC 'A. Fleming', VIB Center for Inflammation Research and University of Ghent under a 12 h light cycle and were given a regular chow diet (Harlan diet no. 2918 or Prolab Isopro RMH3000 5P76) ad libitum. All of the animal procedures were conducted in accordance with European national and institutional guidelines, and protocols were approved by the local government authorities (Landesamt für Natur, Umwelt und Verbraucherschutz Nordrhein-Westfalen; the ethics committee of Ghent University and the Institutional Animal Care and Use Committee of BSRC 'Alexander Fleming' in conjunction with the Veterinary Service Management of the Hellenic Republic Prefecture of Attika). Animals requiring medical attention were provided with the appropriate care and excluded from the experiments described. No other exclusion criteria existed.

For the generation of A20-ZnF7 KI mice, Cas9 mRNA (Sigma) and protein (VIB Protein Service Facility) together with a 151 bp single-stranded repair template (IDT) containing the homologous sequence around the mutations and two short guide RNAs (sgRNAs, Synthego) targeting the ZnF7 domain of the murine A20 gene were micro-injected into the pronucleus of zygotes obtained from C57BL/6 mice. The embryos were incubated overnight in KSOM medium and transferred to foster mothers the next day through oviduct transfer. The two sgRNAs used were: sgRNA1, 5′-AGCCATACATCTGCTTGAACTGG-3′ and sgRNA2, 5′-ATTGCAGTAACCATTACACTTGG-3′. A single-stranded DNA oligo was used as repair template containing two Cys-to-Ala point mutations (TGC < GCC (C764A) and TGC < GCT (C767A)) and two silent mutations (GCC < GCT (A758) and TAC < TAT (Y768)) to avoid re-editing after recombination: 5′-GCCTGAAGAGCCCCCTAAACAGCGCTGCCGGGCCCCT GCTTGTGATCACTTTGGCAATGCTAAGTGTAATGGTTACGCCAATGAGGC TTATCAGTTCAAGCAGATGTATGGCTAAGTGCGAACACATTGACAGGTCC AGCAAGAAGGAGCC-3′.

Bone-marrow transplantation. The bone marrow of the mice with the indicated genotypes was obtained from the femurs and tibia. Bone marrow cells (5×10^6 cells in 200 µl HBSS) were intravenously injected into lethally γ-irradiated sex-matched mice of the indicated genotypes (MDS Nordion Gammacell 3000 Elan; 2 × 600 rad, 3 h interval). The mice were maintained in isolated/specific-pathogen-free conditions and kept on an antibiotic regime for two weeks. Reconstituted mice were followed up weekly and killed 26 weeks after the bone-marrow transfer. At the end of the study, reconstitution was assessed by specific staining via cell count analysis of peripheral blood of each mouse.

Clinical scoring. The mice were scored once a week as previously described[23]. A score of 0–3 was assigned to each paw as follows: 0, normal; 0.5, swelling of toes; 1, swelling of the wrist and/or ankle or carpus and/or tarsus; 2, moderate swelling of the wrist and/or ankle or carpus and/or tarsus or mild swelling of both and 3, severe swelling of the entire paw.

Blood cell analysis. Blood-cell-count analysis was performed in 50 µl of peripheral blood using an Abacus Junior Vet analyser or an ADVIA 2120i Hematology System according to the manufacturer's instructions.

Histology. Formalin-fixed, EDTA-decalcified, paraffin-embedded mouse tissue specimens were sectioned and stained with haematoxylin and eosin, toluidine blue and TRAP (Leukocyte Acid Phosphatase kit; Sigma-Aldrich). The stained joint sections were semi-quantitatively and blindly evaluated for the following parameters: synovial inflammation/hyperplasia (scale of 0–5), cartilage erosion (scale of 0–5) and bone loss (scale of 0–5), as described previously[63].

Immunohistochemistry. Following deparaffinization, slides were subjected to antigen-retrieval treatment by either proteinase K (37 °C, 20 µm ml^{-1}, 20 min; for anti-B220, anti-neutrophil and F4/80) or HCl (37 °C, 2N, 1 h; for anti-CD3) and endogenous peroxidase quenching (3% hydrogen peroxide in PBS, 10 min). Following blocking, the slides were incubated with the following antibodies: rat anti-B220 (BD, cat no. 553084; 1:700), rat anti-F4/80 (Serotech, MCA497; 1/40), rat anti-neutrophil antibody (Abcam, ab2557; 1:40) and rabbit anti-CD3 (Abcam, ab16669; 1:50). The biotin-conjugated antibodies were applied for 1 h (anti-rat IgG; 1:500; Southern Biotech, cat no. 3052–08 and anti-rabbit IgG; 1:500; Vector, BA-5000) and visualization was performed using the ABC and DAB kit (Vector; PK-6100 and SK-4105, respectively). Quantification of positive cells was performed using ImageJ software. All of the antibodies used in this study are listed in Supplementary Table 1.

Micro-computed tomography. Micro-computed tomography of dissected formalin-fixed joints was carried out by a SkyScan 1172 CT scanner (Bruker). Briefly, scanning was conducted at 50 kV and 100 mA using a 0.5 mm aluminium filter at a resolution of 8.8 µm pixel^{-1}. Reconstruction of sections was achieved using the NRECON software (Bruker) with beam hardening correction set to 40%. The three-dimensional imaging was performed using CTVox software (Bruker).

Isolation and culture of BMDMs. For the preparation of BMDMs, bone marrow cells were plated on 10 cm bacterial Petri dishes (Greiner) in DMEM medium (Invitrogen) supplemented with 10 µM mM-CSF (ImmunoTools, cat no. 12343113), 10% fetal calf serum, penicillin/streptomycin and sodium pyruvate. The cells were plated in tissue-coated dishes at Day 6 of culture. The experiments were performed on Day 7/8 of culture. The BMDMs were stimulated with either 1 µg ml^{-1} or 20 ng ml^{-1} ultrapure LPS (Enzo Life Sciences, ALX-581–010-L002) for different periods of time before the collection of samples. Alternatively, BMDMs were stimulated with 20 ng ml^{-1} murine TNF (VIB Protein Service Facility). For the detection of proteins in cell culture medium, cells were washed with PBS and the medium was replaced with OptiMEM (Life Technologies, cat no. 31985–062) before the addition of LPS. When required, macrophages were pre-incubated for 1 h with Necrostatin-1s (20 µm; BioVision, cat no. 2263), z-VAD-fmk (20 µm; Enzo Life Sciences, ALX-260–020-M005) or a combination of both.

Isolation and culture of synovial fibroblasts. Primary mouse synovial fibroblasts were isolated and cultured for at least four passages, as previously described[64]. Synovial fibroblasts were stimulated with 1 µg ml^{-1} ultrapure LPS (Enzo Life Sciences, ALX-581–010-L002) or 20 ng ml^{-1} IL-1β (ImmunoTools, cat no. 12340012).

Immunoblotting. Cell lysates and culture supernatants were denatured in 2×Laemmli buffer (150 mM Tris–HCl pH 6.8, 20% glycerol, 10% SDS, 10% dithiothreitol, 4% β-mercaptoethanol and bromophenol blue). The protein samples were subsequently boiled at 95 °C for 10 min and separated by SDS–PAGE. Separated proteins were transferred to PVDF membranes. Blocking, incubation with secondary antibody and washing of the membrane were done in TBS supplemented with 0.1% Tween-20 (v/v) and 5% (w/v) non-fat dry milk. Incubation of the membranes with primary antibodies was performed in TBS supplemented with 0.1% Tween-20 (v/v) and 1% (w/v) BSA. The immunoblots were incubated overnight with primary antibodies against A20 (Santa Cruz Biotechnology, sc-166692; 1:1,000), IL-1β (Abcam, ab9722; 1:1,000), RIPK3 (Enzo Life Sciences, ADI-905–242–100; 1:1,000), MLKL (Millipore, MABC604; 1:1,000), phospho-IκBα (Cell Signalling, cat no. 9246; Ser32/36, 1:1,000), IκBα (Santa Cruz Biotechnology, sc-371; 1:1,000), pJNK (Cell Signalling, cat no. 9251; 1:1,000), JNK (Cell Signalling, cat no. 9252; 1:1,000), p-p38 (Cell Signalling, cat no. 9211; 1:1,000), p38 (Cell Signalling, cat no. 2371; 1:1,000), p-ERK1/2 (Cell Signalling, cat no. 9101; 1:1,000), ERK1/2 (Cell Signalling, cat no. 9102; 1:1,000), TRADD (Bio-Rad, AHP2533; 1:1,000), RIPK1 (Cell Signalling, cat no. 3493; 1:1,000), TNFR1 (R&D Systems, AF-425-SP; 1:1,000), β-actin (Santa Cruz Biotechnology, sc-1616; 1:1,000), GAPDH (Novus Biologicals, NB300–221; 1:5,000). Horseradish-peroxidase-conjugated anti-mouse (Amersham Pharmacia, NA931V; 1:10,000), anti-rabbit secondary antibody (Amersham Pharmacia, NA934V; 1:10,000) or anti-rat secondary antibody (Jackson Immuno Research, cat no. 112–035–003; 1:10,000) was used to detect proteins by enhanced chemiluminescence (GE Healthcare, RPN2236).

Synovial fibroblasts were lysed in RIPA buffer containing 1% Triton X-100, 0.1% SDS, 150 mM NaCl, 10 mM Tris–HCl, pH 7.4, 1 mM EDTA, protease inhibitors (Roche), and phosphatase inhibitors (Sigma-Aldrich), separated by SDS–PAGE (8–12.5%), transferred to nitrocellulose membranes (Millipore) and probed with the following antibodies: pJNK1/2 (cat no. 4668; 1:1,000) and p-p38 (cat no. 9215; 1:1,000) from Cell Signalling, and JNK2 (cat no. 7345, 1:300), p-ERK1/2 (sc-7383; 1:1,000), ERK1/2 (sc-154-G; 1:500), p38 (sc-7972; 1:1,000), IκBα (sc-371; 1:1,000), tubulin (sc-9104; 1:2,000) and actin (sc-1615; 1:2,000) from Santa Cruz Biotechnology. Chemiluminescent signals were detected by the Bio-Rad Gel Doc EZ imaging system. All of the antibodies used in this study are listed in Supplementary Table 1.

Immunoprecipitation studies. BMDMs were stimulated with human FLAG–TNF (VIB Protein Service Facility) as indicated. Cells were lysed in NP40 buffer (150 mM NaCl, 1% NP40, 10% glycerol and 10 mM Tris–HCl pH 8) and FLAG pulldown was performed using M2 beads (Sigma). The TNF-R1 signalling complex was eluted from beads using 3×FLAG peptide (Sigma) as described in the manufacturer's instructions. For USP2 and PPase treatment, the beads were incubated with 24 µg ml^{-1} USP2 (Enzo Life Sciences) and 8 U µl^{-1} λPPase (NEB) for 30 min at 37 °C before FLAG peptide elution.

Quantitative real-time PCR. RNA was isolated from cells using TRIzol reagent (Life Technologies, cat no. 15596018) and RNeasy columns (QIAGEN, cat no. 74106). The RNA was used for reverse transcription with SuperScript III reverse transcriptase (Invitrogen, cat no. 18080–44). The reaction was topped up to 200 µl with water and 2 µl was used for quantitative real-time PCR reactions with the TaqMan qPCR kit from Eurogentec. Normalization was performed with primers for *Tbp*. Information on the primers used for quantitative real-time PCR is provided in Supplementary Table 2.

Cytokine analysis. The cytokine levels in the serum of mice or supernatants from macrophage cultures were determined by a customized magnetic-bead-based mouse seven-plex multiplex assay (eBioscience, EPX070–24031–801) or ELISA kits for IL-1α (Thermo Fisher Scientific, cat no. 88–5019–22,) and IL-1β (Thermo Fisher Scientific, cat. no. 88–7013–88) according to the manufacturers' instructions.

Real-time single-cell imaging of cell death and IL-1α and IL-1β release. Imaging of the release of IL-1β and IL-1α by live-cell imaging for secretion activity were performed as described previously[50] with some modifications. Briefly, time-resolved measurements were performed with a completely automated inverted microscope (ECLIPSE Ti-E, Nikon) equipped with a high numerical aperture objective lens (CFI Apo TIRF ×60 Oil, numerical aperture = 1.49, Nikon), a stage-top incubator (INUBG2TF-WSKM, Tokai Hit Co.) and an EM-CCD camera (ImagEM C9100–17, Hamamatsu Photonics K.K.) or scientific CMOS camera (ORCA-flash4.0 V2, Hamamatsu Photonics). The light sources used were as follows: a high-pressure mercury lamp (Intensilight, Nikon) was used for epi-fluorescence imaging for SYTOX staining; for single-probe observation of secretion, home-made total internal reflection fluorescent optics with a diode laser (CUBE 640–40C, Coherent) was used; for multi probes observation of secretion, an LED light source (BGX:505–545 nm and RLX:615–655 nm, X-Cite XLED1; Excelitas technologies Corp.) was used through a TI-SFL high performance Epi-fl illuminator (Nikon). The following sets of excitation (Ex) and emission (Em) filters, and dichroic mirrors (DMs) were used: FF02–438/24–25 (Ex), FF01–483/32–25 (Em) and FF458-Di02–25 × 36 (DM) for SYTOX blue; FF02–472/30–25 (Ex), FF01–520/35–25 (Em) and FF495-Di03–25 × 36 (DM) for SYTOX green; FF01–530/43–25 (Ex), FF01–593/40–25 (Em) and FF560/659-Di01–25 × 36 (DM) for Cy3 and FF01–635/18–25 (Ex), FF01–692/40–25 (Em) and FF560/659-Di01–25 × 36 (DM) for CF660R. These optical filters were purchased from Semrock.

BMDMs from each mouse genotype were harvested at Day 7 and cultured on UpCell culture dishes (CellSeed) for 1 or 2 d. We stimulated the cells with crude LPS (2 µg ml^{-1}, from *Salmonella enterica* serotype enteritidis; Sigma, L6011) or ultrapure LPS (1 µg ml^{-1}, from *Escherichia coli* O55:B5; Sigma, L6529) for 1 h, then detached and introduced the cells into a PDMS-glass hybrid nanolitre well array chip, where anti-IL-1β antibodies (clone 30311; R&D Systems, MAB401) with or without anti-IL-1α antibodies (clone 40508; R&D Systems, MAB400) were immobilized on the glass surface of the base of the nanolitre wells. After the cells had settled on the bottom of the nanolitre wells, the supernatant was replaced with a freshly prepared detection medium containing 1% BSA, LPS, SYTOX reagent and detection antibodies that were fluorescently labelled individually and blocked with biotin-PEG. The detection antibody for IL-1β (polyclonal; R&D Systems, BAF401) was conjugated with CF660R streptavidin (biotinum) and that for IL-1α (polyclonal; R&D Systems, BAF400) was conjugated to Cy3 streptavidin (BioLegend). Mineral oil was layered on top of the medium to prevent evaporation. For the first serial of trials, we observed IL-1β secretion, SYTOX blue staining and the change in morphology from the cells in 2,500 nanolitre wells per genotype at 30-min intervals for 9.5 h. In the trials performed after that, we observed secretion of both IL-1β and IL-1α, SYTOX green staining and the change in morphology from the cells in 996 nanolitre wells per genotype at 1-h intervals for 12 h.

The time-course analysis of each fluorescence was performed using NIS Elements 4.6 (Nikon). The fluorescence intensity of the secretion signal as well as that of the dead-cell staining were measured over the entire time for all the regions of interest (ROIs) that were set to contain each well. Bright field imaging was used to determine whether each well contained a single cell. Background estimation was done with the fluorescence intensities in ROIs that were set on wells containing no cells (referred to as 'empty ROIs'). The median value of intensity from all of the empty ROIs of each ROI position (four positions in the view) in each scan cycle was regarded as the background level at that time. The location-specific background signal was corrected by subtracting the initial value of each field of view. The s.d. could be estimated as 1.4826× the median absolute deviation when the distribution of the intensity in empty ROIs followed a normal distribution and then we used 5× the s.d. estimated from the median absolute deviation as the threshold for signal detection.

Statistics and reproducibility. Continuous variables were summarized by the mean ± s.e.m. Regarding mean values, pairwise comparisons of groups were evaluated by the non-parametric Mann–Whitney test contingent. Multiple pairwise comparisons of groups over time were evaluated by ordinary or Kruskal–Wallis one-way ANOVAs with post-Bonferronni corrections. Moreover, multiple pairwise comparisons of groups over time by repeated or non-repeated measures were evaluated by two-way ANOVAs with Bonferronni correction (the corrected *P* values are given for comparison between genotypes at each time point or for the main effect over time). The usual family-wise type I error of 5% was adopted to assess statistical significance. All statistical tests were two-tailed and were performed using Prism (GraphPad Software). The number of mice analysed in each experiment is described in the respective figure legends. The experiments were repeated two or three times independently, as indicated in the respective figure legends.

Reporting Summary. Further information on research design is available in the Nature Research Reporting Summary linked to this article.

Data availability

Source data for Figs. 1–8 and Supplementary Figs. 1–4, 6 and 7 have been provided in Supplementary Table 3. Uncropped images of the immunoblots presented in the figures are included in Supplementary Fig. 9. All other data supporting the findings of this study are available from the corresponding author on reasonable request[55,56,58,61].

References

55. Pasparakis, M. et al. TNF-mediated inflammatory skin disease in mice with epidermis-specific deletion of IKK2. *Nature* **417**, 861–866 (2002).
56. Vlantis, K. et al. TLR-independent anti-inflammatory function of intestinal epithelial TRAF6 signalling prevents DSS-induced colitis in mice. *Gut* **65**, 935–943 (2016).
57. Drexler, S. K. et al. Tissue-specific opposing functions of the inflammasome adaptor ASC in the regulation of epithelial skin carcinogenesis. *Proc. Natl Acad. Sci. USA* **109**, 18384–18389 (2012).
58. Sodhi, C. P. et al. Intestinal epithelial Toll-like receptor 4 regulates goblet cell development and is required for necrotizing enterocolitis in mice. *Gastroenterology* **143**, 708–718 (2012).
59. Clausen, B. E., Burkhardt, C., Reith, W., Renkawitz, R. & Forster, I. Conditional gene targeting in macrophages and granulocytes using LysMcre mice. *Transgenic Res.* **8**, 265–277 (1999).
60. Newton, K., Sun, X. & Dixit, V. M. Kinase RIP3 is dispensable for normal NF-κBs, signaling by the B-cell and T-cell receptors, tumor necrosis factor receptor 1, and Toll-like receptors 2 and 4. *Mol. Cell. Biol.* **24**, 1464–1469 (2004).
61. Lin, J. et al. RIPK1 counteracts ZBP1-mediated necroptosis to inhibit inflammation. *Nature* **540**, 124–128 (2016).
62. Adachi, O. et al. Targeted disruption of the *MyD88* gene results in loss of IL-1- and IL-18-mediated function. *Immunity* **9**, 143–150 (1998).
63. Armaka, M., Ospelt, C., Pasparakis, M. & Kollias, G. The p55TNFR–IKK2–Ripk3 axis orchestrates arthritis by regulating death and inflammatory pathways in synovial fibroblasts. *Nat. Commun.* **9**, 618 (2018).
64. Armaka, M., Gkretsi, V., Kontoyiannis, D. L. & Kollias, G. A standardized protocol for the isolation and culture of normal and arthritogenic murine synovial fibroblasts. *Protoc. Exch.* https://doi.org/10.1038/nprot.2009.102 (2009).

nature cell biology

SUPPLEMENTARY INFORMATION

https://doi.org/10.1038/s41556-019-0324-3

In the format provided by the authors and unedited.

A20 prevents inflammasome-dependent arthritis by inhibiting macrophage necroptosis through its ZnF7 ubiquitin-binding domain

Apostolos Polykratis[1,11], Arne Martens[2,3,11], Remzi Onur Eren[1,11], Yoshitaka Shirasaki[4,5], Mai Yamagishi[5], Yoshifumi Yamaguchi[6,7], Sotaro Uemura[5], Masayuki Miura[6], Bernhard Holzmann[8], George Kollias[9,10], Marietta Armaka[9,12], Geert van Loo[2,3,12*] and Manolis Pasparakis[1,12*]

[1]Institute for Genetics, Cologne Excellence Cluster on Cellular Stress Responses in Aging-Associated Diseases (CECAD) and Center for Molecular Medicine (CMMC), University of Cologne, Cologne, Germany. [2]VIB Center for Inflammation Research, Ghent, Belgium. [3]Department of Biomedical Molecular Biology, Ghent University, Ghent, Belgium. [4]JST PRESTO, Tokyo, Japan. [5]Department of Biological Sciences, Graduate School of Science, The University of Tokyo, Tokyo, Japan. [6]Department of Genetics, Graduate School of Pharmaceutical Science, The University of Tokyo, Tokyo, Japan. [7]Institute of Low Temperature Science, Hokkaido University, Sapporo, Japan. [8]Department of Surgery, School of Medicine, Technical University of Munich, Munich, Germany. [9]Biomedical Sciences Research Center 'Alexander Fleming', Vari, Greece. [10]Department of Physiology, Medical School, National and Kapodistrian University of Athens, Athens, Greece. [11]These authors contributed equally: Apostolos Polykratis, Arne Martens, Remzi Onur Eren. [12]These authors jointly supervised this work: Marietta Armaka, Geert van Loo, Manolis Pasparakis. *e-mail: geert.vanloo@irc.vib-ugent.be; pasparakis@uni-koeln.de

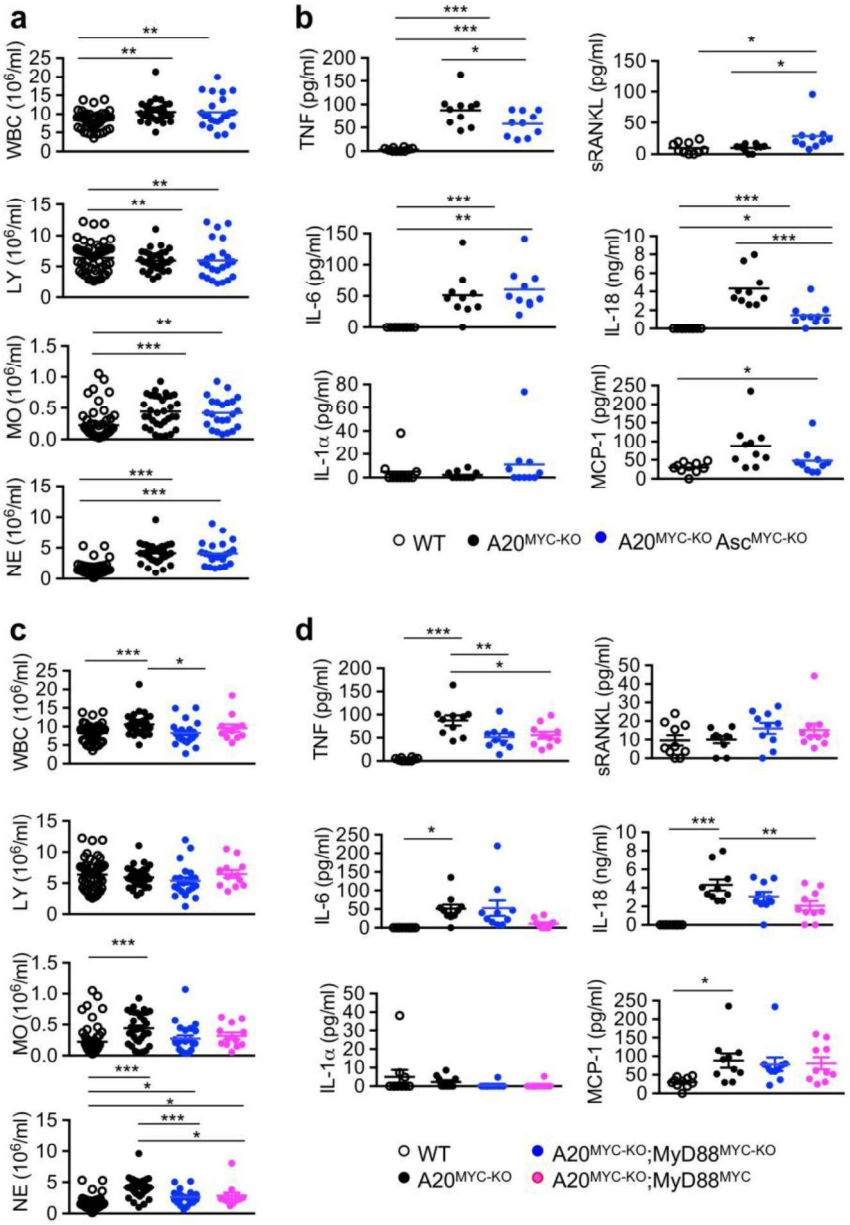

Supplementary Figure 1

Leucocyte and cytokine analysis in the blood of wild type, A20^{MYC-KO}, A20^{MYC-KO} ASC^{MYC-KO}, A20^{MYC-KO} MyD88^{MYC-KO}, and A20^{MYC-KO} MyD88^{MYC} mice.

(a) Graphs indicating the number of white blood cells (WBC), lymphocytes (LY), monocytes (MO), and neutrophils (NE) in peripheral blood from mice with the indicated genotypes (wt, n=54; A20^{MYC-KO}, n=33; A20^{MYC-KO} Asc^{MYC-KO}, n=23 mice). (b) Levels of the indicated cytokines and chemokines in the serum of mice with the indicated genotypes (n=10 mice per genotype). (c) Graphs indicating the number of white blood cells (WBC), lymphocytes (LY), monocytes (MO), and neutrophils (NE) in peripheral blood from mice with the indicated genotypes. Wild type and A20^{MYC-KO} mice are the same shown in Supplementary Fig. 1 and are included for comparison (wt, n=54; A20^{MYC-KO}, n=33; A20^{MYC-KO} MyD88^{MYC-KO}, n=22; A20^{MYC-KO} MyD88^{MYC,} n=12 mice). (d) Levels of the indicated cytokines and chemokines in the serum of mice with the indicated genotypes (n=10 mice per genotype). Dots in the graphs indicate individual mice. In all graphs average ± SEM is also shown for each group of mice. *, ** and *** represent $p<0.05$, $p<0.01$ and $p<0.001$ respectively (one-way ANOVA post-Bonferonni test between indicated genotypes). All statistical tests are two-tailed. Raw data are provided in Supplementary Table 3.

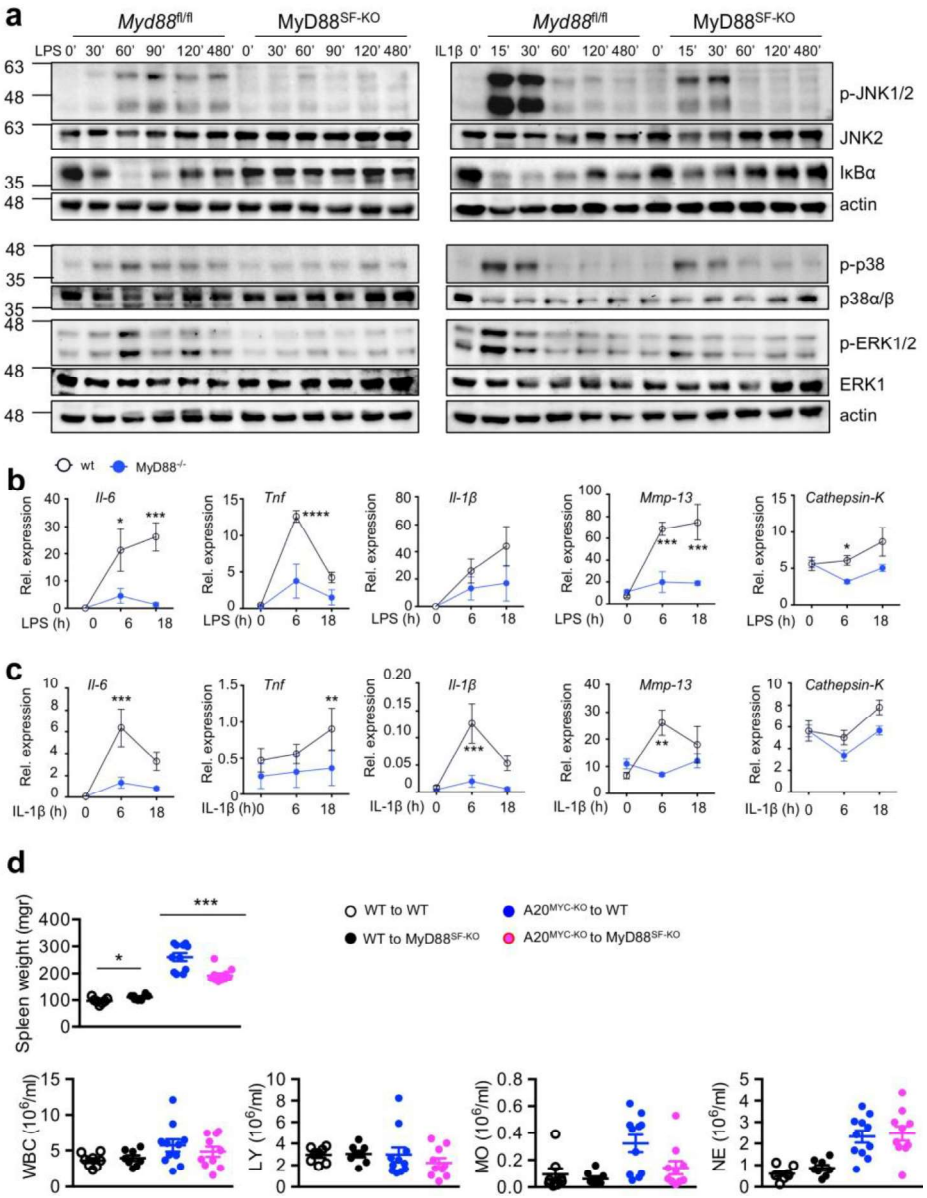

Supplementary Figure 2

MyD88 regulates LPS- and IL-1β-induced inflammatory signalling in synovial fibroblasts.

a) Synovial fibroblasts with the indicated genotypes were stimulated with 1 μg/ml of LPS (left panel) or 10 ng/ml of IL-1β (right panel) and analysis of NF-κB and MAPK signalling was performed by immunoblotting with the indicated antibodies. Results of one representative out of two independent experiments are shown. (b-c) Synovial fibroblasts with the indicated genotypes were incubated with 1 μg/ml of LPS (b) or 10 ng/ml of IL-1β (c) and mRNA expression of the indicated genes was evaluated at the indicated time points after stimulation. Graphs depict pooled results from two independent experiments in which five independent isolations of synovial fibroblasts for each genotype (n=5 independent isolations of synovial fibroblasts) were used. (d) Graphs depicting spleen weight as well as the numbers of white blood cells (WBC), lymphocytes (LY), monocytes (MO), and neutrophils (NE) in peripheral blood from mice with the indicated genotypes. Dots indicate individual mice (wt to wt, n=7; wt to MyD88^{SF-KO} n=8; A20^{MYC-KO} to wt, n=11, A20^{MYC-KO} to MyD88^{SF-KO}, n=10 mice). In all graphs average ± SEM is also shown for each group of mice. *, ** and *** represent $p<0.05$, $p<0.01$ and $p<0.001$ respectively (non-parametric Mann-Whitney test between indicated genotypes for d; two way ANOVA post Bonferroni for b, c). All statistical tests are two-tailed. Raw data are provided in Supplementary Table 3 and unprocessed immunoblots are provided in Supplementary Figure 9.

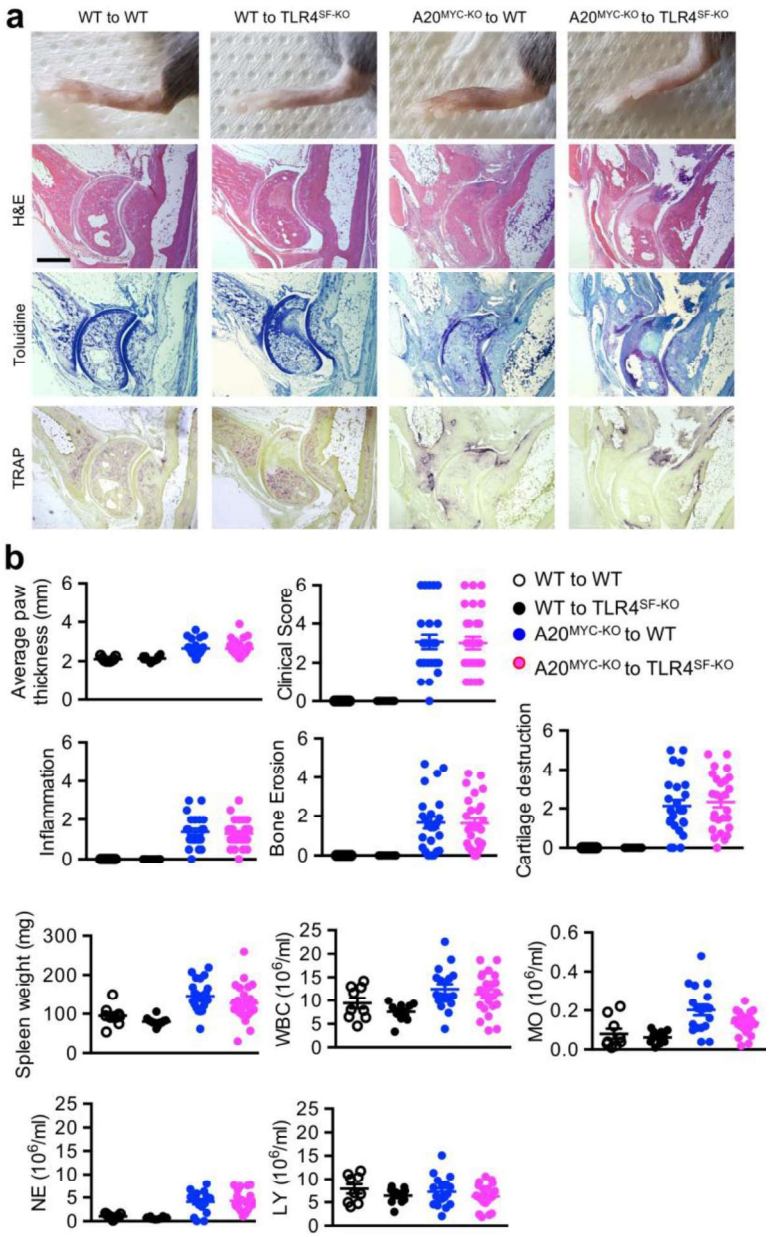

Supplementary Figure 3

Synovial fibroblast-specific TLR4 knockout does not inhibit arthritis caused by myeloid cell specific A20 deficiency

a) Representative macroscopic and histological images of the ankle joints of mice with the indicated genotypes analysed 32 weeks after adoptive transfer of bone marrow from wt or $A20^{MYC-KO}$ animals (scale bar: 500µm). (b) Graphs depicting clinical scores, average thickness of rear paws at the ankle area, as well as histological scores for inflammation, bone erosion, and cartilage destru ction in mice with the indicated genotypes transferred with bone marrow from wt or $A20^{MYC-KO}$ animals. Dots in the graphs indicate individual mice (wt to wt, n=9; wt to $TLR4^{SF-KO}$ n=12; $A20^{MYC-KO}$ to wt, n=24, $A20^{MYC-KO}$ to $TLR4^{SF-KO}$, n=27 mice for a-b). (c) Graphs depicting spleen weight, the number of white blood cells (WBC), lymphocytes (LY), monocytes (MO), and neutrophils (NE) in peripheral blood from mice with the indicated genotypes. (wt to wt, n=9; wt to $TLR4^{SF-KO}$ n=10; $A20^{MYC-KO}$ to wt, n=18, $A20^{MYC-KO}$ to $TLR4^{SF-KO}$, n=22 mice). In all graphs average ± SEM is shown for each group of mice (non-parametric Mann-Whitney test between indicated genotypes). All statistical tests are two-tailed. Raw data are provided in Supplementary Table 3.

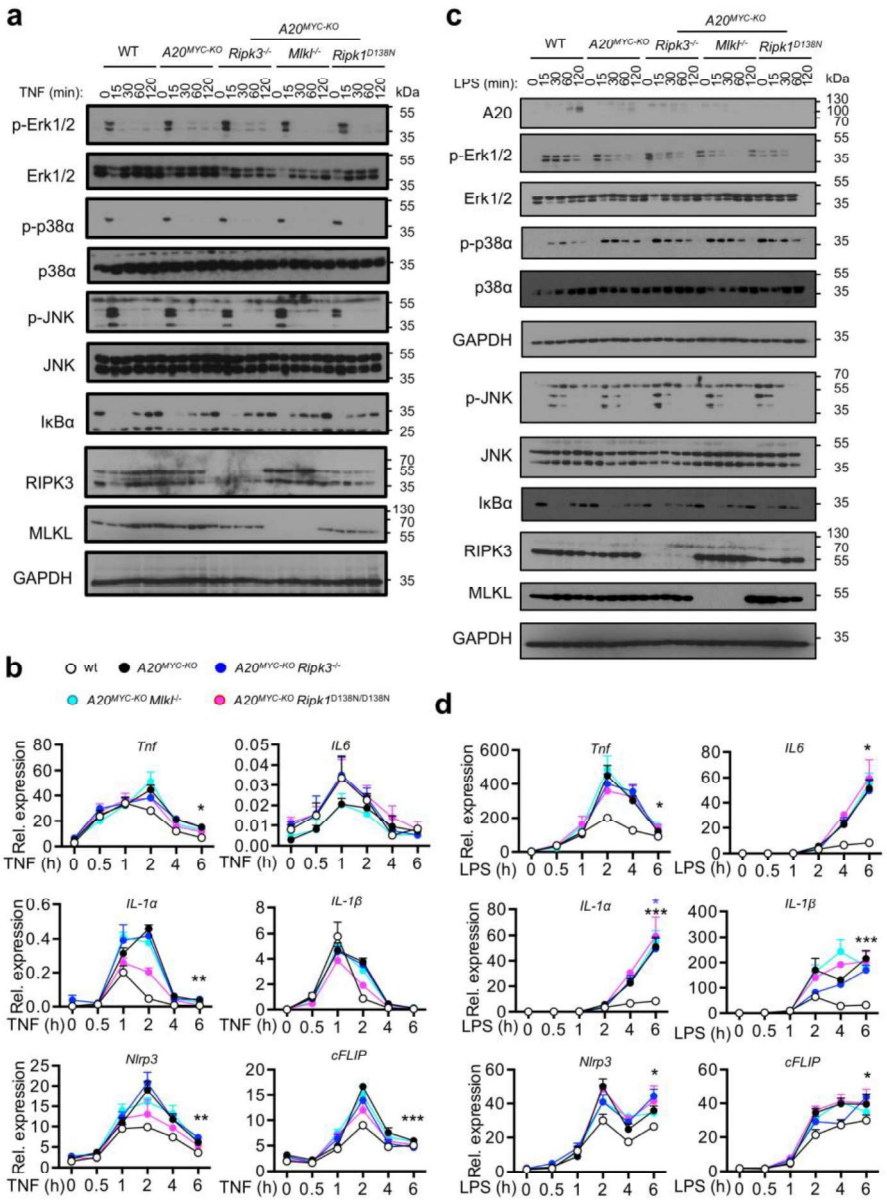

Supplementary Figure 4

RIPK3 or MLKL deficiency or lack of RIPK1 kinase activity, does not affect TNF- and LPS-induced NF-κB and MAPK activation as well as inflammatory gene expression in *A20*$^{-/-}$ macrophages.

(a-b) BMDMs with the indicated genotypes were stimulated with 20 ng/ml of TNF for the indicated time points. (a) Analysis of NF-κB and MAPK signalling was performed by immunoblotting with the indicated antibodies. Results of one representative out of two independent experiments are shown. (b) mRNA expression of the indicated genes was analysed by qRT-PCR Results shown were obtained from one experiment in which three independent isolations of BMDMs for each genotype (n=3 independent BMDM isolations) were included. (c-d) BMDMs with the indicated genotypes were stimulated with 20 ng/ml of LPS for the indicated time points. (c) Analysis of NF-κB and MAPK signalling was performed by immunoblotting with the indicated antibodies. Results of one representative out of two independent experiments are shown. (d) mRNA expression of the indicated genes was analysed by qRT-PCR. Results shown were obtained from one experiment in which three independent isolations of BMDMs for each genotype (n=3 independent BMDM isolations) were included. In all graphs average ± SEM is shown for each group of mice. *, ** and *** represent $p<0.05$, $p<0.01$ and $p<0.001$ respectively (two way ANOVA post Bonferroni). All statistical tests are two-tailed. Raw data are provided in Supplementary Table 3 and unprocessed immunoblots are provided in Supplementary Figure 9.

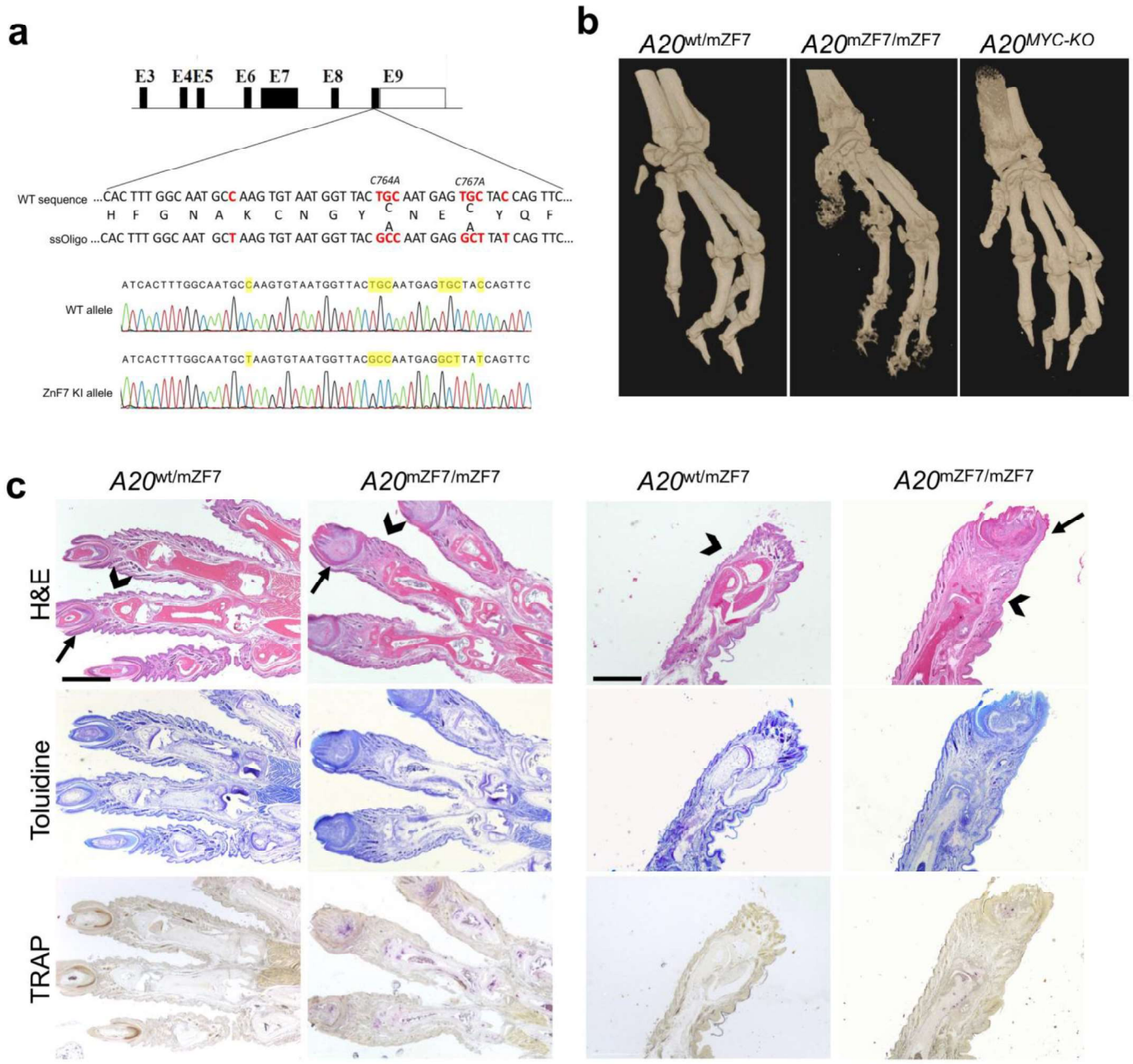

Supplementary Figure 5

A20$^{mZnF7/mZnF7}$ knock-in mice generated using CRISPR/Cas9-mediated gene targeting develop dactylitis.

(a) Schematic representation of the A20 gene indicating the location of the point mutations introduced in exon 9 to change cys teine (C) residues at positions 764 and 767 to alanines (A). Two silent mutations were also introduced to avoid re-editing of the DNA by Cas9 after homology-directed repair. Sanger sequencing of wt and *A20*$^{mZnF7/mZnF7}$ mouse tail DNA to confirm correct introduction of the designed mutations into the genome. **(**b) mCT analysis of forepaws of mice with the indicated genotypes depicts the extensive bone erosions in the digits of *A20*$^{mZnF7/mZnF7}$ and the milder erosions in carpal bones compared to *A20*$^{MYC-KO}$ mice (c) Representative histological images from forepaws (right panel; transversal sections) and hindpaws (left panel; sagittal sections) of mice with the indicated genotypes. Note the development of dactylitis in *A20*$^{mZnF7/mZnF7}$ mice with a characteristic severe tenosynovitis leading to disruption of muscle/tendon fibres and the pannus orchestrating destruction of bones (arrow), all being more evident in the d istal and intermediate (arrowhead) than in proximal phalanxes (scale bar: 1mm) (*A20*$^{wt/mZnF7}$, n=8 and *A20*$^{mZnF7/mZnF7}$, n=10 mice).

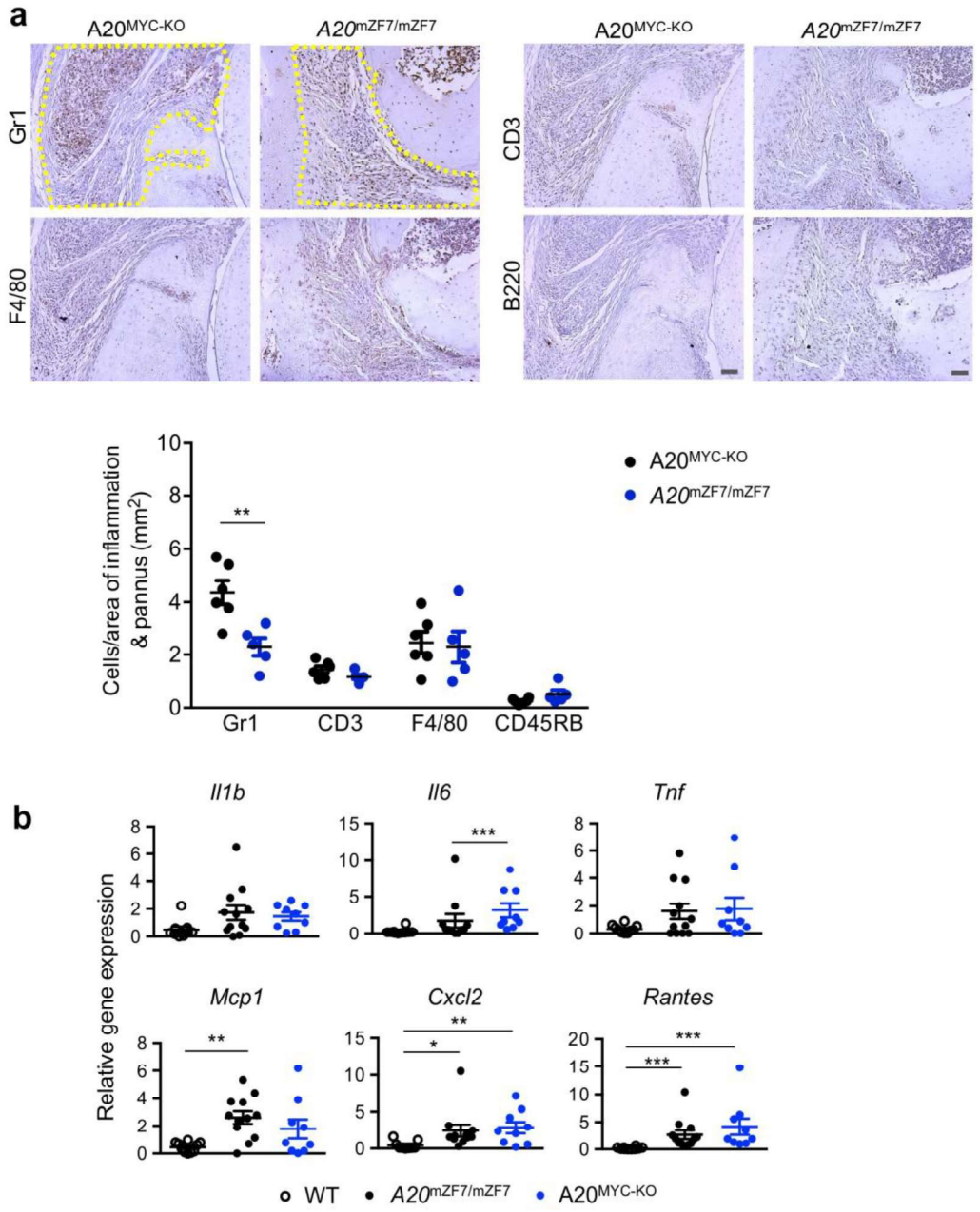

Supplementary Figure 6

Comparison of immune cell infiltration and inflammatory cytokine and chemokine expression in joints from A20^{MYC-KO} and *A20*$^{mZnF7/mZnF7}$ mice.

(a) Representative images of histological serial sections from the ankle joints of mice with the indicated genotypes, which were immunostained with the indicated antibodies (*A20*$^{MYC-KO}$,n=6 and *A20*^{ZnF7} n=5 mice). Immune cell numbers were evaluated within the affected areas (dotted line). Data represents mean ± SEM (non-parametric Mann-Whitney test between indicated genotypes). (b) The mRNA expression of the indicated cytokines and chemokines was analyzed by qRT-PCR in RNA from hind paws of mice with the indicated genotypes. Each dot represents an individual mouse (*A20*$^{wt/wt}$, n=9-10; *A20*wt$^{/mZnF7}$, n=11-12 and *A20*$^{MYC-KO}$, n=9 mice). Average ± SEM is also shown for each group of mice. *, ** and *** represent p<0.05, p<0.01 and p<0.001 respectively (Kruskal-Wallis one-way ANOVA test between indicated genotypes). All statistical tests are two-tailed. Raw data are provided in Supplementary Table 3.

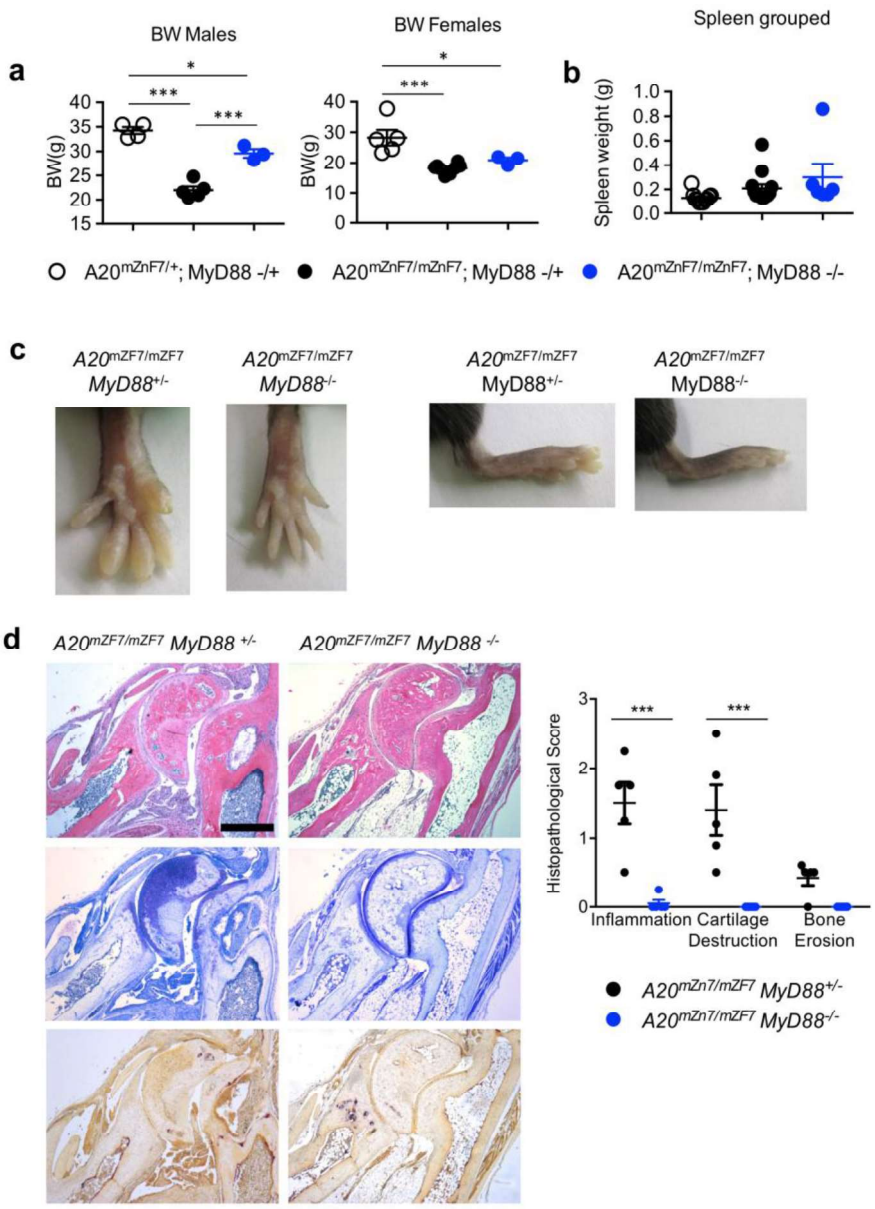

Supplementary Figure 7

MyD88 deficiency prevents the development of arthritis and dactylitis in *A20*$^{mZnF7/mZnF7}$ mice.

a) Graphs depicting the body weight (BW) of mice with the indicated genotypes at the age of 20-30 weeks. (b) Graph depicting spleen / BW ratio of mice with the indicated genotypes. (c) Representative pictures of forepaws and hindpaws of mice with the indicated genotypes at the age of 20 weeks. (d) Representative histological images of ankle joints from 20-30-week-old littermate mice with the indicated genotypes. Scale bar: 500 µm. Graph depicts histological scores for inflammation, bone erosion, and cartilage destruction in mice with the indicated genotypes. Dots in the graphs indicate individual mice (*A20*$^{mZnF7/+}$ *MyD88*$^{-/+}$ n=4; *A20*$^{mZnF7/mZnF7}$ *MyD88*$^{-/+}$ n=5; *A20*$^{mZnF7/mZnF7}$ *MyD88*$^{-/-}$ n=3 mice for a,b; *A20*$^{mZnF7/mZnF7}$ *MyD88*$^{-/+}$ n=5; *A20*$^{mZnF7/mZnF7}$ *MyD88*$^{-/-}$ n=5 mice for d). In all graphs average ± SEM is also shown for each group of mice. *, **, and *** represent $p<0.05$, $p<0.01$, and $p<0.001$ respectively (One-way ANOVA post-Bonferroni test for a; two-way ANOVA post-Bonferroni test for b). All statistical tests are two-tailed. Raw data are provided in Supplementary Table 3.

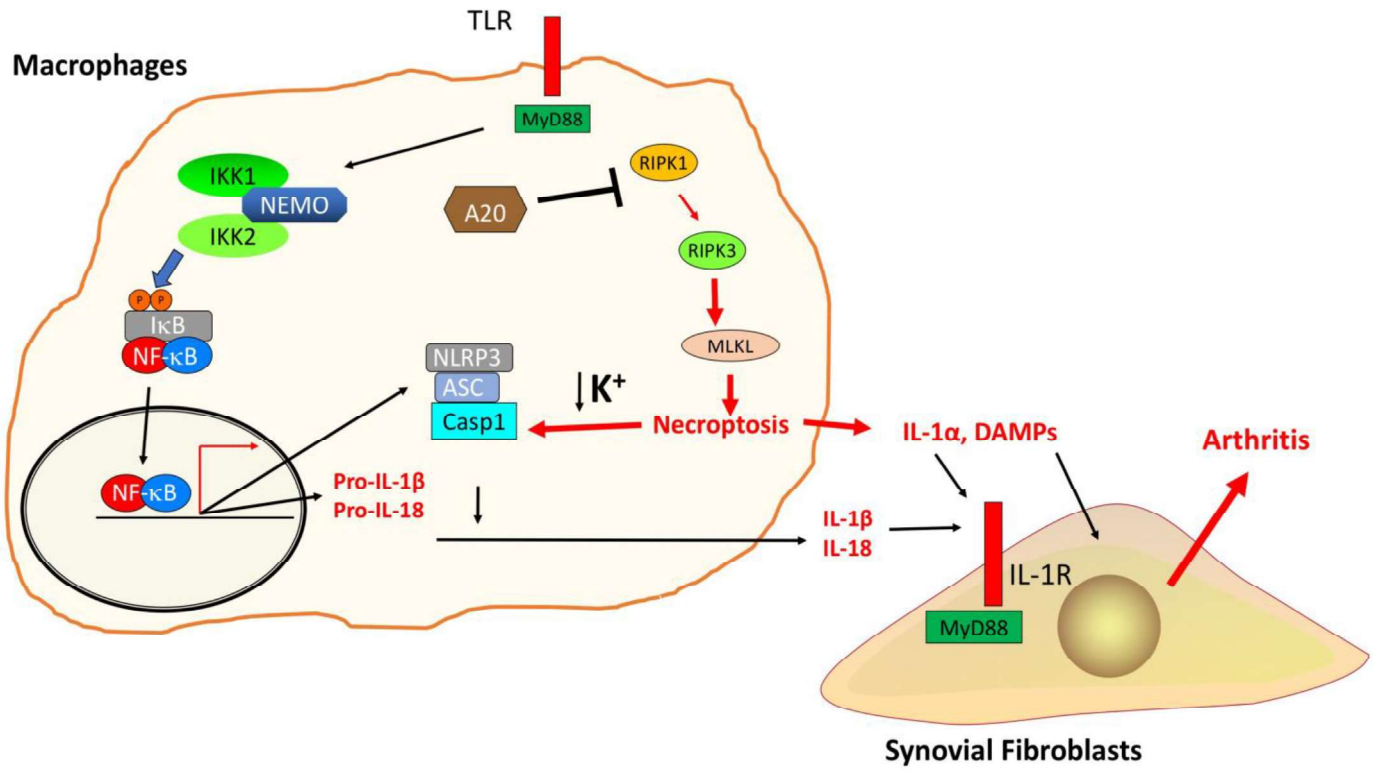

Supplementary Figure 8

Schematic model depicting the mechanisms regulating the pathogenesis of inflammatory arthritis in A20$^{MYC\text{-}KO}$ mice.

A20 prevents inflammasome activation and the release of mature IL-1β and IL-18 but also IL-1α in macrophages by inhibiting RIPK1-RIPK3-MLKL-dependent necroptosis. In A20-deficient macrophages, RIPK1-RIPK3-MLKL-dependent signalling causes necroptosis that results in the release of IL-1α and other DAMPs. In addition, MLKL-dependent plasma membrane permeabilization triggers K+ efflux, which activates the NLRP3 inflammasome and the caspase-1-dependent processing and subsequent release of IL-1β and IL-18. IL-1α and IL-1β, likely together with IL-18 and other DAMPs released by necroptotic A20-deficient macrophages activate MyD88-dependent proinflammatory signalling in synovial fibroblasts causing joint tissue inflammation, as well as cartilage and bone destruction resulting in the development of arthritis.

Addendum: A20 prevents inflammasome-dependent arthritis by inhibiting macrophage necroptosis through its ZnF7 ubiquitin-binding domain

We hypothesize that in myeloid specific A20 deficient mice, IL-1α and IL-1β likely together with IL-18 and other DAMPs released by necroptotic macrophages activate MyD88-dependent proinflammatory signalling in synovial fibroblasts causing the development of arthritis[1]. Blocking inflammasome activation or necroptosis in $A20^{MYC\text{-}KO}$ mice, by crossing these mice in an ASC deficient or RIPK1 kinase dead ($RIPK1^{D138N}$) background, rescues from arthritis development[1]. To test whether necroptosis and NLRP3 inflammasome activation are also involved in the RA pathology seen in $A20^{ZnF7/ZnF7}$ mice, these mice were crossed in a $NLRP3^{-/-}$ or $RIPK1^{D138N}$ genetic background. Surprisingly, $A20^{ZnF7/ZnF7}NLRP3^{-/-}$ and $A20^{ZnF7/ZnF7}RIPK1^{D138N}$ mice still have reduced bodyweight and develop splenomegaly. Furthermore, these mice develop arthritis to the same extend as $A20^{ZnF7/ZnF7}$ mice, as seen macroscopically by symmetric swelling of ankles, wrists and toes, and by histological analysis (Fig. 1,2). Since these mice are full body $A20^{ZnF7/ZnF7}$ mice, most likely the pathology is caused by the mutated ZnF7 in non-myeloid cells. Together, the ZnF7 domain prevents macrophage necroptosis and IL-1α/β release, however the phenotype seen in $A20^{ZnF7}$ mice is partly caused by mechanisms relying on non-myeloid cells, independent of necroptosis and NLRP3-inflammasome activation.

In addition, the inflammatory toe pathology seen in $A20^{ZnF7/ZnF7}$ mice is never observed in myeloid-specific A20 deficient mice. Removing a downstream sub-TAD domain, containing 4 enhancers, at the A20 locus significantly reduces the basal and induced levels of A20[2]. Also, these mice develop spontaneous inflammatory arthritis and dactylitis with synovitis involving the digits of all paws[2], comparable to what was seen in $A20^{ZnF7/ZnF7}$ mice[1,2]. This observation suggests that the phenotype observed in the toes of $A20^{ZnF7/ZnF7}$ mice is probably also caused by the mutation in non-myeloid cells.

Finally, previous research using conditional A20 knockout mice suggests that also apoptosis of A20-deficient cells could contribute to the systemic inflammation seen in A20 deficient mice[3,4]. To assess the specific role of cell death, both apoptosis and necroptosis, in the inflammatory phenotype of $A20^{ZnF7/ZnF7}$ mice or more general in the systemic and lethal inflammation of A20-deficient mice, it would be interesting to cross these lines into a FADD/Caspase-8 and RIPK3/MLKL deficient

background to inhibit both apoptosis and necroptosis, in order to see if the inflammatory phenotype seen in these mice can be rescued.

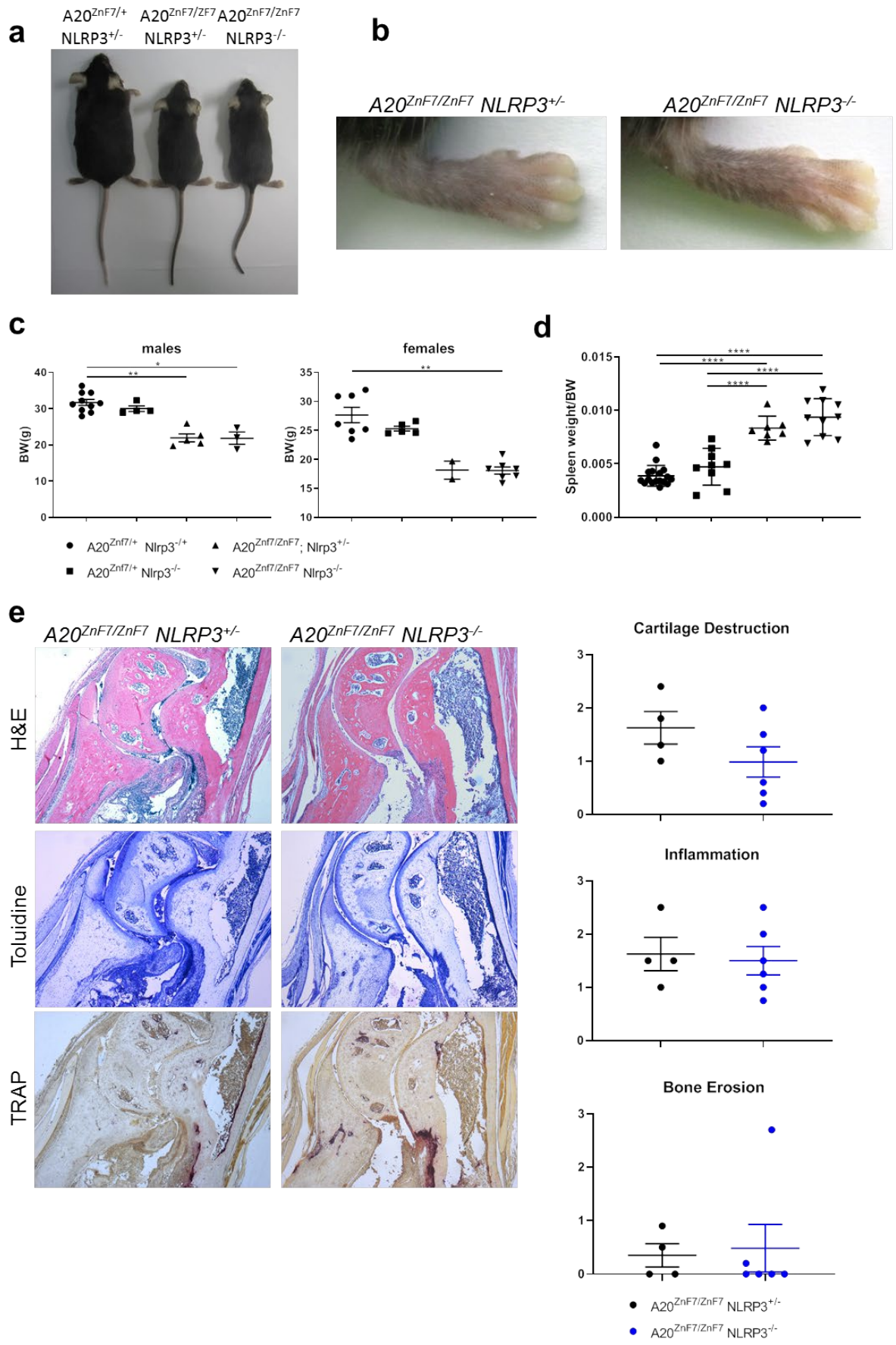

Fig. 1 **(a)** Gross appearance of A20$^{ZnF7/+}$ NLRP3$^{+/-}$, A20$^{ZnF7/ZnF7}$ NLRP3$^{+/-}$ and A20$^{ZnF7/ZnF7}$ NLRP3$^{-/-}$ mice. **(b)** Representative pictures of hindpaws of mice with the indicated genotypes at the age of 20 weeks.

(c) Body weight of 20-week-old male and female mice with indicated genotypes (male: $A20^{ZnF7/+}$ $NLRP3^{+/-}$ n=10, $A20^{ZnF7/+}$ $NLRP3^{-/-}$ n=4, $A20^{ZnF7/ZnF7}$ $NLRP3^{+/-}$ n=5, $A20^{ZnF7/ZnF7}$ $NLRP3^{-/-}$ n=3; female: $A20^{ZnF7/+}$ $NLRP3^{+/-}$ n=7, $A20^{ZnF7/+}$ $NLRP3^{-/-}$ n=5, $A20^{ZnF7/ZnF7}$ $NLRP3^{+/-}$ n=2, $A20^{ZnF7/ZnF7}$ $NLRP3^{-/-}$ n=7) **(d)** Spleen:body weight ratio in 20-week-old mice with indicated genotypes ($A20^{ZnF7/+}$ $NLRP3^{+/-}$ n=17, $A20^{ZnF7/+}$ $NLRP3^{-/-}$ n=9, $A20^{ZnF7/ZnF7}$ $NLRP3^{+/-}$ n=7, $A20^{ZnF7/ZnF7}$ $NLRP3^{-/-}$ n=10). Symbols used are identical as in panel c. **(e)** Representative histological images and histological scores for inflammation, bone erosion and cartilage destruction of the ankle joints of 20-week-old littermate mice with the indicated genotypes ($A20^{ZnF7/ZnF7}$ $NLRP3^{+/-}$ n=4, $A20^{ZnF7/ZnF7}$ $NLRP3^{-/-}$ n=6). The dots in all the graphs indicate individual mice In all graphs average ± SEM is also shown for each group of mice. *, **, and *** represent $p<0.05$, $p<0.01$, and $p<0.001$ respectively (One-way ANOVA with Bonferroni correction for c,d; Non-parametric Mann–Whitney test for e)

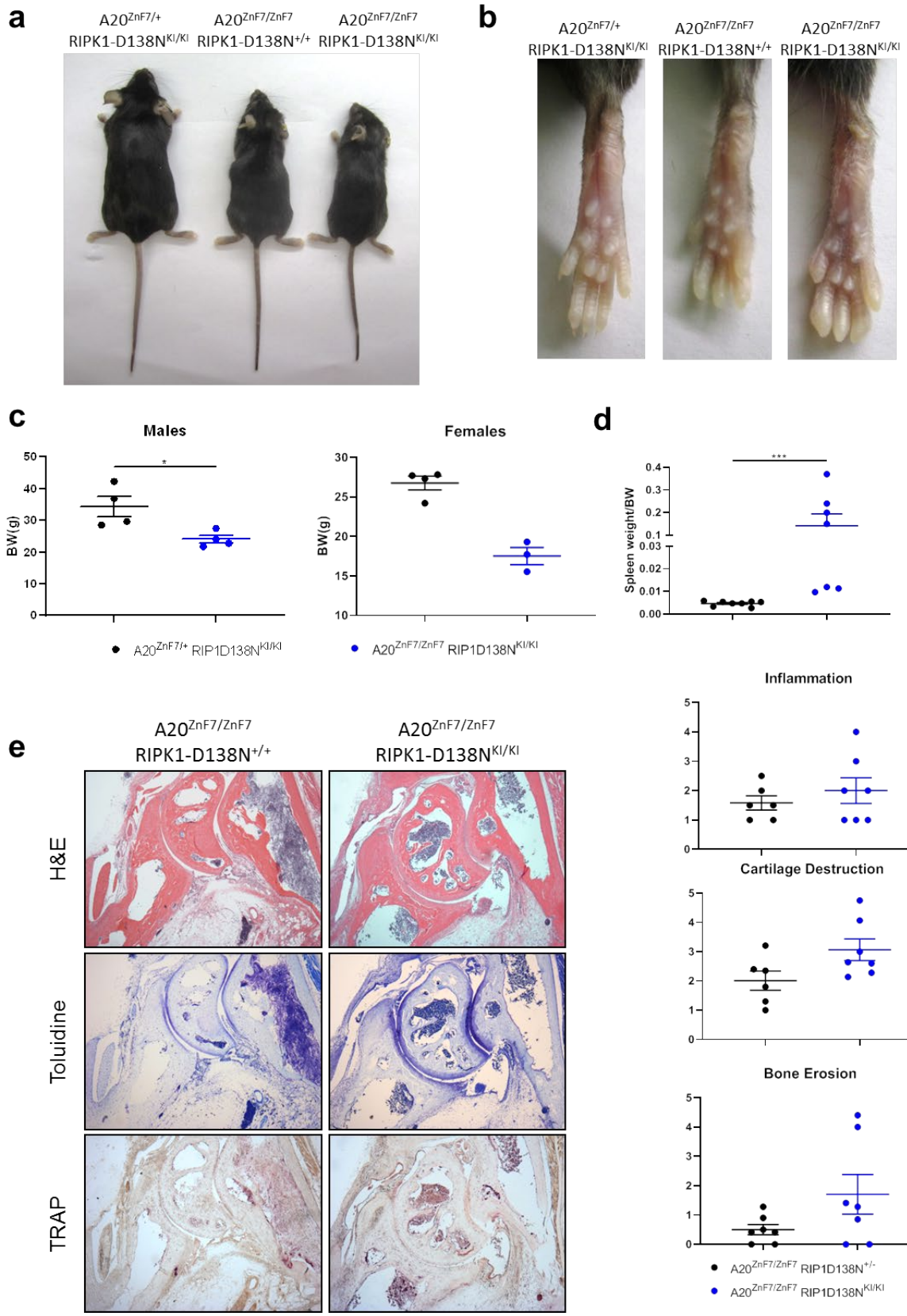

Fig. 2 **(a)** Gross appearance of $A20^{ZnF7/+}$ RIPK1-$D138N^{KI/KI}$, $A20^{ZnF7/ZnF7}$ RIPK1-$D138N^{+/+}$ and $A20^{ZnF7/ZnF7}$ RIPK1-$D138N^{KI/KI}$. **(b)** Representative pictures of hindpaws of mice with the indicated genotypes at the age of 20 weeks. **(c)** Body weight of 20-week-old male and female mice with indicated genotypes (male: $A20^{ZnF7/+}$ RIPK1-$D138N^{KI/KI}$ n=4, $A20^{mZnF7/mZnF7}$ RIPK1-$D138N^{KI/KI}$ n=4;

female: $A20^{ZnF7/+}$ $RIPK1\text{-}D138N^{KI/KI}$ n=4, $A20^{ZnF7/ZnF7}$ $RIPK1\text{-}D138N^{KI/KI}$ n=3 **(d)** Spleen:body weight ratio in 20-week-old mice with indicated genotypes ($A20^{ZnF7/+}$ $RIPK1\text{-}D138N^{KI/KI}$ n=8, $A20^{ZnF7/ZnF7}$ $RIPK1\text{-}D138N^{KI/KI}$ n=7). Symbols used are identical as in panel c. **(e)** Representative histological images and histological scores for inflammation, bone erosion and cartilage destruction of the ankle joints of 20-week-old littermate mice with the indicated genotypes ($A20^{ZnF7/ZnF7}$ $RIPK1\text{-}D138N^{+/+}$ n=6, $A20^{ZnF7/ZnF7}$ $RIPK1\text{-}D138N^{KI/KI}$ n=7). The dots in all the graphs indicate individual mice In all graphs average ± SEM is also shown for each group of mice. *, **, and *** represent $p<0.05$, $p<0.01$, and $p<0.001$ respectively (One-way ANOVA with Bonferroni correction for c,d; Non-parametric Mann–Whitney test for e)

References

1 Polykratis, A. *et al.* A20 prevents inflammasome-dependent arthritis by inhibiting macrophage necroptosis through its ZnF7 ubiquitin-binding domain. *Nat Cell Biol* **21**, 731-742, doi:10.1038/s41556-019-0324-3 (2019).

2 Sokhi, U. K. *et al.* Dissection and function of autoimmunity-associated TNFAIP3 (A20) gene enhancers in humanized mouse models. *Nat Commun* **9**, 658, doi:10.1038/s41467-018-03081-7 (2018).

3 Vereecke, L. *et al.* Enterocyte-specific A20 deficiency sensitizes to tumor necrosis factor-induced toxicity and experimental colitis. *J Exp Med* **207**, 1513-1523, doi:10.1084/jem.20092474 (2010).

4 Catrysse, L. *et al.* A20 prevents chronic liver inflammation and cancer by protecting hepatocytes from death. *Cell Death Dis* **7**, e2250, doi:10.1038/cddis.2016.154 (2016).

III. A20 critically controls RANK-dependent osteoclastogenesis and bone physiology

Arne Martens[1,2], Dario Priem[1,2], Els Louagie[1,3], Julie Coudenys[1,3], Amélie De Muynck[4], Djoere Gaublomme[1,3], Mozes Sze[1,2], Kalliopi Iliaki[5], Jolanda van Hengel[6], Jeffrey D Zajac[7] , Rachel A Davey[7], Luc Van Hoorebeke[4], Mathieu JM Bertrand[1,2], Marietta Armaka[5], Dirk Elewaut[1,3] and Geert van Loo[1,2]

1. Center for Inflammation Research Center, VIB, B-9052 Ghent, Belgium.
2. Department of Biomedical Molecular Biology, Ghent University, B-9052 Ghent, Belgium.
3. Laboratory for Molecular Immunology and Inflammation, Department of Rheumatology, Ghent University Hospital, B-9000 Ghent, Belgium.
4. UGent Centre for X-ray Tomography, Department of Physics and Astronomy, Ghent University, B-9000 Ghent, Belgium.
5. Biomedical Sciences Research Center 'Alexander Fleming', G-16672 Vari, Greece
6. Laboratory for Medical Stem Cell Biology, Department of Basic Medical Sciences, Ghent University Hospital, B-9000 Ghent, Belgium.
7. Department of Medicine, Austin Health, University of Melbourne, Heidelberg, Victoria, Australia

Author contributions

A.M. and G.v.L. conceived the study and designed the experiments. A.M., D.P., E.L., J.C., A.D.M., M.S., M.B. and M.A.. performed and/or analysed the experiments. A.D.M. and L.V.H. provided help for the µCT analysis and D.G. provided the software for µCT analysis. J.V.H provided help for the femur strength analysis. J.D.Z. and R.A.D provided the mice. A.M. and G.v.L. supervised the experiments, interpreted the data and wrote the paper.

A20 critically controls RANK-dependent osteoclastogenesis and bone physiology

Abstract

A20 (TNFAIP3) serves as a critical brake on NF-κB signaling and NF-κB-dependent inflammation. In humans, polymorphisms in or near the *A20* gene have been associated with several inflammatory disorders, including rheumatoid arthritis (RA). In agreement, previous studies have demonstrated that mice with myeloid-specific A20 deficiency spontaneously develop a severe polyarthritis resembling human RA. Myeloid A20 deficiency, however, was also shown to promote osteoclastogenesis in mice, suggesting a role for A20 in the regulation of osteoclast differentiation and bone remodeling. We show here that osteoclast-specific A20 knockout mice develop severe osteoporosis, but no signs of inflammatory arthritis. *In vitro*, we demonstrate that A20 inhibits RANK-induced NF-κB signaling independent from its deubiquitinating activity but dependent on its zinc finger (ZnF) 4 and 7 ubiquitin-binding function. In addition, A20 expression is shown to be induced by the activation of RANK signaling in osteoclast cultures. Together, these data demonstrate that A20 acts as a negative regulator of RANK-induced NF-κB signaling to control osteoclastogenesis assuring proper bone development and turnover.

Introduction

Bone is continuously being remodeled in a process of bone matrix synthesis by osteoblasts and bone resorption by osteoclasts[1]. This is a highly regulated process requiring "coupling" of bone resorption and reformation, and perturbations in this balance lead to a loss in bone mineral density, a disease called osteoporosis, or in to dense bones, known as osteopetrosis[2]. Osteoclasts are large, multinucleated cells formed by the cytoplasmatic but not nuclear fusion of cells that differentiate from the macrophage/monocyte lineage[3]. Activated mature osteoclasts adhere to the bone surface and form tightly sealed compartments with the bone surface, called resorption pits, in which osteoclasts release lytic enzymes such as tartrate-resistant acid phosphatase (TRAP) and pro-cathepsinK (CATK) next to hydrogen ions to acidify the environment[4].

Osteoclastogenesis critically relies on two factors, *viz.* macrophage colony-stimulating factor (M-CSF) and receptor activator of nuclear factor kappa-B ligand (RANKL), which are sufficient to induce osteoclast differentiation *in vitro*[5]. Binding of RANKL to its receptor RANK, a member of the TNF superfamily expressed on the surface of osteoclast precursors, recruits TRAF6 which will induce the activation of several downstream signaling pathways leading to the activation of the transcription factors nuclear factor-κB (NF-κB) and activator protein-1 (AP-1)[6]. RANK signaling also induces the activation of nuclear factor-activated T cells c1 (NFATc1), the so called "master regulator of osteoclast differentiation" responsible for the expression of critical osteoclast genes coding for TRAP, cathepsin K and the calcitonin receptor (CalcR)[7].

The NF-κB family of transcription factors play critical roles in a wide variety of cellular processes of which inflammation is the best described. Several mechanisms are known to control NF-κB activation assuring a tight control of the inflammatory response. The anti-inflammatory protein A20 (also known as tumor necrosis factor alpha-induced protein 3, TNFAIP3) is one of the key molecules involved in the regulation of NF-κB signaling and inflammatory gene expression, and genetic deletion of A20 in mice leads to a lethal multi-organ inflammation, confirming the importance of A20 in the control of inflammatory responses[8]. Myeloid A20 deficiency in mice was shown to result in the spontaneous development of a severe destructive polyarthritis with many features of rheumatoid arthritis (RA) in humans[9], and single nucleotide polymorphisms in the human *TNFAIP3* locus were shown to be associated with increased susceptibility to RA[10,11]. Besides its role in inflammation, A20 may also regulate NF-κB signaling pathways controlling developmental processes. In this context, we previously identified A20 as a negative regulator of NF-κB signaling downstream of the Ectodysplasin A receptor (EDAR), a pathway important for the development of epidermal appendages such as skin, hair, nails, teeth, and sweat glands[12]. Since NF-κB is important for osteoclast differentiation, and NF-

κB inhibition blocks osteoclastogenesis[13], A20 may also play a regulatory role in the control of RANKL-induced NF-κB signaling and osteoclastogenesis. Cylindromatosis (CYLD), a deubiquitinating protein with functions similar to A20, was shown to negatively regulate RANK signaling and osteoclastogenesis[14], and CYLD deficient mice develop severe osteoporosis due to aberrant osteoclast formation and activation. CYLD was shown to negatively regulate RANK signaling by inhibiting TRAF6 ubiquitination and activation of downstream signaling events[14]. A20 may perform similar activities, since leukocyte cultures from myeloid-specific A20 deficient mice were shown to form many more TRAP-positive osteoclasts in presence of RANKL and M-CSF compared to wild-type leukocyte cultures, suggesting a role for A20 in the process of osteoclastogenesis[9]. However, the enhanced osteoclastogenesis in myeloid A20 knockout mice may also be the result of the more general inflammatory phenotype of these mice, since inflammatory cytokines such as TNF, IL-1β and IL-6 promote osteoclastogenesis [15,16].

For this study we generated transgenic mice with osteoclast-specific A20 deficiency, and show that these mice spontaneously develop severe osteoporosis with increased numbers of TRAP-positive osteoclasts. *In vitro,* bone marrow cells from osteoclast-specific A20 deficient mice produce more osteoclasts with increased expression of osteoclast specific markers upon incubation with M-CSF and RANKL, compared to control cells. Moreover, we show that A20 is upregulated under conditions of RANKL-induced osteoclastogenesis Together, these data identify A20 as a critical negative regulator of RANK-induced osteoclastogenesis and bone formation.

Results

Myeloid-specific A20 deficiency promotes osteoclastogenesis

Myeloid-specific A20 deficient ($A20^{myel\text{-}KO}$) mice spontaneously develop a severe destructive polyarthritis with many features of human RA[9]. This inflammatory phenotype was shown to be caused by the necroptosis of A20 deficient macrophages triggering inflammasome activation and IL-1β release, which induces MyD88-dependent signaling in synovial fibroblasts causing joint destruction and inflammation[17,18]. Myeloid A20 deficient mice also show an expansion of peripheral $CD^{115+}CD^{117+}$ osteoclast precursors, and blood leukocytes from these mice produce more and larger osteoclasts *in vitro* upon stimulation with RANKL and M-CSF than cells derived from wild type mice[9]. These findings suggest that A20 deficiency promotes osteoclastogenesis, a condition which may contribute to the severe bone degradation seen in these mice. We here confirmed these findings and demonstrate that stimulation of bone marrow-derived osteoclast precursor cells with RANKL and M-

CSF results in a significant increase in the number of tartrate-resistant acid phosphatase (TRAP) positive osteoclasts in A20 deficient conditions. These osteoclasts are also significantly larger and contain substantially more nuclei than osteoclasts derived from wild type progenitor cells (Fig. 1a). Next, we assessed the expression analysis of osteoclast specific markers in ankle joints isolated from $A20^{myel\text{-}KO}$ mice and control littermates, and demonstrate that their expression is significantly higher in $A20^{myel\text{-}KO}$ tissue compared to that of control wild-type mice (Fig. 1b). These data indeed suggest that increased osteoclast differentiation in the absence of A20 might contribute to the severe osteoporosis in myeloid A20 deficient mice. This phenotype may, however, also result from the more general inflammatory phenotype of $A20^{myel\text{-}KO}$ mice[9], since inflammatory cytokines such as TNF, IL-1β and IL-6 are known to promote osteoclastogenesis[15,16]. Indeed, incubation of bone marrow cultures with M-CSF and RANKL to induce osteoclastogenesis results in an increased expression of the inflammatory cytokines IL-1β and IL-6 in A20 deficient conditions at the later stages of osteoclastogenesis (Fig. 1c). Also, increased IL-6 levels can be detected in the supernatant of A20 deficient cultures after treatment with M-CSF and RANKL (Fig. 1d).

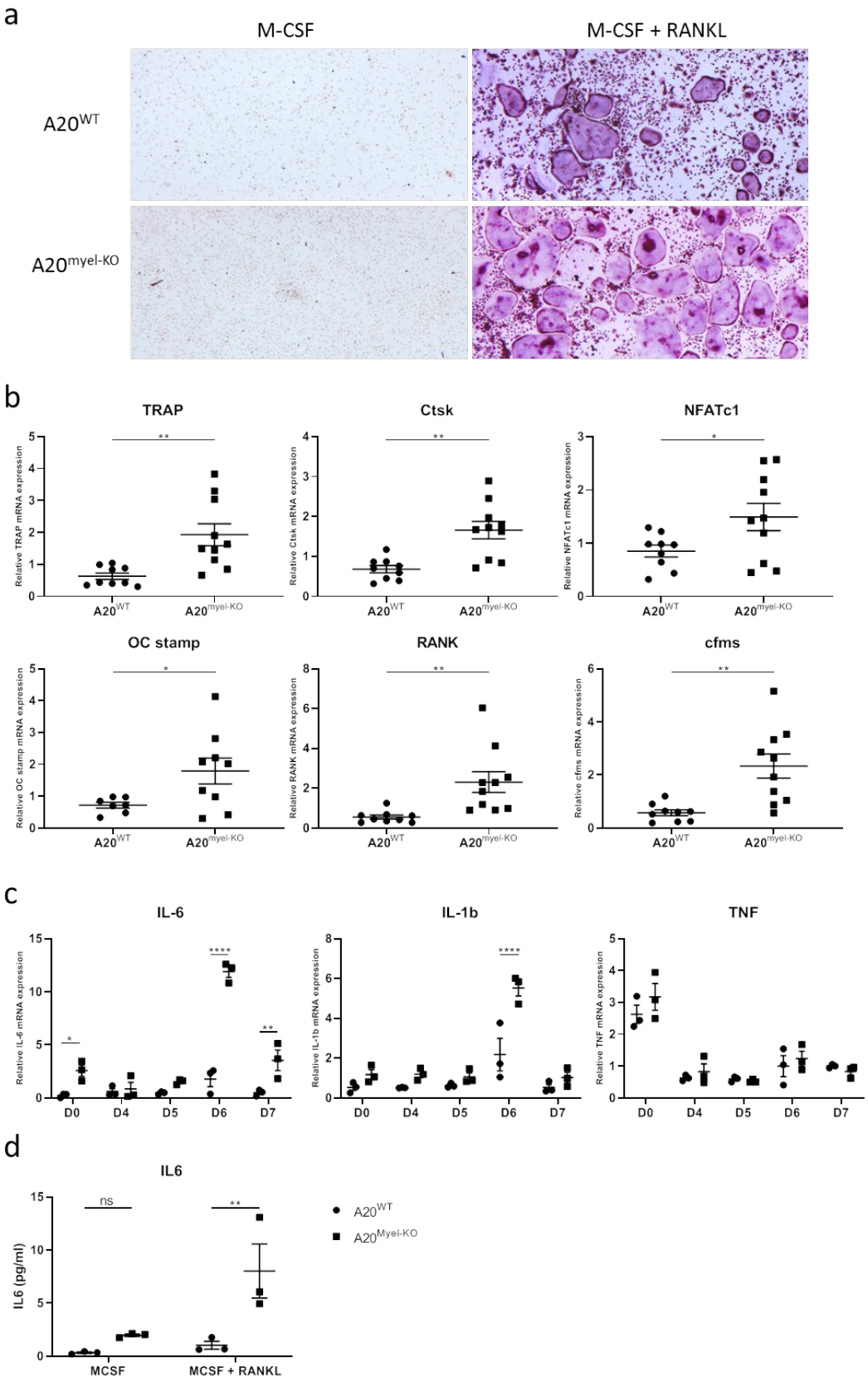

Fig. 1 Myeloid specific A20 deficiency results in increased osteoclastogenesis *in vivo* and upregulated inflammatory cytokine expression *in vitro*. (a) TRAP staining on osteoclast cultures

derived from bone marrow cells isolated from hind paws of wild-type (WT) and A20$^{myel\text{-}KO}$ mice and incubated for 7 days with M-CSF only or with M-CSF + RANKL. (b) qRT-PCR mRNA expression analysis of the indicated genes on RNA isolated from ankles of mice with the indicated genotypes (A20^{WT}, n=9; A20$^{myel\text{-}KO}$, n=10). Data are expressed as mean ± SEM. * and **represent p<0.05, p<0.01, respectively (parametric one-way ANOVA test between indicated genotypes). (c) qRT-PCR mRNA expression analysis of inflammatory cytokines on bone marrow cultures from A20^{WT} and A20$^{myel\text{-}KO}$ mice, incubated with M-CSF (25 ng/ml) and RANKL (100 ng/ml) for 7 days to induce osteoclastogenesis. (A20^{WT}, n=3; A20$^{myel\text{-}KO}$, n=3). Data are expressed as mean ± SEM. ****represents p<0.0001 respectively (Kruskal-Wallis one-way ANOVA test between indicated genotypes). (d) IL-6 levels in supernatant of bone marrow cultures from A20^{WT} and A20$^{myel\text{-}KO}$ mice, incubated with M-CSF (25 ng/ml) and RANKL (100 ng/ml) for 7 days to induce osteoclastogenesis. Data are expressed as mean ± SEM. ** represents p<0.01 (Two-way ANOVA test with Sidak's multiple comparisons between indicated genotypes for each timepoint).

Osteoclast-specific A20 deficient mice develop severe osteoporosis

To assess if A20 plays a direct regulatory role in RANK-induced NF-κB signaling and osteoclastogenesis, we generated transgenic mice with osteoclast-specific A20 deficiency by crossing the floxed A20 line with mice expressing Cre recombinase under control of the Cathepsin K promoter, which is selectively active in differentiated osteoclasts[19]. Osteoclast-specific A20 deficient (A20$^{OC\text{-}KO}$) mice develop normally and do not show signs of arthritis development as seen in A20$^{myel\text{-}KO}$ mice (data not show). Also, A20$^{OC\text{-}KO}$ mice do not have elevated levels of the inflammatory cytokine IL-6 in their serum in contrast to A20$^{myel\text{-}KO}$ mice (Fig. 2a). To investigate the consequence of osteoclast-specific A20 deletion for bone physiology, we next analyzed the structure, bone mass and bone density of both the femur and tibia of A20$^{OC\text{-}KO}$ and control littermate mice by microcomputed tomography (microCT) analysis. As shown in Fig. 2b and suppl. Fig. 1, A20$^{OC\text{-}KO}$ mice at the age of 27 weeks display severe loss of trabecular bone compared to wild-type mice. In agreement, the volume and density of trabecular bone is significantly reduced in A20$^{OC\text{-}KO}$ mice (Fig. 2c). However and in line with what is visually seen on microCT images, no significant differences between A20$^{OC\text{-}KO}$ and control mice could be observed for cortical bone parameters (Suppl. Fig. 2). Next we tested the strength of the femoral diaphysis by measuring ultimate load until failure (N) via a three-point bending test, representing the highest force the bone can withstand. A20$^{OC\text{-}KO}$ mice require significant less force (N) before they break, as could be expected based on the severe bone loss observed by microCT analysis (Fig. 2d). Finally, histological analysis of tibia of 20 week-old mice shows significantly more TRAP-positive osteoclasts in A20$^{OC\text{-}KO}$ mice compared to control littermates (Fig. 2e, f). Although old A20$^{OC\text{-}KO}$ mice (50 weeks of age) have reduced numbers of osteoclasts present in their tibia, they still have significantly more osteoclasts than wild-type controls of that age (Suppl. Fig. 3). Together, these data

indicate that A20 plays a direct role in regulating osteoclastogenesis *in vivo*, independent of its anti-inflammatory functions.

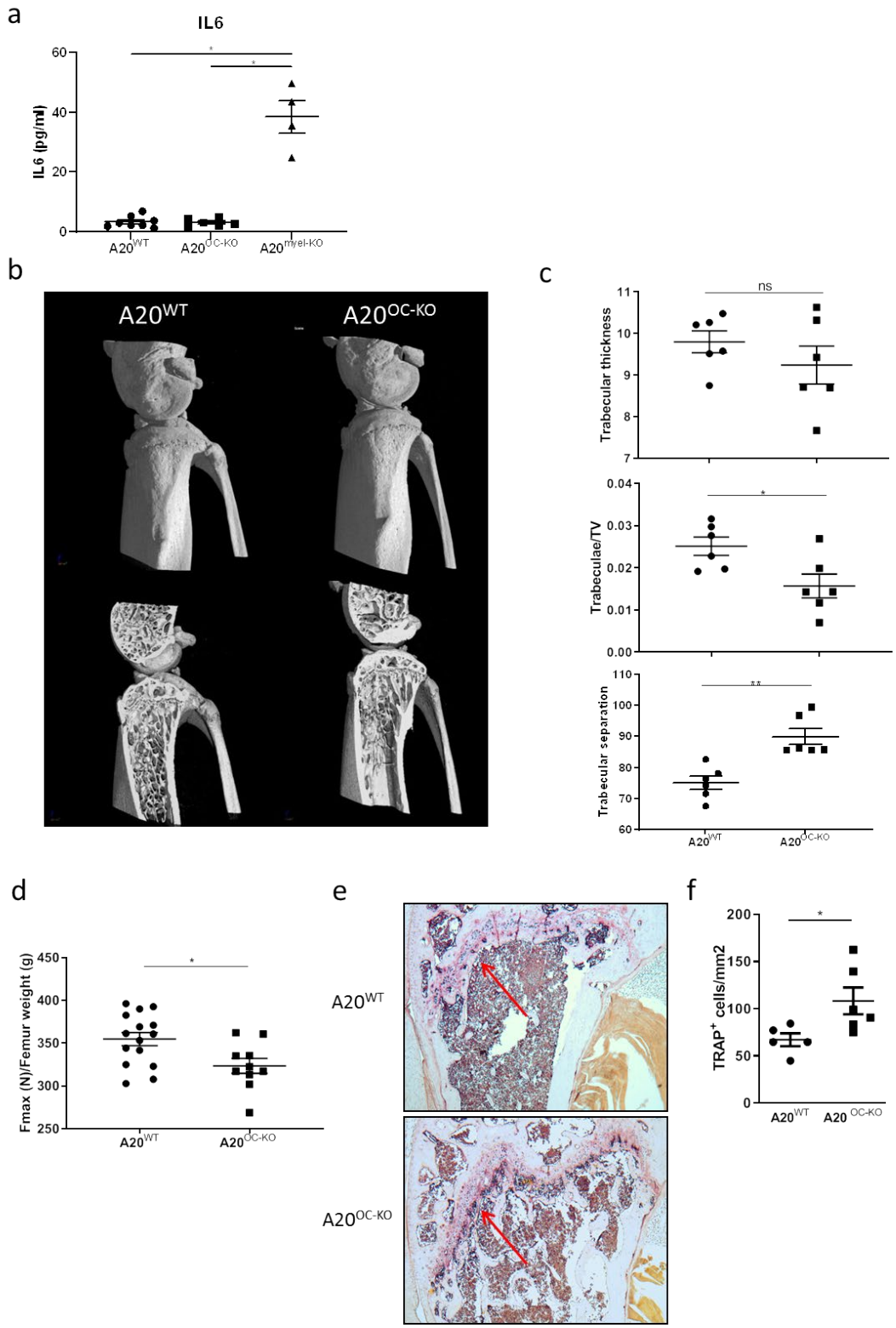

Fig. 2 Osteoclast-specific deletion of A20 in mice induces severe osteoporosis due to hyperactive osteoclastogenesis. (a) Levels of IL-6 in serum of $A20^{WT}$, $A20^{OC\text{-}KO}$ and $A20^{myel\text{-}KO}$ mice. Each dot represents an individual mouse ($A20^{WT}$, n=9; $A20^{OC\text{-}KO}$, n=6 and $A20^{myel\text{-}KO}$, n=4). Data are expressed as

mean ± SEM. * represents p<0.05 (parametric one-way ANOVA between indicated genotypes). (b) Representative micro-CT pictures of hind legs of 27 week-old control ($A20^{WT}$) and $A20^{OC-KO}$ littermates. Note the severe osteoporosis in $A20^{OC-KO}$ mice. (c) Trabecular parameters, calculated on micro-CT scans of hind legs of 27 week-old control ($A20^{WT}$) and $A20^{OC-KO}$ littermates. Each dot represents an individual mouse ($A20^{WT}$, n=6; $A20^{OC-KO}$, n=6). Data are expressed as mean ± SEM. *, ** represent p<0.05 and p<0.01, respectively (Non-parametric Mann Whitney test between indicated genotypes). (d) Functional femur strength was determined by the three-point bending test and is expressed as the maximum force (Fmax, Newton) bones can resist before breaking corrected for femur weight, with higher values mirroring stronger bones. Each dot represents an individual mouse ($A20^{WT}$, n=9; $A20^{OC-KO}$, n=6). Data are expressed as mean ± SEM. * represents p<0.05 (Non-parametric Mann Whitney test between indicated genotypes). (e) Representative pictures of TRAP-stained sections from tibia of 20 week-old $A20^{WT}$ and $A20^{OC-KO}$ mice. (f) Quantification of the number of TRAP-positive cells on sections from tibia of 20 week-old $A20^{WT}$ and $A20^{OC-KO}$ mice. . Each dot represents an individual mouse ($A20^{WT}$, n=6; $A20^{OC-KO}$, n=6). Data are expressed as mean ± SEM. * represents p<0.05 (Non-parametric Mann Whitney test between indicated genotypes).

A20 regulates RANK-induced NF-κB activation and osteoclastogenesis

Next we assessed the consequence of osteoclast-specific A20 deletion for RANK-induced osteoclastogenesis *in vitro*. Upon culturing of bone marrow-derived osteoclast precursor cells in the presence of M-CSF and RANKL, equal numbers of TRAP-positive multinucleated osteoclasts are observed in $A20^{OC-KO}$ and control cultures after 7 days of incubation (Fig. 3a). Also, at this timepoint, similar expression levels of osteoclast-specific markers are seen in both cultures. However, at day 4-5, a stronger expression of TRAP, Ctsk and NFATc1 is observed in $A20^{OC-KO}$ cultures compared to control cultures (Fig. 3b). Given that osteoclasts rapidly undergo apoptosis in the absence of sufficient amounts of growth factors and/or substrates *in vitro*, A20 deficiency possibly results in enhanced and earlier osteoclast formation (around day 5), which can no longer be detected at later time-points. Follow-up experiments should be performed at early stages of osteoclast differentiation to confirm the importance of A20 in the regulation of osteoclastogenesis.

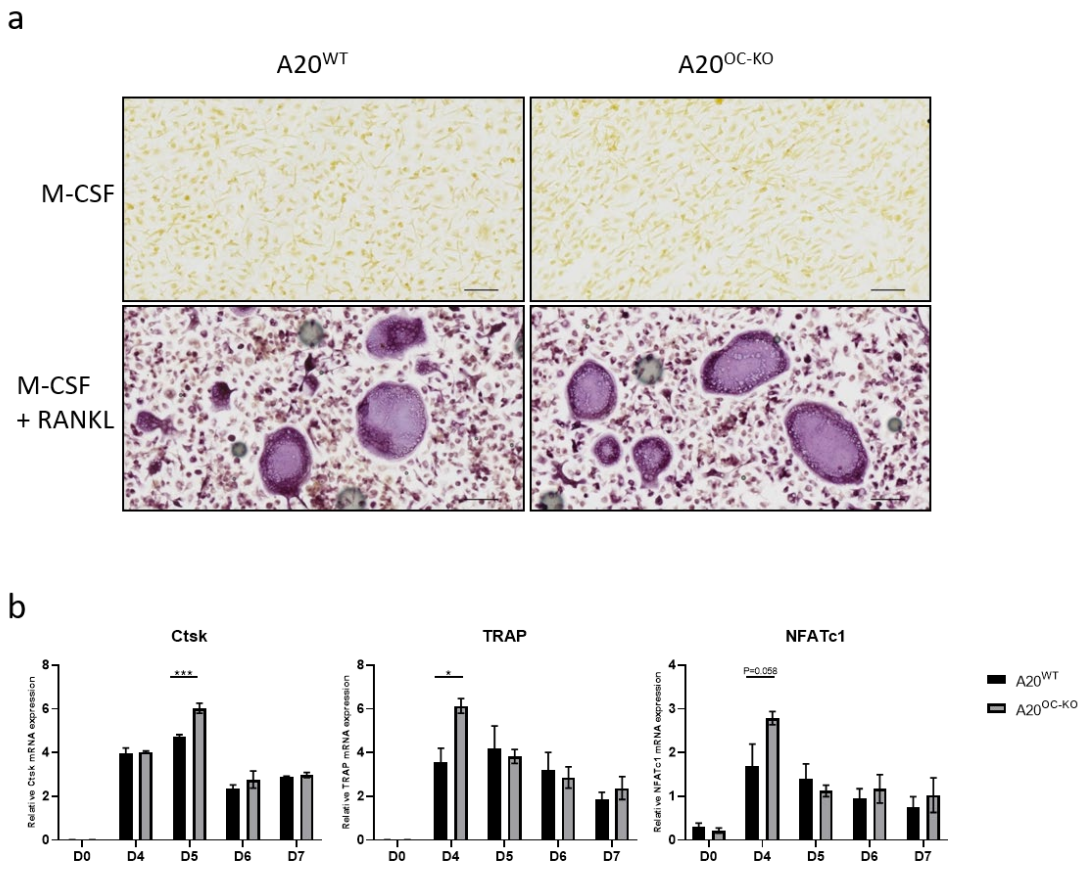

Fig. 3 Increased osteoclastogenesis in bone marrow cells from A20^{OC-KO} mice. (a) Bone marrow from A20^{WT} and A20^{OC-KO} mice was cultured on glass coverslips for 7 days in α-MEM medium supplemented with M-CSF (25 ng/ml) alone or with M-CSF and RANKL (100 ng/ml). On day 7, TRAP staining was performed. (b) qRT-PCR mRNA expression analysis on RNA isolated from bone marrow cultures incubated for the indicated time-points with M-CSF (25 ng/ml) and RANKL (100 ng/ml) (D0 represents a 7 day culture with M-CSF alone). Data are expressed as mean ± SEM. * and *** represent $p<0.05$, $p<0.001$ respectively (Two-way ANOVA test with Sidak's multiple comparisons between indicated genotypes for each time-point).

In most cell types, A20 expression levels are low at steady state, but are rapidly upregulated in inflammatory conditions as a result of NF-κB activation[20]. A20 expression is also low in unstimulated BMDMs, however becomes rapidly upregulated upon incubation with RANKL, indicating that A20 is an NF-kB response gene in the RANK pathway acting as a negative feedback regulator of RANK-induced NF-kB signaling (Fig. 4a, b). As the loss of A20 in osteoclasts results in enhanced osteoclastogenesis *in vitro*, we hypothesized that A20 might be a negative regulator of the RANK-induced NF-kB pathway. Indeed, by using an NF-κB-dependent luciferase reporter assay we demonstrated that A20 blocks RANK-induced activation of NF-kB in HEK293T cells (Fig. 4c). We next tested an A20 point mutant (A20 C103A), which is critically mutated in its N-terminal de-

ubiquitinating (DUB) activity, and could show that this A20 variant is as effective as wild-type A20 in inhibiting RANK-induced NF-kB activation, indicating that the A20 DUB activity is not required for this effect [21] (Fig. 4d). However, an A20 mutant affected in its zinc finger 7 (ZnF7) domain (C775A/C779A), which was previously shown to have high binding affinity for linear ubiquitin[22,23], showed slightly reduced NF-κB-inhibiting activity, while an A20 variant mutated in both its ZnF4 (C624A/C627A) and ZnF7 ubiquitin-binding domains completely lost its ability to suppress RANK-induced NF-κB signaling (Fig. 4d). These results indicate that A20 negatively regulates RANK-induced NF-κB activation via its ubiquitin-binding activity, at least in *in vitro* overexpression studies in HEK293T cells.

We next examined the effect of A20 deficiency on RANKL-stimulated NF-κB and MAP kinase signaling. A20 deficient BMDMs show slightly increased NF-κB signaling in response to RANKL, as shown by stronger and prolonged IκBα phosphorylation and degradation, than wild-type cells. Also increased phosphorylation of the MAP kinase p38 is observed in A20 deficient BMDMs, while no difference could be observed for phosphorylated JNK in response to RANKL (Fig. 4e). Next to canonical NF-κB signaling, RANK signaling is also known to induce the non-canonical NF-κB pathway which involves processing of the NF-κB2 precursor protein p100 to generate p52[24]. Interestingly, A20 deficient BMDMs have higher levels of p100, a non-canonical NF-κB response protein[25], in agreement with increased NF-κB activation in these cells. Moreover, increased processing of p100 to p52 could be observed in A20 deficient cells compared to wild-type cells upon treatment with RANKL, confirming increased activation of the non-canonical NF-κB pathway. Together these results indicate that A20 is directly involved in controlling signaling downstream of the RANK receptor driving the process of osteoclastogenesis.

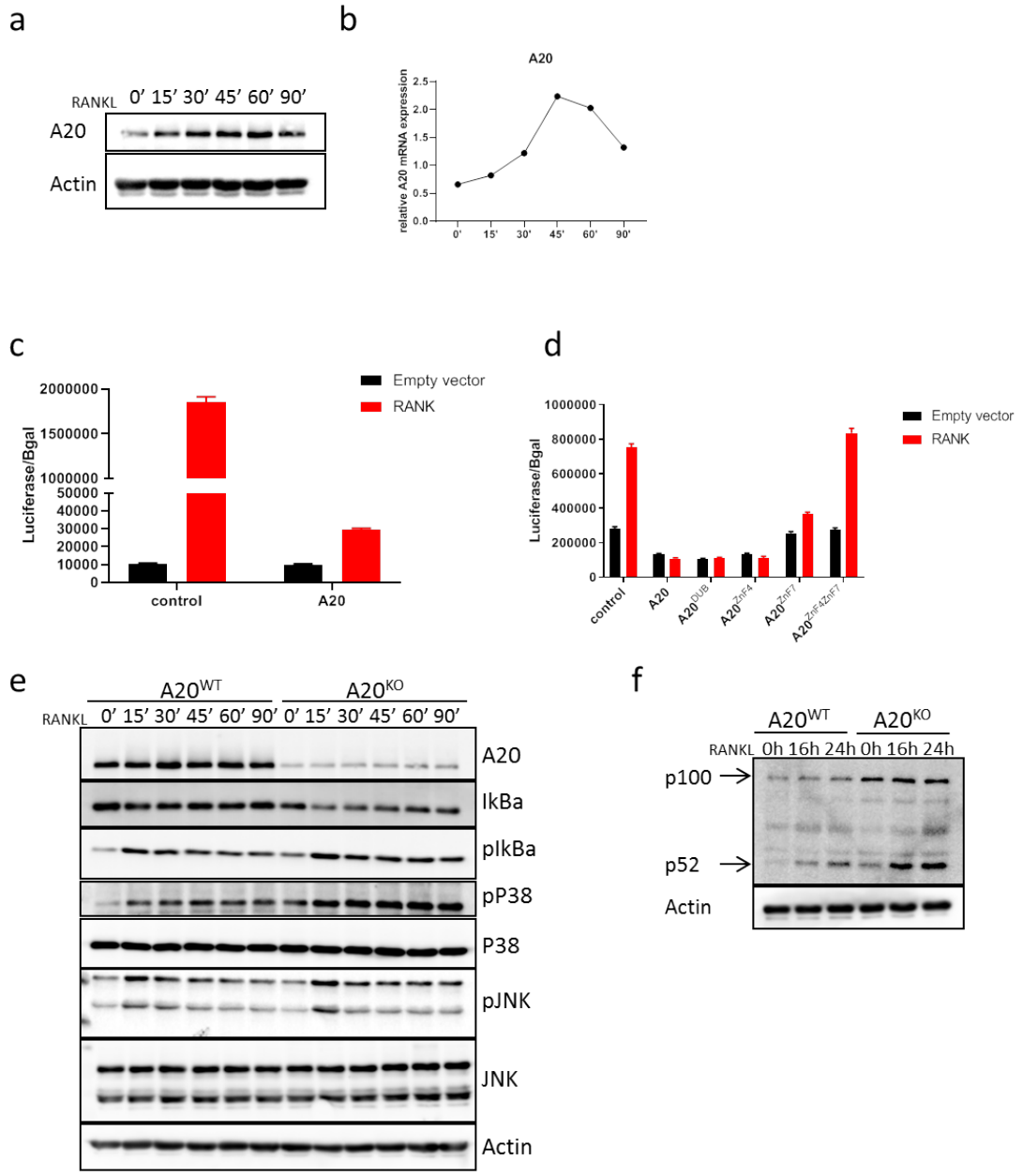

Fig. 4 A20 regulates RANK-induced NF-κB signalling. (a) Immunoblot analysis for A20 on wild-type BMDMs stimulated for the indicated time-points with RANKL (100 ng/ml). Actin was used as a loading control. (b) qRT-PCR mRNA expression analysis on RNA isolated from BMDM cultures isolated from control ($A20^{WT}$) mice incubated for the indicated time-points with RANKL (100 ng/ml). Data are representative of 2 independent experiments (c) Measurement of NF-kB luciferase activity in lysates of HEK293T cells transfected with combinations of an NF-κB luciferase reporter plasmid and plasmids encoding A20 and RANK. Data are expressed as the mean of technical triplicates ± SD. Results are representative of two independent experiments. (d) Inhibition of RANK-induced NF-kB luciferase activity by different A20 mutant variants. $A20^{DUB}$ (D100A - C103A), $A20^{ZF4}$ (C624A - C627A), $A20^{ZF7}$ (C775A - C779A), and $A20^{ZF4/ZF7}$ (C624A - C627A/C775A - C779A). Data are expressed as the mean of technical triplicates ± SD. Results are representative of two independent experiments. (e,f) Western blot analysis of whole cell lysates from BMDMs differentiated from $A20^{WT}$ and $A20^{myel\text{-}KO}$ mice, stimulated with RANKL (100 ng/ml) for the indicated time periods. Actin is shown as a loading control.

Discussion

Bone formation is a highly dynamic process involving bone-forming osteoblasts and bone-resorbing osteoclasts. Perturbations in the balance between both cell types will lead to either low bone density, a disease called osteoporosis, or to abnormally dense bones or osteopetrosis[2]. In this study we identified the NF-κB-inducible protein A20 as a negative feedback regulator of RANKL-induced osteoclastogenesis, independent of its anti-inflammatory functions. Osteoclast-specific A20 deletion in mice induces the development of severe osteoporosis, and increased numbers of $TRAP^+$ osteoclasts can be detected in bone tissue of A20 deficient mice, indicating that A20 acts as a critical regulator of osteoclastogenesis and bone homeostasis. Increased osteoclastogenesis is also observed *in vitro* at early stages of osteoclast differentiation, while these differences are no longer clear at later stages possibly due to osteoclast apoptosis in culture conditions. RANK stimulation of BMDMs induces the expression of A20, and absence of A20 in BMDMs enhances NF-κB signaling, demonstrating that A20 acts as a negative regulator of RANK-induced NF-κB signaling. The mechanism by which A20 regulates RANK-induced signaling is however not clear. Previous studies have shown that the deubiquitinating enzyme CYLD directly regulates RANK-induced NF-κB signaling by restricting TRAF6 ubiquitination[14]. Although A20 has also been described to act as a deubiquitinating enzyme which may affect the ubiquitination status of TRAF6 and possibly other targets[26], we have no evidence of such role in RANK-induced osteoclastogenesis *in vitro*. Although we could not demonstrate a role for the DUB activity of A20 in the inhibition of RANK signaling, we could demonstrate that expression of A20 variants mutated in their ability to bind ubiquitin chains via its ZnF4 and ZnF7 domains no longer suppress RANK-induced NF-κB signaling. This in agreement with recent reports that demonstrate that A20 function critically relies on its ubiquitin binding property to control inflammation *in vivo*[17]. However, these observations need to be validated in more physiological models, including mice with disruptive mutations in the A20 ZnF4 and ZnF7 domains, to clarify the mechanism by which A20 controls osteoclastogenesis *in vivo*.

Materials and Methods

Myeloid and Osteoclast-specific A20 knockout mice. Conditional A20/*tnfaip3* knockout mice, in which exons IV and V of the *tnfaip3* gene are flanked by two LoxP sites, were generated as described before[27]. A20 floxed mice were crossed with LysM-Cre[28] or CathepsinK-Cre transgenic mice[19] to generate a myeloid-specific ($A20^{myel\text{-}KO}$) or osteoclast-specific A20 knockout mouse ($A20^{OC\text{-}KO}$). All experiments were performed on mice of C57BL/6 genetic background. Mice were housed in individually ventilated cages at the VIB Center for Inflammation Research in a conventional animal facility. All experiments on mice were performed according to institutional, national and European animal regulations.

Isolation of bone marrow-derived macrophages. BMDMs were obtained from bone marrow cells flushed from mouse femurs and tibia with sterile RPMI medium, and cultured in RPMI 1640 supplemented with 40 ng/ml recombinant mouse M-CSF, 10% FCS, 1% penicillin/streptavidin and glutamine. Fresh M-CSF was added on day 3 and medium was refreshed on day 5. On day 7 cells were seeded and stimulated with 100 ng/ml RANKL (Peprotech) for the indicated timepoints.

Isolation of bone marrow-derived osteoclasts. Osteoclasts were obtained from bone marrow cells flushed from mouse femurs and tibia with sterile RPMI medium, and cultured overnight in αMEM medium (Gibco) containing 20% FCS in a petridish. The next day, the cells were seeded on glass coverslips in αMEM medium containing 20% FCS, 25 ng/ml M-CSF and 100 ng/ml RANKL (Peprotech). Medium was refreshed on day 5 ,and on day 7 cells were stained or processed for further analysis.

***In vitro* TRAP staining.** Osteoclasts were obtained as described above. TRAP staining was performed according to the manufacturers instruction (Sigma-Aldrich). Staining solutions were freshly prepared before use. Bright-field microscopy was done using an Axio Scan.Z1 (Zeiss, Germany). $TRAP^{+}$ multinucleated cells with three or more nuclei were defined as osteoclasts.

TRAP Histology. Formalin-fixed, EDTA-decalcified, paraffin-embedded mouse tissue specimens were sectioned and stained with haematoxylin and eosin and TRAP [Leukocyte Acid Phosphatase Kit; Sigma-Aldrich], and TRAP-positive cells were quantified.

Bone microCT analysis. All samples were scanned at the Centre for X-Ray tomography of the Ghent University (UGCT, www.ugct.ugent.be). Optimal scanner settings were selected based on the sample size and composition. The samples were scanned on HECTOR[29] using a directional X-ray source set at 130kV and 10 Watt beam power with a 1 mm Aluminum filtration, with a detector (Perkin-Elmer) measuring 40 x 40 cm and a pixel pitch of 200 µm. A total of 2000 projections of 1 sec exposure time

each was recorded. Resulting scan images had a voxel size of 4 µm. Projection images were reconstructed using Octopus Software for quantification of X-ray microtomography[30], and 3D visualisations were made using the commercial rendering software VGStudioMAX (Volume Graphics). Analysis of bone morphology was performed using a custom script in ImageJ. A tibial region of interest (ROI) with a length of 1200 µm was manually defined, starting 200 µm below the growth plate. The bone structures within this ROI were then automatically classified using an algorithm similar to that of Buie et al[31]. For quantification purposes, we measured both the average thickness of these structures (using the Thickness plugin from BoneJ and their entire volume (determined by the number of voxels). The trabecular spacing measure is the average thickness of the non-bone volume between the trabeculae.

Mechanical testing. On the day of sacrifice, mouse femurs were collected, cleaned from soft tissue, wrapped in saline moistened gauze, and frozen at −20°C for later *ex vivo* biomechanical measurements. The strength of the femoral diaphysis was determined by a three-point bending test on a Lloyd Instruments universal testing machine (LRXplus, Lloyd Instruments, Fareham, UK), after rehydration in a saline solution at room temperature. For this, a loading point is applied on the mid-diaphysis of the femur and is moved downwards with increasing force and displacement. The maximum force (Newton) reflects the load applied right before the femur fractures.

Quantitative real-time PCR. Total RNA was isolated using TRIzol reagent (Invitrogen) and Aurum Total RNA Isolation Mini Kit (Biorad), according to manufacturer's instructions. Synthesis of cDNA was performed using SensiFAST™ cDNA Synthesis Kiy according to the manufacturer's instructions. cDNA was amplified for quantitative PCR in a total volume of 5 µl with SensiFAST SYBR® No-ROX Kit (Bioline) and specific primers on a LightCycler 480 (Roche). The reactions were performed in triplicates. The following mouse-specific primers were used: A20 fwd AAACCAATGGTGATGGAAACTG; A20 rev GTTGTCCCATTCGTCATTCC; OC-Stamp fwd TGGGCCTCCATATGACCTCGAGTAG; OC-Stamp rev TCAAAGGCTTGTAAATTGGAGGAGT; TRAP fwd TGGTCCAGGAGCTTAACTGC; TRAP rev GTCAGGAGTGGGAGCCATATG; Ctsk fwd AGGCATTGACTCTGAAGATGCT; Ctsk rev TCCCCACAGGAATCTCTCTG; RANK fwd ATGAGTACACGGACCGGCC; RANK rev GCTGGATTAGGAGCAGTGAACC; NFATc1 fwd AGGCTGGTCTTCCGAGTTCA; NFATc1 rev ACCGCTGGGAACACTCGAT; HPRT fwd AGTGTTGGATACAGGCCAGAC; HPRT rev CGTGATTCAAATCCCTGAAGT; cFms fwd TGGCATCTGGCTTAAGGTGAA; cFms rev GAATCCGCACCAGCTTGCTA; IL-6 fwd GAGGATACCACTCCCAACAGACC; IL-6 rev AAGTGCATCATCGTTGTTCATACA; IL-1β fwd TGGGCCTCAAAGGAAAGA IL-1β rev

GGTGCTGATGTACCAGTT TNF fwd ACCCTGGTATGAGCCCATATAC; TNF rev ACACCCATTCCCTTCACAGAG

Cytokine detection. Cytokine levels in culture medium were determined by magnetic bead-based multiplex assay using Luminex technology (Bio-Rad), according to the manufacturers' instructions.

Western blotting. Cells were lysed directly in 2 x Laemlli and boiled for 5 min. Lysates were separated by SDS polyacrylamide gel electrophoresis, transferred to nitrocellulose membranes with a semi-dry blot system (Invitrogen), and immunoblotted with anti-IκBα (Santa Cruz Biotechnology, Inc., sc-371), anti-phospho-IκBα (Cell Signaling, CST9246), anti-A20 (Santa Cruz Biotechnology, Inc., sc-166692), anti-p38 (cell signaling, CST9212), anti-phospho-p38 (cell signaling, CST9215), anti-SAPK/JNK (cell signaling, CST9252), anti-phospho-SAPK/JNK (cell signaling, CST4668), anti-NF-kB2 p100/p52 (cell signaling, CST4882), and anti-β-actin (Santa Cruz Biotechnology, Inc., sc-47778) antibodies.

NF-κB-dependent reporter assays. HEK293T cells were seeded at 2×10^5 cells/well in 6-well plates. Cells were transiently transfected the next day by DNA calcium phosphate coprecipitation. Each transfection contained 100 ng of pNFconluc, 100 ng pactβgal and 100 ng of a specific A20 expression plasmid. The total amount of DNA per well was kept constant at 1 µg by adding empty pCAGGS vector. After 24 h, cells were lysed in luciferase lysis buffer (25mM Tris phosphate pH 7,8; 2 mM DTT; 2 mM CDTA(1,2 diaminocyclohexane-N.N.N.N-tetraacetic acid); 10 % glycerol; 1 % Triton X-100). Substrate buffer was added (658 mM luciferin, 378 mM coenzyme A and 742 mM ATP) and Luciferase activity (Luc) was assayed in a GloMax 96 Microplate Luminometer (Promega). B-Galactosidase (Gal) activity in cell extracts was assayed with chlorophenol-red β-D-galactopyranoside substrate (Roche Applied Science, Basel, Switzerland) and the optical density was read at 595 nm in a Benchmark microplate Reader (Bio-Rad Laboratories, Nazareth, Belgium). Luc values were normalized for Gal values to correct for differences in transfection efficiency (plotted as Luc/Gal). The data represent the average ± S.D. of technical triplicates.

Statistics. GraphPad Prism V8 software was used for statistical analysis. Results are expressed as the mean ± SEM or mean ± SD, as indicated in figure legend. Statistical significance between experimental groups was assessed using a nonparametric Mann–Whitney U-statistical test. Statistical significance between multiple groups was assessed using either one- or two-way ANOVA with Tukey correction for multiple comparison.

Acknowledgments

A. Martens is supported by a grant from the “Concerted Research Actions” (GOA) of the Ghent University. Research in the G. van Loo lab is supported by research grants from the FWO, the “Geneeskundige Stichting Koningin Elisabeth” (GSKE), the CBC Banque Prize, the Charcot Foundation, the “Belgian Foundation against Cancer”, “Kom op tegen Kanker”, and the GOA of the Ghent University. M.A. lab is supported by a startup grant from the Stavros Niarchos Foundation donation to BSRC “Al. Fleming.

Competing interests statement

The authors declare no competing financial interests.

References

1 Chang, J. *et al.* Inhibition of osteoblastic bone formation by nuclear factor-kappaB. *Nat Med* **15**, 682-689, doi:10.1038/nm.1954 (2009).

2 Wada, T., Nakashima, T., Hiroshi, N. & Penninger, J. M. RANKL-RANK signaling in osteoclastogenesis and bone disease. *Trends Mol Med* **12**, 17-25, doi:10.1016/j.molmed.2005.11.007 (2006).

3 Itzstein, C., Coxon, F. P. & Rogers, M. J. The regulation of osteoclast function and bone resorption by small GTPases. *Small GTPases* **2**, 117-130, doi:10.4161/sgtp.2.3.16453 (2011).

4 Boyle, W. J., Simonet, W. S. & Lacey, D. L. Osteoclast differentiation and activation. *Nature* **423**, 337-342, doi:10.1038/nature01658 (2003).

5 Quinn, J. M., Elliott, J., Gillespie, M. T. & Martin, T. J. A combination of osteoclast differentiation factor and macrophage-colony stimulating factor is sufficient for both human and mouse osteoclast formation in vitro. *Endocrinology* **139**, 4424-4427, doi:10.1210/endo.139.10.6331 (1998).

6 Asagiri, M. & Takayanagi, H. The molecular understanding of osteoclast differentiation. *Bone* **40**, 251-264, doi:10.1016/j.bone.2006.09.023 (2007).

7 Takayanagi, H. *et al.* Induction and activation of the transcription factor NFATc1 (NFAT2) integrate RANKL signaling in terminal differentiation of osteoclasts. *Dev Cell* **3**, 889-901 (2002).

8 Lee, E. G. *et al.* Failure to regulate TNF-induced NF-kappaB and cell death responses in A20-deficient mice. *Science* **289**, 2350-2354, doi:10.1126/science.289.5488.2350 (2000).

9 Matmati, M. *et al.* A20 (TNFAIP3) deficiency in myeloid cells triggers erosive polyarthritis resembling rheumatoid arthritis. *Nat Genet* **43**, 908-912, doi:10.1038/ng.874 (2011).

10 Plenge, R. M. *et al.* Two independent alleles at 6q23 associated with risk of rheumatoid arthritis. *Nat Genet* **39**, 1477-1482, doi:10.1038/ng.2007.27 (2007).

11 Thomson, W. *et al.* Rheumatoid arthritis association at 6q23. *Nat Genet* **39**, 1431-1433, doi:10.1038/ng.2007.32 (2007).

12 Lippens, S. *et al.* Keratinocyte-specific ablation of the NF-kappaB regulatory protein A20 (TNFAIP3) reveals a role in the control of epidermal homeostasis. *Cell Death Differ* **18**, 1845-1853, doi:10.1038/cdd.2011.55 (2011).

13 Novack, D. V. Role of NF-kappaB in the skeleton. *Cell Res* **21**, 169-182, doi:10.1038/cr.2010.159 (2011).

14 Jin, W. *et al.* Deubiquitinating enzyme CYLD negatively regulates RANK signaling and osteoclastogenesis in mice. *J Clin Invest* **118**, 1858-1866, doi:10.1172/JCI34257 (2008).

15 Lam, J. *et al.* TNF-alpha induces osteoclastogenesis by direct stimulation of macrophages exposed to permissive levels of RANK ligand. *J Clin Invest* **106**, 1481-1488, doi:10.1172/JCI11176 (2000).

16 Dai, J. *et al.* Chronic alcohol ingestion induces osteoclastogenesis and bone loss through IL-6 in mice. *J Clin Invest* **106**, 887-895, doi:10.1172/JCI10483 (2000).

17 Polykratis, A. *et al.* A20 prevents inflammasome-dependent arthritis by inhibiting macrophage necroptosis through its ZnF7 ubiquitin-binding domain. *Nat Cell Biol* **21**, 731-742, doi:10.1038/s41556-019-0324-3 (2019).

18 Vande Walle, L. *et al.* Negative regulation of the NLRP3 inflammasome by A20 protects against arthritis. *Nature* **512**, 69-73, doi:10.1038/nature13322 (2014).

19 Chiu, W. S. *et al.* Transgenic mice that express Cre recombinase in osteoclasts. *Genesis* **39**, 178-185, doi:10.1002/gene.20041 (2004).

20 Krikos, A., Laherty, C. D. & Dixit, V. M. Transcriptional activation of the tumor necrosis factor alpha-inducible zinc finger protein, A20, is mediated by kappa B elements. *J Biol Chem* **267**, 17971-17976 (1992).

21 Wertz, I. E. *et al.* De-ubiquitination and ubiquitin ligase domains of A20 downregulate NF-kappaB signalling. *Nature* **430**, 694-699, doi:10.1038/nature02794 (2004).
22 Verhelst, K. *et al.* A20 inhibits LUBAC-mediated NF-kappaB activation by binding linear polyubiquitin chains via its zinc finger 7. *EMBO J* **31**, 3845-3855, doi:10.1038/emboj.2012.240 (2012).
23 Tokunaga, F. *et al.* Specific recognition of linear polyubiquitin by A20 zinc finger 7 is involved in NF-kappaB regulation. *EMBO J* **31**, 3856-3870, doi:10.1038/emboj.2012.241 (2012).
24 Sun, S. C. The non-canonical NF-kappaB pathway in immunity and inflammation. *Nat Rev Immunol* **17**, 545-558, doi:10.1038/nri.2017.52 (2017).
25 Lombardi, L. *et al.* Structural and functional characterization of the promoter regions of the NFKB2 gene. *Nucleic Acids Res* **23**, 2328-2336, doi:10.1093/nar/23.12.2328 (1995).
26 Boone, D. L. *et al.* The ubiquitin-modifying enzyme A20 is required for termination of Toll-like receptor responses. *Nat Immunol* **5**, 1052-1060, doi:10.1038/ni1110 (2004).
27 Vereecke, L. *et al.* Enterocyte-specific A20 deficiency sensitizes to tumor necrosis factor-induced toxicity and experimental colitis. *J Exp Med* **207**, 1513-1523, doi:10.1084/jem.20092474 (2010).
28 Clausen, B. E., Burkhardt, C., Reith, W., Renkawitz, R. & Forster, I. Conditional gene targeting in macrophages and granulocytes using LysMcre mice. *Transgenic Res* **8**, 265-277 (1999).
29 Masschaele, B. *et al.* HECTOR: A 240kV micro-CT setup optimized for research. *Journal of Physics: Conference Series* **463**, 012012 (2013).
30 Vlassenbroeck, J. *et al.* Nuclear Instruments and Methods in Physics Research. **580**, 442-445 (2007).
31 Buie, H. R., Campbell, G. M., Klinck, R. J., MacNeil, J. A. & Boyd, S. K. Automatic segmentation of cortical and trabecular compartments based on a dual threshold technique for in vivo micro-CT bone analysis. *Bone* **41**, 505-515, doi:10.1016/j.bone.2007.07.007 (2007).

Supplementary figures

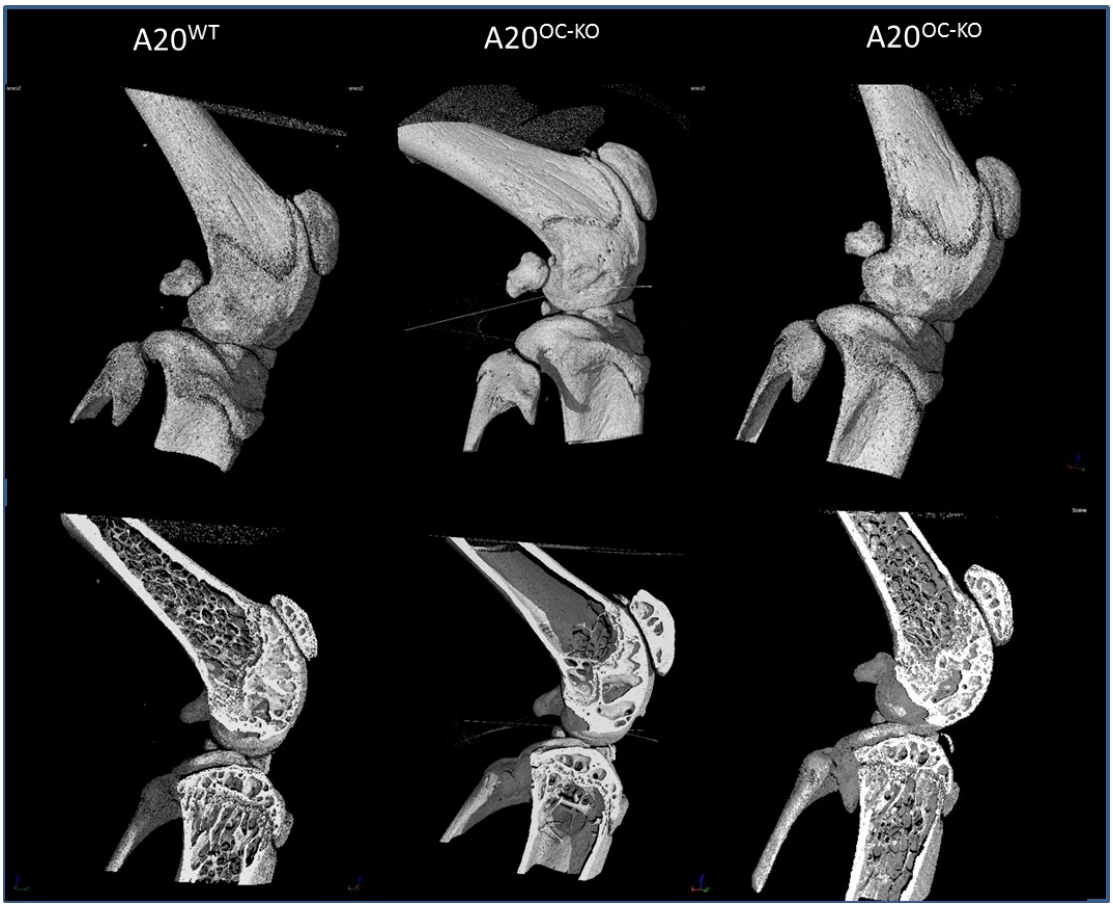

Suppl. Fig. 1 Osteoclast specific A20 deficient mice develop severe osteoporosis. Representative micro-CT pictures of hind legs of control ($A20^{WT}$) and $A20^{OC-KO}$ littermates at the age between 16 and 27 weeks old. Note the severe osteoporosis in $A20^{OC-KO}$ mice.

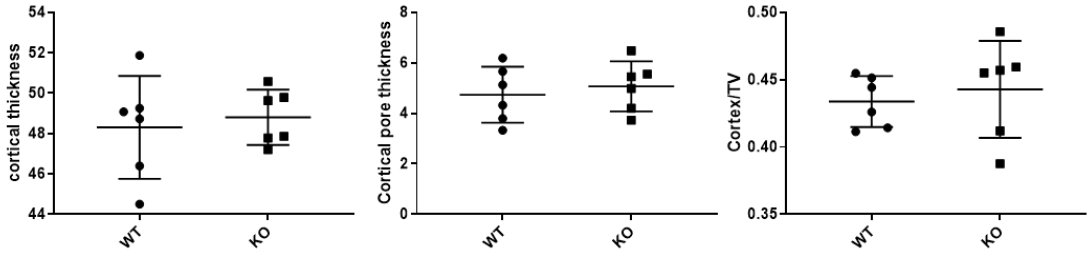

Suppl. Fig. 2 Osteoclast specific A20 deficiency does not affect cortical bone. Cortical bone parameters, calculated on micro-CT scans of hind legs of 27 week-old control ($A20^{WT}$) and $A20^{OC-KO}$ littermates. Each dot represents an individual mouse ($A20^{WT}$, n=6; $A20^{OC-KO}$, n=6). Data are expressed as mean ± SEM (Non-parametric Mann Whitney test between indicated genotypes).

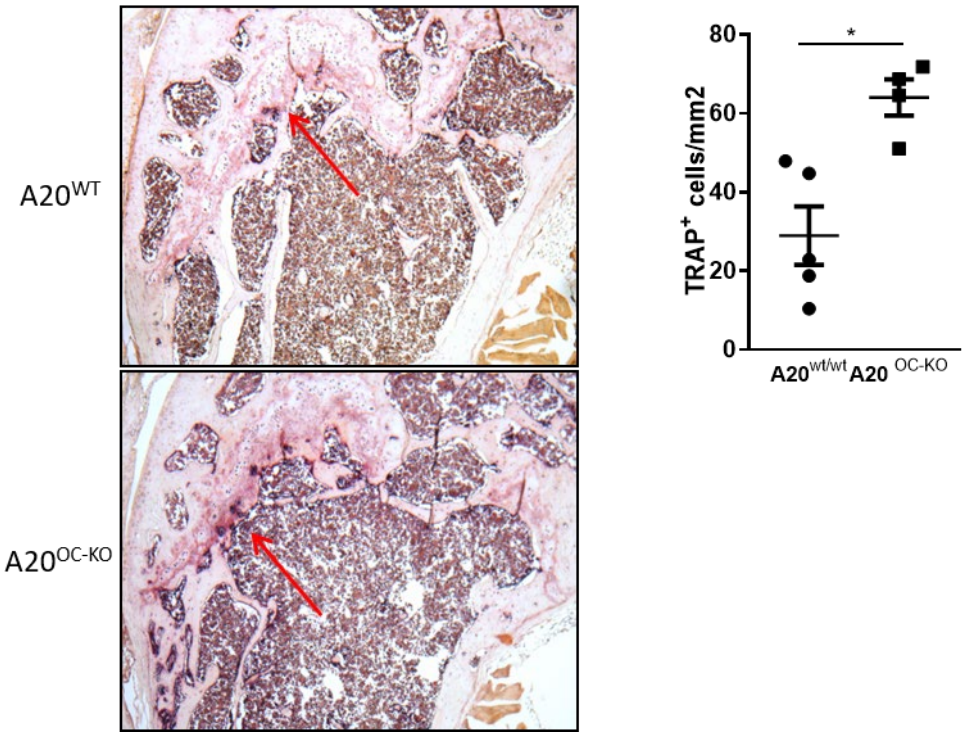

Suppl. Fig. 3 50-week old A20^{OC-KO} mice still show increased numbers of osteoclasts. (a) Representative pictures of TRAP-stained sections from tibia of 50 week-old A20^{WT} and A20^{OC-KO} mice. (b) Quantification of the number of TRAP-positive cells on sections from tibia of 50 week-old A20^{WT} and A20^{OC-KO} mice. Each dot represents an individual mouse (A20^{WT}, n=5; A20^{OC-KO}, n=4). Data are expressed as mean ± SEM. * represents $p<0.05$ (Non-parametric Mann Whitney test between indicated genotypes).

Part IV
General conclusion, discussion and future perspectives

General conclusions, discussion and future perspectives

The protein A20 is best known for its role as a negative regulator of pro-inflammatory NF-κB signaling and cell death, and several genome wide association studies (GWAS) have identified *A20/TNFAIP3* as a disease susceptibility gene for numerous inflammatory and autoimmune diseases[1]. Next to its role in the control of NF-κB-dependent inflammation, A20 might also be involved in regulating NF-κB signaling pathways controlling developmental processes. Initially, A20 was characterized as a ubiquitin-editing enzyme modifying the ubiquitination status of specific signaling proteins via its deubiquitinating (DUB) activity (OTU domain) and E3 ligase activity (ZnF4 domain)[2]. However, mice with a disruptive point mutation abolishing either the DUB or the E3 ligase activity do not develop spontaneous inflammatory disease as seen in A20 knockout mice, questioning the importance of these catalytic functions of A20 *in vivo*[3-5]. A20 has also been identified as a ubiquitin-binding protein which has strong binding affinity for both K63-specific ubiquitin chains via its ZnF4 domain and for linear (M1) ubiquitin chains via its ZnF7 domain. *In vitro* studies have also shown that A20's ZnF7 domain is critical for limiting NF-κB signaling and preventing cell death[6-9]. To further investigate the mechanisms by which A20 regulates inflammation and cell death *in vivo* and to examine the role of A20's ubiquitin binding functions, we have generated mice with disruptive mutations in the ZnF7 domain as well as in both the ZnF4 and ZnF7 domains. These mice were analyzed for spontaneous pathologies as well as in established models of inflammatory stress. In a second study, and based on earlier observations regarding the phenotype of myeloid A20 knockout mice[10], we investigated the role of A20 in bone development. For this we generated osteoclast-specific A20 deficient mice ($A20^{OC\text{-}KO}$) to investigate A20's role in RANK signaling and osteoclastogenesis.

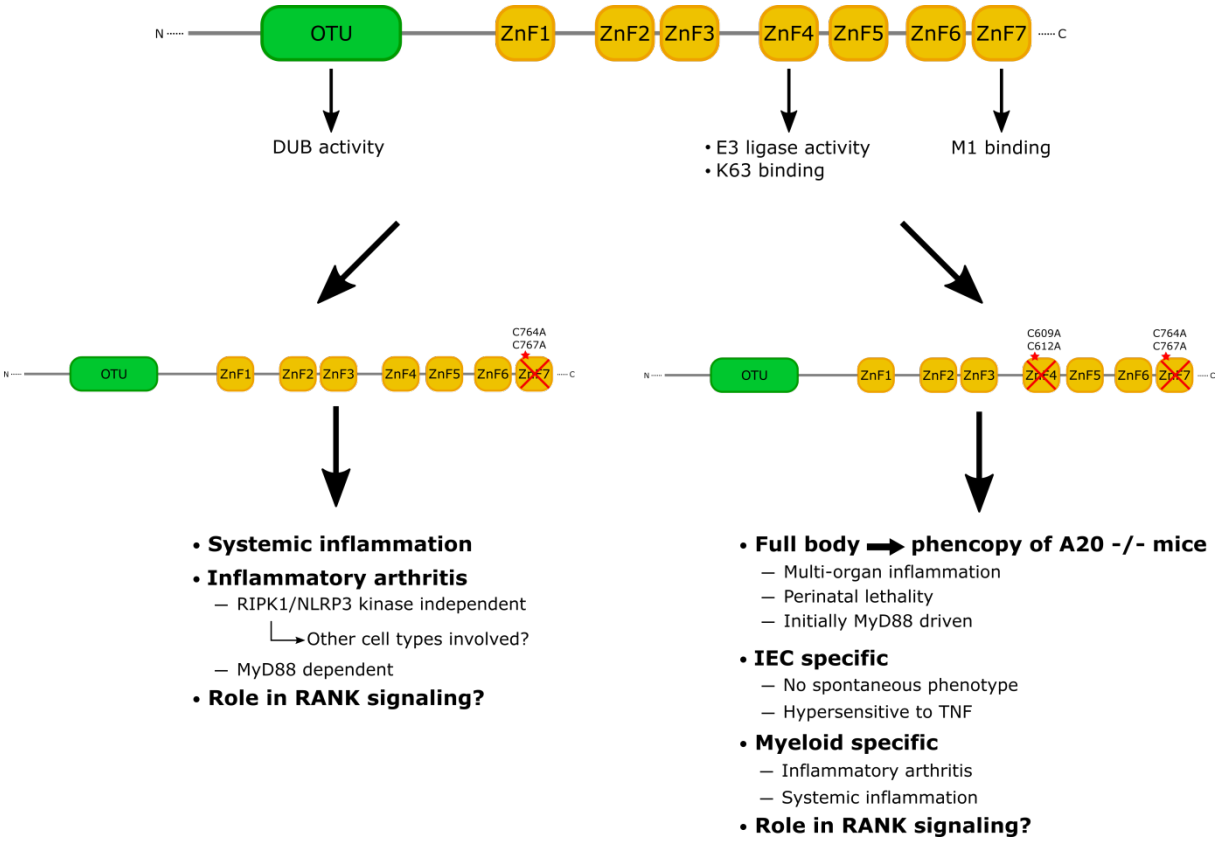

Fig. 1 Summary of the findings. Domain structure of the A20 protein. The N-terminus of A20 contains an ovarian tumor (OTU) domain, which has deubiquitinating (DUB) activity. The C-terminal part of A20 contains 7 zinc finger (ZnF) domains. The 4th ZnF domain has K63-linked polyubiquitin binding affinity and possesses E3 ubiquitin ligase activity, while the 7th ZnF domain has strong binding affinity for linear (M1) ubiquitin chains. Mice were generated with disruptive mutations in the ZnF7 domain abolishing M1 binding, or in both the ZnF4 and ZnF7 domains abolishing K63- and M1-Ub binding, and mice were analyzed for the presence of inflammatory pathology.

Two distinct ubiquitin-binding motifs in A20 mediate its anti-inflammatory and cell- protective activities

We have shown that the 7th ZnF domain of A20 is critical for controlling inflammatory responses *in vivo*. Mice with a disruptive mutation in the ZnF7 domain (A20^{ZnF7} mice) spontaneously develop mild systemic inflammation characterized by splenomegaly and lymphadenopathy, high levels of circulating inflammatory cytokines, increased inflammatory cell infiltration in liver, and increased levels of monocytes, macrophages and neutrophils in blood and spleen. Consistent with the essential role of A20 as a negative feedback regulator of inducible NF-κB–dependent gene expression, MEF cells and BMDMs stimulated with TNF or LPS, respectively, show increased inflammatory signaling and release of inflammatory cytokines in A20^{ZnF7} cells. Since binding of NEMO to linear ubiquitin chains is critical for NF-κB activation, A20 might compete with NEMO for binding to M1 chains,

thereby preventing downstream NF-κB activation[11]. However, if increased inflammatory signaling is a direct effect of A20 deficiency on NF-κB signaling or a secondary response to aberrant cell death induction still remains elusive. A20 deficiency enhances pro-inflammatory and pro-survival signaling, however also sensitizes cells to TNF induced cell death[12-15]. Myeloid-specific A20 deficient ($A20^{myel\text{-}KO}$) mice develop systemic inflammation, splenomegaly and polyarthritis, which is not rescued by myeloid-specific IKK2/IKKβ deficiency[16]. This argues against a direct effect of A20 deficiency on NF-κB activation and suggests that an NF-κB-independent function of A20 in myeloid cells is critical for preventing inflammation *in vivo*. Furthermore, the 7th ZnF domain of A20 was shown to suppress TNF induced apoptosis[17].

Previous research using conditional A20-knockout mice has demonstrated that apoptosis of A20-deficient cells, as shown for intestinal epithelial cells and liver parenchymal cells, could contribute to the systemic inflammation seen in A20 deficient mice[14,18]. Significant numbers of cleaved caspase 3-positive cells could be detected in livers of $A20^{ZnF7}$ mice. Moreover, we showed that $A20^{ZnF7}$ mice are hypersensitive to TNF-induced lethality due to the TNF-induced apoptosis of the intestinal epithelium. Mechanistically, in BMDMs we could show that the ZnF7 mutation in A20 prevents the recruitment of A20 to the TNFR1 complex, confirming earlier findings in cell lines[7,9]. Previous studies had suggested that A20 binds M1 chains via its ZnF7 domain, thereby protecting these chains from CYLD-mediated degradation[9]. Indeed, reduced recruitment of $A20^{ZnF7}$ to TNFR1 leads to a strong reduction in linear ubiquitin chains present at the complex, while increased ubiquitination on RIPK1 (most likely K63 chains) could be observed. Since linear ubiquitin chains are known to stabilize complex 1 and prevent cell death induction[19-21], reduced levels of M1 chains results in the formation of complex 2 and cell death as seen in TNF-stimulated MEF cell cultures isolated from $A20^{ZnF7}$ mice, which we showed to be sensitized to TNF-induced apoptosis, similar to what was described for $A20^{-/-}$ MEFs[12]. M1 ubiquitin pulldown assays should be performed to identify the targets in the TNFR1 complex that show a reduction in linear ubiquitination in absence of a functional ZnF7 domain, compared to the WT situation. In cell lines, CYLD deficiency was shown to result in increased levels of M1 and K63 on RIPK1, TNFR1 and TRADD, while A20 deficiency was shown to result in reduced M1 ubiquitination of TNFR1[9]. Since TNF is a potent inducer of cell death in A20 deficient conditions[22], and $A20^{ZnF7}$ mice have high levels of TNF in their serum, TNF might be an important mediator of the inflammatory phenotype of $A20^{ZnF7}$ mice. In this context, recent studies have identified inflammation as a consequence of aberrant TNF-induced cell death in models of inflammatory pathology[23]. To clarify if TNF drives the inflammatory phenotype of $A20^{ZnF7}$ mice, $A20^{ZnF7}$ mice are being crossed with TNFR1 and TNF knockout mice. However, A20 is also critically involved in regulating TNF-independent signaling, such as in signaling downstream of TLRs and NLRs, and the backcross of A20 deficient mice

($A20^{-/-}$) in a TNFR1 or TNF knockout background could not rescue these mice from the severe inflammatory pathology and perinatal lethality[24,25].

MyD88 deficiency or treatment with broad spectrum antibiotics was shown to rescue the perinatal lethal phenotype of $A20^{-/-}$ mice, indicating that A20 restricts TLR signaling induced by the commensal intestinal flora [26]. In agreement, deletion of MyD88 in $A20^{ZnF7}$ mice partly restored body weight and $A20^{ZnF7}MyD88^{-/-}$ mice developed less severe splenomegaly and were protected from developing spontaneous tissue inflammation, demonstrating that MyD88-dependent mechanisms contributed to the local inflammatory pathology in $A20^{ZnF7}$ mice. However, $A20^{ZnF7}MyD88^{-/-}$ still demonstrate systemic inflammation, as evidenced by detection of inflammatory cytokines in serum of these mice. To undeniably assess if the intestinal flora crucially contributes to the pathology of $A20^{ZnF7}$ mice, these mice will need to be rederived in germ free conditions.

Cell death has long been considered a consequence of sustained inflammation in many diseases, however recent studies identified cell death as a driver of inflammation. Particularly lytic forms of cell death, including necroptosis and pyroptosis, were shown to induce inflammation by the release of Danger Associated Molecular Patterns (DAMPS)[27,28]. To test if necroptosis is involved in the inflammatory pathology seen in $A20^{ZnF7}$ mice, $A20^{ZnF7}$ mice were crossed into a RIP1 kinase death (KD, $RIPK1^{D138N}$) background. These mice were, however, not rescued from systemic inflammation. Previously, it was shown that RIPK3 deficiency significantly restored the survival of A20-deficient mice, though these A20-$RIPK3^{-/-}$ mice still succumb to severe inflammation[29]. It was suggested that A20 prevents RIPK1-RIPK3 complex formation by interfering with RIPK3 ubiquitination via its deubiquitinating OTU domain[15]. However, A20 mutant mice that have a catalytically inactive OTU domain do not develop spontaneous disease, questioning the importance of RIPK3 ubiquitination by A20. Another study confirmed the partial rescue of $A20^{-/-}$ mice in a RIPK3 deficient background and further showed that a RIPK1 KD background also extended the survival time of $A20^{-/-}$ mice. However, MLKL deficiency could not rescue or delay the perinatal death of $A20^{-/-}$ mice[29], questioning the involvement of necroptosis in the inflammatory lethality of $A20^{-/-}$ mice and indicating that necroptosis-independent functions of RIPK1 and RIPK3 are involved in the pathology. Indeed, RIPK1 and RIPK3 have been shown to have necroptosis-independent pro-inflammatory functions and to induce apoptosis[30]. Furthermore, RIPK3 was shown to promote NLRP3 inflammasome activation, independent of its role in MLKL activation and necroptosis[31]. Based on this, $A20^{ZnF7}$ mice should be crossed with MLKL deficient mice rather than with RIPK1 KD or RIPK3 deficient mice to assess the involvement of necroptosis.

In myeloid cells, A20 was shown to regulate the activation of the NLRP3 inflammasome and the execution of pyroptotic cell death. Studies on BMDMs demonstrated that A20 deficiency enhanced NLRP3 inflammasome activation, IL1β and IL18 release and pyroptosis upon stimulation with LPS and ATP[32]. Also in primary microglia cultures, A20 deficiency was shown to induce NLRP3 inflammasome hyperactivation and pyroptosis[33]. BMDMs isolated from $A20^{ZnF7}$ mice also show NLRP3 inflammasome hyperactivation upon stimulation with LPS and ATP, to the same extend as seen in A20 deficient BMDMs. LPS/ATP treatment also induced massive pyroptosis of $A20^{ZnF7}$ BMDMs, comparable to what is seen in $A20^{-/-}$ BMDMs. This indicates that A20 critically relies on its ZnF7 ubiquitin binding domain to prevent inflammasome activation.

In vivo, $A20^{myel\text{-}KO}$ mice were shown to develop spontaneous polyarthritis resembling rheumatoid arthritis. Treatment with neutralizing IL-6 antibodies offered significant protection from arthritis development, identifying IL-6 as an important mediator of disease progression[10]. Furthermore, arthritis development in $A20^{myel\text{-}KO}$ mice was prevented by crossing these mice with $IL\text{-}1R^{-/-}$, $NLRP3^{-/-}$ or Caspase $1/11^{-/-}$ mice, indicating that excessive NLRP3 inflammasome activation and IL1β release are driving arthritis pathology[32]. NLRP3 or Caspase 1/11 deficiency also prevented excessive IL-6 production, showing that elevated IL-6 levels are a consequence of NLRP3 inflammasome hyperactivation. Since A20 critically relies on its ZnF7 domain to control the activation of the NLRP3 inflammasome, and excessive NLRP3 inflammasome activation leads to the development of arthritis , we hypothesized $A20^{ZnF7}$ mice might develop arthritis pathology. Indeed, we could demonstrate that $A20^{ZnF7}$ mice progressively develop an inflammatory joint pathology, although the overall disease severity in these mice was generally milder compared with age-matched $A20^{myel\text{-}KO}$ mice. However, increased numbers of infiltrating neutrophils could be detected in the joints of $A20^{myel\text{-}KO}$ mice compared to $A20^{ZnF7}$ animals. Since neutrophils are considered a key pathogenic component in joint inflammation both in humans and in animal models[34], this could account for the more severe arthritis development in $A20^{myel\text{-}KO}$ mice. In agreement with the phenotype of $A20^{myel\text{-}KO}$ mice, $A20^{ZnF7}$ $MyD88^{-/-}$ mice no longer developed arthritis pathology, indicating that the arthritis phenotype seen in $A20^{ZnF7}$ mice is caused by aberrant MyD88-dependent signaling locally at the site of arthritic pathology, and not by the systemic increase in inflammatory cytokines.

The mechanisms by which A20, via its ZnF7 domain, limits NLRP3 inflammasome activation remain poorly understood. In collaboration with the research group of Prof. Manolis Pasparakis (University of Cologne), we have demonstrated that A20 prevents NLRP3 inflammasome-mediated arthritis by preventing macrophage necroptosis. Myeloid-specific deletion of ASC, an adaptor protein crucial for inflammasome assembly, ameliorates the arthritis phenotype of $A20^{myel\text{-}KO}$ mice, confirming the importance of inflammasome hyperactivation in myeloid cells in the absence of A20. However,

crossing of A20$^{myel\text{-}KO}$ mice into a RIPK3$^{-/-}$, RIPK1 KD or MLKL$^{-/-}$ genetic background completely prevented arthritis development, identifying myeloid cell necroptosis as a crucial driver of arthritis pathology in A20$^{myel\text{-}KO}$ mice. Dynamic real-time imaging of cell death and IL-1β release simultaneously at the single cell level in BMDMs could demonstrate that IL-1β release from A20-deficient macrophages requires RIPK3-dependent cell death, consistent with the *in vivo* genetic data showing that necroptosis drives IL-1β production and the development of arthritis in A20$^{myel\text{-}KO}$ mice. The upstream ligands triggering macrophage necroptosis are, however, currently not known. TLR4-MyD88 signaling might function in a redundant and cooperative fashion with TRIF-dependent TLR3/TLR4 and/or type I and type II interferon (IFN) signaling. TLR3/4 signaling can induce necroptosis in BMDMs via TRIF, but independently of TNF[35,36], and TRIF can induce IFNβ via activation of TBK1 and IFN regulatory factor-3 (IRF-3)[37]. Interestingly, IFNs signal via the JAK-STAT pathway, and our previous research has shown that A20 negatively regulates JAK-STAT1 signaling in BMDMs and demonstrated that pharmacological inhibition of JAK reduced enthesitis development in A20$^{myel\text{-}KO}$ mice [38].

BMDMs isolated from A20^{ZnF7} mice release IL-1β as well as IL-1α upon treatment with LPS, although at lower levels compared with A20-knockout cells. This shows that A20 is, at least partly, relying on its M1-binding ZnF7 domain to prevent macrophage necroptosis and arthritis development. Our mechanistic studies further showed that A20 is recruited to the TNFR1 via its ZnF7 domain. However, ZnF7 might also be essential to recruit A20 to the TLR4 complex. Although A20 was previously shown to limit IKK activation and NF-κB signaling downstream of TLR4 by removing K63 chains from TRAF6 [5,24], the role of LUBAC and linear ubiquitination in TLR4/IL-1R signaling is not clear. K63-M1-hybrid chains can be detected on IRAK-1, IRAK-4 and MyD88 upon activation of the IL-1R[39], which might be applicable to other signaling complexes including TLR4. Further experiments should be performed to investigate if the ZnF7 mutation in A20 prevents A20 recruitment to the TLR4 signaling complex preventing downstream signaling. Indeed, A20 binding to M1-chains via its ZnF7 might prevent downstream NF-κB activation by competing with NEMO/IKK for M1-ubiquitin binding. We showed that A20^{ZnF7} BMDMs treated with LPS have sustained NF-κB activation and increased IL-6 and TNF production compared to control BMDMs. Furthermore, since CYLD was shown to promote LPS-induced necroptosis in BMDMs[40], A20 might also protect ubiquitin chains in the TLR4 complex from being degraded by CYLD, preserving signaling complex stability, similar to what is seen in the TNFR1 signaling complex. Since mutating the ZnF4 domain of A20 does not render mice susceptible to LPS induced lethality, nor interferes with A20's ability to limit NF-κB activation in LPS treated BMDMs, A20 does not rely on its K63 binding activity to control TLR4 signaling[5].

Although A20$^{myel\text{-}KO}$RIPK3$^{-/-}$, A20$^{myel\text{-}KO}$RIPK1 ^{D138N} or A20$^{myel\text{-}KO}$MLKL$^{-/-}$ mice are completely protected from arthritis development, A20^{ZnF7}RIPK1^{D138N} are not and develop pathology to the same extent as A20^{ZnF7} mice. Also, NLRP3 deficiency could also not prevent arthritis development in A20^{ZnF7} mice. However and in contrast to our previous studies using A20$^{myel\text{-}KO}$ mice[16,32], A20^{ZnF7} mice are full body knockin mice, and the mutant ZnF7 domain is expressed in all cells, also in cells other than the myeloid cells, which may also contribute to the arthritis phenotype, independent of NLRP3 inflammasome activation and necroptosis. In contrast to A20$^{myel\text{-}KO}$ mice, A20^{ZnF7} mice also show severe inflammatory pathology and bone erosion in fingers and toes, hence, A20 deficiency in non-myeloid cells is likely responsible for this. Mice expressing low levels of A20, due to the genetic removal of a sub-TAD domain containing 4 enhancers at the A20 locus, develop an inflammatory arthritis involving inflammation in the digits of the paws, similar to what is observed in A20^{ZnF7} mice[41]. Furthermore, mice lacking A20 specifically in the keratinocytes develop ectodermal organ abnormalities, due to aberrant EDAR-signaling in the absence of A20[42]. These mice also develop mild skin inflammation and increased sensitivity to experimental psoriasis[43], but also display pronounced swelling of their digits which may represent a form of psoriatic arthritis. These observations suggest that part of the phenotype of A20^{ZnF7} mice may result from the expression of the mutant A20 in keratinocytes. Keratinocytes, together with T-cells and dendritic cells are central players in psoriasis and psoriatic arthritis[44]. Although we observed a small reduction in CD3^{+} T-cells in A20^{ZnF7} mice, more in-depth immunophenotyping through flow cytometry should be performed to investigate if there are differences in immune mediators critical for psoriasis and arthritis. Overall, we conclude that both myeloid and non-myeloid cells contribute to the arthritis phenotype of A20^{ZnF7} mice, and that blocking macrophage necroptosis or inflammasome activation is not sufficient to prevent arthritis development in these mice.

Although A20^{ZnF7} mice develop a spontaneous inflammatory phenotype, they do not fully recapitulate the phenotype of A20$^{-/-}$ mice that develop severe multi-organ inflammation and cachexia and die in the first weeks after birth[12]. Furthermore, a small portion of A20^{ZnF7} proteins is still detected at the TNFR1 complex upon stimulation of BMDMs with TNF. Also in HOIP$^{-/-}$ cells, which are defective in linear ubquitination, A20 is still recruited to the TNFR1 complex, although to a much lesser extent than in wild-type cells[45]. This suggests that A20 exerts additional protective functions independent of its ZnF7 linear ubiquitin binding activity. In this respect, the ZnF4 domain of A20 has been demonstrated to bind K63-linked polyubiquitin, and mutations in the A20 ZnF4 ubiquitin-binding interface were shown to result in slightly impaired regulation of NF-κB signaling. However, mice with a disruptive mutation in their ZnF4 domain do not develop spontaneous disease[3,5,6]. In a M1 sufficient situation, A20 solely relies on its ZnF7 domain for the recruitment to TNFR1, while in a

M1 deficient context (e.g. HOIP deficiency) A20 recruitment becomes dependent on its ZnF4 domain[45]. To clarify the physiological role of A20's ZnF4 domain in suppressing inflammation, we introduced point mutations in the ZnF4 motif of $A20^{ZnF7}$ mice, generating mice which express A20 that is no longer able to bind both K63 ubiquitin as well as M1 ubiquitin ($A20^{ZnF4ZnF7}$ mice). $A20^{ZnF4ZnF7}$ mice are born in normal numbers but die before weaning age due to severe inflammation in multiple organs, including intestine, liver, and skin, comparable to what is seen in A20 deficient mice[12]. $A20^{ZnF4ZnF7}MyD88^{-/-}$ survive past weaning age and do not longer develop the severe multi-organ pathology, however, they still have significantly reduced bodyweight with presence of inflammatory cytokines in serum, and do not get older than 20 weeks. This indicates that MyD88 dependent signaling is involved in the initial, post-natal, inflammatory response in these mice, while at later age MyD88-independent contribute to pathology. Crossing $A20^{ZnF4ZnF7}$ mice in a RIPK1 KD background unexpectedly did not prevent nor delay postnatal lethality, contrasting to what has been described for $A20^{-/-}$ mice before[29]. Most likely there is a difference in genetic background and/or microbiome between both mouse lines, since in our hands $A20^{-/-}$ all die within 2 weeks after birth, in contrast to the $A20^{-/-}$ mice described by Newton et al. that have a median survival of 5 weeks [29]. To address the role of cell death in the lethal inflammatory pathology of $A20^{ZnF4ZnF7}$ mice, these mice should be crossed into a FADD or Caspase-8 and MLKL deficient background to inhibit both apoptosis and necroptosis. These crosses are currently ongoing. Given that $A20^{ZnF4ZnF7}$ mice largely phenocopy A20 deficient mice, we conclude that A20 primarily acts in a non-enzymatic way to suppress inflammation by allowing its recruitment and the stabilization of ubiquitin chains in the receptor complex. However, also the E3-ligase activity of the ZnF4 domain is disrupted in our model, which might also contribute to the observed phenotype. Furthermore A20's DUB activity may still have important functions in the downstream regulation of signaling. Indeed, since the mutation in the ZnF4 and ZnF7 domains prevents A20 recruitment to the TNFR1 complex and likely also to other signaling receptor complexes, the A20 OTU domain is no longer brought in close proximity with its possible substrates.

$A20^{ZnF4ZnF7}$ mice are not viable, preventing further research to determine the *in vivo* physiological functions of A20's ZnF4 and ZnF7 activity. Therefore we generated a conditional $A20^{ZnF4ZnF7}$ knockin mouse line, allowing us to assess the tissue-specific role of these ubiquitin binding ZnF domains. We previously demonstrated that A20 deficiency in intestinal epithelial cells (IECs, $A20^{IEC\text{-}KO}$), sensitizes IECs to TNF-induced apoptosis, leading to intestinal barrier disruption and lethality in mice[14]. Similarly, mutating the ZnF4 and ZnF7 domains of A20 in IECs renders mice susceptible to TNF-induced lethality due to severe IEC apoptosis. However, these mice show a delay in lethality compared to $A20^{IEC\text{-}KO}$ mice. Myeloid-specific $A20^{ZnF4ZnF7}$ mice develop splenomegaly and show high serum levels of TNF and IL-6, as seen in $A20^{myel\text{-}KO}$ cells. These mice also develop a progressive

polyarthritis, although to a lesser extend as seen in $A20^{myel\text{-}KO}$ mice. However, no swelling of digits, as seen in $A20^{ZnF7}$ mice, was observed, further proving that part of the $A20^{ZnF7}$ phenotype is caused by non-myeloid cells. *In vitro*, BMDMs isolated from myeloid-specific $A20^{ZnF4ZnF7}$ mice show increased release of inflammatory cytokines TNF and IL-6, although still not to the same level as seen in A20 deficient BMDMs. Together, these results identified the ZnF4 and ZnF7 domains as critical for A20's anti-inflammatory and cytoprotective activities.

Although $A20^{ZnF4ZnF7}$ mice phenocopy A20 deficient mice, tissue-specific $A20^{ZnF4ZnF7}$ mice develop milder pathology compared to tissue-specific $A20^{-/-}$ mice. We hypothesize that the mutation of the ZnF4 and the ZnF7 domain in the whole organism is sufficient to trigger a cascade of responses leading to severe inflammation and perinatal death, while tissue-specific mutation results in milder phenotypes revealing subtle differences between the $A20^{-/-}$ and $A20^{ZnF4ZnF7}$ condition. However, next to its function as a ubiquitin-binding protein, A20 is also recruited to signaling complexes via interaction with other proteins. In this context, ABIN-1 recruits A20 to the IKK complex where it removes ubiquitin chains from NEMO[46,47]. Also tax1-binding protein 1 (TAX1BP1) was shown to recruit A20 to TRAF6 and RIPK1[48,49]. These and possibly other A20 binding proteins might still recruit A20 to signaling complexes in absence of A20's ubiquitin binding functions. Furthermore, as already mentioned, also the OTU-DUB domain may still control regulatory functions once A20 is recruited upon activation of the inflammatory pathway. In that respect, A20 was recently shown to rely on its DUB function to prevent TNF induced cell death in M1 deficient conditions *in vitro*[45].

A20 critically controls RANK-dependent osteoclastogenesis and bone physiology

Next to its role in the control of NF-κB-dependent inflammation, A20 also regulates NF-κB signaling pathways controlling developmental processes. In this context, A20 was previously shown to regulate Ectodysplasin A receptor (EDAR)-induced NF-κB signaling, important for the development of epidermal appendages such as skin, hair, nails, teeth, and sweat glands[42]. We have now also demonstrated a role for A20 as a direct negative feedback regulator of RANKL-induced osteoclastogenesis. Bone is a dynamic organ which is constantly renewed in a process called 'bone remodeling'. This is a highly regulated process and uncontrolled remodeling can result in a disease called osteoporosis, characterized by low bone density, or in osteopetrosis caused by too dense bones[50]. We have developed mice which lack A20 only in mature osteoclasts ($A20^{OC\text{-}KO}$). These mice develop severe osteoporosis, and increased numbers of TRAP-positive osteoclasts can be demonstrated in the bones of these mice. $A20^{OC\text{-}KO}$ mice do not show increased levels of

inflammatory cytokines in their serum, indicating that A20 regulates osteoclastogenesis independent of its anti-inflammatory functions. *In vitro*, increased expression of osteoclast specific markers were detected in osteoclast cultures derived from $A20^{OC\text{-}KO}$ bone marrow progenitor cells in the early stages of osteoclast differentiation but not at the final stages of osteoclastogenesis. Osteoclasts are short-lived cells, that undergo apoptotic cell death to prevent excessive bone degradation and sustain homeostasis. Differentiating osteoclasts upregulate Fas expression, and mice lacking functional Fas develop osteroporosis due to increased numbers of osteoclasts[51]. In culture, osteoclasts survive significantly longer when grown on bone matrix compared to plastic[52]. Therefore, $A20^{OC\text{-}KO}$ bone marrow might show enhanced osteoclastogenesis resulting in more osteoclasts at early stages of osteoclast differentiation, while this is no longer visible at later stage due to rapid osteoclast apoptosis in absence of bone matrix. In-depth analysis at the initial stages of osteoclast differentiation *in vitro* should be performed to further characterize the importance of A20 for osteoclastogenesis.

Mechanistically we showed that A20 is upregulated in BMDMs by RANKL stimulation, and demonstrated that A20 deficiency results in increased RANK-induced NF-κB signaling. This demonstrates that A20 can directly control signaling downstream of RANK. However, the mechanisms by which A20 regulates RANK signaling still remains elusive. Upon binding of RANKL to its receptor RANK, different TRAF molecules are recruited to the receptor of which TRAF6 was shown to be critical for osteoclast differentiation and maturation[53]. TRAF6 was shown to auto-ubiquitinate in response to RANKL[54], and K63 polyubiquitin chains on TRAF6 were shown to be crucial for the recruitment of the IKK complex and the induction of downstream signaling[55]. Expression of a RING mutant of TRAF6 preventing TRAF6 auto-ubiquitination fails to rescue NF-κB signaling and osteoclastogenesis in RANKL-stimulated TRAF6 deficient monocytes[54]. A20 was previously shown to regulate TRAF6 ubiquitination downstream of TLRs via its DUB domain[24], however there is currently no evidence that A20 is also involved in the deubiquitinating of TRAF6 downstream of RANK, in contrast to the deubiquitinating enzyme CYLD which was previously shown to directly regulate RANK-induced NF-κB signaling by restricting TRAF6 ubiquitination[56]. Overexpression of an A20-DUB mutant could not affect A20's ability to suppress RANK induced NF-κB signaling, questioning the role of A20's DUB function in regulating RANK signaling. Pulldown experiments of TRAF6 should be performed to see if A20 deficiency alters the TRAF6 ubiquitination status upon RANKL stimulation. In contrast to the DUB mutant, overexpression of a ZnF7 mutant slightly impaired inhibition, but expression of a double ZnF4/ZnF7 mutant completely prevented A20 mediated inhibition of RANK-induced NF-κB signaling in overexpression experiments. This is in agreement with our previous study showing that A20 primarily functions as a ubiquitin binding protein to prevent cell death and inflammation[16].

Additional studies using bone marrow from $A20^{ZnF7}$ and $A20^{ZnF4ZnF7}$ mice will be needed to unravel the specific role of these domains in RANK signaling and osteoclast maturation. Also, osteoclast-specific $A20^{ZnF4ZnF7}$ mice will need to be generated in order to find out if these mice would develop osteoporosis similar to what is observed in $A20^{OC\text{-}KO}$ mice.

The role of linear ubiquitination in RANK signaling is currently not known. Mice deficient for Sharpin, a component of the LUBAC complex, develop TNF-dependent multi-organ inflammation and show significantly reduced levels of linear ubiquitinylation at the TNFR1 signaling complex[57]. However, these mice also show reduced trabecular and cortical bone volume, and cells from Sharpin deficient mice show significantly reduced osteoclast formation and function *in vitro*[58]. This indicates that linear ubiquitination may be important for RANK signaling, however further research is needed to identify the targets that are ubiquitinated by the LUBAC complex.

References

1 Martens, A. & van Loo, G. A20 at the Crossroads of Cell Death, Inflammation, and Autoimmunity. *Cold Spring Harb Perspect Biol*, doi:10.1101/cshperspect.a036418 (2019).

2 Wertz, I. E. *et al.* De-ubiquitination and ubiquitin ligase domains of A20 downregulate NF-kappaB signalling. *Nature* **430**, 694-699, doi:10.1038/nature02794 (2004).

3 Lu, T. T. *et al.* Dimerization and ubiquitin mediated recruitment of A20, a complex deubiquitinating enzyme. *Immunity* **38**, 896-905, doi:10.1016/j.immuni.2013.03.008 (2013).

4 De, A., Dainichi, T., Rathinam, C. V. & Ghosh, S. The deubiquitinase activity of A20 is dispensable for NF-kappaB signaling. *EMBO Rep* **15**, 775-783, doi:10.15252/embr.201338305 (2014).

5 Wertz, I. E. *et al.* Phosphorylation and linear ubiquitin direct A20 inhibition of inflammation. *Nature* **528**, 370-375, doi:10.1038/nature16165 (2015).

6 Bosanac, I. *et al.* Ubiquitin binding to A20 ZnF4 is required for modulation of NF-kappaB signaling. *Mol Cell* **40**, 548-557, doi:10.1016/j.molcel.2010.10.009 (2010).

7 Tokunaga, F. *et al.* Specific recognition of linear polyubiquitin by A20 zinc finger 7 is involved in NF-kappaB regulation. *EMBO J* **31**, 3856-3870, doi:10.1038/emboj.2012.241 (2012).

8 Verhelst, K. *et al.* A20 inhibits LUBAC-mediated NF-kappaB activation by binding linear polyubiquitin chains via its zinc finger 7. *EMBO J* **31**, 3845-3855, doi:10.1038/emboj.2012.240 (2012).

9 Draber, P. *et al.* LUBAC-Recruited CYLD and A20 Regulate Gene Activation and Cell Death by Exerting Opposing Effects on Linear Ubiquitin in Signaling Complexes. *Cell Rep* **13**, 2258-2272, doi:10.1016/j.celrep.2015.11.009 (2015).

10 Matmati, M. *et al.* A20 (TNFAIP3) deficiency in myeloid cells triggers erosive polyarthritis resembling rheumatoid arthritis. *Nat Genet* **43**, 908-912, doi:10.1038/ng.874 (2011).

11 Rahighi, S. *et al.* Specific recognition of linear ubiquitin chains by NEMO is important for NF-kappaB activation. *Cell* **136**, 1098-1109, doi:10.1016/j.cell.2009.03.007 (2009).

12 Lee, E. G. *et al.* Failure to regulate TNF-induced NF-kappaB and cell death responses in A20-deficient mice. *Science* **289**, 2350-2354, doi:10.1126/science.289.5488.2350 (2000).

13 Kreuz, S., Siegmund, D., Scheurich, P. & Wajant, H. NF-kappaB inducers upregulate cFLIP, a cycloheximide-sensitive inhibitor of death receptor signaling. *Mol Cell Biol* **21**, 3964-3973, doi:10.1128/MCB.21.12.3964-3973.2001 (2001).

14 Vereecke, L. *et al.* Enterocyte-specific A20 deficiency sensitizes to tumor necrosis factor-induced toxicity and experimental colitis. *J Exp Med* **207**, 1513-1523, doi:10.1084/jem.20092474 (2010).

15 Onizawa, M. *et al.* The ubiquitin-modifying enzyme A20 restricts ubiquitination of the kinase RIPK3 and protects cells from necroptosis. *Nat Immunol* **16**, 618-627, doi:10.1038/ni.3172 (2015).

16 Polykratis, A. *et al.* A20 prevents inflammasome-dependent arthritis by inhibiting macrophage necroptosis through its ZnF7 ubiquitin-binding domain. *Nat Cell Biol* **21**, 731-742, doi:10.1038/s41556-019-0324-3 (2019).

17 Yamaguchi, N. & Yamaguchi, N. The seventh zinc finger motif of A20 is required for the suppression of TNF-alpha-induced apoptosis. *FEBS Lett* **589**, 1369-1375, doi:10.1016/j.febslet.2015.04.022 (2015).

18 Catrysse, L. *et al.* A20 prevents chronic liver inflammation and cancer by protecting hepatocytes from death. *Cell Death Dis* **7**, e2250, doi:10.1038/cddis.2016.154 (2016).

19 Gerlach, B. *et al.* Linear ubiquitination prevents inflammation and regulates immune signalling. *Nature* **471**, 591-596, doi:10.1038/nature09816 (2011).

20 Ikeda, F. *et al.* SHARPIN forms a linear ubiquitin ligase complex regulating NF-kappaB activity and apoptosis. *Nature* **471**, 637-641, doi:10.1038/nature09814 (2011).

21 Peltzer, N. *et al.* HOIP deficiency causes embryonic lethality by aberrant TNFR1-mediated endothelial cell death. *Cell Rep* **9**, 153-165, doi:10.1016/j.celrep.2014.08.066 (2014).

22 Opipari, A. W., Jr., Hu, H. M., Yabkowitz, R. & Dixit, V. M. The A20 zinc finger protein protects cells from tumor necrosis factor cytotoxicity. *J Biol Chem* **267**, 12424-12427 (1992).
23 Annibaldi, A. & Meier, P. Checkpoints in TNF-Induced Cell Death: Implications in Inflammation and Cancer. *Trends Mol Med* **24**, 49-65, doi:10.1016/j.molmed.2017.11.002 (2018).
24 Boone, D. L. *et al.* The ubiquitin-modifying enzyme A20 is required for termination of Toll-like receptor responses. *Nat Immunol* **5**, 1052-1060, doi:10.1038/ni1110 (2004).
25 Hitotsumatsu, O. *et al.* The ubiquitin-editing enzyme A20 restricts nucleotide-binding oligomerization domain containing 2-triggered signals. *Immunity* **28**, 381-390, doi:10.1016/j.immuni.2008.02.002 (2008).
26 Turer, E. E. *et al.* Homeostatic MyD88-dependent signals cause lethal inflamMation in the absence of A20. *J Exp Med* **205**, 451-464, doi:10.1084/jem.20071108 (2008).
27 Welz, P. S. *et al.* FADD prevents RIP3-mediated epithelial cell necrosis and chronic intestinal inflammation. *Nature* **477**, 330-334, doi:10.1038/nature10273 (2011).
28 Gunther, C. *et al.* Caspase-8 regulates TNF-alpha-induced epithelial necroptosis and terminal ileitis. *Nature* **477**, 335-339, doi:10.1038/nature10400 (2011).
29 Newton, K. *et al.* RIPK3 deficiency or catalytically inactive RIPK1 provides greater benefit than MLKL deficiency in mouse models of inflammation and tissue injury. *Cell Death Differ* **23**, 1565-1576, doi:10.1038/cdd.2016.46 (2016).
30 Moriwaki, K. & Chan, F. K. The Inflammatory Signal Adaptor RIPK3: Functions Beyond Necroptosis. *Int Rev Cell Mol Biol* **328**, 253-275, doi:10.1016/bs.ircmb.2016.08.007 (2017).
31 Lawlor, K. E. *et al.* RIPK3 promotes cell death and NLRP3 inflammasome activation in the absence of MLKL. *Nat Commun* **6**, 6282, doi:10.1038/ncomms7282 (2015).
32 Vande Walle, L. *et al.* Negative regulation of the NLRP3 inflammasome by A20 protects against arthritis. *Nature* **512**, 69-73, doi:10.1038/nature13322 (2014).
33 Voet, S. *et al.* A20 critically controls microglia activation and inhibits inflammasome-dependent neuroinflammation. *Nat Commun* **9**, 2036, doi:10.1038/s41467-018-04376-5 (2018).
34 Wright, H. L., Moots, R. J. & Edwards, S. W. The multifactorial role of neutrophils in rheumatoid arthritis. *Nat Rev Rheumatol* **10**, 593-601, doi:10.1038/nrrheum.2014.80 (2014).
35 He, S., Liang, Y., Shao, F. & Wang, X. Toll-like receptors activate programmed necrosis in macrophages through a receptor-interacting kinase-3-mediated pathway. *Proc Natl Acad Sci U S A* **108**, 20054-20059, doi:10.1073/pnas.1116302108 (2011).
36 Kaiser, W. J. *et al.* Toll-like receptor 3-mediated necrosis via TRIF, RIP3, and MLKL. *J Biol Chem* **288**, 31268-31279, doi:10.1074/jbc.M113.462341 (2013).
37 Sato, S. *et al.* Toll/IL-1 receptor domain-containing adaptor inducing IFN-beta (TRIF) associates with TNF receptor-associated factor 6 and TANK-binding kinase 1, and activates two distinct transcription factors, NF-kappa B and IFN-regulatory factor-3, in the Toll-like receptor signaling. *J Immunol* **171**, 4304-4310, doi:10.4049/jimmunol.171.8.4304 (2003).
38 De Wilde, K. *et al.* A20 inhibition of STAT1 expression in myeloid cells: a novel endogenous regulatory mechanism preventing development of enthesitis. *Ann Rheum Dis* **76**, 585-592, doi:10.1136/annrheumdis-2016-209454 (2017).
39 Emmerich, C. H. *et al.* Activation of the canonical IKK complex by K63/M1-linked hybrid ubiquitin chains. *Proc Natl Acad Sci U S A* **110**, 15247-15252, doi:10.1073/pnas.1314715110 (2013).
40 Legarda, D. *et al.* CYLD Proteolysis Protects Macrophages from TNF-Mediated Auto-necroptosis Induced by LPS and Licensed by Type I IFN. *Cell Rep* **15**, 2449-2461, doi:10.1016/j.celrep.2016.05.032 (2016).
41 Sokhi, U. K. *et al.* Dissection and function of autoimmunity-associated TNFAIP3 (A20) gene enhancers in humanized mouse models. *Nat Commun* **9**, 658, doi:10.1038/s41467-018-03081-7 (2018).

42 Lippens, S. *et al.* Keratinocyte-specific ablation of the NF-kappaB regulatory protein A20 (TNFAIP3) reveals a role in the control of epidermal homeostasis. *Cell Death Differ* **18**, 1845-1853, doi:10.1038/cdd.2011.55 (2011).
43 Devos, M. *et al.* Keratinocyte Expression of A20/TNFAIP3 Controls Skin Inflammation Associated with Atopic Dermatitis and Psoriasis. *J Invest Dermatol* **139**, 135-145, doi:10.1016/j.jid.2018.06.191 (2019).
44 Diani, M., Altomare, G. & Reali, E. T cell responses in psoriasis and psoriatic arthritis. *Autoimmun Rev* **14**, 286-292, doi:10.1016/j.autrev.2014.11.012 (2015).
45 Priem, D. *et al.* A20 protects cells from TNF-induced apoptosis through linear ubiquitin-dependent and -independent mechanisms. *Cell Death Dis* **10**, 692, doi:10.1038/s41419-019-1937-y (2019).
46 Heyninck, K. *et al.* The zinc finger protein A20 inhibits TNF-induced NF-kappaB-dependent gene expression by interfering with an RIP- or TRAF2-mediated transactivation signal and directly binds to a novel NF-kappaB-inhibiting protein ABIN. *J Cell Biol* **145**, 1471-1482, doi:10.1083/jcb.145.7.1471 (1999).
47 Mauro, C. *et al.* ABIN-1 binds to NEMO/IKKgamma and co-operates with A20 in inhibiting NF-kappaB. *J Biol Chem* **281**, 18482-18488, doi:10.1074/jbc.M601502200 (2006).
48 Iha, H. *et al.* Inflammatory cardiac valvulitis in TAX1BP1-deficient mice through selective NF-kappaB activation. *EMBO J* **27**, 629-641, doi:10.1038/emboj.2008.5 (2008).
49 Shembade, N., Harhaj, N. S., Liebl, D. J. & Harhaj, E. W. Essential role for TAX1BP1 in the termination of TNF-alpha-, IL-1- and LPS-mediated NF-kappaB and JNK signaling. *EMBO J* **26**, 3910-3922, doi:10.1038/sj.emboj.7601823 (2007).
50 Wada, T., Nakashima, T., Hiroshi, N. & Penninger, J. M. RANKL-RANK signaling in osteoclastogenesis and bone disease. *Trends Mol Med* **12**, 17-25, doi:10.1016/j.molmed.2005.11.007 (2006).
51 Wu, X., McKenna, M. A., Feng, X., Nagy, T. R. & McDonald, J. M. Osteoclast apoptosis: the role of Fas in vivo and in vitro. *Endocrinology* **144**, 5545-5555, doi:10.1210/en.2003-0296 (2003).
52 Xing, L. & Boyce, B. F. Regulation of apoptosis in osteoclasts and osteoblastic cells. *Biochem Biophys Res Commun* **328**, 709-720, doi:10.1016/j.bbrc.2004.11.072 (2005).
53 Lomaga, M. A. *et al.* TRAF6 deficiency results in osteopetrosis and defective interleukin-1, CD40, and LPS signaling. *Genes Dev* **13**, 1015-1024, doi:10.1101/gad.13.8.1015 (1999).
54 Lamothe, B. *et al.* TRAF6 ubiquitin ligase is essential for RANKL signaling and osteoclast differentiation. *Biochem Biophys Res Commun* **359**, 1044-1049, doi:10.1016/j.bbrc.2007.06.017 (2007).
55 Hacker, H. & Karin, M. Regulation and function of IKK and IKK-related kinases. *Sci STKE* **2006**, re13, doi:10.1126/stke.3572006re13 (2006).
56 Jin, W. *et al.* Deubiquitinating enzyme CYLD negatively regulates RANK signaling and osteoclastogenesis in mice. *J Clin Invest* **118**, 1858-1866, doi:10.1172/JCI34257 (2008).
57 Rickard, J. A. *et al.* TNFR1-dependent cell death drives inflammation in Sharpin-deficient mice. *Elife* **3**, doi:10.7554/eLife.03464 (2014).
58 Xia, T. *et al.* Loss-of-function of SHARPIN causes an osteopenic phenotype in mice. *Endocrine* **39**, 104-112, doi:10.1007/s12020-010-9418-1 (2011).

Curriculum Vitae

Curriculum Vitae

Degrees

PhD in Biotechnology (2014 – ongoing)

Title: 'Mechanistic insights into the regulation of inflammatory pathology by A20'
University of Ghent
Department of Biomedical Molecular Biology
VIB Center for Inflammation Research
Prof. Dr. Geert van Loo (promotor)

Master in Biochemistry and Biotechnology (2012 – 2014)

Thesis: 'Study of the ubiquitin-editing protein A20 in osteoclastogenesis and bone pathology'
University of Ghent
Department for Biomedical Molecular Biology
VIB Center for Inflammation Research
Prof. Dr. Geert van Loo (promotor)

Bachelor in Biochemistry and Biotechnology (2009 – 2012)

University of Ghent

Courses and training followed

- Animal Sciences: Part 1 and 2 – University of Ghent (Prof. Dr. Katleen Hermans)
- Research Ethics
- Career Guidance
- BITS training on qbase+
- BITS training on GIMP and INKSCAPE
- Basic Microscopy course
- BioImaging Core slide scanner workshop
- Effective Oral Presentation
- VIB - CRISPR User Meeting

Scientific output

Martens, A., Priem, D., Hoste, E., Vetters, J., Rennen, S., Catrysse, L., Voet, S., Deelen, L., Sze, M., Vikkula, H., Slowicka, K., Hochepied, T., Iliaki, K., Wullaert, A., Janssens, S., Lamkanfi, M., Beyaert, R., Armaka, M., Bertrand, M.J.M. & van Loo, G. Two distinct ubiquitin-binding motifs in A20 mediate its anti-inflammatory and cell- protective activities Nat. Immunol. (In Press)

Verboom, L., Martens, A., Priem, D., Hoste, E., Sze, M., Vikkula, H., Van Hove, L., Voet, S., Roels, J., Maelfait, J., Bongiovanni, L., de Bruin, A., Scott, C.L., Saeys, Y., Pasparakis, M., Bertrand, M.J.M., & van Loo, G.OTULIN prevents liver inflammation and hepatocellular carcinoma by inhibiting FADD- and RIPK1 kinase-mediated hepatocyte apoptosis. (In Press)

Martens, A. & van Loo, G. A20 phosphorylation controls A20 function. Nat Immunol 20, 1261-1262, doi:10.1038/s41590-019-0481-3 (2019).

Priem, D., Devos, M., Druwe, S., Martens, A., Slowicka, K., Ting, A. T., Pasparakis, M., Declerq, W., Vandenabeele, P., van Loo, G. & Bertrand, M. J. M. A20 protects cells from TNF-induced apoptosis through linear ubiquitin-dependent and -independent mechanisms. Cell Death Dis 10, 692, doi:10.1038/s41419-019-1937-y (2019).

Martens, A. & van Loo, G. A20 at the Crossroads of Cell Death, Inflammation, and Autoimmunity. Cold Spring Harb Perspect Biol, doi:10.1101/cshperspect.a036418 (2019).

Polykratis, A.*, Martens, A.*, Eren, R. O.*, Shirasaki, Y., Yamagishi, M., Yamaguchi, Y., Uemura, S., Miura, M., Holzmann, B., Kollias, G., Armaka, M.#, van Loo, G.# & Pasparakis, M.# A20 prevents inflammasome-dependent arthritis by inhibiting macrophage necroptosis through its ZnF7 ubiquitin-binding domain. Nat Cell Biol 21, 731-742, doi:10.1038/s41556-019-0324-3 (2019). (*, equally first author; #, equally last author)

Slowicka, K., Serramito-Gomez, I., Boada-Romero, E., Martens, A., Sze, M., Petta, I., Vikkula, H. K., De Rycke, R., Parthoens, E., Lippens, S., Savvides, S. N., Wullaert, A., Vereecke, L., Pimentel-Muinos, F. X. & van Loo, G. Physical and functional interaction between A20 and ATG16L1-WD40 domain in the control of intestinal homeostasis. Nat Commun 10, 1834, doi:10.1038/s41467-019-09667-z (2019).

Vetters, J., van Helden, M. J., Wahlen, S., Tavernier, S. J., Martens, A., Fayazpour, F., Vergote, K., Vanheerswynghels, M., Deswarte, K., Van Moorleghem, J., De Prijck, S., Takahashi, N., Vandenabeele, P., Boon, L., van Loo, G., Vivier, E., Lambrecht, B. N. & Janssens, S. The ubiquitin-editing enzyme A20 controls NK cell homeostasis through regulation of mTOR activity and TNF. J Exp Med 216, 2010-2023, doi:10.1084/jem.20182164 (2019).

Van Quickelberghe, E., Martens, A., Goeminne, L. J. E., Clement, L., van Loo, G. & Gevaert, K. Identification of Immune-Responsive Gene 1 (IRG1) as a Target of A20. J Proteome Res 17, 2182-2191, doi:10.1021/acs.jproteome.8b00139 (2018).

Voet, S., Mc Guire, C., Hagemeyer, N., Martens, A., Schroeder, A., Wieghofer, P., Daems, C., Staszewski, O., Vande Walle, L., Jordao, M. J. C., Sze, M., Vikkula, H. K., Demeestere, D., Van Imschoot, G., Scott, C. L., Hoste, E., Goncalves, A., Guilliams, M., Lippens, S., Libert, C., Vandenbroucke, R. E., Kim, K. W., Jung, S., Callaerts-Vegh, Z., Callaerts, P., de Wit, J., Lamkanfi, M., Prinz, M. & van Loo, G. A20 critically controls microglia activation and inhibits inflammasome-dependent neuroinflammation. *Nat Commun* **9**, 2036, doi:10.1038/s41467-018-04376-5 (2018).

De Wilde, K., Martens, A., Lambrecht, S., Jacques, P., Drennan, M. B., Debusschere, K., Govindarajan, S., Coudenys, J., Verheugen, E., Windels, F., Catrysse, L., Lories, R., McGonagle, D., Beyaert, R., van Loo, G. & Elewaut, D. A20 inhibition of STAT1 expression in myeloid cells: a novel endogenous regulatory mechanism preventing development of enthesitis. *Ann Rheum Dis* **76**, 585-592, doi:10.1136/annrheumdis-2016-209454 (2017).

Attendance of symposia and conferences

TNF conference 2019

03-07 June 2019
Monterey, USA
Oral presentation

25th conference of the European Cell Death Organization (ECDO) 2017

27-29 September 2017
Leuven, Belgium
Poster presentation

Deubiquitinases - from structure to physiology 2017

26-28 June 2019
Oxford, Great Britain
Poster presentation (Poster prize)

CRISPR based Genome Engineering 2016

27 October 2016
Leuven, Belgium

Molecular mechanisms of Inflammation 2016

30 May – 02 June 2016
Trondheim, Norway
Poster presentation

Genome Engineering and Synthetic Biology 2016

28-29 January 2016
Gent, Belgium

IRC – FWO Symposium on "Molecular Mechanisms of Inflammation" 2015

8 December 2015
Gent, Belgium

IRC Symposium 'ER Stress & Inflammation' 2015

27 November 2015
Ghent, Belgium

The CRISPR/Cas 9 Revolution meeting 2015

24-27 September 2015
Cold Spring Harbor, USA
Poster presentation

Training of students

Master I student, Lien Demeyer (2015-2016): 'Study of the ubiquitin-editing protein A20 in octeoclastogenesis and bone pathology.'

Master II student, Laura Deelen (2017-2018): 'Analysis of new A20 mutant knock-in mice.'

Additional papers

EXTENDED REPORT

A20 inhibition of STAT1 expression in myeloid cells: a novel endogenous regulatory mechanism preventing development of enthesitis

Katelijne De Wilde,[1,2] Arne Martens,[3,4] Stijn Lambrecht,[1,2] Peggy Jacques,[1,2] Michael B Drennan,[1,2] Karlijn Debusschere,[1,2] Srinath Govindarajan,[1,2] Julie Coudenys,[1,2] Eveline Verheugen,[1,2] Fien Windels,[1,2] Leen Catrysse,[3,4] Rik Lories,[5,6] Dennis McGonagle,[7] Rudi Beyaert,[4,8] Geert van Loo,[3,4] Dirk Elewaut[1,2]

Handling editor Tore K Kvien

► Additional material is published online only. To view please visit the journal online (http://dx.doi.org/10.1136/annrheumdis-2016-209454)

For numbered affiliations see end of article.

Correspondence to
Dr Dirk Elewaut, Unit for Molecular Immunology and Inflammation, VIB Inflammation Research Center Ghent and Department of Rheumatology, Ghent University, De Pintelaan 185, Ghent 9000, Belgium; Dirk.Elewaut@UGent.be

Part of these data were presented at the International TNF Conference in 2015 (poster presentation), the Belgian Congress of Rheumatology in 2015 (oral presentation), the ACR/ARHP Annual Meeting in 2015 (oral presentation) and at the European Workshop on Rheumatology Research 2016 (poster presentation).

Received 27 February 2016
Revised 26 June 2016
Accepted 11 July 2016
Published Online First 17 August 2016

To cite: De Wilde K, Martens A, Lambrecht S, *et al. Ann Rheum Dis* 2017;**76**:585–592.

ABSTRACT

Objectives A20 is an important endogenous regulator of inflammation. Single nucleotide polymorphisms in A20 have been associated with various immune-mediated inflammatory diseases, and cell-specific deletion of A20 results in diverse inflammatory phenotypes. Our goal was to delineate the underlying mechanisms of joint inflammation in myeloid-specific A20-deficient mice ($A20^{myelKO}$ mice).

Methods Inflammation in $A20^{myelKO}$ mice was assessed in a time-dependent manner. Western blot analysis and quantitative PCR analysis were performed on bone marrow-derived macrophages from $A20^{myelKO}$ and littermate control mice to study the effect of A20 on STAT1/STAT3 expression and STAT1/STAT3-dependent gene transcription in myeloid cells. The in vivo role of Janus kinase-Signal Transducer and Activator of Transcription (JAK-STAT) signalling in the development of enthesitis in $A20^{myelKO}$ mice was assessed following administration of a JAK inhibitor versus placebo control.

Results Enthesitis was found to be an early inflammatory lesion in $A20^{myelKO}$ mice. A20 negatively modulated STAT1-dependent, but generally not STAT3-dependent gene transcription in myeloid cells by suppressing STAT1 but not STAT3 expression, both in unstimulated conditions and after interferon-γ or interleukin-6 stimulation. The increase in STAT1 gene transcription in the absence of A20 was shown to be JAK-STAT-dependent. Moreover, JAK inhibition in vivo resulted in significant reduction of enthesitis, both clinically and histopathologically.

Conclusions Our data reveal an important and novel interplay between myeloid cells and tissue resident cells at entheseal sites that is regulated by A20. In the absence of A20, STAT1 but not STAT3 expression is enhanced leading to STAT1-dependent inflammation. Therefore, A20 acts as a novel endogenous regulator of STAT1 that prevents onset of enthesitis.

INTRODUCTION

A20, also known as tumour necrosis factor-α-induced protein 3, is a crucial negative regulator of nuclear factor-κB (NF-κB)-dependent inflammation.[1 2] It has been identified as a susceptibility gene for several immune-mediated inflammatory diseases, including rheumatoid arthritis, systemic lupus erythematosus and psoriasis.[1 2] Whereas germline A20 knockout (KO) mice die prematurely due to multiorgan inflammation,[3] the specific function of A20 in different cell types has been extensively studied using conditional KO mice. This showed that A20 deficiency can result in distinct phenotypes, depending on the cell type in which A20 is deleted.[1 2] For example, epidermis-specific A20 deficiency leads to keratinocyte hyperproliferation, while A20 deficiency in myeloid cells leads to the spontaneous development of a progressive arthritis.[4 5] Here, we focused on mice with a myeloid cell-specific A20 deficiency, referred to as $A20^{myelKO}$ mice. The inflammation in these mice is dependent on Nlrp3 inflammasome activation, interleukin (IL)-6 and IL-1 receptor signalling, but independent of TNF.[5 6]

A20 is known to function as a negative regulator of inflammation by restricting NF-κB signalling.[1 2] In addition to the NF-κB signalling pathway, the Janus kinase-Signal Transducer and Activator of Transcription (JAK-STAT) pathway is also of great importance in the immune system.[1 2 7] Given the role of the JAK-STAT pathway in several immune-mediated inflammatory disorders,[7] we aimed to study the effect of A20 on JAK-STAT signalling in myeloid cells. Several cytokines and growth factors are known to signal through the JAK-STAT pathway;[8] with two prototypic examples: IL-6 and interferon (IFN)-γ. While IFN-γ signalling predominantly phosphorylates STAT1, IL-6 signalling strongly phosphorylates STAT3.[7 9] Phosphorylated STAT proteins form homodimers or heterodimers, followed by nuclear translocation and transcriptional activation of their target genes.[8]

Enthesitis is an important hallmark of spondyloarthritis (SpA). A marked characteristic of SpA-associated enthesitis is that the inflammation is not confined to the enthesis itself, but is also present in the adjacent tissues. Because the synovium and the enthesis are located in close proximity to one another and because there is a functional association between the two, they can be regarded as a synovio-entheseal complex (SEC). If microdamage arises in the enthesis, this can lead to inflammation of the synovium or even to inflammation of the entire SEC.[10 11] Although enthesitis is an important hallmark of SpA, much remains unknown about the underlying mechanisms.

Journal of proteome research

Article

Cite This: J. Proteome Res. 2018, 17, 2182−2191

pubs.acs.org/jpr

Identification of Immune-Responsive Gene 1 (IRG1) as a Target of A20

Emmy Van Quickelberghe,[†,‡] Arne Martens,[¶,∥] Ludger J. E. Goeminne,[†,‡,§,⊥] Lieven Clement,[§,⊥] Geert van Loo,[¶,∥] and Kris Gevaert*[,†,‡]

[†]VIB-UGent Center for Medical Biotechnology, B-9000 Ghent, Belgium

[‡]Department of Biochemistry, [§]Department of Applied Mathematics, Computer Science and Statistics, and [⊥]Bioinformatics Institute Ghent, Ghent University, B-9000 Ghent, Belgium

[¶]VIB-UGent Center for Inflammation Research, B-9052 Ghent, Belgium

[∥]Department of Biomedical Molecular Biology, Ghent University, B-9052 Ghent, Belgium

Supporting Information

ABSTRACT: A20 is a negative regulator of NF-κB signaling; it controls inflammatory responses and ensures tissue homeostasis. A20 is thought to restrict NF-κB activation both by its ubiquitin-editing activity as well as by its nonenzymatic activities. Besides its role in NF-κB signaling, A20 also acts as a protective factor inhibiting apoptosis and necroptosis. Because of the ability of A20 to both ubiquitinate and deubiquitinate substrates, and its involvement in many cellular processes, we hypothesized that deletion of A20 might generally impact on protein levels, thereby disrupting cellular signaling. We performed a differential proteomics study on bone marrow-derived macrophages (BMDMs) from control and myeloid-specific A20 knockout mice, both in untreated conditions and after LPS or TNF treatment, and demonstrated A20-dependent changes in protein expression. Several inflammatory proteins were found up-regulated in the absence of A20, even without an inflammatory stimulus, but, depending on the treatment and the treatment time, more proteins were found regulated. Together these protein changes may affect normal signaling events, which may disturb tissue homeostasis and induce (autoimmune) inflammation, in agreement with A20s proposed identity as a susceptibility gene for inflammatory disease. We further verify that immune-responsive gene 1 (IRG1) is up-regulated in the absence of A20 and that its levels are transcriptionally regulated.

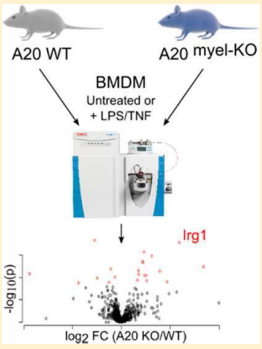

KEYWORDS: *A20, TNFAIP3, bone marrow-derived macrophages, differential proteomics, IRG1, CAD*

INTRODUCTION

The transcription factor Nuclear Factor kappa B (NF-κB) plays crucial roles in the regulation of inflammation and immune responses, and inappropriate NF-κB activity has been linked to many autoimmune and inflammatory diseases. NF-κB signaling is tightly regulated by negative feedback mechanisms to ensure tissue homeostasis.[1] One of the proteins controlling NF-κB signaling is A20, which was initially identified as a tumor necrosis factor (TNF)-induced primary response gene (tumor necrosis factor alpha-induced protein 3 (*TNFAIP3*)) that protects cells from TNF-induced cell death.[2,3] A20 was later identified as a strong anti-inflammatory protein through the inhibition of NF-κB signaling.[4] The first *in vivo* evidence demonstrating the anti-inflammatory and tissue protective function of A20 was found upon examining the phenotype of A20-deficient mice, which die prematurely due to severe multiorgan inflammation and cachexia.[5] Mice with tissue-specific deletion of A20 also demonstrate spontaneous or induced inflammatory phenotypes caused by hyperactivation of NF-κB signaling or enhanced cell death responses.[6] In agreement, genome-wide association studies have identified polymorphisms in A20/*TNFAIP3* in patients suffering from inflammatory and autoimmune pathology,[7] and loss-of-function mutations in A20 leading to A20 haploinsufficiency have been identified in patients suffering from an early onset auto-inflammatory disease, resembeling Behçet's disease.[6,8] A20 loss-of-function mutations have also been identified in B cell lymphomas, proposing A20 as a tumor suppressor protein, although in other cell types A20 has been described as a tumor enhancer.[6]

A20 inhibits NF-κB signaling by acting as a ubiquitin-editing enzyme.[9] The A20 protein contains an N-terminal ovarian tumor (OTU) domain responsible for its deubiquitinase (DUB) activity to remove lysine 63 (K63)-linked polyubiquitin chains from specific NF-κB signaling molecules, as well as a C-terminal domain containing seven zinc fingers (ZnF), of which ZnF4 is thought to have ubiquitin E3 ligase activity to promote K48-linked polyubiquitination of substrate proteins, targeting them for proteasome-mediated degradation. In TNF signaling, A20 inhibits NF-κB activation by sequential deubiquitination and ubiquitin-mediated degradation of receptor-interacting serine/threonine-protein kinase (RIP) 1.[9] A20 can also inhibit toll-like receptor (TLR) 4 and nucleotide-binding oligomeriza-

Received: March 1, 2018
Published: May 7, 2018

DOI: 10.1021/acs.jproteome.8b00139
J. Proteome Res. 2018, 17, 2182−2191

nature COMMUNICATIONS

ARTICLE

DOI: 10.1038/s41467-018-04376-5 OPEN

A20 critically controls microglia activation and inhibits inflammasome-dependent neuroinflammation

Sofie Voet[1,2], Conor Mc Guire[1,2,3,4], Nora Hagemeyer[5], Arne Martens[1,2], Anna Schroeder[6,7], Peter Wieghofer[5,14], Carmen Daems[8], Ori Staszewski[5], Lieselotte Vande Walle[1,9], Marta Joana Costa Jordao[5], Mozes Sze[1,2], Hanna-Kaisa Vikkula[1,2], Delphine Demeestere[1,2], Griet Van Imschoot[1,2], Charlotte L. Scott[1,2], Esther Hoste[1,2], Amanda Gonçalves[1,2,10], Martin Guilliams[1,2], Saskia Lippens[1,2,10], Claude Libert[1,2], Roos E. Vandenbroucke[1,2], Ki-Wook Kim[11,15], Steffen Jung[11], Zsuzsanna Callaerts-Vegh[12], Patrick Callaerts[8], Joris de Wit[6,7], Mohamed Lamkanfi[1,9], Marco Prinz[5,13] & Geert van Loo[1,2]

Microglia, the mononuclear phagocytes of the central nervous system (CNS), are important for the maintenance of CNS homeostasis, but also critically contribute to CNS pathology. Here we demonstrate that the nuclear factor kappa B (NF-κB) regulatory protein A20 is crucial in regulating microglia activation during CNS homeostasis and pathology. In mice, deletion of A20 in microglia increases microglial cell number and affects microglial regulation of neuronal synaptic function. Administration of a sublethal dose of lipopolysaccharide induces massive microglia activation, neuroinflammation, and lethality in mice with microglia-confined A20 deficiency. Microglia A20 deficiency also exacerbates multiple sclerosis (MS)-like disease, due to hyperactivation of the Nlrp3 inflammasome leading to enhanced interleukin-1β secretion and CNS inflammation. Finally, we confirm a Nlrp3 inflammasome signature and IL-1β expression in brain and cerebrospinal fluid from MS patients. Collectively, these data reveal a critical role for A20 in the control of microglia activation and neuroinflammation.

[1] VIB Center for Inflammation Research, B-9052 Ghent, Belgium. [2] Department of Biomedical Molecular Biology, Ghent University, B-9052 Ghent, Belgium. [3] VIB Center for Medical Biotechnology, B-9052 Ghent, Belgium. [4] Department of Biochemistry and Microbiology, Ghent University, B-9052 Ghent, Belgium. [5] Institute of Neuropathology, Faculty of Medicine, University of Freiburg, D-79106 Freiburg, Germany. [6] VIB Center for Brain & Disease Research, B-3000 Leuven, Belgium. [7] Department of Neurosciences, KU Leuven, B-3000 Leuven, Belgium. [8] Department of Human Genetics, KU Leuven, B-3000 Leuven, Belgium. [9] Department of Internal Medicine, Ghent University, B-9052 Ghent, Belgium. [10] VIB Bio-Imaging Core, B-9052 Ghent, Belgium. [11] Department of Immunology, Weizmann Institute of Science, I-76100 Rehovot, Israel. [12] Laboratory of Biological Psychology, KU Leuven, B-3000 Leuven, Belgium. [13] BIOSS Centre for Biological Signalling Studies, University of Freiburg, D79106 Freiburg, Germany. [14] Institute of Anatomy, University of Leipzig, Leipzig D-04103, Germany. [15] Present address: Department of Pathology and Immunology, Washington University of Medicine, St. Louis, MO 63110, USA. These authors contributed equally: Sofie Voet, Conor Mc Guire, Nora Hagemeyer. These authors jointly supervised this work: Marco Prinz, Geert van Loo. Correspondence and requests for materials should be addressed to G. van L. (email: geert.vanloo@irc.vib-ugent.be)

nature COMMUNICATIONS

ARTICLE

https://doi.org/10.1038/s41467-019-09667-z OPEN

Physical and functional interaction between A20 and ATG16L1-WD40 domain in the control of intestinal homeostasis

Karolina Slowicka[1,2,3,10], Inmaculada Serramito-Gómez[4,10], Emilio Boada-Romero[4,10], Arne Martens[1,2], Mozes Sze[1,2,3], Ioanna Petta[1,3,5], Hanna K. Vikkula[1,2,3], Riet De Rycke[1,2,6,7], Eef Parthoens[1,2,6], Saskia Lippens[1,2,6], Savvas N. Savvides[1,8], Andy Wullaert[1,3,9], Lars Vereecke[1,3,5,11], Felipe X. Pimentel-Muiños[4,11] & Geert van Loo[1,2,3,11]

Prevention of inflammatory bowel disease (IBD) relies on tight control of inflammatory, cell death and autophagic mechanisms, but how these pathways are integrated at the molecular level is still unclear. Here we show that the anti-inflammatory protein A20 and the critical autophagic mediator Atg16l1 physically interact and synergize to regulate the stability of the intestinal epithelial barrier. A proteomic screen using the WD40 domain of ATG16L1 (WDD) identified A20 as a WDD-interacting protein. Loss of A20 and Atg16l1 in mouse intestinal epithelium induces spontaneous IBD-like pathology, as characterized by severe inflammation and increased intestinal epithelial cell death in both small and large intestine. Mechanistically, absence of A20 promotes Atg16l1 accumulation, while elimination of Atg16l1 or expression of WDD-deficient Atg16l1 stabilizes A20. Collectively our data show that A20 and Atg16l1 cooperatively control intestinal homeostasis by acting at the intersection of inflammatory, autophagy and cell death pathways.

[1] VIB Center for Inflammation Research, 9052 Ghent, Belgium. [2] Department of Biomedical Molecular Biology, Ghent University, 9052 Ghent, Belgium. [3] Ghent Gut Inflammation Group (GGIG), Ghent University, 9000 Ghent, Belgium. [4] Instituto de Biología Molecular y Celular del Cáncer (IBMCC), Centro de Investigación del Cáncer, CSIC-Universidad de Salamanca, 37007 Salamanca, Spain. [5] Department of Rheumatology, Ghent University, 9000 Ghent, Belgium. [6] VIB BioImaging Core Ghent, 9052 Ghent, Belgium. [7] UGent TEM Expertise Centre, Ghent University, 9000 Ghent, Belgium. [8] Department of Biochemistry and Microbiology, Ghent University, 9000 Ghent, Belgium. [9] Department of Internal Medicine and Pediatrics, Ghent University, 9000 Ghent, Belgium. [10] These authors contributed equally: Karolina Slowicka, Inmaculada Serramito-Gómez, Emilio Boada-Romero. [11] These authors jointly supervised this work: Lars Vereecke, Felipe X. Pimentel-Muiños and Geert van Loo. Correspondence and requests for materials should be addressed to F.X.P-Mño. (email: fxp@usal.es) or to G.v.L. (email: geert.vanloo@irc.vib-ugent.be)

JEM Journal of Experimental Medicine

BRIEF DEFINITIVE REPORT

The ubiquitin-editing enzyme A20 controls NK cell homeostasis through regulation of mTOR activity and TNF

Jessica Vetters[1,2,3,4*], Mary J. van Helden[1,4*], Sigrid Wahlen[5], Simon J. Tavernier[1,4], Arne Martens[6,9], Farzaneh Fayazpour[2,3,4], Karl Vergote[1,4], Manon Vanheerswynghels[1,4], Kim Deswarte[1,4], Justine Van Moorleghem[1,4], Sofie De Prijck[1,4], Nozomi Takahashi[6,7], Peter Vandenabeele[6,7], Louis Boon[8], Geert van Loo[6,9], Eric Vivier[10,11], Bart N. Lambrecht[1,3,4,12**], and Sophie Janssens[2,3,4**]

The ubiquitin-editing enzyme A20 is a well-known regulator of immune cell function and homeostasis. In addition, A20 protects cells from death in an ill-defined manner. While most studies focus on its role in the TNF-receptor complex, we here identify a novel component in the A20-mediated decision between life and death. Loss of A20 in NK cells led to spontaneous NK cell death and severe NK cell lymphopenia. The few remaining NK cells showed an immature, hyperactivated phenotype, hallmarked by the basal release of cytokines and cytotoxic molecules. NK-A20$^{-/-}$ cells were hypersensitive to TNF-induced cell death and could be rescued, at least partially, by a combined deficiency with TNF. Unexpectedly, rapamycin, a well-established inhibitor of mTOR, also strongly protected NK-A20$^{-/-}$ cells from death, and further studies revealed that A20 restricts mTOR activation in NK cells. This study therefore maps A20 as a crucial regulator of mTOR signaling and underscores the need for a tightly balanced mTOR pathway in NK cell homeostasis.

Introduction

Natural killer (NK) cells are the cytotoxic members of the heterogeneous population of innate lymphoid cells (ILCs; Vivier et al., 2018). NK cells kill target cells via the binding of death receptors or by the release of lytic granules that contain granzymes and perforin. They also regulate the function of other immune cells by producing chemokines and cytokines such as TNF and IFNγ (Vivier et al., 2008). Under normal conditions, their activation is inhibited by ligands expressed on healthy cells that engage germline-encoded inhibitory receptors on the NK cells. Viral infection (Waggoner et al., 2016), malignant transformation (Vivier et al., 2012), or cellular stress (Raulet and Guerra, 2009) can lead to up-regulation of ligands that are recognized by a vast array of activating receptors. The relative balance of inhibitory and activating signals eventually determines the activity of the NK cell. Several signaling pathways have been identified to play a crucial role in NK cell functioning. Recently, the mechanistic target of rapamycin (mTOR) pathway was shown to be a hallmark of NK activity (Marçais et al., 2014, 2017). Although NK cell activation has been studied thoroughly, relatively little is known about how activated NK cells are switched off after termination of an inflammatory response.

The NF-κB family of transcription factors plays a key role in inflammatory responses triggered by a plethora of signaling receptors. NF-κB dimers induce expression not only of a large proinflammatory gene program, but also of their own negative regulators, such as inhibitor of κB (IκB) or A20 (encoded by the gene TNFα induced protein 3 (*Tnfaip3*; Renner and Schmitz, 2009). Absence of A20 leads to prolonged NF-κB activation and elevated production of inflammatory cytokines (Catrysse et al., 2014). A20-deficient mice show widespread tissue inflammation and perinatal death (Lee et al., 2000). Also in humans, polymorphisms in the *Tnfaip3* gene are

[1]Laboratory of Immunoregulation and Mucosal Immunology, VIB Center for Inflammation Research, Ghent, Belgium; [2]Laboratory for Endoplasmic Reticulum Stress and Inflammation, VIB Center for Inflammation Research, Ghent, Belgium; [3]GROUP-ID Consortium, Ghent University and Ghent University Hospital, Ghent, Belgium; [4]Department of Internal Medicine and Pediatrics, Ghent University, Ghent, Belgium; [5]Department of Diagnostic Sciences, Ghent University, Ghent, Belgium; [6]Department of Biomedical Molecular Biology, Ghent University, Ghent, Belgium; [7]Molecular Signaling and Cell Death, VIB Center for Inflammation Research, Ghent, Belgium; [8]Bioceros BV, Utrecht, Netherlands; [9]Cellular and Molecular (Patho)physiology, VIB Center for Inflammation Research, Ghent, Belgium; [10]Innate Pharma Research Laboratories, Innate Pharma, Marseille, France; [11]Aix-Marseille University, Assistance Publique–Hôpitaux de Marseille, Centre d'Immunologie de Marseille-Luminy, Hôpital de la Timone, Marseille Immunopôle, Marseille, France; [12]Department of Pulmonary Medicine, Erasmus University Medical Center, Rotterdam, Netherlands.

*J. Vetters and M.J. van Helden contributed equally to this paper; **B.N. Lambrecht and S. Janssens contributed equally to this paper; Correspondence to Sophie Janssens: sophie.janssens@irc.vib-ugent.be; Bart N. Lambrecht: bart.lambrecht@irc.vib-ugent.be.

Priem et al. *Cell Death and Disease* (2019)10:692
https://doi.org/10.1038/s41419-019-1937-y

Cell Death & Disease

ARTICLE Open Access

A20 protects cells from TNF-induced apoptosis through linear ubiquitin-dependent and -independent mechanisms

Dario Priem[1,2], Michael Devos[1,2], Sarah Druwé[1,2], Arne Martens[1,2], Karolina Slowicka[1,2], Adrian T. Ting[3], Manolis Pasparakis[4], Wim Declerq[1,2], Peter Vandenabeele[1,2], Geert van Loo[1,2] and Mathieu J. M. Bertrand[1,2]

Abstract

The cytokine TNF promotes inflammation either directly by activating the MAPK and NF-κB signaling pathways, or indirectly by triggering cell death. A20 is a potent anti-inflammatory molecule, and mutations in the gene encoding A20 are associated with a wide panel of inflammatory pathologies, both in human and in the mouse. Binding of TNF to TNFR1 triggers the NF-κB-dependent expression of A20 as part of a negative feedback mechanism preventing sustained NF-κB activation. Apart from acting as an NF-κB inhibitor, A20 is also well-known for its ability to counteract the cytotoxic potential of TNF. However, the mechanism by which A20 mediates this function and the exact cell death modality that it represses have remained incompletely understood. In the present study, we provide in vitro and in vivo evidences that deletion of A20 induces RIPK1 kinase-dependent and -independent apoptosis upon single TNF stimulation. We show that constitutively expressed A20 is recruited to TNFR1 signaling complex (Complex I) via its seventh zinc finger (ZF7) domain, in a cIAP1/2-dependent manner, within minutes after TNF sensing. We demonstrate that Complex I-recruited A20 protects cells from apoptosis by stabilizing the linear (M1) ubiquitin network associated to Complex I, a process independent of its E3 ubiquitin ligase and deubiquitylase (DUB) activities and which is counteracted by the DUB CYLD, both in vitro and in vivo. In absence of linear ubiquitylation, A20 is still recruited to Complex I via its ZF4 and ZF7 domains, but this time protects the cells from death by deploying its DUB activity. Together, our results therefore demonstrate two distinct molecular mechanisms by which constitutively expressed A20 protect cells from TNF-induced apoptosis.

Introduction

TNF is a well-established inducer of inflammation, and a pharmacological target in several inflammatory disorders[1]. Binding of TNF to TNFR1 induces the rapid assembly of a membrane-bound signaling complex known as TNFR1 Complex I. The initial binding of TRADD and RIPK1 to the receptor allows the subsequent recruitment of TRAF2 and of the E3 ubiquitin ligases cIAP1/2 and LUBAC. Together, these E3s generate a dense network of ubiquitin chains resulting in the stabilization of Complex I and in the recruitment of the kinases that activate the MAPKs and NF-κB signaling pathways[2,3]. The K63-ubiquitin chains generated by cIAP1/2 operate as binding stations for the adapter proteins TAB2/3 and for the recruitment of the kinase TAK1, which subsequently activates the MAPK pathway by phosphorylation[3–5]. On the other hand, the multiprotein E3 complex LUBAC (composed of Sharpin, HOIP, and HOIL-1) docks on these newly formed K63-linked ubiquitin chains and further conjugates Complex I components with linear (M1)-ubiquitin chains; in this way creating, in some cases, hybrid K63/M1 chains[2,6]. The adapter protein NEMO

Correspondence: Mathieu J. M. Bertrand (mathieu.bertrand@irc.vib-ugent.be)
[1]Center for Inflammation Research, VIB, Ghent, Belgium
[2]Department of Biomedical Molecular Biology, Ghent University, Ghent, Belgium
Full list of author information is available at the end of the article.
Edited by G. Raschellà

Acknowledgements

Eerst en vooral wil ik mijn promotor, Geert van Loo, bedanken. Precies 6 jaar geleden ben ik gestart met mijn masterthesis in het U_Gvl labo. Ondanks de moeilijkheden om osteoclasten in cultuur te groeien was dit toch een geslaagde, interessante en leuke periode, waardoor ik ook beslist heb om een PhD te doen. Geert, ook gekend als G, bedankt om me de kans te geven om mijn masterthesis te doen in uw labo en om me daarna aan boord te houden voor een PhD. Je geeft ons veel vrijheid om ons projecten uit te werken, maar we kunnen altijd bij u terecht om problemen of nieuwe ideeën te bespreken. De eerste 2 jaar was het wat zoeken en doorbijten om A20 domein mutante muizen te maken via de CRISPR technologie, maar gezien de recentelijk mooie publicaties met deze muizen was het dit zeker waard. Ik blijf nog wat langer in het labo, maar misschien wordt het toch eens tijd om nog eens een man aan te nemen 😊.

In die 6 jaar die ik in het labo al heb doorgebracht is er wel wat veranderd. Toen ik startte was de "gender balance" in evenwicht, maar na het vertrek van Conor en Lars staan Mozes en ikzelf er alleen voor met al het vrouwelijk geweld. Conor en Lars, ook al was ik nog wat stil in het begin, ik heb toch vaak moeten lachen met alle (soms ongepaste) moppen en opmerkingen. Veel succes nog in jullie verdere carrière. Mozes, je bent al van bij het begin deel van U_GvL en weet dus wel van alles iets af. Ik kan bij u dan ook terecht voor hulp bij vele dingen, ook al moet je het iedere keer opnieuw uitleggen omdat ik geen notities neem. Bedankt om mijn genotyperingen over te nemen en alle buffers te maken voor mij, zonder u was ik waarschijnlijk nog niet kunnen beginnen schrijven aan mijn doctoraat. Ik blijf nog wat langer in het labo en ik zal proberen in de toekomst mijn eigen materiaal (tipjes, whatman papier,epjes,…) te gebruiken in plaats van alles van u te stelen, al lijkt dit weinig geloofwaardig. Ik zal u binnenkort eens een duveltje trakteren, maar we zullen het bij eentje houden voor uw eigen welzijn ☺.

Hanna you also helped me a lot with all the mouse experiments and my histology work. Now you are leaving, maybe it's time to learn and do these things on my own (otherwise Mozes might get a burnout). Congratulations with your Master's degree and good luck with your next adventure in Germany. Esther, you always make time for discussions about experiments and scientific problems in between all your experiments and funding applications. I hope you manage to become independent and start your own group soon, you would do great. Lisette, when you arrived in the lab you were quiet, but now we really notice the silence when you're not in the lab. Under bad influence of Sofie, you turned into a partygirl (hence the nickname "Lizatje"), but your wild times seem to be over since she left. You don't have to stress too much about your papers and PhD, you still have 2 years and in the end everything will be fine. See you on the train 😉. Sahana, thanks to you our lab knows how to dance on Indian music, including the "sweeping with an imaginary broom"-move. Too bad your

wedding was so far away, otherwise I would probably have done something memorable again that you could use for my movie. I wish you all the best with your PhD. (Otu)Lien, the youngster of the lab. In the beginning you were quiet, but you slowly started to open up. You already have a paper in your first year, so no stress for your PhD. Since you don't like wine or beer, maybe we should go on a cocktail night once with the lab (although I don't think Mozes would survive that).

I would also like to thank Leen, Sofie and Karolina who more recently left the lab. You were there already since I started my master thesis, and probably saw me evolving from a very quiet person to "a less quiet" person that likes to make fun of other people. We had a lot of fun and I even got pretty good at gossiping. Leen, you were the mommy of the group with excellent conflict handling skills, trying to make and keep everyone happy in the lab. Good luck at your new job! I'm pretty sure you will easily be integrated in the new team, since it's almost impossible not to like you. Voetje, your bench in the lab is still a big mess, but that's just because I crossed the imaginary border between our benches and I'm now using both of them. We had a lot of fun at work, but also outside work at parties and weddings where you, after a couple of "wijntjes", demonstrated some typical Sofie dance moves and shouted along with some dance hits like "Give me a hand after midnight". I wish you all the best in Argenx and I'll keep you updated with the latest gossips 😉. Karolina, thank you for helping me with all the gut stuff! As far as I remember I had a lot of fun at your wedding in Poland, and I learned that I'm not very good at drinking wodka, although after a couple of wodka's I could suddenly sing songs in Polish. You were always very ambitious and I wish you good luck with your job and career.

Next to the people from the lab, I would also like to thank some other people from the building. Special thanks to the people from the Bertrand group for adopting me at social events, saving me from all the girl talk. Although I always aim to take the last train home after a party, I often end up taking the first train in the morning or wake up in a couch due the persuasiveness of some persons (or my lack of character). In this context, Dario and Yves, thanks for all the fun nights out and for letting me crash on your couch when parties took longer than originally planned. Gillian, thank you for dropping me off at home in the first years, when you were still by car from Oostrozebeke. I told you a lot I would drive the next party, but at least I was BOB once. Also thank to the Berx unit for the nice weekend in the Ardennes.

Daarnaast wil ik ook nog mijn ouders bedanken. Danku om me altijd de vrijheid te geven in mijn studiekeuzes. Ik ben nooit echt een voorbeeldstudent geweest, maar jullie vertrouwden mij (of dachten we laten hem maar even doen) toen ik zei dat jullie zich geen zorgen hoefden te maken en dat alles wel goedkwam. Floor, ook bedankt om mijn scan en knieoperatie zo snel te regelen, anders

zou ik hier nu misschien nog niet kunnen staan. Daarnaast wil ik nog mijn schoonouders Piet en Conny bedanken voor het schilderen en klaar maken van de kinderkamers, terwijl ik mijn doctoraat en paper moest schrijven en daarna niet kon rondlopen door mijn knieblessure.

Finaal wil ik ook nog Tine bedanken voor alle moral support en de leuke dingen die we samen beleven. Ook bedankt om me te helpen met het opmaken van mijn thesis, vooraleer mijn laptop door de lucht vloog omdat alles maar blijft verspringen. Nu staan we voor een dubbel groot avontuur, maar ik ben er zeker van dat we dat samen supergoed gaan doen ☺.